Inflammation and endothelium-platelet interaction in pulmonary thrombosis

Manz, Xue Daphne

2023

DOI (link to publisher)
10.5463/thesis.163

document version
Publisher's PDF, also known as Version of record

Inflammation and endothelium-platelet interaction in pulmonary thrombosis

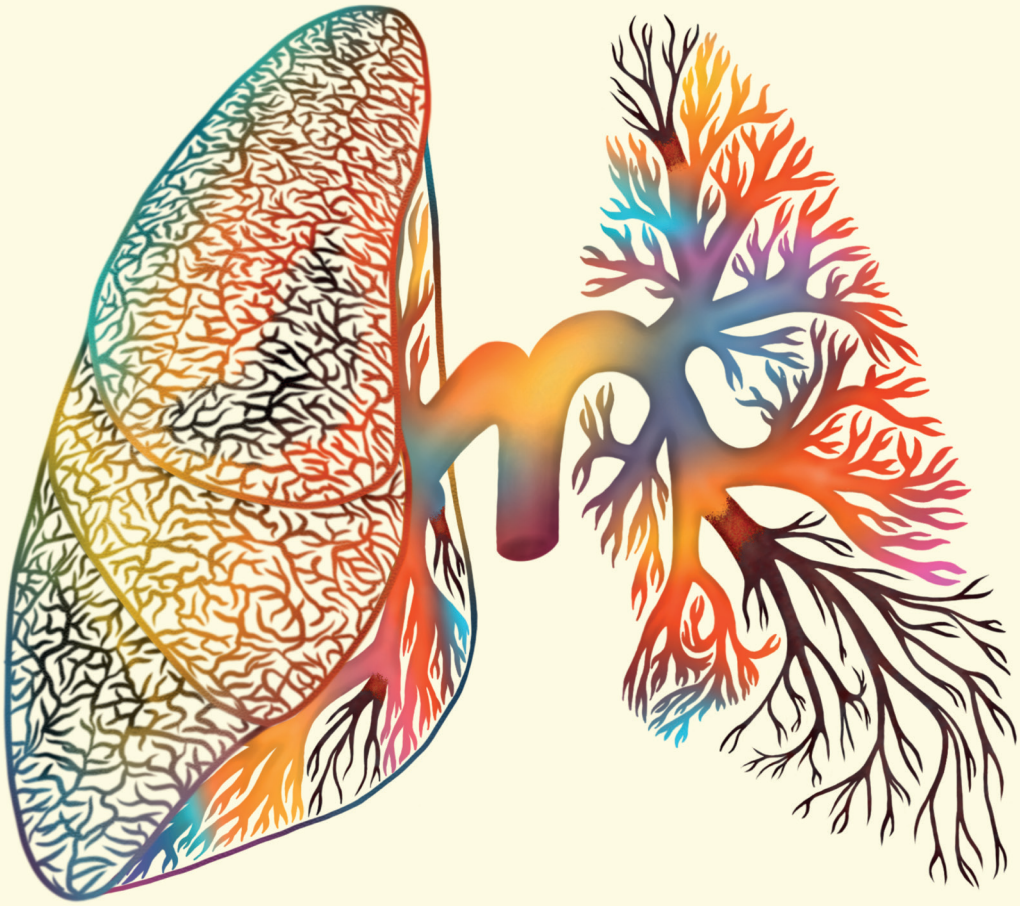

Xue Manz

Inflammation and endothelium-platelet interaction in pulmonary thrombosis

Xue Manz

Cover image by Choënne Straatman

Printing by Ridderprint | www.ridderprint.nl

ISBN: 978-94-6483-028-6

Xue D. Manz is funded by a research grant of the Institute for CardioVascular Research (ICaR-VU) at the VU University Medical Center, Amsterdam, the Netherlands.

The research described in this thesis was supported by the Dutch CardioVascular Alliance (DCVA) [2012-08, 2014-11], awarded to the Phaedra and the Reconnect consortium as well as the Impulse grant 2018 awarded to the Phaedra IMPACT consortium. These grants include collective funding by the Dutch Heart Foundation. Furthermore, this work was supported by The Dutch Federation of University Medical Centers, The Netherlands Organization for Health Research and Development, and the Royal Netherlands Academy of Sciences.

Financial support by the Dutch Heart Foundation for the publication of this thesis is gratefully acknowledged.

VRIJE UNIVERSITEIT

Inflammation and endothelium-platelet interaction in pulmonary thrombosis

ACADEMISCH PROEFSCHRIFT

ter verkrijging van de graad Doctor of Philosophy
aan de Vrije Universiteit Amsterdam,
op gezag van de rector magnificus
prof.dr. J.J.G. Geurts,
in het openbaar te verdedigen
ten overstaan van de promotiecommissie
van de Faculteit der Geneeskunde
op woensdag 17 mei 2023 om 13.45 uur
in een bijeenkomst van de universiteit,
De Boelelaan 1105

door

Xue Daphne Manz

geboren te Wuhan, China

promotor:	prof.dr. H.J. Bogaard
copromotoren:	dr. J. Aman
	dr. R. Szulcek
promotiecommissie:	prof.dr. A. Vonk Noordegraaf
	prof.dr. P.L. Hordijk
	prof.dr. M.J.T.H. Goumans
	prof.dr. J.J. Voorberg
	prof.dr. M. Delcroix

Table of Contents

CHAPTER 1

General introduction

Cardiovascular physiology

The human body is composed of eleven physiological organ systems, which are highly interconnected through an eleventh system: the cardiovascular system. The primary function of the cardiovascular system is transport of materials throughout the body. The heart pumps oxygen and nutrients to, and eliminates carbon dioxide and waste products from the organs via a closed circulatory network of blood vessels. This circulatory network can be divided into a systemic and pulmonary circulation (**Figure 1**). The pulmonary circulation is responsible for the exchange of oxygen and carbon dioxide with the external environment, also known as pulmonary respiration. Pulmonary respiration takes place in the smallest units of the lungs: the alveoli, consisting of alveolar epithelial cells surrounded by a vast network of blood capillaries. Oxygen diffuses through the very thin layer between air and blood (alveolocapillary barrier) and is transported to the heart, which pumps oxygen-rich blood through the systemic circulation. When oxygenated blood reaches tissue, oxygen is released to the peripheral tissues, where it is consumed during cellular respiration leading to the production of carbon dioxide. Deoxygenated blood circulates back to the right heart, which in turn pumps oxygen-poor blood into the pulmonary arteries for new circuit of respiration[1,2].

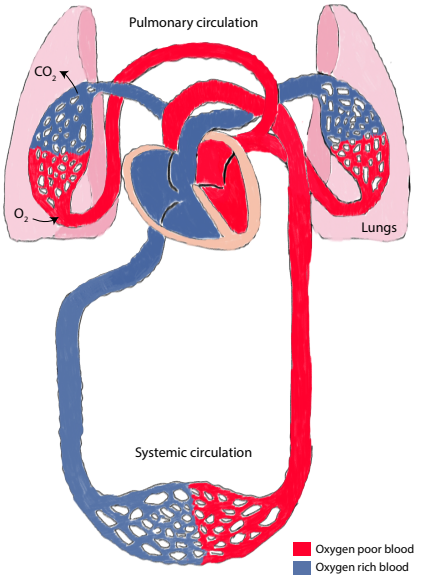

Figure 1. The cardiovascular circulation

The pulmonary circulation

The lungs are the only organ system receiving the entire cardiac output during one heartbeat. With a mean pulmonary artery pressure of about 14 mmHg at rest, the pulmonary circulation is a high-flow and low-pressure system. Flow rates vary between 5 liters per minute at rest to 25 liters per minute during exercise, at a constant pulmonary pressure. This unique feature is mainly explained by a low resistance to blood flow for optimal gas exchange, and a high compliance of thin walled precapillary arterioles[3]. The inner layer of the pulmonary vasculature is formed by endothelial cells, forming the interface between the bloodstream and lung tissue. Besides gas exchange, the pulmonary endothelium plays a key role in vasomotor balance and vascular tissue homeostasis. The endothelium is highly metabolically active to sense and respond to signals from extracellular environments, maintains a thrombus-free surface and controls immune responses to assure normal angiogenesis and integrity of the vascular wall[4]. Alterations of the pulmonary endothelium play a central role in the pathogenesis of several chronic and acute lung diseases, including pulmonary edema, emphysema, thrombosis and pulmonary hypertension[3].

Pulmonary thrombosis

Hemostasis and thrombosis are described as a process of blood clot formation. While hemostasis refers to a controlled response to blood vessel injury by forming a plug to prevent bleeding, thrombosis is initiated in the absence of bleeding, and often actively participates in various cardiovascular diseases[5]. The underlying mechanism of clot formation involves initial binding of platelets to the endothelium, and amplification of further platelet aggregation. This leads to the production of tissue factor that initiates the coagulation cascade to form a thrombin induced platelet-fibrin thrombus[6].

The endothelium plays a key role in coagulation and maintaining blood flow by regulating vascular tone. A healthy endothelium provides a non-thrombogenic environment by preventing the adhesion of platelets and other blood cells. Endothelial cells release prostacyclin and nitric oxide that act as potent inhibitors of platelet and monocyte activation. In addition, the endothelial cell surface expresses anti-adhesive molecules such as ecto-adenoside diphosphatase, preventing platelet aggregation[7]. In addition, the endothelium forms a barrier between blood and the subendothelial matrix. Hemostasis is initiated by exposure of tissue factor in the subendothelium or during pathological conditions such as trauma and inflammation. Disruption of vascular integrity leads to a rapid reaction that induces vascular constriction and the formation of a platelet plug for the initiation of clot formation. Von Willebrand Factor (VWF) is the first protein that captures platelets from the blood stream. It is exclusively produced by endothelial cells and megakaryocytes and requires post-translational modifications through multimerization and glycosylation for appropriate function. VWF is stored within endothelial cells in Weibel-Palade Bodies (WPBs) and released by endothelial cells upon activation by injury or infection8. In **chapter 2**, we review the regulation of VWF on transcriptional and translational level, and describe how VWF is controlled in inflammatory conditions.

Inflammation

Endothelial cells are key regulators of the inflammatory response. Resting endothelial cells maintain an anti-inflammatory environment that prevents coagulation and activation of immune cells[9]. In case of infection or tissue injury, and triggered by various stimuli including bacterial endotoxins, inflammatory cytokines or pattern recognition receptor activation, endothelial cells undergo morphological and functional changes[9]. The upregulation of an inflammatory response that follows endothelial activation leads to sustained inflammation with local and systemic complications, often associated with an increased risk of thrombosis.

Physiologically, inflammation-dependent activation of the coagulation system is part of the host response to locally contain micro-organisms and to prevent systemic spreading via the blood stream[10]. This response involves activation of endothelial cells and an interplay between immune cells and platelets. Innate immune cells express molecular signatures which initiate platelet adhesion and fibrin

network formation. Central in this communication is the formation of neutrophil extracellular traps (NETs) and the expression of intravascular tissue factor by monocytes, resulting in VWF release and platelet binding. The NFκB signaling cascade plays a key role in this stress response and consists of a group of transcription factors that interact to form transcriptionally active homo- and heterodimeric complexes that bind the NFκB consensus sequence in target genes[11]. Important target genes are endothelial cell adhesion molecules such as ICAM-1, VCAM-1 and E-selectin that mediate adherence of immune cells, such as neutrophils and macrophages[12]. Neutrophils interact with constitutively expressed P-selectin on the surface of endothelial cells to initiate rolling along the vessel wall. In addition, WPBs can be released by activators of the NFκB pathway that can promote VWF dependent leukocyte extravasation[13].

Dysregulated thrombosis impairs organ perfusion and may thus form a major threat for the host organism, as is well recognized in acute conditions of sepsis[14], ischemia-reperfusion injury and recently COVID-19[15,16]. In addition to these acute conditions, accumulating evidence suggests that sustained, low-grade inflammation may contribute to chronic thrombotic diseases including atherosclerosis, deep vein thrombosis and chronic thromboembolic pulmonary hypertension (CTEPH)[17]. Many of these clinical conditions show elevated systemic VWF concentrations, and are characterized by signs of local thrombosis, suggesting that local VWF release by the endothelium plays an important role in immunothrombosis. To investigate how the endothelium contributes to thrombosis, we implement a new model to study endothelial function in pulmonary thrombosis in **chapter 3** We introduce a unique protocol for the isolation of pulmonary artery endothelial cells that can be used to study endothelial-platelet or endothelial-whole blood interaction. We show that the thrombotic response is not only different in diseased conditions such as in CTEPH, but also among different vascular beds.

Chronic thromboembolic pulmonary hypertension

Pulmonary hypertension (PH) is a condition characterized by a mean pulmonary artery pressure that exceeds 20 mmHg at rest. This increase in pressure is caused by narrowing of the pulmonary vessels which makes it harder for the heart to pump blood through the lungs. This impaired blood flow results in reduced gas exchange and an increased work load for the right side of the heart, which in the end results in heart failure[18]. Chronic thromboembolic pulmonary hypertension (CTEPH) is a distinct type of PH that is characterized by thrombotic obstructions of the pulmonary arteries after at least three months of effective anticoagulative treatment for acute pulmonary embolism (PE)[19]. Although it is unknown which pathophysiological mechanisms contribute to the chronic transformation, it is thought to involve an interplay between three factors: defective angiogenesis, impaired thrombus resolution and fibrinolysis and endothelial dysfunction[20]. However, the exact mechanisms remain a topic of ongoing discussion.

Although CTEPH is regarded as a long-term complication of an acute venous thromboembolic event, many patients do not have a history of PE or deep vein thrombosis. Moreover, at the time of acute PE diagnosis, signs of CTEPH are often already present. Furthermore, CTEPH patients have a different thromboembolic pulmonary arterial morphology compared to acute PE patients[21]. These observations indicate that besides non-resolving emboli, additional processes such as in situ thrombosis may contribute to the development and progression of CTEPH. In **chapter 4**, we provide evidence of a mechanism of in situ thrombosis that contributes to the progression of the disease. We describe a direct molecular link between inflammation and VWF expression, consequently leading to increased platelet adhesion on the pulmonary endothelium of CTEPH patients.

The role of inflammation in CTEPH is further supported in **chapter 5**, where we describe a multi-omics analysis on CTEPH-PAEC. Expression profiles of CTEPH pulmonary artery endothelial cells show that extracellular matrix organization and cell-cell contacts in CTEPH are disturbed due to the transcription permissive epigenome of these genes in endothelial cells. Moreover, we describe an association between inflammatory signaling and disrupted endothelial barrier function.

The current treatment options of CTEPH consist of lifelong anticoagulation to prevent in situ thrombosis and recurrent VTE. Eligible patients undergo pulmonary endarterectomy (PEA): surgical removal of organized blood clots and scar tissue from the pulmonary arteries, leading to improved blood flow and relief of right heart pressure overload. Operability is based on surgical accessibility of the lesions and the absence of relevant comorbidities[22]. Balloon pulmonary angioplasty (BPA) and PH-specific pharmacotherapy are treatment options indicated for inoperable CTEPH patients. During BPA, preferably performed after optimised medical therapy, stenotic obstructions are opened using a balloon catheter.

Riociguat was the first approved medical therapy in many countries for inoperable CTEPH[23]. It is a selective vasodilator that acts on the nitric oxide pathway and reduces pulmonary vasoconstriction by stimulating soluble guanylate cyclase (sGC). Clinically, it has been shown that riociguat improves exercise capacity, hemodynamics and cardiac function in CTEPH patients for short and longer durations[24-26]. However, the combined use of some selective pulmonary vasodilators and anticoagulants, can be associated with an increased risk of bleeding[27]. It was found that CTEPH patients with a combined therapy of sGC stimulators and vitamin K antagonists experience bleeding events. In **chapter 6**, we attempt to define the mechanism by which riociguat affects endothelial function and increases the increased risk of bleeding. We describe how endothelial cells stimulated with riociguat inhibit ultra large VWF formation, reducing initial platelet binding and interfering with normal hemostasis.

Coronavirus disease 2019

Opposed to the chronic and low-grade inflammation observed in CTEPH, Coronavirus disease 2019 (COVID-19) is associated with acute and severe inflammation, affecting the pulmonary vasculature. COVID-19 is caused by the severe acute respiratory syndrome coronavirus 2 (SARS-CoV-2). The majority of patients presents with common symptoms related to upper tract respiratory infection, such as cough, shortness of breath, fatigue and fever. However, some patients experience a wide range of complications requiring hospitalization for bilateral pneumonia, that may rapidly deteriorate into acute respiratory distress syndrome and pulmonary thrombosis[28,29]. Strikingly, worsening of the disease is often observed around one to two weeks after onset of symptoms, suggesting a disturbed adaptive immune response to infection[30]. The adaptive immune response is characterized by the production of antibodies that counteract infections via various mechanisms, including pathogen neutralization and cytokine production. However, patients with severe COVID-19 symptoms have altered antibody glycosylation, which amplifies the inflammatory response, frequently described as the so called 'cytokine storm'[31]. This excessive inflammatory response often leads to pulmonary edema and thrombosis, in which endothelial cells play a key role. In **chapter 7**, we have show that antibodies from critically ill COVID-19 patients amplify pro-inflammatory responses by alveolar macrophages, subsequently inducing endothelial barrier disruption and pulmonary thrombosis.

Summary

Pulmonary thrombosis is associated with both acute and chronic inflammatory conditions. Focusing on the endothelium, we try to identify how inflammation and thrombosis are linked, with Von Willebrand Factor (VWF) as a key regulator (**chapter 2**). To study this in a preclinical set-up, we implement an in vitro model of vascular thrombosis and endothelial-platelet interaction (**chapter 3**). We investigate how VWF is regulated in CTEPH and thereby provide strong evidence of a link between CTEPH and inflammation (**chapter 4-5**). Current medical therapy for CTEPH patients includes vasodilators in parallel with anticoagulation. We describe how this combination of therapies may lead to an increased risk of bleeding (**chapter 6**). Lastly, an excessive inflammatory response plays a key role in critically ill COVID-19 patients. We describe how the immune response contributes to microvascular leakage and thrombosis in this disease (**chapter 7**).

References

1. Silverthorn DU. Human physiology. Jones & Bartlett Publishers; 2015.
2. Tortora GJ, Derrickson BH. Principles of anatomy and physiology. John Wiley & Sons; 2018.
3. Huertas A, Guignabert C, Barbera JA, Bartsch P, Bhattacharya J, Bhattacharya S, Bonsignore MR, Dewachter L, Dinh-Xuan AT, Dorfmuller P, et al. Pulmonary vascular endothelium: the orchestra conductor in respiratory diseases: Highlights from basic research to therapy. Eur Respir J. 2018;51. doi: 10.1183/13993003.00745-2017
4. Ryan US. Pulmonary endothelium: a dynamic interface. Clin Invest Med. 1986;9:124-132.
5. Versteeg HH, Heemskerk JW, Levi M, Reitsma PH. New fundamentals in hemostasis. Physiol Rev. 2013;93:327-358. doi: 10.1152/physrev.00016.2011
6. Sim D, Flaumenhaft R, Furie B, Furie B. Interactions of platelets, blood-borne tissue factor, and fibrin during arteriolar thrombus formation in vivo. Microcirculation. 2005;12:301-311. doi: 10.1080/10739680590925682
7. Wu KK, Thiagarajan P. Role of endothelium in thrombosis and hemostasis. Annu Rev Med. 1996;47:315-331. doi: 10.1146/annurev.med.47.1.315
8. Lenting PJ, Christophe OD, Denis CV. von Willebrand factor biosynthesis, secretion, and clearance: connecting the far ends. Blood. 2015;125:2019-2028. doi: 10.1182/blood-2014-06-528406
9. Loof TG, Morgelin M, Johansson L, Oehmcke S, Olin AI, Dickneite G, Norrby-Teglund A, Theopold U, Herwald H. Coagulation, an ancestral serine protease cascade, exerts a novel function in early immune defense. Blood. 2011;118:2589-2598. doi: 10.1182/blood-2011-02-337568
10. Stark K, Massberg S. Interplay between inflammation and thrombosis in cardiovascular pathology. Nat Rev Cardiol. 2021;18:666-682. doi: 10.1038/s41569-021-00552-1
11. Oeckinghaus A, Ghosh S. The NF-kappaB family of transcription factors and its regulation. Cold Spring Harb Perspect Biol. 2009;1:a000034. doi: 10.1101/cshperspect.a000034
12. Iba T, Levy JH, Connors JM, Warkentin TE, Thachil J, Levi M. The unique characteristics of COVID-19 coagulopathy. Crit Care. 2020;24:360. doi: 10.1186/s13054-020-03077-0
13. Petri B, Broermann A, Li H, Khandoga AG, Zarbock A, Krombach F, Goerge T, Schneider SW, Jones C, Nieswandt B, et al. von Willebrand factor promotes leukocyte extravasation. Blood. 2010;116:4712-4719. doi: 10.1182/blood-2010-03-276311
14. Angus DC, van der Poll T. Severe sepsis and septic shock. N Engl J Med. 2013;369:840-851. doi: 10.1056/NEJMra1208623
15. Jackson SP, Darbousset R, Schoenwaelder SM. Thromboinflammation: challenges of therapeutically targeting coagulation and other host defense mechanisms. Blood. 2019;133:906-918. doi: 10.1182/blood-2018-11-882993
16. Bonaventura A, Vecchie A, Dagna L, Martinod K, Dixon DL, Van Tassell BW, Dentali F, Montecucco F, Massberg S, Levi M, et al. Endothelial dysfunction and immunothrombosis as key pathogenic mechanisms in COVID-19. Nat Rev Immunol. 2021;21:319-329. doi: 10.1038/s41577-021-00536-9
17. Skoro-Sajer N, Gerges C, Gerges M, Panzenbock A, Jakowitsch J, Kurz A, Taghavi S, Sadushi-Kolici R, Campean I, Klepetko W, et al. Usefulness of thrombosis and inflammation biomarkers in chronic thromboembolic pulmonary hypertension-sampling plasma and surgical specimens. J Heart Lung Transplant. 2018;37:1067-1074. doi: 10.1016/j.healun.2018.04.003
18. Orfanos SE, Giannakoulas G. Pulmonary Hypertension: Current Diagnosis, Approach and Treatment at the Dawn of the New European Guidelines. J Clin Med. 2022;11. doi: 10.3390/jcm11195804
19. Wilkens H, Konstantinides S, Lang IM, Bunck AC, Gerges M, Gerhardt F, Grgic A, Grohe C, Guth S, Held M, et al. Chronic thromboembolic pulmonary hypertension (CTEPH): Updated Recommendations from the Cologne Consensus Conference 2018. Int J Cardiol. 2018;272S:69-78. doi: 10.1016/j.ijcard.2018.08.079
20. Hoeper MM, Madani MM, Nakanishi N, Meyer B, Cebotari S, Rubin LJ. Chronic thromboembolic pulmonary hypertension. Lancet Respir Med. 2014;2:573-582. doi: 10.1016/S2213-2600(14)70089-X
21. Braams NJ, Boon G, de Man FS, van Es J, den Exter PL, Kroft LJM, Beenen LFM, Huisman MV, Nossent EJ, Boonstra A, et al. Evolution of CT findings after anticoagulant treatment for acute pulmonary embolism in patients with and without an ultimate diagnosis of CTEPH. Eur Respir J. 2021. doi: 10.1183/13993003.00699-2021
22. Jenkins D. Pulmonary endarterectomy: the potentially curative treatment for patients with chronic thromboembolic pulmonary hypertension. Eur Respir Rev. 2015;24:263-271. doi: 10.1183/16000617.00000815

23. Pepke-Zaba J, Ghofrani HA, Hoeper MM. Medical management of chronic thromboembolic pulmonary hypertension. Eur Respir Rev. 2017;26. doi: 10.1183/16000617.0107-2016
24. Ghofrani HA, D'Armini AM, Grimminger F, Hoeper MM, Jansa P, Kim NH, Mayer E, Simonneau G, Wilkins MR, Fritsch A, et al. Riociguat for the treatment of chronic thromboembolic pulmonary hypertension. N Engl J Med. 2013;369:319-329. doi: 10.1056/NEJMoa1209657
25. Simonneau G, D'Armini AM, Ghofrani HA, Grimminger F, Hoeper MM, Jansa P, Kim NH, Wang C, Wilkins MR, Fritsch A, et al. Riociguat for the treatment of chronic thromboembolic pulmonary hypertension: a long-term extension study (CHEST-2). Eur Respir J. 2015;45:1293-1302. doi: 10.1183/09031936.00087114
26. Simonneau G, D'Armini AM, Ghofrani HA, Grimminger F, Jansa P, Kim NH, Mayer E, Pulido T, Wang C, Colorado P, et al. Predictors of long-term outcomes in patients treated with riociguat for chronic thromboembolic pulmonary hypertension: data from the CHEST-2 open-label, randomised, long-term extension trial. Lancet Respir Med. 2016;4:372-380. doi: 10.1016/S2213-2600(16)30022-4
27. Opitz CF, Kirch W, Mueller EA, Pittrow D. Bleeding events in pulmonary arterial hypertension. Eur J Clin Invest. 2009;39 Suppl 2:68-73. doi: 10.1111/j.1365-2362.2009.02122.x
28. Zhang Q, Bastard P, Effort CHG, Cobat A, Casanova JL. Human genetic and immunological determinants of critical COVID-19 pneumonia. Nature. 2022;603:587-598. doi: 10.1038/s41586-022-04447-0
29. Merad M, Blish CA, Sallusto F, Iwasaki A. The immunology and immunopathology of COVID-19. Science. 2022;375:1122-1127. doi: 10.1126/science.abm8108
30. Tay MZ, Poh CM, Renia L, MacAry PA, Ng LFP. The trinity of COVID-19: immunity, inflammation and intervention. Nat Rev Immunol. 2020;20:363-374. doi: 10.1038/s41577-020-0311-8
31. Hoepel W, Chen HJ, Geyer CE, Allahverdiyeva S, Manz XD, de Taeye SW, Aman J, Mes L, Steenhuis M, Griffith GR, et al. High titers and low fucosylation of early human anti-SARS-CoV-2 IgG promote inflammation by alveolar macrophages. Sci Transl Med. 2021;13. doi: 10.1126/scitranslmed.abf865

PART I

Thrombosis

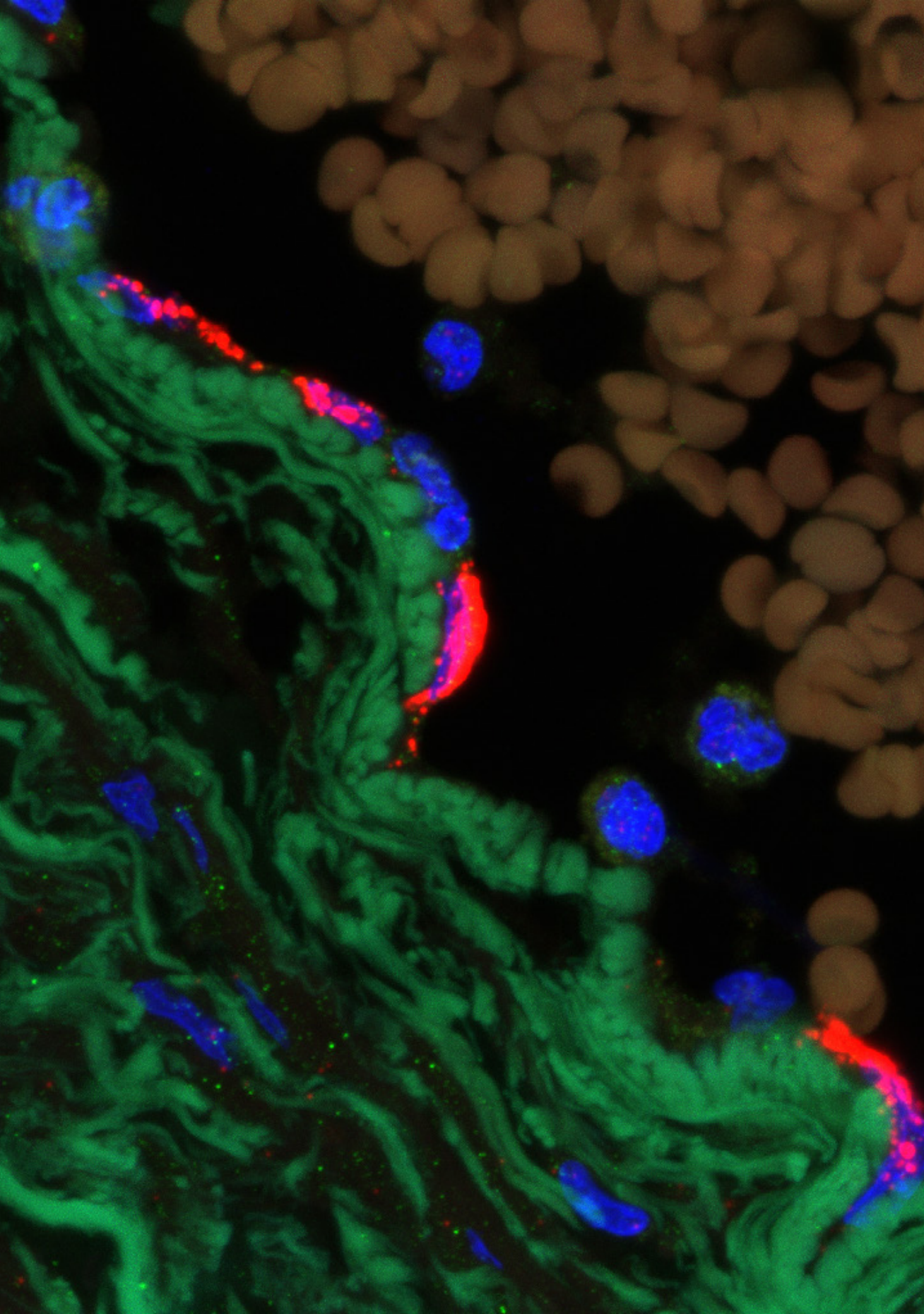

CHAPTER 2

Regulation of VWF (Von Willebrand Factor) in inflammatory thrombosis

Xue D. Manz[1], Harm Jan Bogaard[1,] Jurjan Aman[1]

[1]Department of Pulmonary Medicine, Amsterdam UMC, VU University Medical Center, Amsterdam Cardiovascular Sciences (ACS), Amsterdam, The Netherlands

29 September 2022, Arteriosclerosis, Thrombosis and Vascular Biology

Abstract

Increasing evidence indicates that inflammation promotes thrombosis via a VWF (von Willebrand factor)-mediated mechanism. VWF plays an essential role in maintaining the balance between blood coagulation and bleeding, and inflammation can lead to aberrant regulation. VWF is regulated on a transcriptional and (post-)translational level, and its secretion into the circulation captures platelets upon endothelial activation. The significant progress that has been made in understanding transcriptional and translational regulation of VWF is described in this review. First, we describe how VWF is regulated at the transcriptional and post-translational level with a specific focus on the influence of inflammatory and immune responses. Next, we describe how changes in regulation are linked with various cardiovascular diseases. Recent insights from clinical diseases provide evidence for direct molecular links between inflammation and thrombosis, including atherosclerosis, chronic thromboembolic pulmonary hypertension, and COVID-19. Finally, we will briefly describe clinical implications for antithrombotic treatment.

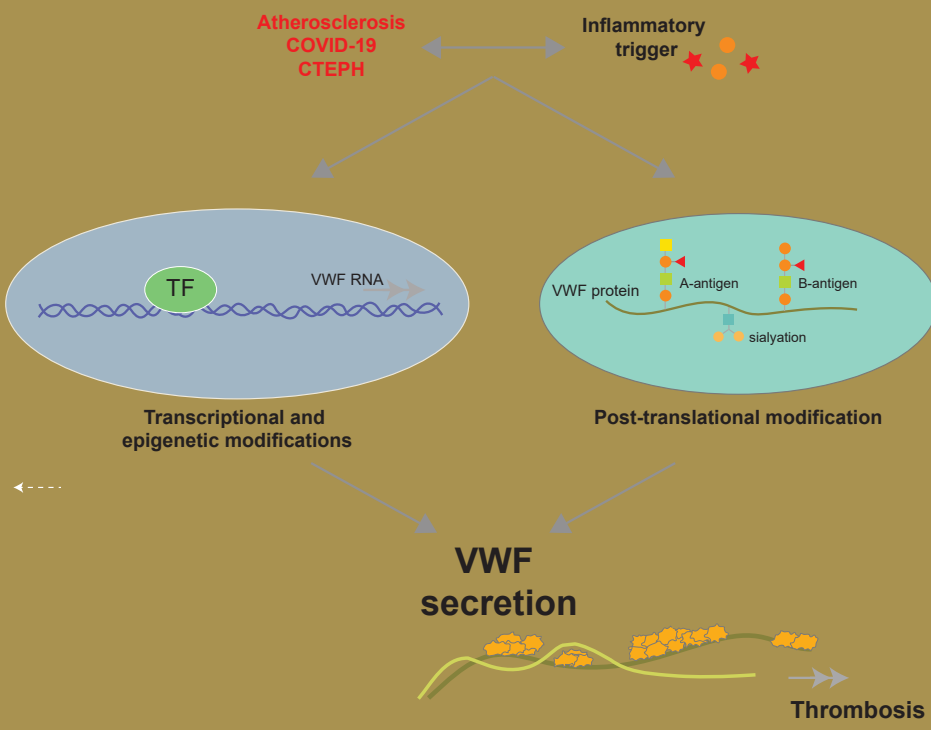

Introduction

Activation of the endothelium plays a central role in various cardiovascular diseases, often resulting in perturbations in hemostasis and thrombosis. Thrombosis involves interactions between the endothelium and platelets, leukocytes, and clotting proteins. A quiescent endothelium acts as an anticoagulant that suppresses platelet activation and promotes fibrinolysis. This occurs via regulatory mechanisms protecting against thrombus formation, including release of nitric oxide and prostacyclin, and expression of heparan sulfate[1]. Activation or damage to the vascular wall causes rapid initiation of hemostasis, an acute response involving the exposure of subendothelial TF (tissue factor), expression of adhesion molecules, and platelet aggregation all directed towards closure of the site of injury. Central players in primary hemostasis include activated platelets as well as VWF (von Willebrand factor). VWF, being both released from injured endothelial cells and present in the subendothelial matrix, provides a major binding site for initial platelet adhesion and subsequent platelet aggregation[2]. Endothelial-platelet activation induces the release of P-selectin and TF, promoting the initiation of the coagulation cascade of serine proteases, which act by cleaving downstream coagulation factors, ultimately resulting in the formation of a firm and stable fibrin clot[3]. Directed at repair of injury, hemostasis serves a physiological function and is self-contained by inhibitors downstream the coagulation cascade. Under certain conditions, however, pathological deviation of hemostasis may result in intravascular thrombus formation and vessel occlusion also referred to as thrombosis[4]. Although bleeding disorders associated with VWF deficiencies clearly illustrate the function and regulation of VWF in hemostasis[5], the contribution of elevated VWF levels to thrombosis is subject to ongoing discussion. Elevated VWF levels are associated with increased cardiovascular risk, but it is unclear whether a high VWF level represents an actual cause of cardiovascular disease. Alternatively, VWF is merely a marker for endothelial dysfunction. Various factors can play a role in the release of VWF during thrombosis, with inflammation being a particular driver of endothelial stimulation and VWF release[6]. Many transcription factors, enzymes, and cytokines that drive inflammatory reactions, also trigger the release of VWF[7]. An example of the intersection of inflammation, and thrombosis was provided during the recent COVID-19 pandemic when VWF was identified as central player in COVID-19 coagulopathy. The link between inflammation and thrombosis is also strong in other clinical conditions, such as atherosclerosis and chronic thromboembolic pulmonary hypertension (CTEPH).

Although the connection between inflammation and thrombosis has been well established in these mentioned diseases, recent molecular insights in COVID-19 and other conditions have further consolidated the prothrombotic role of VWF during the inflammatory response. In this review, we aim to provide an overview of (1) the regulation of VWF expression with a specific focus on inflammation and (2) the contribution of inflammation-induced VWF release to in situ thrombosis. Finally, we will evaluate pharmacological strategies to target VWF.

Immunothrombosis

From an evolutionary point of view, immunity and hemostasis have been closely intertwined, both from a functional and a molecular perspective. Hemostasis forms part of the host defense, as wound closure directly protects against infection by preventing a porte d'entrée for microorganisms. In addition to hemostasis and wound repair, also intravascular thrombosis has been proposed to form part on the innate immune response. Both microorganisms and first-line immune responses may induce thrombosis to limit the spread of blood-borne infections. Microorganisms captured in fibrin networks resulting from intravascular thrombosis are also more accessible to immune cells[8,9]. From a molecular point of view, there is a close intertwinement between immunity and thrombosis, with the serine protease cascades of hemostasis tracing back to the innate immunity of invertebrates[9]. Interestingly, recent work from our group demonstrated binding of the inflammatory transcription factor NFκB2 (nuclear factor κB 2) to highly conserved sites in the VWF promoter, providing a direct molecular link between the immune response and thrombosis[10].

In adults, the relationship between thrombosis and inflammation involves a complex interplay between inflammatory, immune, and hemostatic cells[11]. During stress responses to injury, pathogens or the release of cytokines, PAMPs (pathogen-associated molecular patterns), host-derived DAMPs (damage-associated molecular patterns), and complement activate the immune system[12]. Innate immune cells express molecular signatures which initiate platelet adhesion and fibrin network formation. Central in this communication is the expression of intravascular TF by monocytes, the formation of NETs (neutrophil extracellular traps), and the binding of TF to NETs, altogether leading to platelet recruitment, thrombin generation, and thrombus formation[8,13]. The endothelium plays a key role by localizing this response to the site of injury and infection, both by platelet binding to locally released VWF from Weibel Palade bodies (WPBs) at the site of insult and by release of anticoagulative molecules, such as prostacyclin and nitric oxide, to prevent platelet activation in unaffected regions[14]. Furthermore, endothelial expression of thrombomodulin maintains homeostasis by interaction with thrombin and protein C to dampen the inflammatory response[15].

The NFκB signaling cascade plays a key role in this stress response and consists of a group of transcription factors that interact to form transcriptionally active homodimeric and heterodimeric complexes that bind the NFκB consensus sequence in target genes[16]. Important target genes are endothelial cell adhesion molecules, such as ICAM-1 (intercellular adhesion molecule 1), VCAM-1 (vascular cell adhesion molecule 1), and E-selectin, that mediate adherence of immune cells, such as neutrophils and macrophages[17]. In addition, WPBs content can be released by activators of the NFκB pathway that can promote leukocyte extravasation[18]. Neutrophils interact with constitutively expressed P-selectin on the surface of endothelial cells to initiate rolling along the vessel wall via interaction with PSGL-1 (P-selectin glycoprotein ligand-1). This PSGL-1 expression on leukocytes interacts with platelet P-selectin and supports platelet-leukocyte conjugation with the activated endothelium[19]. In addition, P-selectin is expressed in high concentrations on platelet surface during

platelet activation, mediating the interaction between endothelial cells, platelets, and leukocytes, being an important mediator in inflammation and thrombosis[20].

Although immunothrombosis is supposed to be self-limiting in order to be functional, derangement has been observed, leading to widespread thrombosis (sometimes referred to as thrombo-inflammation[11]). Dysregulated microvascular thrombosis impairs organ perfusion and may thus form a major threat for the host organism, as is well recognized in acute conditions of sepsis[21], ischemia-reperfusion injury, and recently COVID-19[11,22]. In addition to these acute conditions, accumulating evidence suggests that sustained, low-grade inflammation may contribute to chronic thrombotic diseases including atherosclerosis, deep vein thrombosis, and CTEPH[23]. Many of these clinical conditions show elevated systemic VWF and are characterized by signs of local thrombosis, suggesting that local VWF release by the endothelium plays an important role in immunothrombosis. However, the role and regulation of VWF in inflammation remain ongoing topics of investigation, which might be of interest for treatment implications in thromboembolic diseases.

Von Willebrand Factor

VWF is an adhesive glycoprotein synthesized by megakaryocytes and endothelial cells, although the main share of circulating VWF originates from the endothelium and endothelial-derived VWF has a more prominent role in thrombosis than platelet-derived VWF[24]. Most of the VWF is stored in either platelet α-granules or endothelial WPB. These WPBs are formed by VWF multimerization and are assumed to be derivatives of the Golgi apparatus[25]. WPBs rapidly respond to alterations in the integrity of endothelial cells and release VWF via a constitutive or regulatory pathway[25]. The constitutive pathway consists of low molecular weight–VWF multimers that are primarily secreted at the basolateral side of the endothelium and mediate platelet adhesion to the extracellular matrix[26]. In contrast, high molecular weight–VWF is released into the circulation, either spontaneously without being functionally active, or via stimulated WPB release[24,27]. This release can be induced by multiple stimuli including thrombin, histamine, and epinephrine and exerts a highly thrombotic activity (**Figure 1A**)[26].

The human VWF gene is located on chromosome 12 and is composed of 52 exons, encoding for a protein of 2813 amino acids that can be subdivided into a signaling peptide, a propeptide, and a mature subunit[28,29]. The propeptide detaches before VWF is released into the blood, while the major subunit consists of different functional domains that interact with other proteins or molecules[28]. Intermolecular disulfide linkage of the D1:D2 domain is important to form functional active VWF multimers[30]. VWF has a binding domain for factor VIII at D3 and a platelet GPIb (glycoprotein Ib) binding site at A1[31]. The A3 domain serves as a ligand for collagen, while C1 has an RGD (arginylglycylaspartic acid) sequence that is recognized by αIIbβ3 and αvβ3 integrins (**Figure 1B**). These integrins anchor VWF to either the underlying endothelial cells or recruited platelets to form aggregates[25,32].

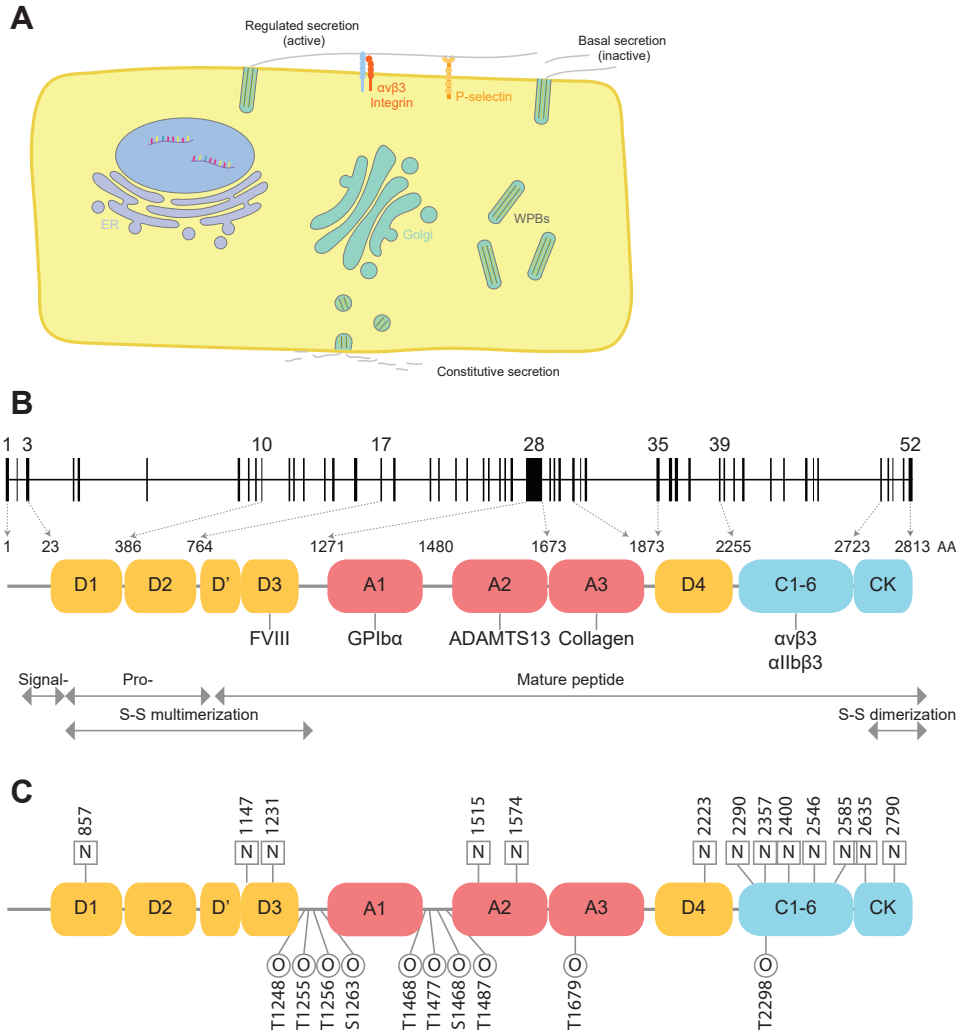

Figure 1. VWF (von Willebrand factor) biosynthesis and composition. **(A)** VWF undergoes synthesis pathway to secretion into the circulation. After transcription and translation, **(B)** VWF composition on genetic and protein level. **(C)** Post-translational modification of N- and O-linked glycosylation on VWF monomers. AA indicates amino acids; ADAMTS-13, a disintegrin and metalloproteinase with thrombospondin motifs; CK, cystine knot domain; FVIII, factor VIII; GPIbα, platelet glycoprotein Ib alpha; and WPB, Weibel Palade bodies.

The different domains are subjected to post-translational modification in the endoplasmic reticulum which involves N-linked and O-linked glycosylation[25]. Before dimerization, high mannose N-linked oligosaccharides are added to specific asparagine residues after which low molecular weight–VWF dimers are formed by C-terminal disulfide bonds. As VWF passes the Golgi system, O-linked oligosaccharides are added to threonine and serine residues and high molecular weight–VWF complexes are formed by N-terminal disulfide bonds. As a result, a VWF contains 13 N-linked and 10 O-linked glycans located at specific sites distributed across the mature monomer (**Figure 1C**). The

highly heterogeneous assembled high molecular weight–VWF complexes are stored in WPBs until secretion. The released VWF multimers can be reduced in size via proteolytic cleavage at the A2 domain by ADAMTS-13 (a disintegrin and metalloproteinase with thrombospondin motifs)[28].

The sequence of events from VWF synthesis to secretion is highly complex, numerous factors can change this pathway and influence VWF plasma levels. Various studies have shown that 60% of VWF plasma levels are genetically determined, suggesting a highly genetic regulation of VWF expression. Genetic variations in the VWF gene have been associated with increased or decreased VWF levels. The phenotypic variability in VWF plasma levels is influenced by several quantitative trait loci that regulate VWF plasma levels and biological mechanisms[33,34]. Variability in VWF expression is also regulated at an epigenetic level. Inflammatory stimuli can induce VWF expression, as well as aging and environmental exposures such as cigarette smoke[35,36]. In addition to the variability in the VWF gene, the ABO blood group is a genetic factor that is strongly associated with VWF expression on a post-translational level[37].

Transcriptional Regulation of VWF

The VWF Promotor and Transcription Factor Binding

It has been acknowledged that VWF protein and mRNA expressions are highly heterogeneous in various vascular beds[38–40] and may change in pathophysiological conditions. Previous investigations demonstrated that VWF expression is highly regulated on a transcriptional regulatory level. The human VWF promoter spans a region between −2182 to the end of the first intron with various binding sites to drive VWF expression. In studies with transgenic mice, it was shown that a region between −487 and +246 directs expression in the brain, whereas a large promoter fragment between −2182 and +1475 also affects VWF expression in the capillary endothelium of the heart (**Table 1**)[41]. The human VWF gene harbors a minimal core promoter region located at −90/+22, a strong negative regulatory element upstream the core promoter at −500/−300, and a positive regulatory region located downstream the core promoter in the first exon[42]. The activity of the promoter is dependent on the binding of transcription factors on these various regions and will result in differential expression.

The investigation of endothelial-specific cis-acting VWF promoter elements resulted in the identification of several trans-acting transcription factors that regulate VWF promoter activity at the 5′ untranslated region (**Table 1**). The promoter region around the first exon of VWF possesses highly conserved GATA (GATA transcription factor) binding sites[43,44], and the induction of mutations in these sites resulted in significantly reduced reporter gene activity in bovine aortic endothelial cells and human umbilical vein endothelial cells[45]. These mutations led to the identification of histone H1 (H1-like protein) as one of the common transcription factors binding to and activating VWF promoter activity on specific CCAAT binding elements[45].

Table 1. **Transcription Factors Involved in VWF Expression**

Promoter activity	Transcription factor	Location	Reference
Activator	**GATA 2, 3, 6**	-89/+244 +220/+225 -89 -2182 and the end of the first intron (LPS mediated)	Liu et al[43], Peng et al[44]
	H1	+155/+184	Wang et al[45], Nassiri et al[46]
	NFAT5	-497 (NaCl induced)	Dmitrieva et al[47]
	ETS1, 2 **ERG**	-56 -36 (not active)	Liu et al[41], Othman et al[48], Schwachtgen et al[49], Peng et al[50], Dong et al[51]
	NFY	-18 -90 (irradiation induced)	Peng et al[44], Nassiri et al[46], Peng et al[50], Bertagna et al[52]
	YY1	Intron 51 via chromatin looping to NF1 binding site	Nassiri et al[46], Mojiri et al[53]
	KLF2	non-consensus DNA binding verified by Luciferase	Chu et al[54]
	TLR2	non-consensus DNA binding verified by ChIP	Singh et al[55]
	SP1	non-consensus DNA binding verified by ChIP	
Repressor	**NF1**	-461	Nassiri et al[46], Peng et al[50], Jahroudi et al[56]
	Oct1	-133	Nassiri et al[46], Peng et al[50], Schwachtgen et al[57]
	NFY	+226	Peng et al[44], Wang et al[45]
	E4BP4	+96	Hough et al[58]
	NFκB	-1793	Wang et al[59]
Tissue specific	**Brain**	-487/+246	Liu et al[41]
	Heart **Skeletal muscle**	-843/-620	Aird et al[60]

ChIP indicates chromatin immunoprecipitation; E4BP4, a basic leucine zipper transcription factor; ERG, Ets-related gene; ETS, E26 transformation-specific transcription factor; GATA, GATA transcription factor; H1, H1-like protein; KLF2, Krüppel-like factor 2; LPS, lipopolysacharide; NF1, nuclear factor 1; NFAT5, nuclear factor of activated T-cells 5; NFY, nuclear transcription factor Y; NFκB, nuclear factor kappa B; Oct1, octamer transcription factor 1; SP1, specificity protein 1; TLR2, Toll-like receptor 2; VWF, von Willebrand factor; and YY1, yin yang 1.

In addition to common transcription factors, specific response or local dependent transcription factors have been identified. For example, the VWF promoter contains an osmotic response element that binds NFAT5 (nuclear factor of activated T-cells 5) upon NaCl increase, consequently leading to increased VWF production in endothelial cells[47]. ERG (Ets-related gene) binding on E twenty-six motifs only activates VWF gene expression in capillary beds while the larger arteries are differently regulated[41]. Although identified as an activator of VWF transcription, ERG responds in a negative feedback to inflammatory stimuli such as TNF (tumor necrosis factor) α. ERG binding represses IL (interleukin)-8 transcription consequently leading to reduced neutrophil activation and VWF expression[61].

In addition, NFY (nuclear transcription factor Y) also functions as either activator or repressor of the VWF gene, depending on the binding site and with organ specificity[46]. In the pulmonary vasculature, for example, NFY acts as repressor, and mutations in the NFY region result in activation of VWF transcription. Other possible repressors of VWF transcription are Octamer transcription factor 1, NF1 (nuclear factor 1), and NFκB. NFκB is a central mediator of inflammation and fundamentally involved in the molecular link between inflammation and thrombosis. Interestingly, we have recently shown that NFκB2, a different protein of the NFκB family, acts as an enhancer of VWF transcription in the pulmonary endothelium[10]. Endothelial cells from patients with chronic pulmonary thrombosis showed increased acetylation of the VWF promoter and enhanced NFκB2 binding, leading to elevated VWF secretion and platelet adhesion. Furthermore, in hypoxemia, VWF transcription in lung endothelial cells is upregulated via inhibition of NF1 and increased YY1 translocation to the VWF promoter[53]. Other nonconsensus binding sites have been identified in the VWF promoter for KLF2 (Krüppel-like factor 2), Toll-like receptor 2, and SP1 (specificity protein 1). KLF2 is activated under external factors such as high and disturbed shear stress[63–65].

Altogether, external stimuli such as hypoxia, trauma, or inflammation can activate transcription factors that can either stimulate or repress VWF transcription, depending on the binding site on the promoter region.

Single Nucleotide Variations

As the promoter plays an important role in the regulation of VWF transcription, several studies focused on the VWF promoter region and single nucleotide polymorphisms (SNPs) that affect VWF plasma concentration. In general, there are 3 major SNPs identified in the VWF gene, all interfering with SP1, GATA2, E twenty-six, and NFκB transcription factors. These SNPs are rs7964777, rs7954855, and rs7965413 and are in strong linkage disequilibrium and segregate into 3 haplotypes (**Figure 2A**)[66]. If VWF is causally linked with the risk of cardiovascular disease, a genetic polymorphism that influences VWF plasma levels should increase the risk of cardiovascular disease to the same extent as predicted by its influence on VWF plasma levels. However, when comparing 4 studies that analyzed the effect of these SNPs on VWF plasma levels, there was no effect on VWF plasma levels and the risk of cardiovascular disease (**Figure 2B**, Table S1, Figure S2)[26,65-67]. After splitting subjects by blood groups, there is only an association between SNPs and VWF expression in blood group O subjects, primarily detectable after the age of 40 (**Figure 2C**)[66]. With haplotype 2/2, group O blood donors have decreased VWF antigen levels compared to haplotype 1/1. This is supported by data that overall mortality and risk for thrombosis are reduced in patients with blood group O. The presence of ABO blood group determinants on VWF glycans were demonstrated to participate in VWF protein expression.

A

haplotype	rs7964777: 2709C>T1234		rs7954855: 2661A>G1185		rs7965413: 2527G>A1051	
1/1	c	c	a	a	g	g
1/2	c	t	a	g	g	a
2/2	t	t	g	g	a	a

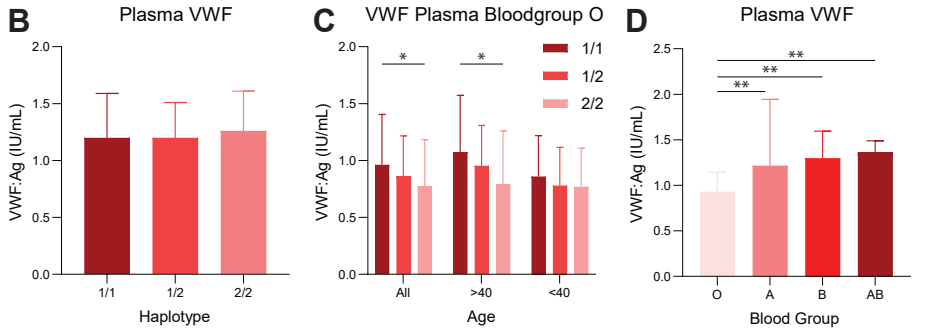

Figure 2. VWF (von Willebrand factor) levels can be affected by genetic and protein modification. **(A)** Identified single nucleotide polymorphism (SNPs) haplotypes on the promotor region of VWF **(B)** Influence of these SNPs on VWF plasma levels. Data presents mean±SD of a meta-analysis from four independent studies. No significant differences were observed. **(C)** The influence of SNPs on VWF expression were associated with blood group O subjects. Data extracted from Keightley et al[66] and presents mean±SD and significance is indicated with *P<0.05 after 2-way ANOVA with Grenhouse-Geisser correction for Tukey multiple comparison test. **(D)** Plasma VWF levels in the ABO blood system. Data presents mean±SD of a meta-analysis of 32 independent studies. Significance is indicated with **P<0.01 after performing a continuous meta-analysis in R 4.0.2 (See Supplemental Material). VWF:Ag indicates VWF antigen levels.

Regulation of VWF by Post-Translational Modification

After translation, the VWF protein is subjected to extensive post-translational modifications including N- and O-linked glycosylation. Both N-linked and O-linked glycans on the mature VWF molecule are involved in regulating VWF secretion and clearance from the plasma. Altered glycosylation of VWF therefore can cause different levels of VWF expression and function[68]. Glycosylated structures are terminated with A, B, and H antigens, which may have significant effects on the level of plasma VWF and are associated with different rates of protein clearance in ABO individuals[69]. Alterations in glycosylation pattern or absence of a glycoside affect protein multimerization, platelet adhesion, ADAMTS-13 proteolysis as well as biosynthesis and secretion of VWF.

Covalently linked ABO blood group determinants are expressed as terminal residues on both N- and O-linked glycans on human VWF. Overall, ≈15% of VWF N-glycans and 1% of O-glycans were shown to carry ABO structures[37]. A major effect of ABO on plasma VWF levels was first reported by Preston and Barr in 1964. From these studies, it is clear that individuals with blood group non-O (A, B, or AB) have at least 25% higher VWF levels than individuals with blood group O[70].

ABO blood groups may alter the rate of VWF synthesis and secretion within endothelial cells. Aberrant glycosyltransferase activity results in low VWF levels, in particular, enhanced clearance of VWF[71]. For example, N-linked glycan chains at N99, N857, N2400, and N2790 influence VWF synthesis and

secretion within endothelial cells[72]. In contrast, low levels of A-antigen correspond to plasma VWF levels; if endothelial cells were stimulated with an inflammatory mediator to secrete VWF, there was a 2-fold increase in A-antigen/VWF ratio[73,74]. When comparing 36 studies investigating VWF plasma levels in different blood group donors revealed that Blood group O significantly showed less VWF antigens in their blood (**Figure 2D**, Table S2, Figure S3 and S4), which is associated with a lower risk of thrombosis and other cardiovascular complications[37].

VWF Release

VWF is stored in endothelial WPBs and can be released in response to various stimuli such as trauma, hypoxia and inflammation. For example, harmful insults or irritants activate resident immune cells and the release of inflammatory mediators, such as IL-1 and TNFα[6]. But also other secretagogues such as thrombin, histamine, epinephrine, vasopressin, and VEGF (vascular endothelial growth factor) induce WPB exocytosis by either activation of cAMP levels or elevating intracellular Ca2 levels[75]. This leads to elevation of local and circulating VWF levels and provides binding potential for platelets to facilitate the thrombotic response[76]. Exacerbated biochemical and biomechanical responses, such as inflammation and high shear stress, can lead to additional endothelial cell activation and abnormal thrombus propagation[77], following the formation of ultra-large, highly reactive VWF multimers. In smaller vessels, these ultra-large multimers may give rise to the thrombotic phenomena as seen in hemolytic uremic syndrome and thrombotic thrombocytopenic purpura where multimer degradation by ADAMTS-13 is impaired[78].

VWF in Inflammation

VWF is an important factor in the development of thrombosis, and epidemiological studies have demonstrated a relationship between elevated plasma levels and the risk for thrombosis. For example, blood group A type 3 antigen is involved in stabilization of VWF during inflammation, whereas non-O blood group individuals showed increased risk for venous thromboembolism[79], atherosclerosis, and more recently, severe COVID-19[80,81]. These associations were confirmed in a recent study of a large population with various ABO blood group phenotypes[82].

Elevated VWF levels were also demonstrated in inflammatory disorders, such as rheumatoid arthritis, vasculitis, sepsis, and diabetes[83]. Inflammatory cytokines released by macrophages activate endothelial cells to release the content of WPBs, consequently leading to elevated VWF levels in the circulation[12].

Atherosclerosis

Atherosclerotic disease develops over decades and involves many cell types from plaque initiation throughout the development of atherothrombotic events, such as acute myocardial infarction and stroke[84]. One of the earliest events in atherosclerosis is the loss of normal endothelial function,

including disruption of antiplatelet mechanisms[85]. The contribution of platelets in plaque development remains a topic of investigation and increasing evidence suggest that chronic inflammation and VWF are important key players in platelet recruitment and the development of atherosclerosis[86,87]. It has been shown that increased VWF levels mediate platelet adhesion to the endothelium before plaque formation[88]. Subsequent to adhesion, platelets become activated and further recruit platelets to adhere, thereby sustaining inflammation and endothelial activation. In numerous preclinical studies, it was demonstrated that early atherosclerotic lesions are smaller and contain fewer macrophages in VWF deficient mice, rabbits, and pigs[89–92]. However, results from clinical studies on atherosclerotic risk in patients with Von Willebrand disease are inconclusive because of limited or poor-quality data[92]. Although strong clinical evidence is lacking, VWF is probably a key player in thrombosis and atherosclerotic plaque formation since the concept of atherosclerotic risk factors, such as hypertension, elevated LDL cholesterol, diabetes, and oxidative stress, can provoke an inflammatory vascular response. This concept is supported by in vivo studies that endothelial VWF promotes atherosclerosis in apoE-deficient mice[93]. In addition, the presence of LDL enhances VWF release and the formation of VWF-mediated platelet plugs on sites of high shear stress[94]. These high shear stresses induce the activation of KLF2, which has been described to activate VWF transcription[54]. Interestingly, KLF2 counteracts NFκB-mediated inflammatory activity. However, in the presence of inflammatory cytokines, NFκB interacts with histone deacetylation of the KLF2 promoter, thereby inhibiting VWF expression[95]. However, NFκB plays a central role in inflammation and is a key transcription factor in atherogenesis. Furthermore, the SNP rs7966230, which has been also found in the VWF promotor, had a strong association with advanced atherosclerosis[96]. Although there is no direct link between these SNPs and binding of transcription factors, these findings may suggest differences in promoter regions with enhanced binding of inflammatory transcription factors.

Atherosclerosis characterizes a variety of vascular disorders including coronary and peripheral artery diseases and stroke. Neutrophils and neutrophil extracellular traps are observed in thrombi from patients with ischemic stroke[97]. Thrombi from acute ischemic stroke patients contain 20% endothelial-derived VWF that has been linked to the presence of leukocytes and extracellular DNA[98]. Like for hemolytic uremic syndrome and thrombotic thrombocytopenic purpura, ADAMTS-13 may play an attenuating role in the accumulation of leukocytes and VWF in stroke[99].

Chronic Thromboembolic Pulmonary Hypertension

Persistence of a pulmonary embolism (PE) after at least three months of effective anti-coagulation treatment is referred to as chronic thromboembolic disease[100]. When it leads to an increase in mean pulmonary artery pressure and pulmonary vascular resistance, this condition is also known as CTEPH[100]. Mechanisms of inflammation and coagulation in the pulmonary circulation have been generally understudied, as the general hypothesis has been that the blood clots seen in the lung circulation in CTEPH result from embolization of clots formed in the systemic circulation (deep vein thrombosis) [101]. However, this hypothesis is challenged by the fact 40% of patients with CTEPH have

no history of acute PE or deep vein thrombosis and that classical risk factors for acute PE, including factor V Leiden and protein C deficiency do not apply to CTEPH, which is rather associated with inflammatory risk factors[102,103].

VWF levels are consistently elevated in patients with CTEPH, although interestingly, such elevated VWF levels are not found in patients with acute PE[104]. Increased levels of VWF are consistently paralleled by increased levels of CRP (C-reactive protein) in patients with CTEPH[23]. In addition, CRP levels in patients with CTEPH were associated with the severity of hemodynamics in patients with CTEPH[105]. Interestingly, stimulation of pulmonary artery endothelial cells from patients with CTEPH with CRP enhanced VWF release by 694%, although CRP did not induce FVIII (factor VIII) or tissue factor[106]. Another study found that the NFκB pathway is enhanced in CRP-stimulated pulmonary artery endothelial cells[107], which paralleled increased IL-6 and VWF secretion. Recent work from our group demonstrated a direct link between the NFκB2 transcription factor and VWF expression in primary pulmonary artery endothelial cells[62]. Epigenetic modifications of the VWF promoter allowed more binding of the NFκB2 transcription factor, leading to increased VWF expression and enhanced platelet aggregation[108]. Besides NFκB2, YY1 (yin yang 1) and SP1 are transcription factors that participate in the hypoxia-induced upregulation of VWF in lung endothelial cells, which correlated to thrombi generation[40]. Furthermore, 77% of patients with CTEPH were found to have non-O blood groups, which may be associated with increased VWF levels[109]. Although venous thromboembolism populations are also associated with elevated VWF levels which are for non-O blood groups[110], VWF levels were higher in CTEPH relative to acute PE[104].

Different study shows that VWF protein was not different between PAH and CTEPH, but remains high in nonsurvivors while ADAMTS-13, which cleaves VWF was similar[111]. Furthermore, VWF levels remain high even after pulmonary endarterectomy treatment[112]. Taken together, these data provide evidence for a pathophysiological picture of CTEPH which involves a local thrombosis driven by low-grade inflammation, combined with reduced clot resolution.

Coronavirus Disease 2019

COVID-19 is caused by infection with SARS-COV-2 and is also characterized by inflammation and pulmonary complications. The clinical spectrum of COVID-19 ranges from asymptomatic to severe disease requiring hospitalization, with up to 20% of admitted patients in need of respiratory support[113]. These patients experience hypoxemia and dyspnea that may develop into acute respiratory distress syndrome and even death[113]. This stage of the disease is characterized by high levels of proinflammatory cytokines such as IL-6, TNFα, and IL-1β, also known as a cytokine storm[114]. Analysis of bronchoalveolar fluid from patients with mild and severe COVID-19 showed that these levels are significantly higher in critically ill patients, and it has been suggested that macrophages induce excessive inflammation in severe COVID-19 pneumonia[115]. Lung macrophages from patients with severe COVID-19 are activated by specific glycosylation of anti-spike IgG, inducing release of IL-6

and TNFα. Consequently, endothelial barrier function was disrupted, leading to excessive platelet adhesion to the pulmonary endothelium, which is driven by increased endothelial VWF secretion[116].

VWF plasma levels have been shown to be markedly increased in COVID-19, which reflects an excessive inflammatory response as a consequence of ULVWF (ultra-large Von Willebrand factor) release from vascular endothelial cells from the cytokine storm. However, elevated VWF levels in patients with COVID-19 often lack ULVWF monomers that are mainly involved in platelet aggregation[117]. In the severely ill patients that are admitted to the intensive care unit, although have shown to have additional markers of vascular endothelial cell damage, such as increased P-selectin along with the so-called cytokine storm.

The occurrence of COVID-19 coagulopathy is strongly associated with elevated VWF levels and may be a predictor of severe disease. Elevated VWF levels are associated with the need for mechanical ventilation[118], and nonhypoxic patients have relatively lower VWF levels[119]. A large meta-analysis comparing VWF plasma levels in patients with COVID-19 has confirmed higher levels in intensive care unit patients compared to other patients with COVID-19[120]. These elevated levels were normalized in mild patients six months after hospital discharge, while survivors with long respiratory recovery still had increased VWF levels and thromboembolic complications[121,122]. Interestingly, a meta-analysis on the nature of these thromboembolisms, revealed that there was no difference in prevalence of deep vein thrombosis although the events of PE are higher in intensive care unit patients with COVID-19[123]. This suggests that at least some of the thrombus encountered in the lungs of patients with COVID-19 is not there because of thromboembolic events, but was formed locally (in situ thrombosis).

There is currently no data to suggest that SNPs or altered transcriptional regulation of VWF are involved in COVID-19. Other risk factors as blood groups have been shown to be involved in infection as non-O blood groups are more likely to be infected with COVID-19 than O blood groups, but it does not associate with disease severity[124]. Mechanistic studies on the regulation of VWF in COVID-19 are lacking. Only one study showed that increased plasma VWF levels were correlated with a decreased sialic acid status of VWF, which makes VWF less susceptible to cleavage[125]. In addition, there is evidence that SARS-COV-2 spike protein induces inflammation via activation of the NFκB pathway that may induce VWF transcription after infection and cause in situ thrombosis as described in this review[126]. Although most COVID-19 literature refers to pulmonary emboli in patients with COVID-19, current pathophysiological insights favor local dysregulated thrombosis rather than migration of emboli from distal veins as cause of the perfusion defects.

Implications for Treatment

VWF production and secretion may represent potential targets for therapy in cardiovascular disease, especially in inflammation-induced thrombosis. Current clinical therapies for preventing thrombosis include antiplatelet therapy such as thromboxane inhibitors or ADP antagonists, or anti-coagulation

therapy with Vitamin K antagonists or direct oral anticoagulants. Antiplatelet therapy with aspirin or clopidogrel have shown to exert both antithrombotic and anti-inflammatory effects by reduced plasma VWF and CRP levels[127,128], suggesting an antithrombotic effect by decreased VWF release from endothelial cells. However, these therapies target platelet function and the coagulation pathway which are associated with the occurrence of serious bleeding events. Alternatively, inflammatory and specific VWF-targeted inhibitors may be suitable to target inflammatory-mediated thrombosis.

Various specific and nonspecific VWF pharmacotherapies have been tested in different inflammatory conditions to limit thrombotic complications. Caplacizumab is an immunoglobin that recognizes the VWF A1 domain and inhibits interaction between VWF and platelet GPIb-IX-V (glycoprotein Ib-IX-V) under high shear conditions[129,130]. However, it has been shown in a phase 2 clinical trial that caplacizumab was associated with an increased tendency towards bleeding[129]. Furthermore, ARC1779 aptamer, another VWF A1 antagonist that is a single-stranded DNA oligonucleotide with a specific 3-dimensional shape, recognizes VWF with high affinity and specificity. Results of a phase 1 study using this aptamer showed proof of shear-dependent inhibition of VWF-platelet interaction[131], followed by 2 phase 2 clinical studies that show reduction in embolic risk[132,133]. Other anti-VWF targets have also been tested in animal models, such as N-acetycysteine, that disrupts the disulfide bounds at the A1 domain of VWF reducing the thrombotic potential[134]. Another strategy is blocking VWF function via the D'D3 domain of VWF, without interfering with its hemostatic function on the A1 domain[135]. However, the use of drugs that directly target VWF is associated with increased risk of bleeding similar to that observed in patients with von Willebrand Disease[136]. To overcome this, treatment with recombinant ADAMTS-13 could be a potential strategy to cleave ultra-large VWF and maintain VWF hemostasis, a strategy that was proven to successfully reduce cerebral infarct size in mice[137].

Besides direct interference with VWF and its related molecules, targeting inflammatory pathways would serve as an alternative to reduce the risk for inflammatory-induced thrombosis. For example, it has been shown that anti-inflammatory therapy such as statins and nonsteroidal anti-inflammatory drugs block the release of VWF and significantly decreased plasma VWF levels[138,139]. However, because emerging evidence show that inflammatory pathways drive thrombosis via the VWF promotor, it would be favorable to target promoter activity in inflammatory thrombosis. Although the GATA promoter region is constitutively active, the NFκB and KLF2 binding, for example, is regulated active in response to specific stimuli. This enables normal hemostasis and targets inflammatory-induced VWF transcription. Alternatively, interfering with epigenetics and accessibility of the promoter region can serve as an alternative to target immunothrombosis. Unselective VWF antagonist that are targeting VWF activation by, for example, inflammation may play beneficial roles in both inflammatory and thrombotic disorders because specific VWF antagonist might cause severe bleeding events and needs extensive testing in preclinical and clinical research.

Conclusions

In summary, inflammation may regulate VWF-mediated platelet adhesion and consequently thrombosis in the systemic and pulmonary circulation. Endothelial VWF expression is regulated on a transcriptional and a translational level, and this regulation is under control by inflammatory mechanisms as described in inflammatory-mediated thromboembolic diseases as atherosclerosis, CTEPH, and COVID-19, as summarized in **Figure 3**. Promoter activity and blood group are important mediators of VWF expression. Elucidation of the mechanism of inflammation-mediated thrombosis may identify new treatment options, targeting thrombosis without impeding hemostasis.

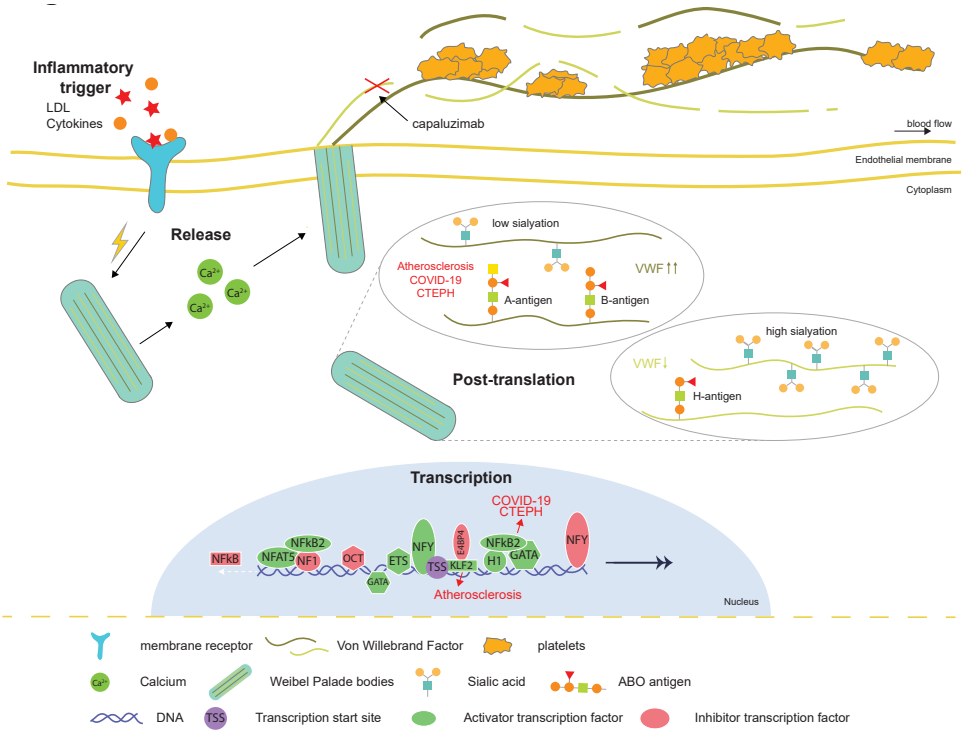

Figure 3. Schematic overview of VWF (von Willebrand factor) regulation on different levels and how these are affected by inflammation and cardiovascular diseases. CTEPH indicates chronic thromboembolic pulmonary hypertension; E4BP4, a basic leucine zipper transcription factor; GATA, GATA transcription factor; KLF2, Krüppel-like factor 2; LDL, low-density lipoprotein; NF1, nuclear factor 1; NFAT5, nuclear factor of activated T-cells 5; NFκB, nuclear factor kappa B; NFY, nuclear transcription factor Y; Oct1, octamer transcription factor 1; and TSS, transcription start site.

References

1. Kanthi YM, Sutton NR, Pinsky DJ. CD39: Interface between vascular thrombosis and inflammation. Curr Atheroscler Rep. 2014;16:425. doi: 10.1007/s11883-014-0425-1
2. Brill A, Fuchs TA, Chauhan AK, Yang JJ, De Meyer SF, Kollnberger M, Wakefield TW, Lammle B, Massberg S, Wagner DD. von Willebrand factormediated platelet adhesion is critical for deep vein thrombosis in mouse models. Blood. 2011;117:1400–1407. doi: 10.1182/blood-2010-05-287623
3. Lowenberg EC, Meijers JC, Levi M. Platelet-vessel wall interaction in health and disease. Neth J Med. 2010;68:242–251.
4. Smith SA, Travers RJ, Morrissey JH. How it all starts: Initiation of the clotting cascade. Crit Rev Biochem Mol Biol. 2015;50:326–336. doi: 10.3109/10409238.2015.1050550
5. Leebeek FW, Eikenboom JC. Von Willebrand's Disease. N Engl J Med. 2016;375:2067–2080. doi: 10.1056/NEJMra1601561
6. Chen J, Chung DW. Inflammation, von Willebrand factor, and ADAMTS13. Blood. 2018;132:141–147. doi: 10.1182/blood-2018-02-769000
7. Bernardo A, Ball C, Nolasco L, Moake JF, Dong JF. Effects of inflammatory cytokines on the release and cleavage of the endothelial cell-derived ultralarge von Willebrand factor multimers under flow. Blood. 2004;104:100–106. doi: 10.1182/blood-2004-01-0107
8. Engelmann B, Massberg S. Thrombosis as an intravascular effector of innate immunity. Nat Rev Immunol. 2013;13:34–45. doi: 10.1038/nri3345
9. Loof TG, Morgelin M, Johansson L, Oehmcke S, Olin AI, Dickneite G, Norrby-Teglund A, Theopold U, Herwald H. Coagulation, an ancestral serine protease cascade, exerts a novel function in early immune defense. Blood. 2011;118:2589–2598. doi: 10.1182/blood-2011-02-337568
10. Manz XD, Szulcek R, Pan X, Symersky P, Dickhoff C, Majolée J, Kremer V, Michielon E, Jordanova ES, Radonic T. et al. Epigenetic modification of the von willebrand factor promoter drives platelet aggregation on the pulmonary endothelium in chronic thromboembolic pulmonary hypertension. Am J Respir Crit Care Med. 2022;205:806–818. doi: 10.1164/rccm.202109-2075OC
11. Jackson SP, Darbousset R, Schoenwaelder SM. Thromboinflammation: challenges of therapeutically targeting coagulation and other host defense mechanisms. Blood. 2019;133:906–918. doi: 10.1182/blood2018-11-882993
12. Mussbacher M, Salzmann M, Brostjan C, Hoesel B, Schoergenhofer C, Datler H, Hohensinner P, Basilio J, Petzelbauer P, Assinger A. et al. Cell type-specific roles of nf-kappab linking inflammation and thrombosis. Front Immunol. 2019;10:85. doi: 10.3389/fimmu.2019.00085
13. Osterud B. Tissue factor expression by monocytes: regulation and pathophysiological roles. Blood Coagul Fibrinolysis. 1998;9:S9–14.
14. Bochenek ML, Schafer K. Role of Endothelial Cells in Acute and Chronic Thrombosis. Hamostaseologie. 2019;39:128–139. doi: 10.1055/s-0038-1675614
15. Conway EM. Thrombomodulin and its role in inflammation. Semin Immunopathol. 2012;34:107–125. doi: 10.1007/s00281-011-0282-8
16. Oeckinghaus A, Ghosh S. The NF-kappaB family of transcription factors and its regulation. Cold Spring Harb Perspect Biol. 2009;1:a000034. doi: 10.1101/cshperspect.a000034
17. Iba T, Levy JH, Connors JM, Warkentin TE, Thachil J, Levi M. The unique characteristics of COVID-19 coagulopathy. Crit Care. 2020;24:360. doi: 10.1186/s13054-020-03077-0
18. Petri B, Broermann A, Li H, Khandoga AG, Zarbock A, Krombach F, Goerge T, Schneider SW, Jones C, Nieswandt B. et al. von Willebrand factor promotes leukocyte extravasation. Blood. 2010;116:4712–4719. doi: 10.1182/blood-2010-03-276311
19. Setiadi H, Yago T, Liu Z, McEver RP. Endothelial signaling by neutrophilreleased oncostatin M enhances P-selectin-dependent inflammation and thrombosis. Blood Adv. 2019;3:168–183. doi: 10.1182/bloodadvances.2018026294
20. Tailor A, Cooper D, Granger DN. Platelet-vessel wall interactions in the microcirculation. Microcirculation. 2005;12:275–285. doi: 10.1080/10739680590925691
21. Angus DC, van der Poll T. Severe sepsis and septic shock. N Engl J Med. 2013;369:840–851. doi: 10.1056/NEJMra1208623
22. Bonaventura A, Vecchie A, Dagna L, Martinod K, Dixon DL, Van Tassell BW, Dentali F, Montecucco F, Massberg S, Levi M. et al. Endothelial dysfunction and immunothrombosis as key pathogenic mechanisms in COVID-19. Nat Rev Immunol. 2021;21:319–329. doi: 10.1038/s41577-021-00536-9

23. Skoro-Sajer N, Gerges C, Gerges M, Panzenbock A, Jakowitsch J, Kurz A, Taghavi S, Sadushi-Kolici R, Campean I, Klepetko W. et al. Usefulness of thrombosis and inflammation biomarkers in chronic thromboembolic pulmonary hypertension-sampling plasma and surgical specimens. J Heart Lung Transplant. 2018;37:1067–1074. doi: 10.1016/j.healun.2018.04.003
24. Lopes da Silva M, Cutler DF. von Willebrand factor multimerization and the polarity of secretory pathways in endothelial cells. Blood. 2016;128:277–285. doi: 10.1182/blood-2015-10-677054
25. Shahidi M. Thrombosis and von Willebrand Factor. Adv Exp Med Biol. 2017;906:285–306. doi: 10.1007/5584_2016_122
26. Sporn LA, Marder VJ, Wagner DD. Inducible secretion of large, biologically potent von Willebrand factor multimers. Cell. 1986;46:185–190. doi: 10.1016/0092-8674(86)90735-x
27. Giblin JP, Hewlett LJ, Hannah MJ. Basal secretion of von Willebrand factor from human endothelial cells. Blood. 2008;112:957–964. doi: 10.1182/blood-2007-12-130740
28. Lenting PJ, Christophe OD, Denis CV. von Willebrand factor biosynthesis, secretion, and clearance: connecting the far ends. Blood. 2015;125:2019–2028. doi: 10.1182/blood-2014-06-528406
29. Denis CV. Molecular and cellular biology of von Willebrand factor. Int J Hematol. 2002;75:3–8. doi: 10.1007/BF02981972
30. Zeng J, Shu Z, Liang Q, Zhang J, Wu W, Wang X, Zhou A. Structural basis of von willebrand factor multimerization and tubular storage. Blood. 2022;139:3314–3324. doi: 10.1182/blood.2021014729
31. Zhou YF, Eng ET, Zhu J, Lu C, Walz T, Springer TA. Sequence and structure relationships within von Willebrand factor. Blood. 2012;120:449–458. doi: 10.1182/blood-2012-01-405134
32. Huang J, Roth R, Heuser JE, Sadler JE. Integrin alpha(v)beta(3) on human endothelial cells binds von Willebrand factor strings under fluid shear stress. Blood. 2009;113:1589–1597. doi: 10.1182/blood-2008-05-158584
33. Bittar LF, de Paula EV, Mello TB, Siqueira LH, Orsi FL, Annichino-Bizzacchi JM. Polymorphisms and mutations in vWF and ADAMTS13 genes and their correlation with plasma levels of FVIII and vWF in patients with deep venous thrombosis. Clin Appl Thromb Hemost. 2011;17:514–518. doi: 10.1177/1076029610375815
34. Swystun LL, Lillicrap D. Genetic regulation of plasma von Willebrand factor levels in health and disease. J Thromb Haemost. 2018;16:2375–2390. doi: 10.1111/jth.14304
35. van Loon J, Dehghan A, Weihong T, Trompet S, McArdle WL, Asselbergs FW, Chen M-H, Lopez LM, Huffman JE, Leebeek FWG. et al. Genome-wide association studies identify genetic loci for low von Willebrand factor levels. Eur J Hum Genet. 2016;24:1035–1040. doi: 10.1038/ejhg.2015.222
36. Bladbjerg EM, de Maat MP, Christensen K, Bathum L, Jespersen J, Hjelmborg J. Genetic influence on thrombotic risk markers in the elderly—a Danish twin study. J Thromb Haemost. 2006;4:599–607. doi: 10.1111/j.1538-7836.2005.01778.x
37. Ward SE, O'Sullivan JM, O'Donnell JS. The relationship between ABO blood group, von Willebrand factor, and primary hemostasis. Blood. 2020;136:2864–2874. doi: 10.1182/blood.2020005843
38. Guan J, Guillot PV, Aird WC. Characterization of the mouse von Willebrand factor promoter. Blood. 1999;94:3405–3412.
39. Bahnak BR, Wu QY, Coulombel L, Assouline Z, Kerbiriou-Nabias D, Pietu G, Drouet L, Caen JP, Meyer D. Expression of von Willebrand factor in porcine vessels: heterogeneity at the level of von Willebrand factor mRNA. J Cell Physiol. 1989;138:305–310. doi: 10.1002/jcp.1041380212
40. Mojiri A, Alavi P, Lorenzana Carrillo MA, Nakhaei-Nejad M, Sergi CM, Thebaud B, Aird WC, Jahroudi N. Endothelial cells of different organs exhibit heterogeneity in von Willebrand factor expression in response to hypoxia. Atherosclerosis. 2019;282:1–10. doi: 10.1016/j.atherosclerosis.2019.01.002
41. Liu J, Yuan L, Molema G, Regan E, Janes L, Beeler D, Spokes KC, Okada Y, Minami T, Oettgen P. et al. Vascular bed-specific regulation of the von Willebrand factor promoter in the heart and skeletal muscle. Blood. 2011;117:342–351. doi: 10.1182/blood-2010-06-287987
42. Jahroudi N, Lynch DC. Endothelial-cell-specific regulation of von Willebrand factor gene expression. Mol Cell Biol. 1994;14:999–1008. doi: 10.1128/mcb.14.2.999-1008.1994
43. Liu J, Kanki Y, Okada Y, Jin E, Yano K, Shih SC, Minami T, Aird WC. A +220 GATA motif mediates basal but not endotoxin-repressible expression of the von Willebrand factor promoter in Hprt-targeted transgenic mice. J Thromb Haemost. 2009;7:1384–1392. doi: 10.1111/j.1538-7836.2009.03501.x
44. Peng Y, Jahroudi N. The NFY transcription factor inhibits von Willebrand factor promoter activation in non-endothelial cells through recruitment of histone deacetylases. J Biol Chem. 2003;278:8385–8394. doi: 10.1074/jbc.M213156200
45. Wang X, Peng Y, Ma Y, Jahroudi N. Histone H1-like protein participates in endothelial cell-specific activation of the von Willebrand factor promoter. Blood. 2004;104:1725–1732. doi: 10.1182/blood-2004-01-0082

46. Nassiri M, Liu J, Kulak S, Uwiera RR, Aird WC, Ballermann BJ, Jahroudi N. Repressors NFI and NFY participate in organ-specific regulation of von Willebrand factor promoter activity in transgenic mice. Arterioscler Thromb Vasc Biol. 2010;30:1423–1429. doi: 10.1161/ATVBAHA.110.206680
47. Dmitrieva NI, Burg MB. Secretion of von Willebrand factor by endothelial cells links sodium to hypercoagulability and thrombosis. Proc Natl Acad Sci USA. 2014;111:6485–6490. doi: 10.1073/pnas.1404809111
48. Othman M, Chirinian Y, Brown C, Notley C, Hickson N, Hampshire D, Buckley S, Waddington S, Parker AL, Baker A. et al. Functional characterization of a 13-bp deletion (c.-1522_-1510del13) in the promoter of the von Willebrand factor gene in type 1 von Willebrand disease. Blood. 2010;116:3645–3652. doi: 10.1182/blood-2009-12-261131
49. Schwachtgen JL, Janel N, Barek L, Duterque-Coquillaud M, Ghysdael J, Meyer D, Kerbiriou-Nabias D. Ets transcription factors bind and transactivate the core promoter of the von Willebrand factor gene. Oncogene. 1997;15:3091–3102. doi: 10.1038/sj.onc.1201502
50. Peng Y, Jahroudi N. The NFY transcription factor functions as a repressor and activator of the von Willebrand factor promoter. Blood. 2002;99:2408–2417. doi: 10.1182/blood.v99.7.2408
51. Dong F, Zhao X, Wang J, Huang X, Li X, Zhang L, Dong H, Liu F, Fan M. Dihydroartemisinin inhibits the expression of von Willebrand factor by downregulation of transcription factor ERG in endothelial cells. Fundam Clin Pharmacol. 2021;35:321–330. doi: 10.1111/fcp.12622
52. Bertagna A, Jahroudi N. The NFY transcription factor mediates induction of the von Willebrand factor promoter by irradiation. Thromb Haemost. 2001;85:837–844.
53. Mojiri A, Nakhaii-Nejad M, Phan WL, Kulak S, Radziwon-Balicka A, Jurasz P, Michelakis E, Jahroudi N. Hypoxia results in upregulation and de novo activation of von Willebrand factor expression in lung endothelial cells. Arterioscler Thromb Vasc Biol. 2013;33:1329–1338. doi: 10.1161/ATVBAHA.113.301359
54. Chu HR, Sun YC, Gao Y, Guan XM, Yan H, Cui XD, Zhang XY, Li X, Li H, Cheng M. Function of Kruppellike factor 2 in the shear stressinduced cell differentiation of endothelial progenitor cells to endothelial cells. Mol Med Rep. 2019;19:1739–1746. doi: 10.3892/mmr.2019.9819
55. Singh B, Biswas I, Bhagat S, Surya Kumari S, Khan GA. HMGB1 facilitates hypoxia-induced vWF upregulation through TLR2-MYD88-SP1 pathway. Eur J Immunol. 2016;46:2388–2400. doi: 10.1002/eji.201646386
56. Jahroudi N, Ardekani AM, Greenberger JS. An NF1-like protein functions as a repressor of the von Willebrand factor promoter. J Biol Chem. 1996;271:21413–21421. doi: 10.1074/jbc.271.35.21413
57. Schwachtgen JL, Remacle JE, Janel N, Brys R, Huylebroeck D, Meyer D, Kerbiriou-Nabias D. Oct-1 is involved in the transcriptional repression of the von willebrand factor gene promoter. Blood. 1998;92:1247–1258.
58. Hough C, Cuthbert CD, Notley C, Brown C, Hegadorn C, Berber E, Lillicrap D. Cell type-specific regulation of von Willebrand factor expression by the E4BP4 transcriptional repressor. Blood. 2005;105:1531–1539. doi: 10.1182/blood-2002-10-3093
59. Wang X, Dong F, Wang F, Yan S, Chen X, Tozawa H, Ushijima T, Kapron CM, Wada Y, Liu J. Low dose cadmium upregulates the expression of von Willebrand factor in endothelial cells. Toxicol Lett. 2018;290:46–54. doi: 10.1016/j.toxlet.2018.03.020
60. Aird WC, Edelberg JM, Weiler-Guettler H, Simmons WW, Smith TW, Rosenberg RD. Vascular bed-specific expression of an endothelial cell gene is programmed by the tissue microenvironment. J Cell Biol. 1997;138:1117–1124. doi: 10.1083/jcb.138.5.1117
61. Yuan L, Nikolova-Krstevski V, Zhan Y, Kondo M, Bhasin M, Varghese L, Yano K, Carman CV, Aird WC, Oettgen P. Antiinflammatory effects of the ETS factor ERG in endothelial cells are mediated through transcriptional repression of the interleukin-8 gene. Circ Res. 2009;104:1049–1057. doi: 10.1161/CIRCRESAHA.108.190751
62. Deleted in proof.
63. Hough C, Cameron CL, Notley CR, Brown C, O'Brien L, Keightley AM, Berber E, Lillicrap D. Influence of a GT repeat element on shear stress responsiveness of the VWF gene promoter. J Thromb Haemost. 2008;6:1183-1190. doi: 10.1111/j.1538-7836.2008.03011.x
64. Daidone V, Pontara E, Romualdi C, Cattini MG, Scaroni C, Albiger N, Pagnan A, Casonato A. Microsatellite (GT)(n) is part of the von Willebrand factor (VWF) promoter region that influences the glucocorticoid-induced increase in VWF in Cushing's syndrome. Thromb Res. 2010;125:e275–e280. doi: 10.1016/j.thromres.2010.01.031
65. Hickson N, Hampshire D, Castaman G, Eikenboom J, Rodeghiero F, Peake I, Goodeve A, McMdm VWD, Groups Z-VS. Effect of the VWF promoter (GT) n repeat and single-nucleotide polymorphism c.-2527G>A on circulating von Willebrand factor levels under normal conditions. J Thromb Haemost. 2011;9:603–605. doi: 10.1111/j.1538-7836.2010.04161.x

66. Keightley AM, Lam YM, Brady JN, Cameron CL, Lillicrap D. Variation at the von Willebrand factor (vWF) gene locus is associated with plasma vWF:Ag levels: identification of three novel single nucleotide polymorphisms in the vWF gene promoter. Blood. 1999;93:4277–4283.
67. Simon D, Palatnik M, Roisenberg I. Analysis of the -1185A/G von Willebrand factor (VWF) gene polymorphism in two Brazilian ethnic groups and its effect on the plasma VWF levels. Thromb Res. 2002;105:519–522. doi: 10.1016/s0049-3848(02)00060-9
68. Ward S, O'Sullivan JM, O'Donnell JS. The biological significance of von Willebrand factor o-linked glycosylation. Semin Thromb Hemost. 2021;47:855–861. doi: 10.1055/s-0041-1726373
69. Gashash EA, Aloor A, Li D, Zhu H, Xu XQ, Xiao C, Zhang J, Parameswaran A, Song J, Ma C. et al. An insight into glyco-microheterogeneity of plasma von Willebrand factor by mass spectrometry. J Proteome Res. 2017;16:3348–3362. doi: 10.1021/acs.jproteome.7b00359
70. Preston AE, Barr A. The plasma concentration of factor viii in the normal population. ii. the effects of age, sex and blood group. Br J Haematol. 1964;10:238–245. doi: 10.1111/j.1365-2141.1964.tb00698.x
71. Aguila S, Lavin M, Dalton N, et al. Increased galactose expression and enhanced clearance in patients with low von Willebrand factor. Blood. 2019;133:1585–1596. doi: 10.1182/blood-2018-09-874636
72. McKinnon TA, Goode EC, Birdsey GM, Nowak AA, Chan AC, Lane DA, Laffan MA. Specific N-linked glycosylation sites modulate synthesis and secretion of von Willebrand factor. Blood. 2010;116:640–648. doi: 10.1182/blood-2010-02-267450
73. Brown SA, Collins PW, Bowen DJ. Heterogeneous detection of A-antigen on von Willebrand factor derived from platelets, endothelial cells and plasma. Thromb Haemost. 2002;87:990–996.
74. O'Donnell J, Laffan MA. Dissociation of ABH antigen expression from von Willebrand factor synthesis in endothelial cell lines. Br J Haematol. 2003;121:928–931. doi: 10.1046/j.1365-2141.2003.04366.x
75. Rondaij MG, Bierings R, Kragt A, van Mourik JA, Voorberg J. Dynamics and plasticity of Weibel-Palade bodies in endothelial cells. Arterioscler Thromb Vasc Biol. 2006;26:1002–1007. doi: 10.1161/01.ATV.0000209501.56852.6c
76. Reininger AJ. The function of ultra-large von Willebrand factor multimers in high shear flow controlled by ADAMTS13. Hamostaseologie. 2015;35:225–233. doi: 10.5482/HAMO-14-12-0077
77. Rana A, Westein E, Niego B, Hagemeyer CE. Shear-dependent platelet aggregation: mechanisms and therapeutic opportunities. Front Cardiovasc Med. 2019;6:141. doi: 10.3389/fcvm.2019.00141
78. Masias C, Vasu S, Cataland SR. None of the above: thrombotic microangiopathy beyond TTP and HUS. Blood. 2017;129:2857–2863. doi: 10.1182/blood-2016-11-743104
79. Li S, Schooling CM. A phenome-wide association study of ABO blood groups. BMC Med. 2020;18:334. doi: 10.1186/s12916-020-01795-4
80. Zalba Marcos S, Antelo ML, Galbete A, Etayo M, Ongay E, Garcia-Erce JA. Infection and thrombosis associated with COVID-19: possible role of the ABO blood group. Med Clin (Engl Ed). 2020;155:340–343. doi: 10.1016/j.medcle.2020.06.013
81. Gerard C, Maggipinto G, Minon JM. COVID-19 and ABO blood group: another viewpoint. Br J Haematol. 2020;190:e93–e94. doi: 10.1111/bjh.16884
82. Groot HE, Villegas Sierra LE, Said MA, Lipsic E, Karper JC, van der Harst P. Genetically determined ABO Blood group and its associations with health and disease. Arterioscler Thromb Vasc Biol. 2020;40:830–838. doi: 10.1161/ATVBAHA.119.313658
83. Yada N, Yoshimoto K, Kawashima H, Yoneima R, Nishimura N, Tai Y, Tsushima E, Miyamoto M, Ono S, Matsumoto M. et al. Plasma level of von Willebrand factor propeptide at diagnosis: a marker of subsequent renal dysfunction in autoimmune rheumatic diseases. Clin Appl Thromb Hemost. 2020;26:1076029620938874. doi: 10.1177/1076029620938874
84. Wu MD, Atkinson TM, Lindner JR. Platelets and von Willebrand factor in atherogenesis. Blood. 2017;129:1415–1419. doi: 10.1182/blood2016-07-692673
85. Borissoff JI, Spronk HM, ten Cate H. The hemostatic system as a modulator of atherosclerosis. N Engl J Med. 2011;364:1746–1760. doi: 10.1056/NEJMra1011670
86. Theilmeier G, Michiels C, Spaepen E, Vreys I, Collen D, Vermylen J, Hoylaerts MF. Endothelial von Willebrand factor recruits platelets to atherosclerosis-prone sites in response to hypercholesterolemia. Blood. 2002;99:4486–4493. doi: 10.1182/blood.v99.12.4486
87. Massberg S, Brand K, Gruner S, Page S, Muller E, Muller I, Bergmeier W, Richter T, Lorenz M, Konrad I. et al. A critical role of platelet adhesion in the initiation of atherosclerotic lesion formation. J Exp Med. 2002;196:887-896. doi: 10.1084/jem.20012044
88. Shim CY, Liu YN, Atkinson T, Xie A, Foster T, Davidson BP, Treible M, Qi Y, Lopez JA, Munday A. et al. Molecular imaging of platelet-endothelial interactions and endothelial von willebrand factor in early and midstage atherosclerosis. Circ Cardiovasc Imaging. 2015;8:e002765. doi: 10.1161/CIRCIMAGING.114.002765

89. Fuster W, Bowie EJ, Lewis JC, Fass DN, OwenBrown CAL. Resistance to arteriosclerosis in pigs with von Willebrand's disease. Spontaneous and high cholesterol diet-induced arteriosclerosis. J Clin Invest. 1978;61:722–730. doi: 10.1172/JCI108985
90. Methia N, Andre P, Denis CV, Economopoulos M, Wagner DD. Localized reduction of atherosclerosis in von Willebrand factor-deficient mice. Blood. 2001;98:1424–1428. doi: 10.1182/blood.v98.5.1424
91. Kleinschnitz C, De Meyer SF, Schwarz T, Austinat M, Vanhoorelbeke K, Nieswandt B, Deckmyn H, Stoll G. Deficiency of von Willebrand factor protects mice from ischemic stroke. Blood. 2009;113:3600–3603. doi: 10.1182/blood-2008-09-180695
92. van Galen KP, Tuinenburg A, Smeets EM, Schutgens RE. Von Willebrand factor deficiency and atherosclerosis. Blood Rev. 2012;26:189–196. doi: 10.1016/j.blre.2012.05.002
93. Doddapattar P, Dhanesha N, Chorawala MR, Tinsman C, Jain M, Nayak MK, Staber JM, Chauhan AK. Endothelial cell-derived von willebrand factor, but not platelet-derived, promotes atherosclerosis in apolipoprotein e-deficient mice. Arterioscler Thromb Vasc Biol. 2018;38:520–528. doi: 10.1161/ATVBAHA.117.309918
94. Ozawa K, Muller MA, Varlamov O, Tavori H, Packwood W, Mueller PA, Xie A, Ruggeri Z, Chung D, Lopez JA. et al. Proteolysis of von Willebrand factor influences inflammatory endothelial activation and vascular compliance in atherosclerosis. JACC Basic Transl Sci. 2020;5:1017–1028. doi: 10.1016/j.jacbts.2020.08.009
95. SenBanerjee S, Lin Z, Atkins GB, Greif DM, Rao RM, Kumar A, Feinberg MW, Chen Z, Simon DI, Luscinskas FW. et al. KLF2 Is a novel transcriptional regulator of endothelial proinflammatory activation. J Exp Med. 2004;199:1305–1315. doi: 10.1084/jem.20031132
96. van der Meer IM, Brouwers GJ, Bulk S, Leebeek FW, van der Kuip DA, Hofman A, Witteman JC, Gomez Garcia EB. Genetic variability of von Willebrand factor and risk of coronary heart disease: the Rotterdam study. Br J Haematol. 2004;124:343–347. doi: 10.1046/j.1365-2141.2003.04776.x
97. Laridan E, Denorme F, Desender L, Francois O, Andersson T, Deckmyn H, Vanhoorelbeke K, De Meyer SF. Neutrophil extracellular traps in ischemic stroke thrombi. Ann Neurol. 2017;82:223–232. doi: 10.1002/ana.24993
98. Yang J, Wu Z, Long Q, Huang J, Hong T, Liu W, Lin J. Insights into immunothrombosis: the interplay among neutrophil extracellular trap, von Willebrand Factor, and ADAMTS13. Front Immunol. 2020;11:610696. doi: 10.3389/fimmu.2020.610696
99. Falcione S, Munsterman D, Joy T, Kamtchum-Tatuene J, Sykes G, Jickling G. Association of thrombin generation with leukocyte inflammatory profile in patients with acute ischemic stroke. Neurology. 2022;99:1356–1363. doi: 10.1212/WNL.0000000000200909
100. Delcroix M, Torbicki A, Gopalan D, et al. ERS statement on chronic thromboembolic pulmonary hypertension. Eur Respir J. 2021;57: doi: 10.1183/13993003.02828-2020
101. Wilkens H, Konstantinides S, Lang IM, et al. Chronic thromboembolic pulmonary hypertension (CTEPH): updated recommendations from the cologne consensus conference 2018. Int J Cardiol. 2018;272:69–78. doi: 10.1016/j.ijcard.2018.08.079
102. Pepke-Zaba J, Delcroix M, Lang I, et al. Chronic thromboembolic pulmonary hypertension (CTEPH): results from an international prospective registry. Circulation. 2011;124:1973–1981. doi: 10.1161/CIRCULATIONAHA.110.015008
103. Lang IM, Madani M. Update on chronic thromboembolic pulmonary hypertension. Circulation. 2014;130:508–518. doi: 10.1161/CIRCULATIONAHA.114.009309
104. Newnham M, South K, Bleda M, et al. The ADAMTS13-VWF axis is dysregulated in chronic thromboembolic pulmonary hypertension. Eur Respir J. 2019;53: doi: 10.1183/13993003.01805-2018
105. Arthur Ataam J, Amsallem M, Guihaire J, Haddad F, Lamrani L, Stephan F, Jais X, Humbert M, Mercier O, Fadel E. Preoperative C-reactive protein predicts early postoperative outcomes after pulmonary endarterectomy in patients with chronic thromboembolic pulmonary hypertension. J Thorac Cardiovasc Surg. 2021;161:1532–1542 e1535. doi: 10.1016/j.jtcvs.2019.11.133
106. Wynants M, Quarck R, Ronisz A, Alfaro-Moreno E, Van Raemdonck D, Meyns B, Delcroix M. Effects of C-reactive protein on human pulmonary vascular cells in chronic thromboembolic pulmonary hypertension. Eur Respir J. 2012;40:886–894. doi: 10.1183/09031936.00197511
107. Wynants M, Vengethasamy L, Ronisz A, Meyns B, Delcroix M, Quarck R. NF-kappaB pathway is involved in CRP-induced effects on pulmonary arterial endothelial cells in chronic thromboembolic pulmonary hypertension. Am J Physiol Lung Cell Mol Physiol. 2013;305:L934–L942. doi: 10.1152/ajplung.00034.2013
108. Remkova A, Simkova I, Valkovicova T. Platelet abnormalities in chronic thromboembolic pulmonary hypertension. Int J Clin Exp Med. 2015;8:9700–9707.

109. Bohacekova M, Kaldararova M, Valkovicova T, Remkova A, Vesely J, Simkova I. Risk factors detection in chronic thromboembolic pulmonary hypertension, a tool for risk quantification?. Bratisl Lek Listy. 2016;117:577–582. doi: 10.4149/bll_2016_112
110. Edvardsen MS, Hindberg K, Hansen ES, Morelli VM, Ueland T, Aukrust P, Braekkan SK, Evensen LH, Hansen JB. Plasma levels of von Willebrand factor and future risk of incident venous thromboembolism. Blood Adv. 2021;5:224–232. doi: 10.1182/bloodadvances.2020003135
111. Ahmed A, Ahmed S, Radegran G. Plasma ADAMTS13 and von Willebrand factor in diagnosis and prediction of prognosis in pulmonary arterial hypertension. Pulm Circ 2021;11:20458940211041500. doi: 10.1177/20458940211041500
112. Bonderman D, Turecek PL, Jakowitsch J, Weltermann A, Adlbrecht C, Schneider B, Kneussl M, Rubin LJ, Kyrle PA, Klepetko W. et al. High prevalence of elevated clotting factor VIII in chronic thromboembolic pulmonary hypertension. Thromb Haemost. 2003;90:372–376. doi: 10.1160/th03-02-0067
113. Gandhi RT, Lynch JB, Del Rio C. Mild or Moderate Covid-19. N Engl J Med. 2020;383:1757–1766. doi: 10.1056/NEJMcp2009249
114. Jud P, Gressenberger P, Muster V, Avian A, Meinitzer A, Strohmaier H, Sourij H, Raggam RB, Stradner MH, Demel U. et al. Evaluation of endothelial dysfunction and inflammatory vasculopathy after SARS-CoV-2 infection-a cross-sectional study. Front Cardiovasc Med. 2021;8:750887. doi: 10.3389/fcvm.2021.750887
115. Liao M, Liu Y, Yuan J, Wen Y, Xu G, Zhao J, Cheng L, Li J, Wang X, Wang F. et al. Single-cell landscape of bronchoalveolar immune cells in patients with COVID-19. Nat Med. 2020;26:842–844. doi: 10.1038/s41591-020-0901-9
116. Hoepel W, Chen HJ, Geyer CE, et al. High titers and low fucosylation of early human anti-SARS-CoV-2 IgG promote inflammation by alveolar macrophages. Sci Transl Med. 2021;13: doi: 10.1126/scitranslmed.abf8654
117. Fujimura Y, Holland LZ. COVID-19 microthrombosis: unusually large VWF multimers are a platform for activation of the alternative complement pathway under cytokine storm. Int J Hematol. 2022;115:457–469. doi: 10.1007/s12185-022-03324-w
118. Seth R, McKinnon TAJ, Zhang XF. Contribution of the von Willebrand factor/ADAMTS13 imbalance to COVID-19 coagulopathy. Am J Physiol Heart Circ Physiol. 2022;322:H87–H93. doi: 10.1152/ajpheart.00204.2021
119. Fan BE, Ramanathan K, Sum CLL, et al. Global haemostatic tests demonstrate the absence of parameters of hypercoagulability in non-hypoxic mild COVID-19 patients: a prospective matched study. J Thromb Thrombolysis. 2022;53:646–662. doi: 10.1007/s11239-021-02575-4
120. Rostami M, Mansouritorghabeh H, Parsa-Kondelaji M. High levels of Von Willebrand factor markers in COVID-19: a systematic review and meta-analysis. Clin Exp Med. 2022;22:347–357. doi: 10.1007/s10238-021-00769-x
121. Li H, Wu Q, Qin Z, Hou X, Zhang L, Guo J, Li Y, Yang F, Zhang Y, Wu Q. et al. Serum levels of laminin and von Willebrand factor in COVID-19 survivors 6 months after discharge. Int J Infect Dis. 2021;115:134–141. doi:10.1016/j.ijid.2021.11.032
122. Willems LH, Nagy M, Ten Cate H, Spronk HMH, Groh LA, Leentjens J, Janssen NAF, Netea MG, Thijssen DHJ, Hannink G. et al. Sustained inflammation, coagulation activation and elevated endothelin-1 levels without macrovascular dysfunction at 3 months after COVID-19. Thromb Res. 2022;209:106–114. doi: 10.1016/j.thromres.2021.11.027
123. Birocchi S, Manzoni M, Podda GM, Casazza G, Cattaneo M. High rates of pulmonary artery occlusions in COVID-19. A meta-analysis. Eur J Clin Invest. 2021;51:e13433. doi: 10.1111/eci.13433
124. Zietz M, Zucker J, Tatonetti NP. Associations between blood type and COVID-19 infection, intubation, and death. Nat Commun. 2020;11:5761. doi: 10.1038/s41467-020-19623-x
125. Mobayen G, Dhutia A, Clarke C, Prendecki M, McAdoo S, Keniyopoullos R, Malik T, Laffan M, Willicombe M, McKinnon T. Severe COVID-19 is associated with endothelial activation and abnormal glycosylation of von Willebrand factor in patients undergoing hemodialysis. Res Pract Thromb Haemost. 2021;5:e12582. doi: 10.1002/rth2.12582
126. Khan S, Shafiei MS, Longoria C, Schoggins JW, Savani RC, Zaki H. SARSCoV-2 spike protein induces inflammation via TLR2-dependent activation of the NF-kappaB pathway. Elife. 2021;10: doi: 10.7554/eLife.68563
127. Homoncik M, Jilma B, Eichelberger B, Panzer S. Inhibitory activity of aspirin on von Willebrand factor-induced platelet aggregation. Thromb Res. 2000;99:461–466. doi: 10.1016/s0049-3848(00)00297-8
128. Zhao L, Gray L, Leonardi-Bee J, Weaver CS, Heptinstall S, Bath PM. Effect of aspirin, clopidogrel and dipyridamole on soluble markers of vascular function in normal volunteers and patients with prior ischaemic stroke. Platelets. 2006;17:100–104. doi: 10.1080/09537100500235966

129. Peyvandi F, Scully M, Kremer Hovinga JA, et al. Caplacizumab for acquired thrombotic thrombocytopenic purpura. N Engl J Med. 2016;374:511–522. doi: 10.1056/NEJMoa1505533
130. Veyradier A. Von Willebrand factor--a new target for TTP treatment?. N Engl J Med. 2016;374:583–585. doi: 10.1056/NEJMe1515876
131. Gilbert JC, DeFeo-Fraulini T, Hutabarat RM, Horvath CJ, Merlino PG, Marsh HN, Healy JM, Boufakhreddine S, Holohan TV, Schaub RG. Firstin-human evaluation of anti von Willebrand factor therapeutic aptamer ARC1779 in healthy volunteers. Circulation. 2007;116:2678–2686. doi: 10.1161/CIRCULATIONAHA.107.724864
132. Cataland SR, Peyvandi F, Mannucci PM, Lammle B, Kremer Hovinga JA, Machin SJ, Scully M, Rock G, Gilbert JC, Yang S. et al. Initial experience from a double-blind, placebo-controlled, clinical outcome study of ARC1779 in patients with thrombotic thrombocytopenic purpura. Am J Hematol. 2012;87:430–432. doi: 10.1002/ajh.23106
133. Markus HS, McCollum C, Imray C, Goulder MA, Gilbert J, King A. The von Willebrand inhibitor ARC1779 reduces cerebral embolization after carotid endarterectomy: a randomized trial. Stroke. 2011;42:2149–2153. doi: 10.1161/STROKEAHA.111.616649
134. Chen J, Reheman A, Gushiken FC, Nolasco L, Fu X, Moake JL, Ni H, Lopez JA. N-acetylcysteine reduces the size and activity of von Willebrand factor in human plasma and mice. J Clin Invest. 2011;121:593–603. doi: 10.1172/JCI41062
135. Hillgruber C, Steingraber AK, Poppelmann B, Denis CV, Ware J, Vestweber D, Nieswandt B, Schneider SW, Goerge T. Blocking von Willebrand factor for treatment of cutaneous inflammation. J Invest Dermatol. 2014;134:77–86. doi: 10.1038/jid.2013.292
136. Scully M, Cataland SR, Peyvandi F, Coppo P, Knobl P, Kremer Hovinga JA, Metjian A, de la Rubia J, Pavenski K, Callewaert F. et al. Caplacizumab Treatment for Acquired Thrombotic Thrombocytopenic Purpura. N Engl J Med. 2019;380:335–346. doi: 10.1056/NEJMoa1806311
137. Fan M, Xu H, Wang L, Luo H, Zhu X, Cai P, Wei L, Lu L, Cao Y, Ye R. et al. Tissue Plasminogen activator neurotoxicity is neutralized by recombinant ADAMTS 13. Sci Rep. 2016;6:25971. doi: 10.1038/srep25971
138. Sahebkar A, Serban C, Ursoniu S, et al. The impact of statin therapy on plasma levels of von Willebrand factor antigen. Systematic review and meta-analysis of randomised placebo-controlled trials. Thromb Haemost. 2016;115:520–532. doi: 10.1160/TH15-08-0620
139. de Kruif MD, Lemaire LC, Giebelen IA, van Zoelen MA, Pater JM, van den Pangaart PS, Groot AP, de Vos AF, Elliott PJ, Meijers JC. et al. Prednisolone dose-dependently influences inflammation and coagulation during human endotoxemia. J Immunol. 2007;178:1845–1851. doi: 10.4049/jimmunol.178.3.1845

Supplementary materials

Inclusion of publications

PubMed was used to search for relevant literature up to December 2021 and selected as provided in Supplementary Figure 1.

To investigate polymorphisms in the VWF promoter, the following search term was used: ("von willebrand factor"[MeSH Terms] OR ("von"[All Fields] AND "willebrand"[All Fields] AND "factor"[All Fields]) OR "von willebrand factor"[All Fields]) AND ("polymorphic"[All Fields] OR "polymorphics"[All Fields] OR "polymorphism s"[All Fields] OR "polymorphism, genetic"[MeSH Terms] OR ("polymorphism"[All Fields] AND "genetic"[All Fields]) OR "genetic polymorphism"[All Fields] OR "polymorphism"[All Fields] OR "polymorphisms"[All Fields]) AND ("promoter"[All Fields] OR "promoter s"[All Fields] OR "promoters"[All Fields]). This resulted in 41 publications, of which two of them included a review article. After screening the remaining 39 articles, only four papers included VWF levels associated with SNPs in the promoter region as listed in Supplementary Table 1.

To investigate the association of blood groups and VWF antigen levels, the following search term was used: ("abo blood-group system"[MeSH Terms] OR ("abo"[All Fields] AND "blood-group"[All Fields] AND "system"[All Fields]) OR "abo blood-group system"[All Fields] OR ("abo"[All Fields] AND "blood"[All Fields] AND "group"[All Fields]) OR "abo blood group"[All Fields]) AND ("von willebrand factor"[MeSH Terms] OR ("von"[All Fields] AND "willebrand"[All Fields] AND "factor"[All Fields]) OR "von willebrand factor"[All Fields]). This resulted in 307 references, of which 43 of them were review articles. After screening the remaining 264 articles on title and abstract for eligibility on VWF data extraction, 39 publications were included for analysis. 5 publications did not include numerical values which resulted in 34 publications that were used for data extraction as shown in Supplementary Table 2.

Statistical analysis

Data in **Figure 2** are presented as mean ± standard deviation (SD), where mean and SD from the included publications were corrected for the number of patients in each study and calculated with the following equations:

Equation 1: $$mean = \frac{(mean_{\,1} \times n_1)+(mean_{\,2} \times n_2)+\cdots+(mean_{\,k} \times n_k)}{(n_1+n_2+\cdots+n_k)}$$

$mean_k$ = VWF concentration in publication k

n_k = number of patients included in publication k

k = total amount of publications

Equation 2: $$SD_{mean} = \sqrt{\frac{(SD_1{}^2)(n_1-1)+(SD_2{}^2)(n_2-1)+-\cdots+(SD_k{}^2)(n_k-1)}{(n_1+n_2+\ldots+n_k)-k}}$$

SD_k = standard deviation from a single publcation

n_k = number of patients included in publication k

k = total amount of publications

Meta-analysis was performed in R studio version 4.0.3. using meta package. A randomized model for continuous data was adopted, due to possible risk of bias. Based on population size, mean and SD, the standardized mean difference and with 95% confidence interval were calculated. I^2 and Tau^2 statistics were performed to assess heterogeneity among studies. If $p<0.05$, data was considered as significant.

Data availability

The authors declare that all supporting data are available within the article and its online supplementary files.

Supplementary Data

Supplementary Table 1. The effect of single nucleotide polymorphisms in the VWF promoter region on VWF plasma levels (U/mL)

SNP / Publication	Haplotype 1/1		Haplotype 1/2		Haplotype 2/2	
	mean ± SD	n	mean ± SD	n	mean ± SD	n
Keightley et al.[1]	0.96 ± 0.44	33	0.86 ± 0.35	111	0.78 ± 0.41	106
Simon et al.[2]	1.13 ± 0.57	112	1.04 ± 0.44	209	1.00 ± 0.42	99
Bladbjerg et al.[3]	1.99 ± 0.45	68	1.96 ± 0.47	240	2.05 ± 0.54	258
Hickson et al.[4]	0.97 ± 0.44	162	0.98 ± 0.43	521	0.96 ± 0.47	432

SNP = single nucleotide polymorphism | VWF = Von Willebrand Factor

Supplementary Table 2. Relationship between ABO blood type and Von Willebrand Factor plasma levels (U/mL)

	Blood type O			Blood type A			Blood type B			Blood type AB		
Publication	mean	SD	n	mean	SD	n	mean	SD	n	mean	SD	n
Ambika et al. 2021[5]	0.49	0.12	141	0.88	0.21	71	0.89	0.15	172	0.92	0.12	10
Ogiwara et al. 2021[6]	0.80	0.22	18	1.03	0.36	18						
Moller et al. 2020[7]	0.74	0.28	429	0.94	0.34	528						
Archer et al. 2020[8]	0.86	0.42	82	1.18	0.54	41						
Alzahrani et al. 2020[9]	0.95	0.30	54	1.21	0.26	44						
Biguzzi et al. 2021[10]	0.91	0.14	1321	1.24	0.19	1502						
Rejto et al. 2020[11]	0.86	0.43	32	1.26	0.62	50						
Valdares et al. 2020[12]	0.89	0.15	176	0.96	0.15	254						
Alharbi et al. 2018[13]	0.85	0.28	36	0.97	0.27	23	1.11	0.26	17	1.25	0.27	5
Liu et al. 2017[14]	0.87	0.18	34	1.12	0.22	64						
Marianor et al. 2015[15]	0.95	0.36	13	1.48	0.53	17						
Song et al. 2015[16]	0.95	0.38	5005	1.32	0.52	3479	1.38	0.55	1791	1.38	0.57	1398
Kepa et al. 2015[17]	0.91	0.38	21	1.23	0.51	21						
Yuan et al. 2013[18]	0.81	0.26	28	1.08	0.30	33	1.13	0.29	43	1.21	0.24	10
Rios et al. 2012[19]	0.76	0.22	37	0.94	0.26	43						
Davies et al. 2012[20]	0.94	0.29	2330	1.23	0.37	2089	1.30	0.37	452	1.37	0.43	181
Akin et al. 2012[21]	0.87	0.20	100	0.99	0.25	100						
Ay et al. 2010[22]	1.06	0.25	13	1.33	0.40	16	1.21		8	1.08		4
Davies et al. 2009[23]	0.95	0.29	2307	1.24	0.37	2072	1.31	0.37	444	1.37	0.43	179
Yabe et al. 2008[24]	0.90	0.26	86	0.83	0.29	11	1.24	0.16		1.09	0.27	22
Davies et al. 2008[25]	0.97	0.24	50	1.26	0.30	50						
Davies et al. 2007[26]	0.94	0.29	2330	1.23	0.37	2089	1.30	0.37	52	1.37	0.43	181
Garcia et al. 2006[27]	1.31	0.05	128	1.68	0.04	192	1.75	0.08	33	1.77	0.22	10
Chng et al. 2005[28]	0.69	0.19	52	1.01	0.36	54						
Castaman et al. 2002[29]	0.75	0.31	10	1.05	0.24	7						
Simon et al. 2002[2]	0.92	0.41	210	1.29	0.61	210						
He et al. 2001[30]	0.99	0.24	15	1.31	0.40	10	1.28	0.00	1	1.29	0.00	4
Huraux et al. 2001[31]	1.21	0.61	18	1.89	0.70	22						
Moeller et al. 2001[32]	0.76	0.24	60	0.95	0.33	63						
Souto et al. 2000[33]	0.77	0.27	131	1.14	0.41	151	1.03	0.30	30	1.37	0.34	10
Philips et al. 1998[34]	0.75	0.35	456	1.06	0.47	340	1.17	0.46	196	1.23	0.44	109

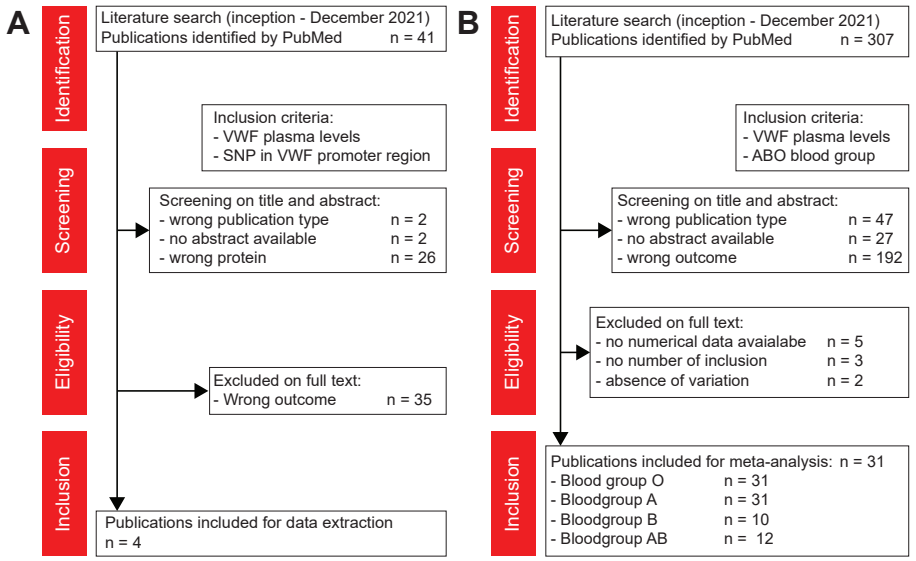

Supplementary Figure 1. Flowchart visualizing selection of publications for meta-analysis (A) Search for single nucleotide polymorphisms (SNPs) influencing Von Willebrand Factor (VWF) levels (B) Search for the influence of ABO blood groups on VWF levels.

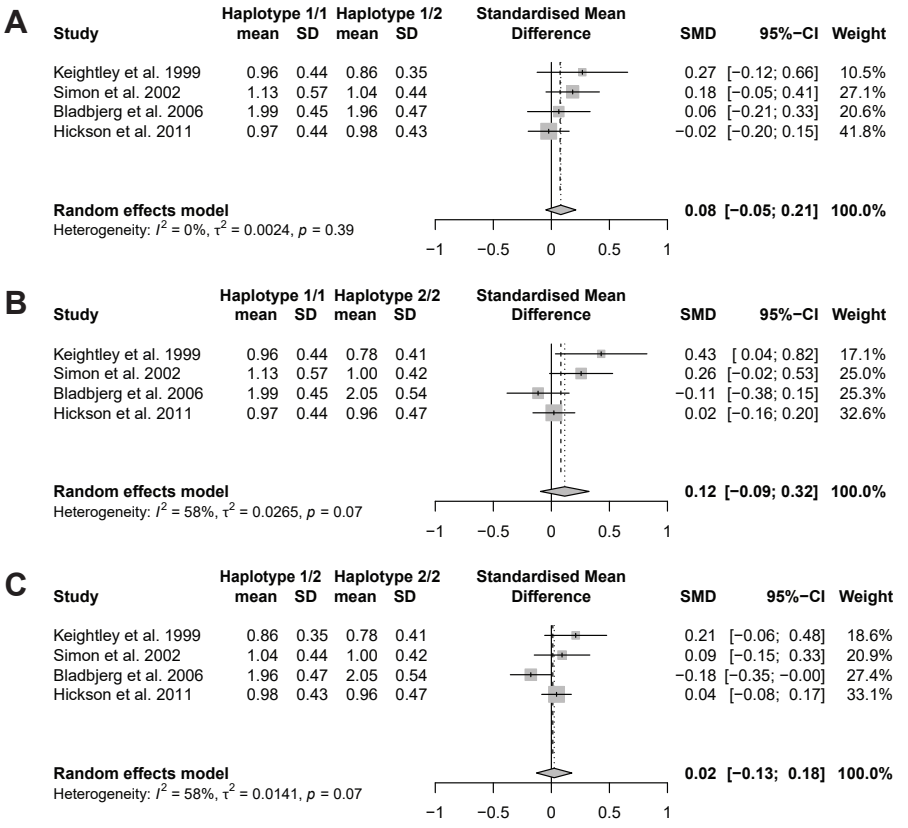

Supplementary Figure 2. Forest plots of selected publications comparing the influence of single nucleotide polymorphism (SNP) on Von Willebrand Factor (VWF) levels (A) SNP haplotype 1/1 vs. haplotype 1/2, (B) SNP haplotype 1/1 vs. 2/2, (C) SNP haplotype 1/2 vs. 2/2. Meta-analysis was performed with standardized mean difference (SMD) with 95% confidence interval (95% CI).

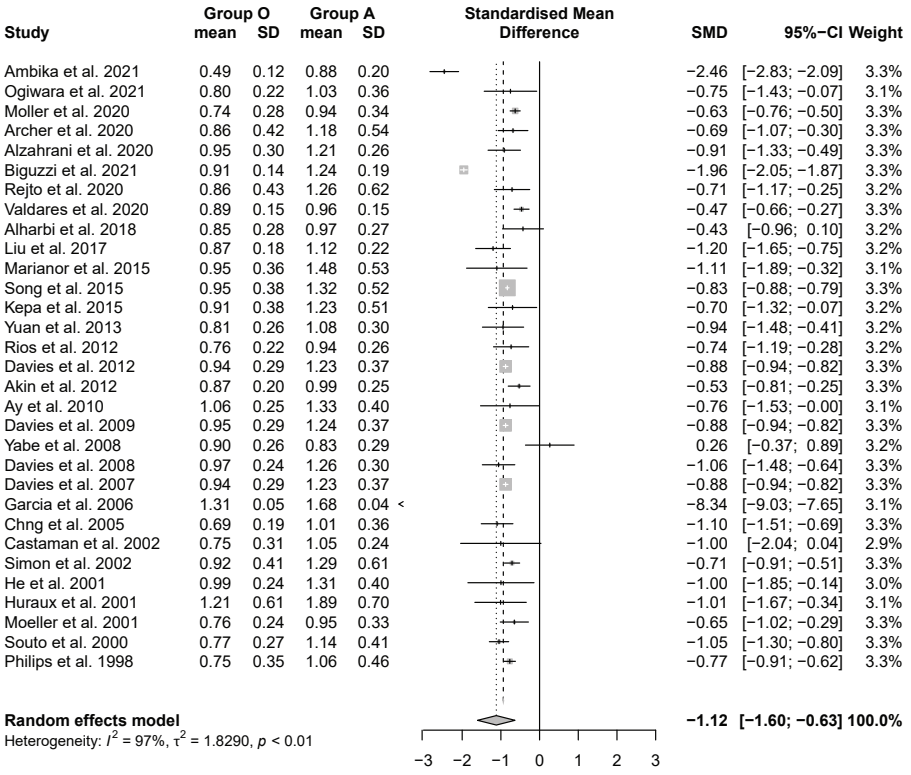

Supplementary Figure 3. Forest plots of selected publications comparing the influence of blood group O versus bloodgroup A on Von Willebrand Factor (VWF) levels. Meta-analysis was performed with standardized mean difference (SMD) with 95% confidence interval (95% CI) of VWF levels.

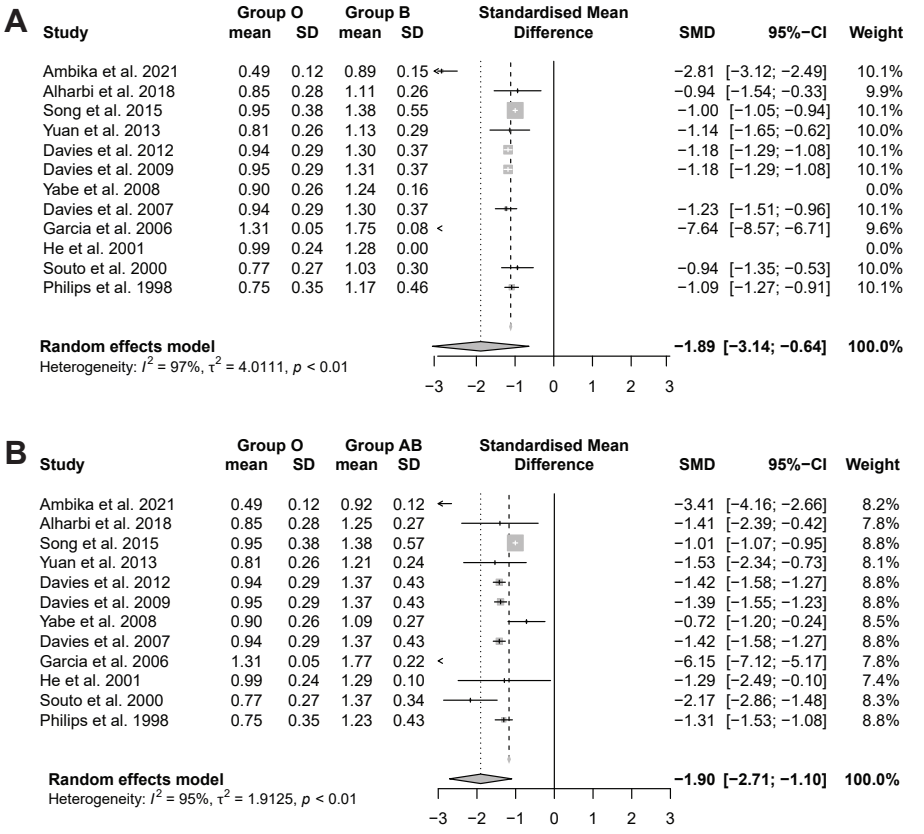

Supplementary Figure 4. Forest plots of selected publications comparing the influence of blood group O versus other blood groups on Von Willebrand Factor (VWF) levels. (A) Blood group O versus Blood group B (B) Blood group O versus blood group AB. Meta-analysis was performed with standardized mean difference (SMD) with 95% confidence interval (95% CI) of VWF levels.

Supplementary references

1. Keightley AM. Lam YM. Brady JN. Cameron CL and Lillicrap D. Variation at the von Willebrand factor (vWF) gene locus is associated with plasma vWF:Ag levels: identification of three novel single nucleotide polymorphisms in the vWF gene promoter. Blood. 1999;93:4277-83.
2. Simon D. Palatnik M and Roisenberg I. Analysis of the -1185A/G von Willebrand factor (VWF) gene polymorphism in two Brazilian ethnic groups and its effect on the plasma VWF levels. Thromb Res. 2002;105:519-22.
3. Bladbjerg EM. de Maat MP. Christensen K. Bathum L. Jespersen J and Hjelmborg J. Genetic influence on thrombotic risk markers in the elderly--a Danish twin study. J Thromb Haemost. 2006;4:599-607.
4. Hickson N. Hampshire D. Castaman G. Eikenboom J. Rodeghiero F. Peake I. Goodeve A. McMdm VWD and Groups Z-VS. Effect of the VWF promoter (GT)n repeat and single-nucleotide polymorphism c.-2527G>A on circulating von Willebrand factor levels under normal conditions. J Thromb Haemost. 2011;9:603-5.
5. Ambika PL. Kar R. Basu D and Kulkarni RG. Influence of ABO Blood Group on von Willebrand Factor Antigen Level in Normal Individuals: A Cross-Sectional Study from Southern India. Indian J Hematol Blood Transfus. 2021;37:505-506.
6. Ogiwara K. Swystun LL. Paine AS. Kepa S. Choi SJ. Rejto J. Hopman W. Pabinger I and Lillicrap D. Factor VIII pharmacokinetics associates with genetic modifiers of VWF and FVIII clearance in an adult hemophilia A population. J Thromb Haemost. 2021;19:654-663.
7. Moller C. Schutte AE. Smith W and Botha-Le Roux S. Von Willebrand factor. its cleaving protease (ADAMTS13). and inflammation in young adults: The African-PREDICT study. Cytokine. 2020;136:155265.
8. Archer NM. Forbes PW. Dargie J. Manganella J. Licameli GR. Kenna MA and Brugnara C. Association of Blood Type With Postsurgical Mucosal Bleeding in Pediatric Patients Undergoing Tonsillectomy With or Without Adenoidectomy. JAMA Netw Open. 2020;3:e201804.
9. Alzahrani FM. Aldossary N and Hassan FM. Phenotypic and Genotypic Characterization of von Willebrand Factor Gene (Exon 18 and 20) in Saudi Healthy Individuals. Med Arch. 2020;74:337-341.
10. Biguzzi E. Castelli F. Lijfering WM. Cannegieter SC. Eikenboom J. Rosendaal FR and van Hylckama Vlieg A. Rise of levels of von Willebrand factor and factor VIII with age: Role of genetic and acquired risk factors. Thromb Res. 2021;197:172-178.
11. Rejto J. Konigsbrugge O. Grilz E. Hofer S. Mauracher LM. Gabler C. Schuster G. Feistritzer C. Sunder-Plassmann R. Quehenberger P. Gebhart J. Ay C and Pabinger I. Influence of blood group. von Willebrand factor levels. and age on factor VIII levels in non-severe haemophilia A. J Thromb Haemost. 2020.
12. Valadares DF. Soares RRP. Di Giacomo G. Rocha T. Reichert CO and Bydlowski SP. von Willebrand factor and factor VIII in a healthy Brazilian population. Association with ABO blood groups. Thromb Res. 2020;188:49-51.
13. Alharbi A. Hassan SB. Al-Momen AK. Al-Saleh K. Nasr R. Kohgear H and Owaidah T. Influence of ABO blood group on von Willebrand factor tests in healthy Saudi blood donors. Blood Coagul Fibrinolysis. 2018;29:211-215.
14. Liu X. Chen X. Yang J and Guo R. Association of ABO blood groups with von Willebrand factor. factor VIII and ADAMTS-13 in patients with lung cancer. Oncol Lett. 2017;14:3787-3794.
15. Marianor M. Zaidah AW and Maraina Ch C. von Willebrand Factor Propeptide: A Potential Disease Biomarker Not Affected by ABO Blood Groups. Biomark Insights. 2015;10:75-9.
16. Song J. Chen F. Campos M. Bolgiano D. Houck K. Chambless LE. Wu KK. Folsom AR. Couper D. Boerwinkle E and Dong JF. Quantitative Influence of ABO Blood Groups on Factor VIII and Its Ratio to von Willebrand Factor. Novel Observations from an ARIC Study of 11.673 Subjects. PLoS One. 2015;10:e0132626.
17. Kepa S. Horvath B. Reitter-Pfoertner S. Schemper M. Quehenberger P. Grundbichler M. Heistinger M. Neumeister P. Mannhalter C and Pabinger I. Parameters influencing FVIII pharmacokinetics in patients with severe and moderate haemophilia A. Haemophilia. 2015;21:343-50.
18. Yuan Z. Chen Y. Zhang Y. Liu H. Liu Q. Zhao J. Hu M. Huang W. Wang G. Zhu T. Zhang J and Zhu P. Changes of plasma vWF level in response to the improvement of air quality: an observation of 114 healthy young adults. Ann Hematol. 2013;92:543-8.
19. Rios DR. Fernandes AP. Figueiredo RC. Guimaraes DA. Ferreira CN. Simoes ESAC. Carvalho MG. Gomes KB and Dusse LM. Relationship between ABO blood groups and von Willebrand factor. ADAMTS13 and factor VIII in patients undergoing hemodialysis. J Thromb Thrombolysis. 2012;33:416-21.
20. Davies JA. Hathaway LS. Collins PW and Bowen DJ. von Willebrand factor: demographics of plasma protein level in a large blood donor cohort from South Wales in the United Kingdom. Haemophilia. 2012;18:e79-81.

21. Akin M. Balkan C. Karapinar DY and Kavakli K. The influence of the ABO blood type on the distribution of von Willebrand factor in healthy children with no bleeding symptoms. Clin Appl Thromb Hemost. 2012;18:316-9.
22. Ay C. Thom K. Abu-Hamdeh F. Horvath B. Quehenberger P. Male C. Mannhalter C and Pabinger I. Determinants of factor VIII plasma levels in carriers of haemophilia A and in control women. Haemophilia. 2010;16:111-7.
23. Davies JA. Collins PW. Hathaway LS and Bowen DJ. C1584: effect on von Willebrand factor proteolysis and von Willebrand factor antigen levels. Acta Haematol. 2009;121:98-101.
24. Yabe M. Matsubara Y. Takahashi S. Ishihara H. Shibano T. Watanabe G. Murata M and Ikeda Y. Alpha 2A adrenergic receptor polymorphism is associated with plasma von Willebrand factor levels in a general population. Blood Coagul Fibrinolysis. 2008;19:395-9.
25. Davies JA. Collins PW. Hathaway LS and Bowen DJ. von Willebrand factor: evidence for variable clearance in vivo according to Y/C1584 phenotype and ABO blood group. J Thromb Haemost. 2008;6:97-103.
26. Davies JA. Collins PW. Hathaway LS and Bowen DJ. Effect of von Willebrand factor Y/C1584 on in vivo protein level and function and interaction with ABO blood group. Blood. 2007;109:2840-6.
27. Garcia AA. van der Heijden JF. Meijers JC. Rosendaal FR and Reitsma PH. The relationship between ABO blood group and the risk of bleeding during vitamin K antagonist treatment. J Thromb Haemost. 2006;4:1418-20.
28. Chng WJ. Yip CY. Baliwag MB and Liu TC. Differential effect of the ABO blood group on von Willebrand factor collagen binding activity and ristocetin cofactor assay. Blood Coagul Fibrinolysis. 2005;16:75-8.
29. Castaman G and Eikenboom JC. ABO blood group also influences the von Willebrand factor (VWF) antigen level in heterozygous carriers of VWF null alleles. type 2N mutation Arg854GIn. and the missense mutation Cys2362Phe. Blood. 2002;100:1927-8.
30. He S. Cao H. Magnusson CG. Eriksson-Berg M. Mehrkash M. Schenck-Gustafsson K and Blomback M. Are increased levels of von Willebrand factor in chronic coronary heart disease caused by decrease in von Willebrand factor cleaving protease activity? A study by an immunoassay with antibody against intact bond 842Tyr-843Met of the von Willebrand factor protein. Thromb Res. 2001;103:241-8.
31. Huraux C. Ankri AA. Eyraud D. Sevin O. Menegaux F. Coriat P and Samama CM. Hemostatic changes in patients receiving hydroxyethyl starch: the influence of ABO blood group. Anesth Analg. 2001;92:1396-401.
32. Moeller A. Weippert-Kretschmer M. Prinz H and Kretschmer V. Influence of ABO blood groups on primary hemostasis. Transfusion. 2001;41:56-60.
33. Souto JC. Almasy L. Muniz-Diaz E. Soria JM. Borrell M. Bayen L. Mateo J. Madoz P. Stone W. Blangero J and Fontcuberta J. Functional effects of the ABO locus polymorphism on plasma levels of von Willebrand factor. factor VIII. and activated partial thromboplastin time. Arterioscler Thromb Vasc Biol. 2000;20:2024-8.
34. Phillips MD and Santhouse A. von Willebrand disease: recent advances in pathophysiology and treatment. Am J Med Sci. 1998;316:77-86.

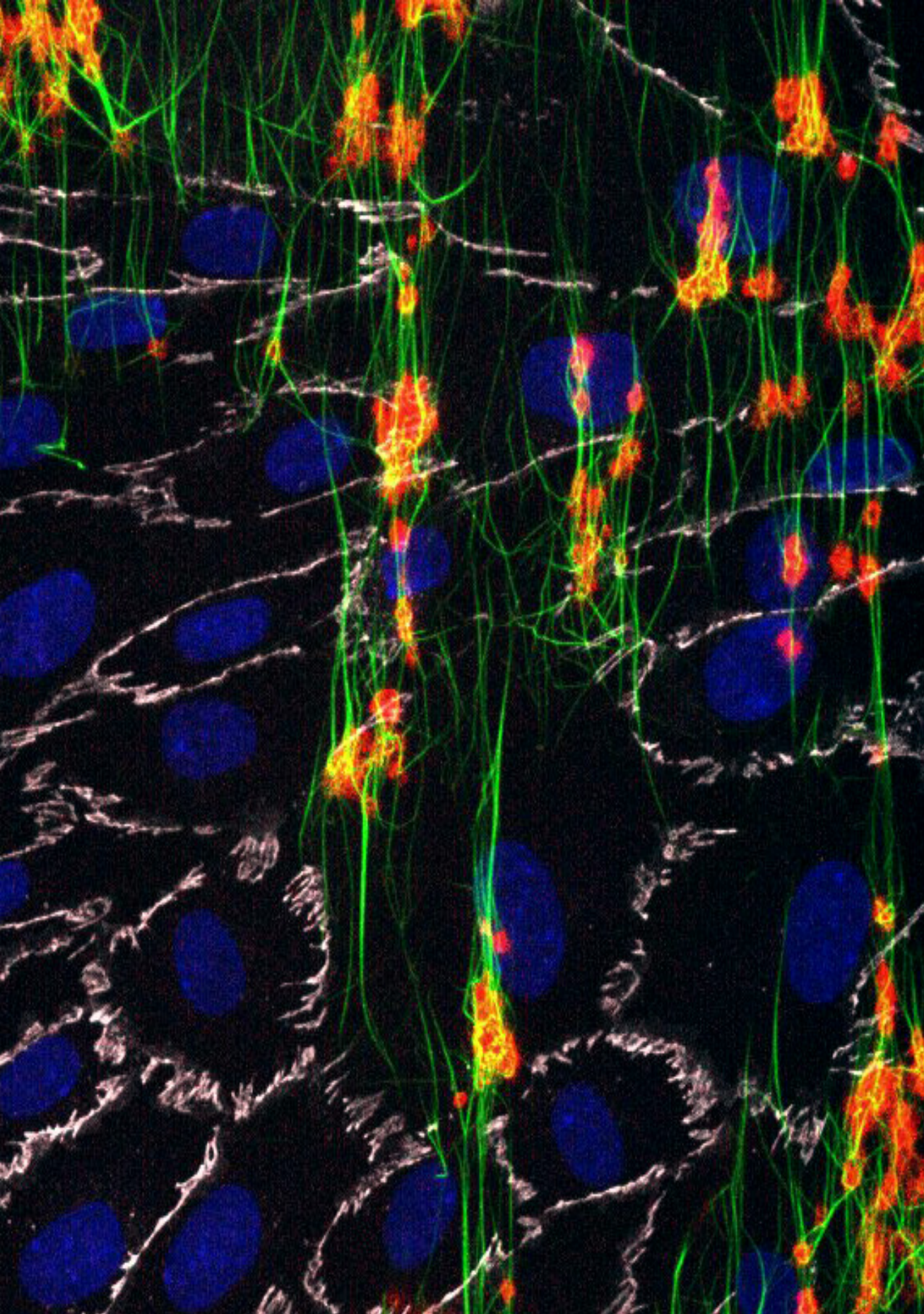

CHAPTER 3

In vitro disease model to study whole blood-endothelial interactions and blood clot dynamics in real-time

Xue D. Manz[1], Hugo J. Albers[2], Petr Symersky[3], Jurjan Aman[1], Andries D. van der Meer[4], Harm Jan Bogaard[1], Robert Szulcek[5]

[1]Department of Pulmonary Diseases, Amsterdam UMC, VU University Medical Center, Amsterdam Cardiovascular Sciences (ACS).
[2]BIOS Lab-on-a-Chip group, University of Twente; Applied Stem Cell Technologies Group, University of Twente.
[3]Department of Cardio-thoracic Surgery, Amsterdam UMC, VU University Medical Center.
[4]Applied Stem Cell Technologies Group, University of Twente.
[5]Department of Pulmonary Diseases, Amsterdam UMC, VU University Medical Center, Amsterdam Cardiovascular Sciences (ACS); Institute of Physiology, Charité-Universitätsmedizin; German Heart Center

24 May 2020, Journal of visualized experiments: JoVE

Abstract

The formation of blood clots involves complex interactions between endothelial cells, their underlying matrix, various blood cells, and proteins. The endothelium is the primary source of many of the major hemostatic molecules that control platelet aggregation, coagulation, and fibrinolysis. Although the mechanism of thrombosis has been investigated for decades, in vitro studies mainly focus on situations of vascular damage where the subendothelial matrix gets exposed, or on interactions between cells with single blood components. Our method allows studying interactions between whole blood and an intact, confluent vascular cell network.

By utilizing primary human endothelial cells, this protocol provides the unique opportunity to study the influence of endothelial cells on thrombus dynamics and gives valuable insights into the pathophysiology of thrombotic disease. The use of custom-made microfluidic flow channels allows application of disease-specific vascular geometries and model specific morphological vascular changes. The development of a thrombus is recorded in real-time and quantitatively characterized by platelet adhesion and fibrin deposition. The effect of endothelial function in altered thrombus dynamics is determined by post-analysis through immunofluorescence staining of specific molecules.

The representative results describe the experimental setup, data collection, and data analysis. Depending on the research question, parameters for every section can be adjusted including cell type, shear rates, channel geometry, drug therapy, and post-analysis procedures. The protocol is validated by quantifying thrombus formation on the pulmonary artery endothelium of patients with chronic thromboembolic disease.

Introduction

The endothelium forms the inner cellular layer of blood vessels and separates blood from the surrounding tissue. It has been described as a dynamic organ that actively regulates its micro-environment and responds to external stimuli[1]. Because of its direct contact with flowing blood, the endothelium is pivotal in the control of hemostasis and thrombosis and is the primary source of many of the major regulatory molecules that control platelet aggregation, coagulation, and fibrinolysis2. Healthy, non-activated endothelial cells (EC) produce several molecules that counteract platelet activation and prevent coagulation and thrombus formation to maintain blood flow, such as prostacyclin, thrombomodulin, or tissue factor pathway inhibitor (TFPI)[2,3]. This prevents the adhesion of platelets, platelet aggregation, and thrombus formation. Injury or activation of the vessel wall results in a pro-coagulant endothelial phenotype that initiates localized platelet adhesion and clot formation[2,4]. Upon endothelial activation platelets adhere to von Willebrand Factor (VWF), a multimeric protein released from ECs, or to exposed binding sites of the underlying subendothelial matrix. Subsequently, molecular changes in platelets and the exposure to tissue factor (TF) initiate the activation of the coagulation system, which induces thrombus formation by fibrin polymerization[5,6]. Together, the resulting clot provides the basis for wound closure by re-endothelialization[7]. Perturbations of the coagulation system may result in bleeding disorders, such as von Willebrand disease, hemophilia, or thrombosis, that often result from a dysregulated pro- and anti-thrombotic balance of the endothelial hemostatic pathway[2,3].

The process of hemostasis occurs in both arterial and venous circulation. However, the mechanisms underlying arterial and venous thrombosis are fundamentally different. While arterial thrombosis, as seen in ischemic heart disease, is mostly driven by the rupture of an atherosclerotic plaque under conditions of high shear stress, venous thrombosis mostly develops in the absence of endothelial injury in a condition of stasis[8,9,10]. A deep vein thrombus may embolize and travel towards the pulmonary arteries, where it causes a pulmonary embolism. This can result in chronic vascular obstructions leading to significant impaired functional capacities that might foster the development of chonic lung diseases including the development of chronic thromboembolic pulmonary hypertension (CTEPH)[11,12,13,14]. CTEPH is characterized by elevated pulmonary pressure due to obstructions of the pulmonary arteries by thromboembolic material following at least three months of anti-coagulation therapy[15]. In addition to lung emboli, it is postulated that the pulmonary endothelium provides a prothrombotic environment in CTEPH that facilitates in situ thrombosis and chronic obstructions of the pulmonary arteries, causing the increase in blood pressure that ultimately can result in heart failure, if untreated[16,17].

Over the past years, various studies have led to the development of assays to examine thrombus formation by measuring platelet function and coagulation[18]. However, most of them either study the interaction of whole blood with single extracellular matrix components like collagens or fibrins, or endothelial function in interaction with single blood components, such as endothelial-platelet or

endothelial-leukocyte interaction[19,20,21,22]. These assays are most commonly performed with human umbilical vein endothelial cells (HUVEC), as these cells are easily obtained. However, hemostatic genes are differentially expressed across the vascular tree, vessel types, and organ systems[23,24], which makes the use of HUVECs to represent endothelial cells involved in arterial thrombosis or pulmonary embolisms problematic[23].

In addition to EC plasticity, disease-specific hemodynamic alterations and changes in vascular morphology can promote thrombus formation at the normal endothelium[25]. Higher shear rates, due to local vasoconstriction or changes in vessel geometry, for example, may result in acute thrombus formation, causing a stenosis that accelerates the cessation of blood flow[26]. The use of custom-made micro engineered flow channels allows to specifically design vascular geometries that are representative of the (patho)biology. In this way, it is possible to study the effect of local biomechanical forces on healthy or diseased EC[27].

There are anti-coagulation therapies available for targeting different phases and molecules in the coagulation cascade, which all pose particular risks and benefits that can be specific to certain disorders. The approach of disease modeling described in this paper is especially suited to test the effects of various anti-coagulation and anti-platelet therapies on thrombus dynamics.

The aim is to present a model of thrombosis that includes primary ECs, yielding a versatile model suitable for the analysis of various forms of thrombosis depending on the type of primary ECs used. As an illustration, we used pulmonary artery endothelial cells from CTEPH patients in interaction with whole human blood containing all components involved in thrombus formation (platelets, leukocytes, erythrocytes, clotting proteins, and co-factors). This approach can be applied in commercial parallel flow channels or in custom-made microfluidic flow channels with a specific vascular design. As such, the model can eventually be used in the study of thrombus formation and resolution, for the assessment of inflammatory responses in disease modeling, for anti-platelet or anti-coagulation therapy, and ultimately for personalized medicine.

Protocol

This study was approved by the institutional Medical Ethical Review Board of the VU Medical Center Amsterdam, The Netherlands (METC VUmc, NL69167.029.19). Primary cell isolation and blood collection of human subjects was performed after written informed consent was obtained in accordance with the Declaration of Helsinki.

This study describes the isolation of primary human pulmonary artery endothelial cells. For the isolation of other primary human endothelial cell types, we refer to previously published methods, including pulmonary microvascular endothelial cells25, human umbilical vein endothelial cells[28], and blood circulating endothelial colony forming cells **Figure 1A**[29].

1. Isolation and culture of primary human pulmonary arterial endothelial cells

1.1. Warm complete endothelial cell medium (cECM) supplemented with 5% fetal bovine serum (FBS), 1% penicillin/streptomycin (P/S), 1% endothelial cell growth supplements (ECGS), and 1% nonessential amino acids (NEAA), in a water bath at 37 °C. Sterilize surgical scissors, forceps, and a scalpel with either a 120 °C heat sterilizer or 70% ethanol. Perform the isolation of pulmonary arterial endothelial cells (PAEC) in a laminar flow cabinet under sterile conditions.

1.2. Coat a high affinity cell binding 60 mm cell culture dish (see **Table of Materials**) with 2 mL of 5 µg/mL fibronectin and incubate at 37 °C for at least 15 min.

1.3. Obtain pulmonary artery (PA) tissue from surgery (e.g., lobectomy or pulmonary endarterectomy), store in 4 °C cold cord buffer (4 mM potassium chloride, 140 mM sodium chloride, 10 mM HEPES, 11 mM D-glucose, and 1% P/S, pH = 7.3), and keep on ice until isolation.

1.4. Isolate endothelial cells from PA within 2 h after tissue removal. Take the PA with forceps and put it in a 10 cm Petri dish to wash with PBS. If the PA is still a ring, cut the pulmonary artery open with scissors. Be very careful to not touch the innermost layer of the vessel with the tools, as the endothelium is easily damaged and/or removed.

1.5. Remove the fibronectin from the cell culture dish and add 4 mL of cECM medium.

1.6. Take the PA tissue with forceps and place it in the medium. Meanwhile, carefully scrape the inner layer of the vessel into the medium with a scalpel. Often, lipid accumulations can be seen in the vessel wall. Try to omit these, as they will impact cell outgrowth.

1.7. Keep the cells in culture until small colonies of endothelial cells start to appear.

1.8. Replace the medium every other day. If fibroblasts contaminate the culture, purify it with magnetic affinity cell separation for CD144 with a kit, in accordance to the manufacturer's instructions (see **Table of Materials**). Use the two-column method for the initial purification and the one-column method for every consecutive purification. Generally, a culture is defined pure when flow cytometry detects ≤10% contaminating cells.

1.9. Split cells in ratios of 1:3 to 1:4 until sufficient PAECs are grown for experimental use. When PAECs are ready to use, continue with the next step.

1.10 After purification, primary endothelial cells need to be characterized for the presence of EC specific markers (e.g., VE-cadherin, CD31, Tie2) and for the absence of smooth muscle cells (α-SMA), fibroblast (vimentin), and epithelial (cytokeratin) markers (**Figure 1B**).

2. Preparation of flow chambers and PAEC monolayers

Depending on the hypothesis, use either the commercially available flow chambers (see **Table of Materials** and **Figure 1C, Option A**, step 2.1 of the protocol) or a custom-made microfluidic flow chamber (**Figure 1C, Option B**, step 2.2 of the protocol).

Option A: Commercially available flow chambers are easy to use and provide a laminar flow pattern throughout the channel that can be used at high shear rates. These microslides are designed to allow multichannel parallel runs and provide an accurate and reproducible flow profile. Because they are optimized for inverted microscopy, it is possible to capture high quality fluorescent images. Furthermore, various dimensions of flow chambers are available in different channel sizes or geometries. The 6-well flow channels are preferred for this assay because these microslides have small dimensions and allow multiparallel runs.

2.1. Cell seeding of endothelial monolayers in commercially available microslides

2.1.1. To coat one channel of a 6-well flow slide (3.5 mm width x 0.4 mm height x 17 mm length) use 30 µL of 0.1% gelatin per channel and incubate at 37 °C for at least 15 min.

2.1.2. To seed one channel, trypsinize 10 cm^2 of confluent PAECs and spin down at 300 xg for 7 min at room temperature (RT).

2.1.3. Suspend PAECs in 600 µL of cECM and pipette 100 µL (1.5 cm^2) of cell suspension in one channel. This covers the microslide through capillary action. If it is going too slow, air bubbles will form. Avoid the formation of air bubbles by using a little bit more force when pipetting.

> **NOTE**: Cell density influences endothelial phenotype. A total of 1.5 cm^2 of confluent cells per channel is overconfluent, because the channel has a surface area of 0.6 cm^2. Before starting the experiment, culture these cells for another 6 days within the channels until they reach maximum confluency.

2.1.4. Add an additional 50 µL of cECM to the channel to provide sufficient medium for overnight incubation at 37 °C, 5% CO_2. Change the medium the next day to wash away unbound cells.

2.1.5. Keep the cells in culture for 6 days at 37 °C, 5% CO2 to allow the PAEC to form a firm, confluent monolayer. Change the medium every other day with 150 µL of cECM.

2.1.6. At day 7, treat the PAEC with 100 µL of 1 µM histamine in ECM and 1% FBS without any other additives for 30 min prior to the assay. The stimulus can be chosen ad libitum. For example, TNF-α has been commonly used as an inflammatory activator.

Option B: Custom-made flow chambers are adapted to the user's needs because the dimensions and geometries can be easily changed to preference. For example, to mimic a more physiologically relevant vessel, a stenosis can be introduced (**Figure 1D**). This approach allows the use of very small blood volumes as seen in microvascular disease.

2.2. Preparation of custom-made microfluidic flow chambers

2.2.1. *Soft lithography of polydimethylsiloxane (PDMS) using patterned wafers*

Combine PDMS curing agent and prepolymer on a microbalance at a 1:10 ratio and thoroughly mix with a general purpose lab mixer.

2.2.1.1. To remove the resulting air bubbles, degas the PDMS in a desiccator for approximately 1 h.

2.2.1.2. Line a glass Petri dish with aluminum foil and add a few droplets of water before placing the wafer in the lined Petri dish. The wafer serves as the mold for the custom-made channel.

NOTE: The wafers or molds are provided by the clean room facilities. Negative photoresist is patterned onto wafers to create protruding channel-like features with the following typical dimensions: 300 µm width x 270 µm height x 14 mm length.

2.2.1.3. Pour the degassed PDMS onto the wafer placed in a glass Petri dish.

2.2.1.4. Degas the PDMS poured onto the wafer in a desiccator for an additional 15 min to remove any bubbles that might have formed during casting.

2.2.1.5. Remove the Petri dish containing the mold and PDMS from the desiccator and place it in a 60 °C oven for a minimum of 4 h to cross-link the PDMS.

2.2.2. *Preparation of cross-linked PDMS for bonding to glass slides*

2.2.2.1. Remove mold and cross-linked PDMS from the oven and move to a cross-flow hood for dust-free handling of the PDMS.

2.2.2.2. Remove any PDMS from the bottom of the mold using a scalpel and remove the top slab of the cross-linked PDMS from the mold.

2.2.2.3. Line the exposed patterned PDMS slab with adhesive tape to prevent any dust particles to come into contact with the PDMS channels.

2.2.2.4. Cut the PDMS chips to size and punch 1 mm diameter inlets and outlets using a biopsy punch.

2.2.3. *Sterilization and bonding of PDMS microfluidic channels and glass slides*

2.2.3.1. Clean glass microscopy slides by thoroughly rinsing with ethanol followed by an isopropyl alcohol rinse. After each rinse, thoroughly dry the slides with a nitrogen gun.

NOTE: Alternatively, cover slips can be used if the analysis is conducted using a confocal microscope.

2.2.3.2. Open the plasma chamber and load the cleaned microscopy slides and microfluidic chips without the protective tape.

2.2.3.3. Close the chamber, purge with nitrogen for 1 min, and fill the chamber with filtered air until a pressure of 500 mTorr is reached.

2.2.3.4. Expose the glass slides and PDMS chips to the plasma for 40 s using a power of 50 W and a frequency of 5 kHz.

2.2.3.5. After exposure to the plasma, immediately bond the glass slides and microfluidic chips. Store the devices in sterile Petri dishes.

2.3. Cell seeding of endothelial monolayers in microfluidic channels

2.3.1. Coat the custom-made microchannel by pipetting 10 µL of 0.1 mg/mL collagen Type I or 0.1% gelatin per channel and incubate at 37 °C for 30 min.

2.3.2. To seed four microchannels, trypsinize 25 cm2 of confluent PAECs and spin down at 300 x g for 7 min at RT.

> **NOTE**: Only a small percentage of cells will adhere to the surface. Therefore, it is necessary to use an excess of cells to achieve a confluent monolayer.

2.3.3. Suspend PAECs in 20 µL of cECM and use 5 µL of cell suspension for each channel. Because of the small channel dimensions, the capillary forces will fill the microslide and prevent air bubble formation.

2.3.4. Change medium after 3–4 h to wash unbound cells.

2.3.5. Keep the cells in culture for 6 days to allow the PAEC to form a firm, confluent monolayer. Because of the small volume, change the medium every day with 150 µL of cECM. Leave the pipette tip filled with medium in the inlet and put an empty tip in the outlet. This will serve as a reservoir providing sufficient nutrients and growth factors to the cells and prevent the slide from drying out.

2.3.6. On day 7, stain the nuclei in the live cells with Hoechst (1:5,000 in cECM) and incubate for a maximum of 10 min at 37 °C and 5% CO2.

2.3.7. Carefully wash 3X with cECM and treat with 1 µM histamine in ECM + 1% FBS for 30 min prior to the assay. The stimulus can be chosen *ad libitum*. For example, TNF-α has been commonly used as an inflammatory activator.

2.3.8. Use 1.27 mm diameter 90° angled stainless steel connectors to connect the outlet of the PDMS chips to tubing.

3. Preparation of human whole blood

3.1. Draw venous blood from subjects in 0.109 M sodium citrate anticoagulant. This can be from healthy or diseased subjects that do not receive anticoagulation treatment. Gently invert the tubes to mix. The total amount of blood required for an experiment mainly depends on the selected flow rate. With a flow rate of 25 mL/h, in ibidi 6-well slides, a total volume of 2 mL with a little excess to fill up tubs and flow channel is sufficient.

3.2. Transfer the blood to a 50 mL tube and add Calcein AM (1:10,000) to fluorescently label blood cells and Alexa488-fibrinogen (15 µg/mL) to conjugate autologous fibrinogen. Let the blood incubate at 37 °C for 15 min to allow complete absorption.

3.3. Dilute the blood 1:1 with recalcification buffer (154 mM sodium chloride, 10.8 mM trisodium citrate, 2.5 mM calcium chloride, and 2 mM magnesium chloride) immediately before the start of experiment.

> **NOTE**: Hemodilution with a maximum of 50% did not influence coagulation reaction time[30]. Furthermore, human blood can contain viruses and other agents. Working with blood samples, therefore, carries a risk of infection. It is highly recommended to use appropriate safety measures and to handle the material with care.

4. Assembling the flow system

4.1. Before connecting the tubing, rinse the flow tubes with a 20 mL syringe filled with wash buffer (36 mM citric acid, 103 mM sodium chloride, 5 mM potassium chloride, 5 mM EDTA, and 0.35% wt/vol bovine serum albumin [BSA], pH = 6.5) to prevent clotting of the blood in the tubes.

4.2. Use a new syringe to fill the flow tubes with HEPES buffer (132 mM sodium chloride, 20 mM HEPES, 6 mM potassium chloride, 1 mM magnesium chloride, 1% BSA, and 5.5 mM D-glucose, pH = 7.4) and carefully connect it with an elbow-shaped Luer connector to the microslide filled with EC in medium. While attaching the connectors to the microchannels, try to prevent the formation of any air bubbles in the slide. Bubbles will damage the endothelium and influence the results of your experiment. Remove wash buffer completely and don't let the buffer get in contact with the cells, as this will inhibit coagulation.

4.3. Set up the flow system as shown in **Figure 1E**. Take up 2 mL of wash buffer in a 20 mL syringe and rinse to prevent clotting when the blood enters the syringe. Insert the empty syringe in the syringe pump and connect the outlet tube with a female Luer connector to this syringe. Put the inlet tube in a container containing the prepared human blood.

4.4. Switch on the syringe pump and calculate the flow rate. Flow profiles follow a parabolic pattern in height. Assuming that the blood acts as a Newtonian fluid, use the following formula to calculate flow rate.

$$\tau = \eta \frac{6Q}{h^2 w} \qquad \text{(Equation 1)}$$

τ = shear stress $\left[\frac{dyn}{cm^2}\right]$

η = dynamical viscosity $\left[\frac{dyn \times s}{cm^2}\right]$

Q = volumetric flow rate $\left[\frac{mm^3}{s}\right]$

h = channel height $[mm]$

w = channel width$[mm]$

> **NOTE**: For pulmonary arterial flow with blood in the commercial 6 channel microslides with rectangular dimensions with 0.4 mm height and 3.5 mm width, a volumetric flow rate of 25 mL/h was used for 5 min. Due to the differences in the dimensions of the custom-made flow channels, these dynamics will also change. Adjust the variables to make sure the shear stress is equal.

4.5. Define the diameter of the 20 mL syringe to 19.05 mm and set the program to Withdraw. Pulling the blood through the cell-coated channel by application of a negative pressure will guarantee constant shear rates and minimal damage to the cell layer.

5. Setting up the microscope for image acquisition

5.1. Use a 20x objective and place the microslide onto the stage of the inverted phase contrast fluorescent microscope. Start the microscope software to move the stage in the Z-direction to focus on the cell monolayer.

5.2. Select a region of interest (ROI) in the beginning, middle, and end of every flow channel. The beginning and end should be at least 3 mm away from the inlet and outlet of the channel. Set the blue, green, and red fluorescent filters with a laser power and light intensity that shows minimal background.

6. Perfusion of whole blood over PAECs

6.1. After everything is connected as in **Figure 1E** and the microscope is ready for recording, push Start to record a video. Push Start on the syringe pump to perfuse the blood over the endothelium.

6.2. As soon as the blood starts flowing over the endothelium, acquire images with the preselected active channels and ROI positions every 15 s for 5 min.

6.3. After 5 min of perfusion, finish recording and stop the syringe pump. Disassemble the flow chamber and very carefully remove the tubing. Often, an air bubble will form if this is done with too much force. Try to prevent this, because this will flush away the endothelium.

7. Fixation and post-analysis

To exclude false positive platelet adhesion by endothelial damage due to the perfusion experiment, it is necessary to characterize the endothelial cells for their gap formation and monolayer. This can be done by regular immunofluorescence staining for VE-cadherin.

7.1. After perfusion and disassembling of the tubing, wash the microfluidic channel with HEPES. Pipette HEPES into the channel so that it will push the blood to the outlet. Remove the excess with another pipette.

Optionally, wash the channel with PBS++ (with 0.5 mM magnesium chloride and 0.9 mM calcium chloride) to prevent precipitation of protein supernatant. This reduces background. However, an extra washing step can change cellular behavior and morphology that could influence post-analysis imaging.

7.2. Remove the HEPES and fix the endothelium with adhered platelets and deposited fibrin by pipetting 37 °C warmed 4% paraformaldehyde (PFA) into the channel and incubate for 15 min at RT.

NOTE: Be extra careful when fixing the custom-made microfluidics as these channels are even smaller, which causes higher shear forces in the channel during every handling step.

7.3. Remove the PFA from the channel and wash 3x with PBS. The microslides are now ready for a standard staining protocol to characterize endothelial cell markers such as VE-cadherin, CD31, P-selectin or integrins, CD42b for adherent platelets, or CD45 for leukocytes.

7.4. After staining, take at least five images with a regular confocal microscope to characterize colocalization.

8. Image analysis

8.1. Open a flow assay image containing either fluorescently labeled platelets or fluorescent fibrin in ImageJ. Drag image of choice to ImageJ.

8.2. The image is taken in RGB color. For analysis, an 8-bit image is preferred, so transform the image into 8-bit: Image | Type | 8-bit.

8.3. To minimize the background, subtract with a sliding paraboloid, where a rolling ball locally calculates and subtracts background pixels from the original image: Process | Subtract Background | Rolling Ball Radius = 50 pixels | Sliding Paraboloid.

> **NOTE**: The image size is defined in pixels. However, to measure area, it is necessary to set the scale. When the images are taken with a 20x objective with a numerical aperture of 0.45, the microscope has a scale of 2 pixels per µm. Most of the time the necessary information to set the scale is stored in the metadata of the image and can automatically be used by ImageJ: Analyze | Set Scale.

8.4. Set a threshold to define adhered platelets or deposited fibrin. Use the Triangle method and the threshold will adjust automatically: Image | Adjust | Threshold.

8.5. Analyze the area covered by the platelets or fibrin with the Analyze Particles command. Set size at 2-Infinity, as the minimal size of a platelet is 2 µm: Analyze | Analyze Particles.

8.6. The results will provide the total area in μm^2, with average size of the aggregates in μm^2 and the percentage of covered area.

Representative Results

The representative results can be divided into three parts, each representing the respective steps of experimental set-up, data collection, and data analysis. Depending on the research question, parameters for each step can be changed. The presented data are applied to study the influence of the endothelium on thrombus formation.

Experimental Set-up

It is well-established that endothelial cells are highly heterogeneous in structure and function, depending on location and time, during health and disease[23]. Various sources of endothelial cells can be used to study endothelial-blood interaction, which in this case were commercially available HUVECs and PAECs (**Figure 1A**). HUVECs have been the most commonly used in laboratory models, while PAECs are patient-derived isolated cells from the pulmonary arteries. Furthermore, there are well-established protocols available to isolate microvascular endothelial cells (MVEC) from the pulmonary circulation or blood circulating endothelial colony forming cells (ECFC)[25,28,29].

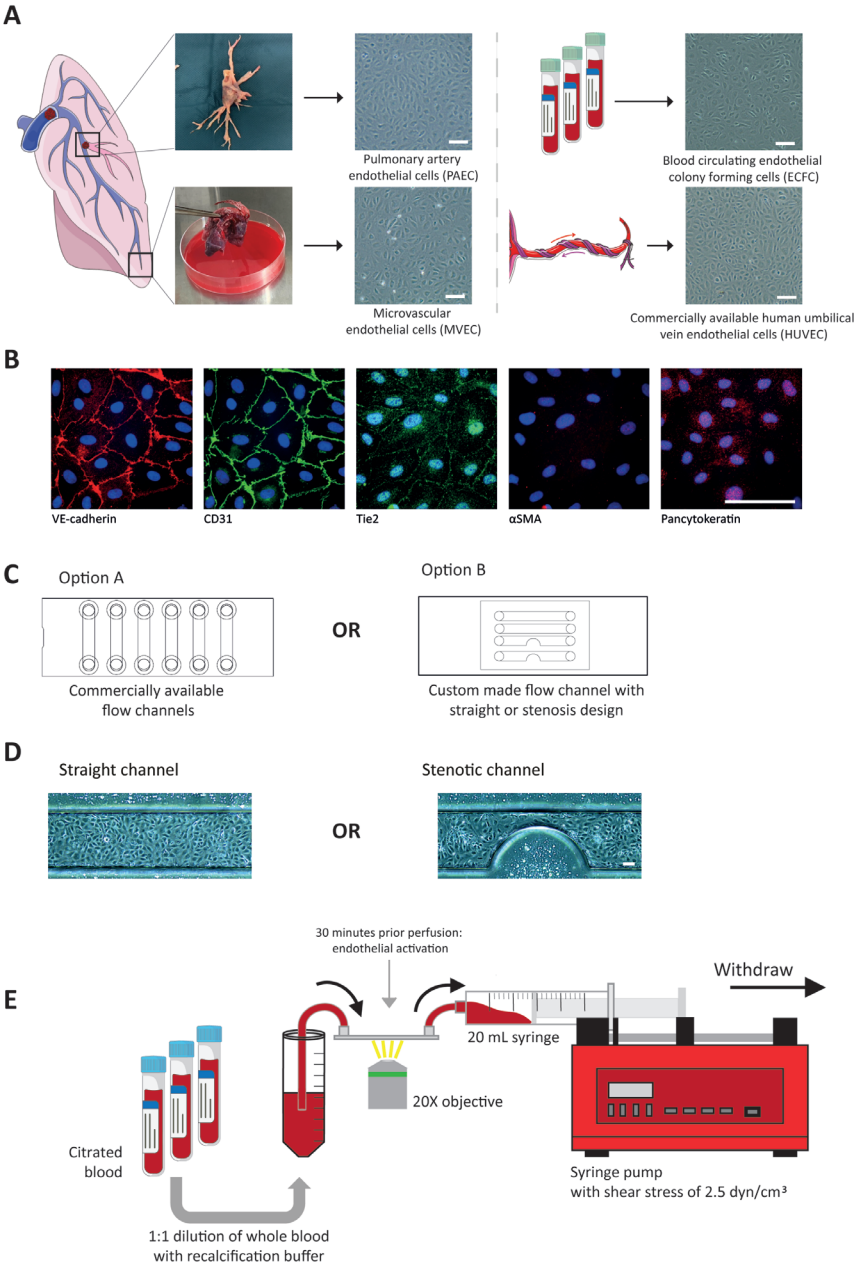

Figure 1: Schematic overview of the protocol. (A) Various sources and different types of endothelial cells were isolated and cultured for usage in a microfluidic flow channel for perfusion experiments. Representative brightfield images of different types of endothelial cells. Scale bar = 50 µm. (B) Isolated cells were characterized by immunofluorescent staining to confirm an endothelial phenotype. Scale bar = 50 µm. (C) Cells can be seeded in either commercial flow slides or custom-made microfluidic channel. (D) Representative brightfield images of HUVEC grown in different channel geometries. Scale bar = 50 µm. (E) Experimental setup of blood perfusion experiments. Citrated blood was collected, diluted with saline buffer, and perfused over endothelial cells with a syringe pump. The lung and umbilical vein in this Figure were modified from Servier Medical Art, licensed under a Creative Common Attribution 3.0 Generic Licence. http://smart.servier.com/

After isolation, endothelial cells were characterized by VE-cadherin, CD31, and Tie2 staining to confirm an endothelial phenotype. Characterization for the presence of αSMA and cytokeratin indicated the absence of a fibroblast or epithelial-like phenotype (**Figure 1B**). After obtaining a highly pure population of ECs, passage 3–5 cells were used to seed either a commercial microslide or custom-made microfluidic flow channels (**Figure 1C**). While the commercially available microslides are primarily parallel flow chambers, or Y-shaped channels with specifically defined parameters in height or bifurcation angle, the use of microfluidic slides makes it possible to adapt the experimental parameters to *in vivo* vessel geometry and blood flow dynamics[31]. However, custom-made microfluidic sizes are smaller and tend to limit cell spread and induce more cell death[32,33]. Using a surplus of cells compensates for the fact that only a small percentage of cells will adhere. This was observed when a stenosis was introduced, where endothelial cells showed a more elongated phenotype compared to a parallel microfluidic channel (**Figure 1D**). Commercial flow chambers have a bigger surface area that cells can bind to. This requires fewer cell numbers for seeding.

To study endothelial cell-blood interaction, whole blood was perfused over an endothelial monolayer. Citrated blood was collected on the day of the experiment and immediately before perfusion recalcified. Cells were stimulated with histamine to induce VWF release and platelet adhesion 30 min prior to perfusion (**Figure 1E**)[34,35]. Because of the small dimensions, the custom-made microfluidic channels allowed use of smaller blood volumes.

Data collection

To investigate thrombus formation on PAECs, Calcein AM-Red fluorescently labeled blood cells and Alexa488-conjugated fibrin were perfused for 5 min at 2.5 dyne/cm^2 (**Figure 2A–C**). Adherent blood cells and deposited fibrin were quantified. Images were acquired every 30 s and quantified with ImageJ. It was important to subtract the background to eliminate the autofluorescence of non-adhered platelets. The triangle algorithm for thresholding has been used to define minimal background. It allowed for measurement of small platelet aggregates (**Figure 2D**).

Expectedly, under non-stimulated conditions, there was no binding of platelets and fibrin to the endothelium. To promote VWF release and platelet binding, PAECs were stimulated with histamine, which resulted in an immediate increase of platelet adhesion reaching a plateau after 2.5 min. At this time, platelets started to secrete autocrine factors that induced platelet aggregation and fibrinogen cleavage into fibrin. Fibrin was deposited after 3 min and formed a stable aggregate with platelets after 4 min (**Figure 2E**).

To investigate whether this effect could be inhibited by a direct oral anticoagulant (DOAC), blood was treated with 10 nM dabigatran. Dabigatran was added to the blood dilution, where it inhibits Factor IIa in the coagulation pathway, and prevented the cleavage of fibrinogen to form fibrin fibers. When dabigatran-treated blood was perfused over stimulated PAECs, clot formation could be directly inhibited mainly by delaying fibrin deposition (**Figure 2F**).

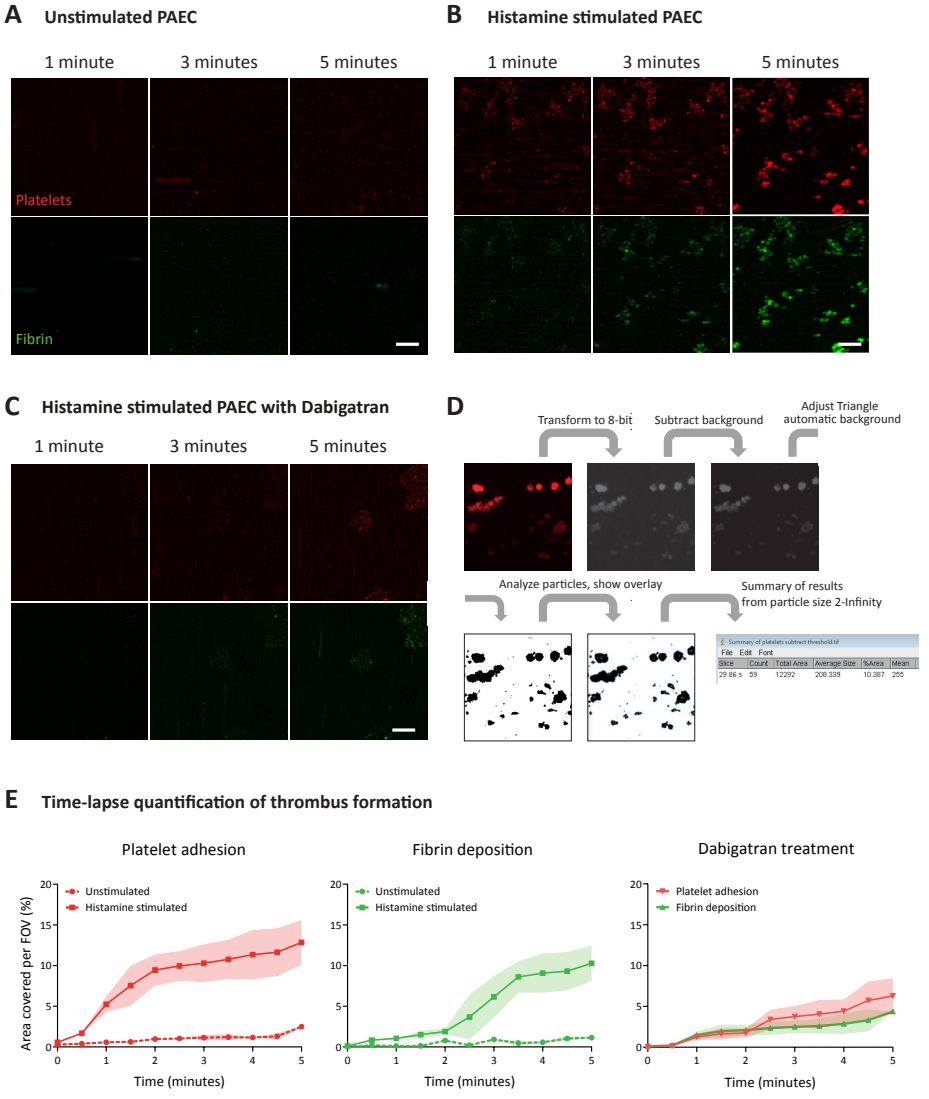

Figure 2: Image acquisition and quantification of thrombus formation. (A) Representative time-lapse imaging of adhered Calcein AM-Red labeled platelets and deposited Alexa488-conjugated fibrin at 1, 3, and 5 min after whole blood perfusion over unstimulated PAECs (B) and over histamine stimulated PAECs. (C) Representative time-lapse images of platelet adhesion and fibrin deposition at 1, 3, and 5 min of perfusion with whole blood incubated with dabigatran perfused over histamine-stimulated PAECs. Scale bar = 50 µm. (D) Schematic overview of image quantification in ImageJ. (E) Quantification of platelet adhesion and fibrin deposition for every 30 s on an unstimulated and histamine stimulated endothelium. (F) Quantification of the effect of dabigatran on thrombus formation quantified by platelet adhesion and fibrin deposition. Data are represented as mean ± SD, n = 3.

Data analysis

To study the influence of various endothelial sources on thrombus formation, the cellular changes upon 5 min blood perfusion were analyzed. The endothelium was fixed and adherent platelets were labeled with CD42b before imaging under a confocal microscope. This provided a detailed analysis for co-localization of platelets and fibrin that could indicate dysfunctional coagulation factors in the blood. The influence of EC in clot formation was determined by standard immunofluorescent staining. Endothelial cell-cell contacts were maintained, as confirmed by VE-cadherin staining, indicating that the blood clots formed on top of the endothelial monolayer rather than on the underlying matrix in between endothelial gaps (**Figure 3**). Furthermore, the use of different cell sources resulted in different patterns of thrombi forming on the endothelium. HUVECs are venous endothelial cells and showed limited platelet adhesion and fibrin deposition, while diseased primary PAEC from CTEPH patients showed abundant platelet adhesion and more fibrin deposition upon histamine stimulation compared to healthy PAEC. This suggests that the endothelium of CTEPH patients show higher responsiveness to vaso-activation that results in increased thrombus formation.

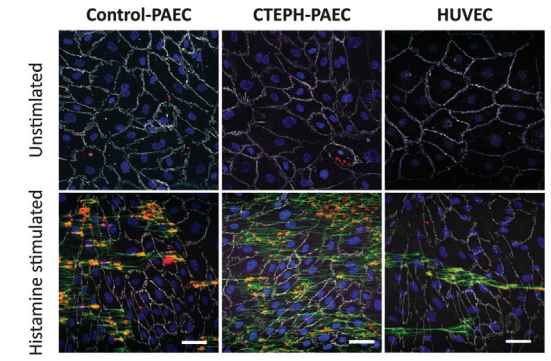

Figure 3: Representative confocal images of flow experiments to characterize thrombus formation in platelet adhesion and fibrin deposition on endothelial cells. Endothelial cell-cell contacts were characterized by VE-cadherin and measured in control PAECs, patient-derived CTEPH PAECs, and HUVEC. Scale bar = 50 µm.

Discussion

Coagulation is a result of the complex and temporally controlled interplay between the endothelium and blood components. This in vitro assay presents a method to investigate thrombogenic properties of endothelial cells in real-time. Various types of primary human endothelial cells can be used, facilitating *in situ* thrombosis in an organ and patient-specific manner. In this study, we illustrated the use of this protocol comparing thrombogenic properties of PAECs isolated from healthy donors versus CTEPH patients. Live thrombus formation was studied by perfusion of whole blood from healthy subjects over histamine-activated endothelium, while the effect of a DOAC was tested as an anti-thrombotic agent.

Besides the use of commercially available microchannels, as shown in the representative results, the introduction of the custom-made microfluidic channels enables the study of the influence of vascular geometry changes on thrombus formation. For example, flow decreases at a branch point or stenosis results in an increase in shear stress and more platelet activation[36]. However, a significant limitation

of these custom-made microfluidic channels is the requirement of high cell numbers to form a stable monolayer of ECs as described in step 2.3.2. This may present a limiting factor when patient-derived cells are scarce. The strengths of the commercially available microslides are that surface areas are modified for cell culture and growth areas are bigger, thereby allowing ECs to form a confluent and stable monolayer. On the other hand, a bigger surface area will result in a bigger lumen. According to **Equation 1**, this requires higher blood volumes to reach similar flow rates as in the custom-made microfluidics.

An improvement to this protocol could be to investigate live EC loss or changes in barrier integrity. EC damage in this protocol is only measured at the end of the experiment. For live tracking, ECs can be tagged with mCherry VE-cadherin, for example[37]. However, as this would need a highly optimized protocol with efficient virus transfection, Electric Cell-substrate Impedance Sensing (ECIS) could be used as an alternative to study endothelial integrity and barrier function[38]. Perfusion over special ECIS flow channels allows longitudinal monitoring of endothelial barrier integrity under flow. These specific ECIS features allow for parallel measurements of endothelial barrier properties and thrombus formation. Alternative ways for parallel EC barrier measurements, especially in the custom-made arrays include the use of fluorescent dextrans in the perfusate, which diffuse out of the lumen, depending on the EC barrier properties.

A limitation of the described protocol is that ECs are removed from the human body and cultured on tissue culture plastic, which is a stiff, artificial substrate. Cells adapt to their biophysical environment. This could possibly affect endothelial response to platelet activation, as there is an association between platelet activation and wall stiffness[39]. Despite these adaptations to culture plastics, cells do keep disease-specific characteristics that can be identified in direct comparison with ECs derived from healthy donors as shown with control, CTEPH-PAEC, and HUVEC that exerted different patterns of platelet adhesion and fibrin deposition after 5 min of blood perfusion.

In contrast to other protocols, this system uses whole blood while others study EC interaction with a single blood component such as platelets and leukocytes[19,20,21]. There have been more advanced microfluidic models developed that allow the study of endothelial function in a vascular model with a round vessel geometry and soft extracellular matrix. However, these are optimized with HUVECs[40,41,42]. The novelty of the described protocol is the use of primary ECs combined with whole blood bringing the modelling of in situ thrombosis one step closer to in vivo conditions. Having optimized the protocol for the use of patient-derived ECs and patient-derived blood further optimizes disease modelling in vitro, allowing the assessment of personalized thrombus formation and drug treatment.

The described protocol can be applied to study the effect of anticoagulation therapies on patient-derived cells. While we used dabigatran to inhibit thrombus formation, it is possible to use other

anticoagulants, such as rivaroxaban, which directly inhibits factor Xa in the coagulation cascade. Direct-platelet inhibitors like clopidogrel or aspirin can be studied as well, as these act on the primary phase of hemostasis where platelets bind to ECs. Ultimately, the thrombogenic capacities of patient-specific ECs in interaction with the patient's own blood can be used to predict the personal effect of anticoagulation therapy on the individual patient. Furthermore, a knockdown of specific proteins can provide additional functional information.

There are some steps in the described protocol that are critical for a successful perfusion experiment. First, during the isolation of primary cells, it is necessary to obtain a highly pure EC culture. Second, it is important that the ECs form a stable confluent monolayer. If this is not the case, a slight change in shear stress can cause endothelial damage and activation of the coagulation cascade, or platelets can start binding to the basement membrane, which will provide false positive results. Third, it is essential to prevent air bubbles, as those can damage the endothelium and thereby influence the results.

After recalcification of the citrated blood with calcium chloride and magnesium chloride, it is important to immediately start the perfusion experiment. Recalcification induces a rapid response in platelet activation and thrombus formation, resulting in fast clotting in the sample.

In conclusion, we describe a highly versatile protocol to study whole blood-endothelial cell interactions during thrombosis.

References

1. Yau, J. W., Teoh, H., Verma, S. Endothelial cell control of thrombosis. BMC Cardiovascular Disorders. 15, 130 (2015).
2. Pearson, J. D. Endothelial cell function and thrombosis. Best Practice & Research: Clinical Haematology. 12, (3), 329-341 (1999).
3. Bochenek, M. L., Schafer, K. Role of Endothelial Cells in Acute and Chronic Thrombosis. Hamostaseologie. 39, (2), 128-139 (2019).
4. Swieringa, F., et al. Platelet Control of Fibrin Distribution and Microelasticity in Thrombus Formation Under Flow. Arteriosclerosis, Thrombosis, and Vascular Biology. 36, (4), 692-699 (2016).
5. Macfarlane, R. G. An Enzyme Cascade in the Blood Clotting Mechanism, and Its Function as a Biochemical Amplifier. Nature. 202, 498-499 (1964).
6. Versteeg, H. H., Heemskerk, J. W., Levi, M., Reitsma, P. H. New fundamentals in hemostasis. Physiological Reviews. 93, (1), 327-358 (2013).
7. Opneja, A., Kapoor, S., Stavrou, E. X. Contribution of platelets, the coagulation and fibrinolytic systems to cutaneous wound healing. Thrombosis Research. 179, 56-63 (2019).
8. Tabas, I., Garcia-Cardena, G., Owens, G. K. Recent insights into the cellular biology of atherosclerosis. Journal of Cell Biology. 209, (1), 13-22 (2015).
9. Karino, T., Motomiya, M. Flow through a venous valve and its implication for thrombus formation. Thrombosis Research. 36, (3), 245-257 (1984).
10. ISTH Steering Committee for World Thrombosis Day. Thrombosis: a major contributor to global disease burden. Thrombosis Research. 134, (5), 931-938 (2014).
11. Witkin, A. S. Acute and chronic pulmonary embolism: the role of the pulmonary embolism response team. Current Opinion in Cardiology. 32, (6), 672-678 (2017).
12. Kim, N. H., et al. Chronic thromboembolic pulmonary hypertension. European Respiratory Journal. 53, (1), 1801915 (2019).
13. Zhang, M., Zhang, Y., Pang, W., Zhai, Z., Wang, C. Circulating biomarkers in chronic thromboembolic pulmonary hypertension. Pulmonary Circulation. 9, (2), 2045894019844480 (2019).
14. Giri, J., et al. Interventional Therapies for Acute Pulmonary Embolism: Current Status and Principles for the Development of Novel Evidence: A Scientific Statement From the American Heart Association. Circulation. 140, (20), 774-801 (2019).
15. Sharma, S., Lang, I. M. Current understanding of the pathophysiology of chronic thromboembolic pulmonary hypertension. Thrombosis Research. 164, 136-144 (2018).
16. Eisenberg, P. R., et al. Fibrinopeptide A levels indicative of pulmonary vascular thrombosis in patients with primary pulmonary hypertension. Circulation. 82, (3), 841-847 (1990).
17. Bochenek, M. L., et al. From thrombosis to fibrosis in chronic thromboembolic pulmonary hypertension. Thrombosis and Haemostasis. 117, (4), 769-783 (2017).
18. Nagy, M., Heemskerk, J. W. M., Swieringa, F. Use of microfluidics to assess the platelet-based control of coagulation. Platelets. 28, (5), 441-448 (2017).
19. Barendrecht, A. D., et al. Live-cell Imaging of Platelet Degranulation and Secretion Under Flow. Journal of Visualized Experiments. (125), e55658 (2017).
20. Vajen, T., et al. Laminar Flow-based Assays to Investigate Leukocyte Recruitment on Cultured Vascular Cells and Adherent Platelets. Journal of Visualized Experiments. (134), e57009 (2018).
21. Michels, A., Swystun, L. L., Mewburn, J., Albanez, S., Lillicrap, D. Investigating von Willebrand Factor Pathophysiology Using a Flow Chamber Model of von Willebrand Factor-platelet String Formation. Journal of Visualized Experiments. (126), e55917 (2017).
22. Smeets, M. W. J., Mourik, M. J., Niessen, H. W. M., Hordijk, P. L. Stasis Promotes Erythrocyte Adhesion to von Willebrand Factor. Arteriosclerosis, Thrombosis, and Vascular Biology. 37, (9), 1618-1627 (2017).
23. Aird, W. C. Endothelial cell heterogeneity. Cold Spring Harbor Perspectives in Medicine. 2, (1), 006429 (2012).
24. Aitsebaomo, J., Portbury, A. L., Schisler, J. C., Patterson, C. Brothers and sisters: molecular insights into arterial-venous heterogeneity. Circulation Research. 103, (9), 929-939 (2008).
25. Szulcek, R., et al. Delayed Microvascular Shear Adaptation in Pulmonary Arterial Hypertension. Role of Platelet Endothelial Cell Adhesion Molecule-1 Cleavage. American Journal of Respiratory and Critical Care Medicine. 193, (12), 1410-1420 (2016).
26. Casa, L. D., Deaton, D. H., Ku, D. N. Role of high shear rate in thrombosis. Journal of Vascular Surgery. 61, (4), 1068-1080 (2015).

27. Jain, A., et al. Assessment of whole blood thrombosis in a microfluidic device lined by fixed human endothelium. Biomedical Microdevices. 18, (4), 73 (2016).
28. van Nieuw Amerongen, G. P., Draijer, R., Vermeer, M. A., van Hinsbergh, V. W. Transient and prolonged increase in endothelial permeability induced by histamine and thrombin: role of protein kinases, calcium, and RhoA. Circulation Research. 83, (11), 1115-1123 (1998).
29. Smits, J., et al. Blood Outgrowth and Proliferation of Endothelial Colony Forming Cells are Related to Markers of Disease Severity in Patients with Pulmonary Arterial Hypertension. International Journal of Molecular Sciences. 19, (12), 3763 (2018).
30. Tobias, M. D., Wambold, D., Pilla, M. A., Greer, F. Differential effects of serial hemodilution with hydroxyethyl starch, albumin, and 0.9% saline on whole blood coagulation. Journal of Clinical Anesthesia. 10, (5), 366-371 (1998).
31. Jain, A., et al. Primary Human Lung Alveolus-on-a-chip Model of Intravascular Thrombosis for Assessment of Therapeutics. Clinical Pharmacology & Therapeutics. 103, (2), 332-340 (2018).
32. Veiseh, M., Veiseh, O., Martin, M. C., Asphahani, F., Zhang, M. Short peptides enhance single cell adhesion and viability on microarrays. Langmuir-ACS. 23, (8), 4472-4479 (2007).
33. Kuo, C. W., Chueh, D. Y., Chen, P. Investigation of size-dependent cell adhesion on nanostructured interfaces. Journal of Nanobiotechnology. 12, 54 (2014).
34. McCormack, J. J., Lopes da Silva, M., Ferraro, F., Patella, F., Cutler, D. F. Weibel-Palade bodies at a glance. Journal of Cell Science. 130, (21), 3611-3617 (2017).
35. Guilarte, M., Sala-Cunill, A., Luengo, O., Labrador-Horrillo, M., Cardona, V. The Mast Cell, Contact, and Coagulation System Connection in Anaphylaxis. Frontiers in Immunology. 8, 846 (2017).
36. Westein, E., et al. Atherosclerotic geometries exacerbate pathological thrombus formation poststenosis in a von Willebrand factor-dependent manner. Proceedings of the National Academy of Sciences. 110, (4), 1357-1362 (2013).
37. Huveneers, S., et al. Vinculin associates with endothelial VE-cadherin junctions to control force-dependent remodeling. Journal of Cell Biology. 196, (5), 641-652 (2012).
38. Szulcek, R., Bogaard, H. J., van Nieuw Amerongen, G. P. Electric cell-substrate impedance sensing for the quantification of endothelial proliferation, barrier function, and motility. Journal of Visualized Experiments. (85), e51300 (2014).
39. Yamasaki, F., et al. Association between arterial stiffness and platelet activation. Journal of Human Hypertension. 19, (7), 527-533 (2005).
40. Tsai, M., et al. In vitro modeling of the microvascular occlusion and thrombosis that occur in hematologic diseases using microfluidic technology. Journal of Clinical Investigation. 122, (1), 408-418 (2012).
41. Zheng, Y., et al. In vitro microvessels for the study of angiogenesis and thrombosis. Proceedings of the National Academy of Sciences. 109, (24), 9342-9347 (2012).
42. Myers, D. R., et al. Endothelialized microfluidics for studying microvascular interactions in hematologic diseases. Journal of Visualized Experiments. (64), e3958 (2012).

Table of Materials (I)

Name	Company	Catalog Number	Comments
NaCl	Merck	106404	
20 mL syringe	BD	300613	
20X objective	Olympus	N1492900	LUCPLFLN20XPH/0.45
2-Propanol (IPA)	Boom	760514555000	
Aladdin Syringe Pump	Word Precision Instruments	AL-4000	
Alexa488-Fibrinogen	Invitrogen	F13191	15 ug/mL
Alexa647-Goat anti Rabbit	Invitrogen	A21245	1:100
Biopsy punch 1 mm diameter	Ted Pella	15110-10	
Bovine Serum Albumin (BSA)	Sigma-Aldrich	A9647	
CaCl2	Sigma-Aldrich	21115	
Calcein AM-Red	Invitrogen	C3099	1:1000
CD42b-APC	Miltenyi Biotec	130-100-208	1:100
Citric Acid	Merck	100244	
Collagen Type I, rat tail	Corning	354249	0.1 mg/mL
Corning CellBIND Surface 60 mm Culture Dish	Corning	3295	
Cross-flow hood	Basan		
Desiccator	Duran	2478269	
D-Glucose	Merck	14431-43-7	
EDTA	Invitrogen	15575020	
Endothelial Cell Medium (ECM)	ScienCell	1001	
Fibronectin Human Plasma	Sigma-Aldrich	F0895	
Flow tubing	ibidi	10831, 10841	
Gelatin	Merck	104070	0.1%
HEPES	Sigma-Aldrich	H4034	
Hoechst 33342	Invitrogen	H1399	1:1000
micron-Slide VI 0.4 flow chambers	ibidi	80606	
ImageJ	NIH	v1.49	
KCl	Merck	7447-40-7	
Lab oven	Quincy	10GC	
LS720 Fluorescent microscope	Etaluma	LS720	
Luer connector	ibidi	10802, 10825	Male elbow connectors, Female tube connectors
MACS magnetic beads (anti-CD144)	Miltenyi Biotec	130-097-857	1:5
MgCl2	Sigma-Aldrich	M1028	
Microscopy slides, 76 x 26 mm	Thermo Scientific	AAAA000001##12E	

Table of Materials (II)

Name	Company	Catalog Number	Comments
Negative photoresist, SU-8	Microchem		
Non-Essential Amino Acids (NEAA)	Lonza	13-114E	
Paraformaldehyde (PFA)	Merck	818715	4% PFA in PBS
Penicillin/streptomycin (P/S)	Gibco	15140-122	1%
Phosphate Buffered Saline (PBS)	Gibco	14190-094	no calcium or magnesium
Plasma chamber, CUTE	Femto Science		
Polydimethylsiloxane (PDMS), Sylgard 184	Dow	101697	
sodium citrate blood collection tubes	BD	363048	
trisodium citrate	Merck	106448	
Trypsin-EDTA (0.05%), phenol red	Gibco	25300-045	
VE-Cadherin (D87F2)-XP	Cell Signaling	2500	1:300

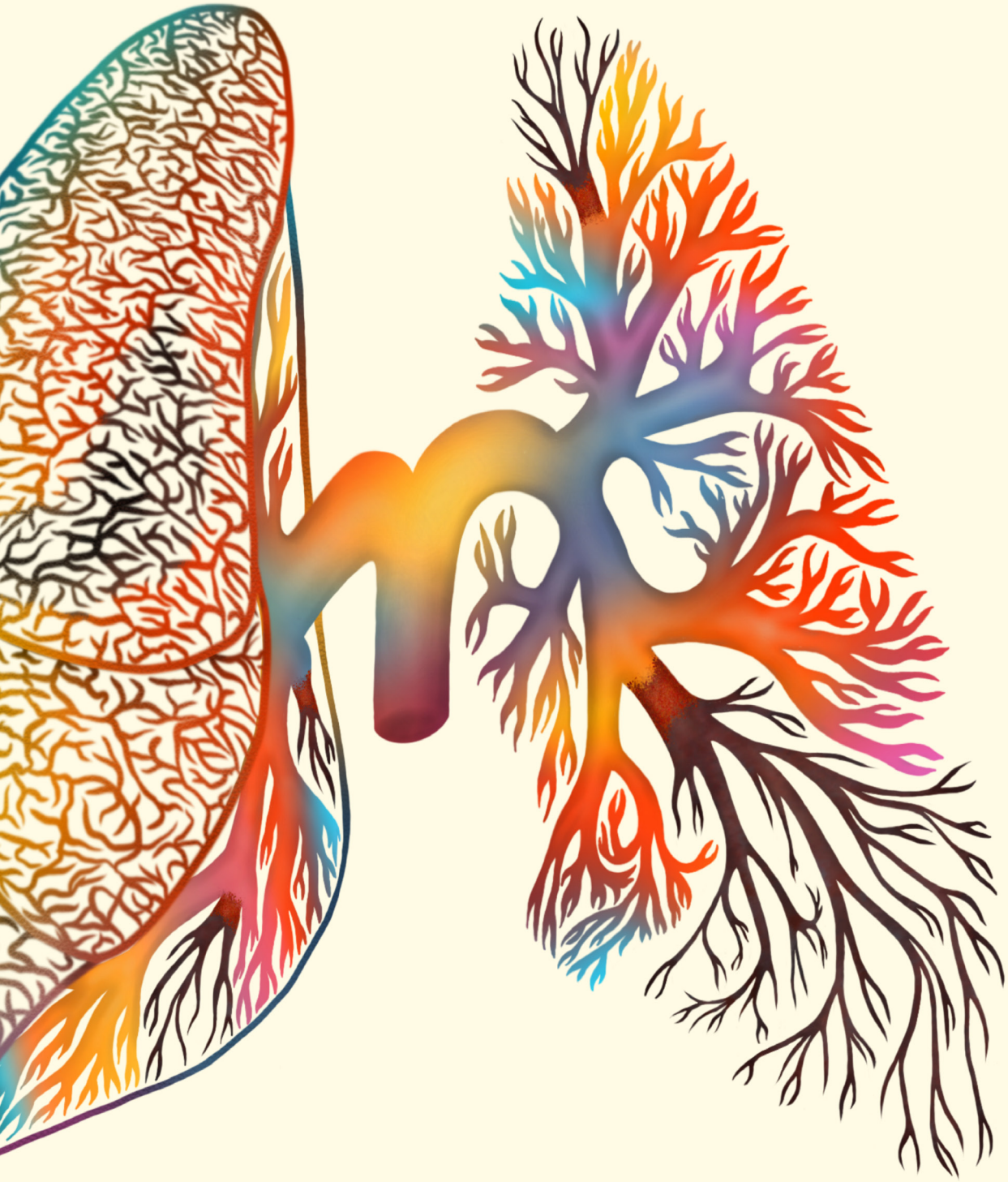

PART II

Chronic thromboembolic pulmonary hypertension

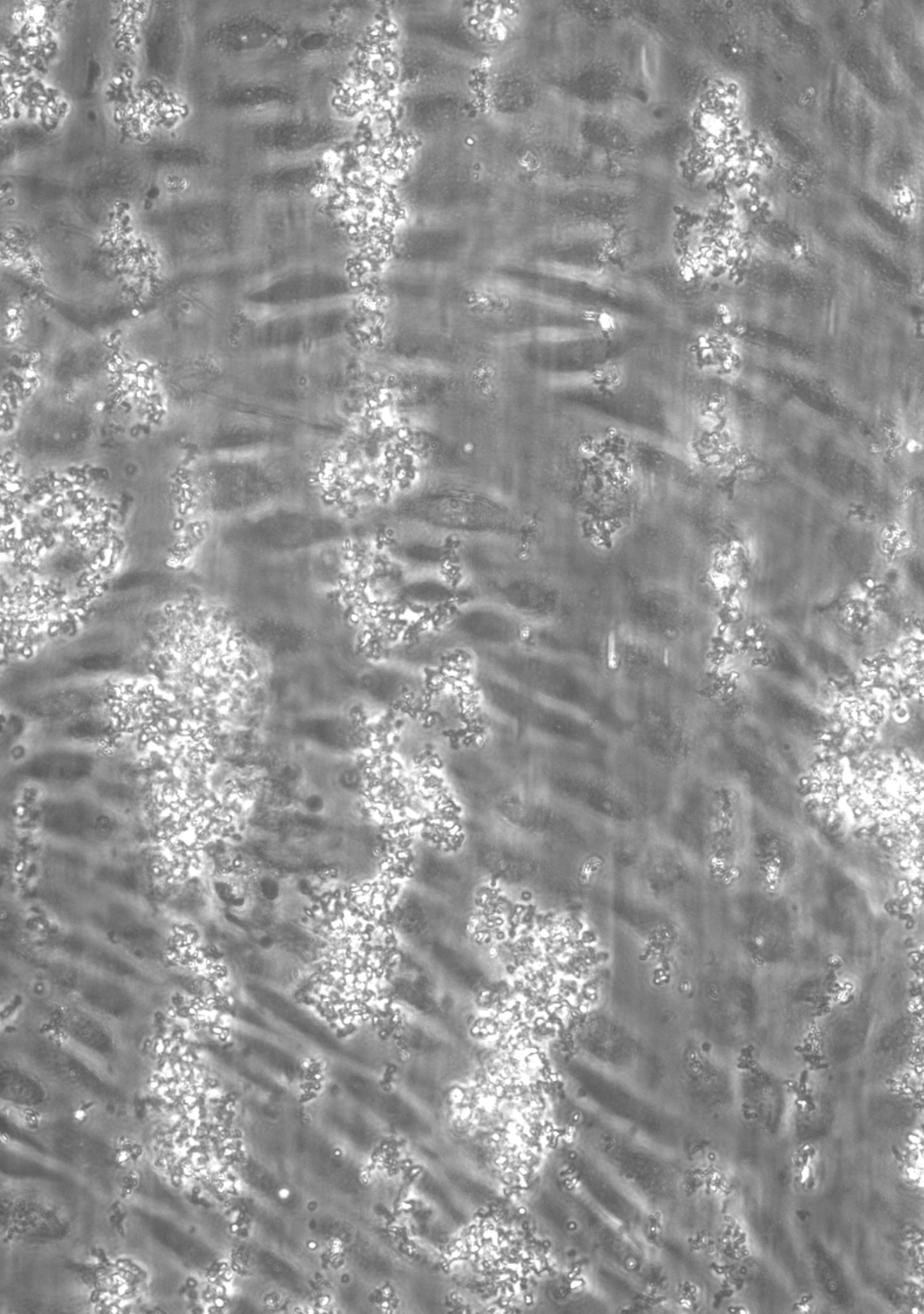

CHAPTER 4

Epigenetic modification of the von Willebrand Factor promoter drives platelet aggregation on the pulmonary endothelium in chronic thromboembolic pulmonary hypertension

Xue D. Manz[1], Robert Szulcek[2], Xiaoke Pan[1], Petr Symersky[3], Chris Dickhoff[3], Jisca Majolée[4], Veerle Kremer[4], Elisabetta Michielon[5], Ekaterina S. Jordanova[6], Teodora Radonic[7], Irene V. Bijnsdorp[8], Sander R. Piersma[8], Thang V. Pham[8], Connie R. Jimenez[8], Anton Vonk Noordegraaf[1], Frances S. de Man[1], Reinier A. Boon[4], Jan Voorberg[9], Peter L. Hordijk[4], Jurjan Aman[1]*, Harm Jan Bogaard[1]*

[1]Department of Pulmonary Medicine, Amsterdam UMC, VU University Medical Center, Amsterdam Cardiovascular Sciences (ACS), Amsterdam, The Netherlands
[2]Institute of Physiology, Charité Universitätsmedizin Berlin, corporate member of Freie Universität Berlin and Humboldt-Universität zu Berlin and German Heart Center Berlin, Germany
[3]Department of Cardio-thoracic Surgery, Amsterdam UMC, VU University Medical Center, Amsterdam, The Netherlands
[4]Department of Physiology, Amsterdam UMC, VU University Medical Center, Amsterdam Cardiovascular Sciences (ACS), Amsterdam, The Netherlands
[5]Department of Molecular Cell Biology and Immunology, Amsterdam UMC, VU University Medical Center, Amsterdam, The Netherlands
[6]Center for Gynecologic Oncology Amsterdam (CGOA), Amsterdam UMC, VU University Medical Center, Cancer Center Amsterdam (CCA), Amsterdam, The Netherlands
[7]Department of Pathology, Amsterdam UMC, VU University Medical Center, Amsterdam, The Netherlands
[8]Department of Medical Oncology, Amsterdam UMC, VU University Medical Center, Cancer Center Amsterdam (CCA), Amsterdam, The Netherlands
[9]Department of Molecular Hematology, Sanquin Research and Landsteiner Laboratory, Amsterdam UMC, Academic Medical Center, Amsterdam, The Netherlands

1 April 2022, American Journal of Respiratory and Critical Care Medicine

Abstract

Rationale: von Willebrand factor (VWF) mediates platelet adhesion during thrombosis. While chronic thromboembolic pulmonary hypertension (CTEPH) is associated with increased plasma levels of VWF, the role of this protein in CTEPH has remained enigmatic.

Objectives: To identify the role of VWF in CTEPH.

Methods: CTEPH-specific patient plasma and pulmonary endarterectomy material from patients with CTEPH were used to study the relationship between inflammation, VWF expression, and pulmonary thrombosis. Cell culture findings were validated in human tissue, and proteomics and chromatin immunoprecipitation were used to investigate the underlying mechanism of CTEPH.

Measurements and Main Results: VWF is increased in plasma and the pulmonary endothelium of CTEPH patients. In vitro, the increase in VWF gene expression and the higher release of VWF protein upon endothelial activation resulted in elevated platelet adhesion to CTEPH endothelium. Proteomic analysis revealed that nuclear factor (NF)-κB2 was significantly increased in CTEPH. We demonstrate reduced histone tri-methylation and increased histone acetylation of the VWF promoter in CTEPH endothelium, facilitating binding of NFκB2 to the VWF promoter and driving VWF transcription. Genetic interference of NFκB2 normalized the high VWF RNA expression levels and reversed the prothrombotic phenotype observed in CTEPH–pulmonary artery endothelial cells.

Conclusions: Epigenetic regulation of the VWF promoter contributes to the creation of a local environment that favors in situ thrombosis in the pulmonary arteries. It reveals a direct molecular link between inflammatory pathways and platelet adhesion in the pulmonary vascular wall, emphasizing a possible role of in situ thrombosis in the development or progression of CTEPH.

Introduction

Chronic thromboembolic pulmonary hypertension (CTEPH) is characterized by the persistence of thrombotic material in the pulmonary arteries. Patients are diagnosed when mean elevated pulmonary artery pressures and persistent perfusion defects are present despite 3 months of adequate anticoagulant treatment[1,2]. It is assumed that CTEPH results from the incomplete resolution of acute pulmonary embolism (PE), but many patients do not have a history of PE or deep vein thrombosis[3]. Moreover, traditional risk factors for acute PE, such as protein C or protein S deficiency, factor V Leiden, and antithrombin or plasminogen deficiency, are not observed in patients with CTEPH[4]. Rather, CTEPH is associated with a different spectrum of risk factors, of which many are linked with chronic inflammation such as inflammatory bowel disease, splenectomy, and autoimmune hypothyroidism[4]. Furthermore, patients with CTEPH have a different thromboembolic pulmonary arterial morphology compared with patients with acute PE[5]. These observations suggest that besides nonresolving emboli, additional processes such as in situ thrombosis may contribute to the development and progression of CTEPH.

Perturbations in hemostasis and thrombosis are initiated when activated endothelial cells secrete von Willebrand factor (VWF) from storage granules called Weibel-Palade bodies[6,7]. The release of VWF recruits platelets to sites of injury, causing activation of the coagulation cascade and thrombus formation[8]. Interestingly, elevated VWF plasma levels are strongly and specifically associated with chronic pulmonary thrombosis. Although large cohort studies demonstrated that plasma VWF levels were not predictive for future development of acute PE[9] and that plasma VWF levels are comparable between control subjects and patients with acute PE[10], VWF plasma levels were elevated in patients with CTEPH[10]. These findings indicate that VWF may play a specific role in CTEPH.

The role and regulation of VWF in CTEPH have not been elucidated. VWF is released by endothelial cells under inflammatory conditions[11,12], and low-grade inflammation has been demonstrated in patients with CTEPH[13,14]. Yet, the acute temporal dynamics of VWF release during inflammation poorly fit the chronic timeframe of CTEPH. The chronic timeframe of CTEPH may suggest genetic abnormalities leading to constitutionally increased VWF, but thus far, no genetic variants have been identified in CTEPH. Regulation of VWF expression by epigenetic modulation of the VWF promoter has not been described before. The aim of the current study is to describe the role of VWF in CTEPH.

To investigate the molecular relationship between inflammatory conditions, VWF expression, and pulmonary thrombosis, we first assessed VWF release in plasma from patients with CTEPH and endothelial VWF expression in lung tissue from patients with CTEPH. To further elucidate the role of VWF in CTEPH, we used a unique human in vitro culture model of endothelium–platelet interaction under flow. We show that CTEPH patient–derived pulmonary artery endothelial cells (PAEC) recruit more platelets due to elevated VWF gene expression and protein release upon endothelial activation. We found that altered epigenetic modifications of the VWF promoter region allow increased binding

of nuclear factor (NF)-κB2 transcription factor, resulting in increased VWF transcription. As interference at NFκB2 or VWF level reduced platelet aggregation, these data reveal a novel mechanism of transcriptional VWF regulation, which promotes a local environment in favor of in situ thrombosis in CTEPH.

Some of the results of this study have been previously reported in the form of an abstract[15,16].

Methods

Blood collection

Citrated blood was taken from healthy volunteers without pulmonary hypertension and/or any bleeding disorders and from patients with CTEPH (1 day before surgery) who were at least 24 hours free from anticoagulant medication. Blood was collected after informed consent was obtained in accordance with the Declaration of Helsinki. This study was approved by the institutional Medical Ethical Review Board of the Amsterdam UMC, location VU University Medical Center, the Netherlands (METC VUmc, NL69167.029.19). Hemodynamic data were collected at the time of baseline right heart catheterization. Baseline group characteristics are summarized in **Table 1** and Table E1 in the online supplement, and donor-specific characteristics are shown in Table E2.

Primary cell isolation

PAEC were isolated from resected pulmonary artery tissue according to the previously published protocol[17]. Control tissue was obtained from lobectomies of suspected or proven lung malignancies (non-PH control), and CTEPH tissue was obtained from pulmonary endarterectomy (PEA) material, both surgeries performed at the Amsterdam UMC, location VU University Medical Center, the Netherlands.

Platelet adhesion under Flow

Platelets were isolated as previously described[18]. If indicated, platelets were treated for 30 minutes with a monoclonal antibody raised to the A1 domain of VWF (CLB-RAg-35, gifted from Sanquin) before perfusion experiments.

PAECs were seeded in 0.1% gelatin-coated µ-Slide VI 0.4 ibiTreat flow slides (ibidi, #80606) and cultured for at least 7 days to form a stable monolayer. Fluorescently labeled platelets were perfused over PAEC with a syringe pump (World Precision Instruments, #AL4000) with a unidirectional shear rate of 2.5 dyn/cm^2. Phase-contrast and fluorescent images of three chosen regions of interest were taken every 30 seconds with an Etaluma LS720 microscope using a 20× phase-contrast objective.

Additional methodologies

The Supplementary Methods section of the online supplement contain detailed procedures of the above-described techniques and description of rotational thromboelastometry, knockdown

procedures with siRNA and lentiviral shRNA, ELISA, real-time quantitative polymerase chain reaction, immunofluorescent imaging, and Western blotting.

Statistical analysis

Data are presented as mean ± SD, and statistics were performed using GraphPad Prism 7. Statistical analysis was performed as described in the figure legends. For comparisons between two groups, an unpaired Student's t test was used if data were normally distributed based on the Shapiro-Wilks test. If these data were not distributed normally, a Mann-Whitney U test was used. For comparisons with more than two groups, two-way ANOVA with Grenhouse-Geisser correction was used, followed by Tukey's or Sidak's post hoc for multiple comparisons when the P value for interaction was less than 0.05. Pearson and Spearman tests were performed for correlation analysis. $P < 0.05$ was considered significant.

Table 1. Clinical group characteristics of controls and CTEPH patients used for PAEC isolation

	CTEPH (n=18)	Control (n=8)	iPAH (n = 5)
Sex (M/F)	13/5	3/5	2/3
Age (years)	62.3 ± 11.9	55.7 ± 16.4	43.6 ± 20.0
mPAP (mmHg)	46.2 ± 11.5	N/A	76.8 ± 26.8
PVR (dyn/s/cm^{-5})	548.5 ± 233.6	N/A	1178.1 ± 490.2
CO (L/min)	5.3 ± 0.9	N/A	4.4 ± 0.7
SvO_2 (%)	63.3 ± 12.6	N/A	51.5 ± 7.8

CTEPH = chronic thromboembolic pulmonary hypertension; iPAH = idiopathic pulmonary arterial hypertension; mPAP = mean pulmonary artery pressure; PVR = pulmonary vascular resistance; CO = cardiac output; SvO_2 = mixed venous oxygen saturation; N/A = not available.

Results

VWF levels are upregulated in CTEPH plasma and pulmonary endothelium

To study the role of VWF in chronic pulmonary thrombosis, we used plasma, pulmonary artery tissue, and isolated endothelial cells from patients who underwent PEA (the surgical treatment for CTEPH), control subjects, and patients with idiopathic pulmonary arterial hypertension without pulmonary thrombosis (iPAH). Baseline characteristics of the patients in whom plasma VWF levels were determined are summarized in Table E1, while baseline characteristics of patients from whom PAECs were isolated are summarized in Table 1. Patients with CTEPH were more often male, which is in line with previous observations that more males undergo PEA[19].

Elevated circulating VWF levels are acknowledged in CTEPH[10,20,21] and were confirmed using the plasma of patients from our hospital (**Figure 1A**). As heterogeneity of the endothelium between different vascular beds confers regional variations of VWF mRNA expression[22], we performed fluorescent in situ hybridization of VWF in formalin-fixed and paraffin-embedded human pulmonary artery tissue from patients with CTEPH and control subjects to study VWF expression in CTEPH (**Figure 1B**). Endothelial VWF RNA was identified with a CD31 counterstain, and nuclear and endothelial

expression was quantified. In situ hybridization showed elevated expression of VWF RNA in the endothelium of patients with CTEPH compared with that from control subjects (**Figure 1C**), suggesting a role for VWF in chronic thrombosis.

To investigate the underlying mechanism of increased VWF expression in CTEPH endothelium, PAECs were isolated from thrombus-free regions of the intima layer of the third or fourth generation of the pulmonary artery from PEA material (**Figures 1D** and **1E**)[23]. Increased endothelial VWF protein and mRNA expression was maintained in isolated CTEPH-PAEC after five to six passages of culture. CTEPH-PAEC showed a 2.5-fold increase in VWF release after activation with histamine compared with PAEC from control subjects (Figure 1F). The higher VWF release was paralleled by a higher level of intracellular VWF under basal conditions (**Figure 1G**), as well as a fivefold increase in VWF expression at mRNA level in CTEPH-PAEC, which was not observed in iPAH-PAEC (**Figure 1H**; Figure E1A). This is in line with plasma studies showing that plasma levels of VWF are elevated in CTEPH but not in PAH[10]. Given the higher pulmonary artery pressures in iPAH-PAEC donors than in CTEPH-PAEC donors (**Table 1**), it is unlikely that the increase in VWF RNA expression is pressure driven. These data indicate that the increased VWF levels in the pulmonary endothelium in patients with CTEPH are mainly driven by a constitutional elevation of VWF transcription, which is specifically observed in CTEPH.

PAECs from patients with CTEPH show enhanced primary hemostasis

Pulmonary artery thrombosis was studied in vitro with a humanized culture model by perfusion of fresh whole blood or isolated platelets over PAEC isolated from patients with CTEPH or control subjects (**Figure 1E**). Perfusion of whole blood revealed a 1.5-fold increase of platelet adhesion and fibrin deposition in CTEPH-PAEC compared with control-PAEC upon histamine stimulation (**Figures 2A–2C**), suggesting increased thrombosis in patients with CTEPH.

To investigate whether this thrombosis is driven by primary or secondary hemostasis, we performed rotational thromboelastometry of whole blood from patients with CTEPH. Anticoagulation treatment of these patients was switched to low-molecular-weight heparins (LMWH) at least 3 days before surgery, and blood was drawn when patients were free from therapeutic LMWH for at least 24 hours. Activation of intrinsic and extrinsic coagulation, fibrin formation, and fibrinolysis showed values within the healthy reference range[2], supporting a central role for primary hemostasis in CTEPH (**Figure 2D**). To confirm this hypothesis, freshly isolated healthy platelets were perfused over PAEC monolayers from patients with CTEPH and control subjects. Platelets barely bound to unstimulated PAEC, but adhesion was enhanced with histamine stimulation (**Figures 2E** and **2F**; Figure E1B). Quantification of the total area covered by platelets over time showed a 1.5-fold increase in adhesion on CTEPH-PAEC compared with that from control subjects (**Figure 2G**). This effect was not observed on PAECs isolated from patients with iPAH, where total platelet adhesion was similar to that from control subjects (Figure E1C). This suggests a specific phenotype in CTEPH-PAECs that promotes platelet adhesion upon endothelial activation, which is correlated to endothelial VWF secretion (**Figure 2H**).

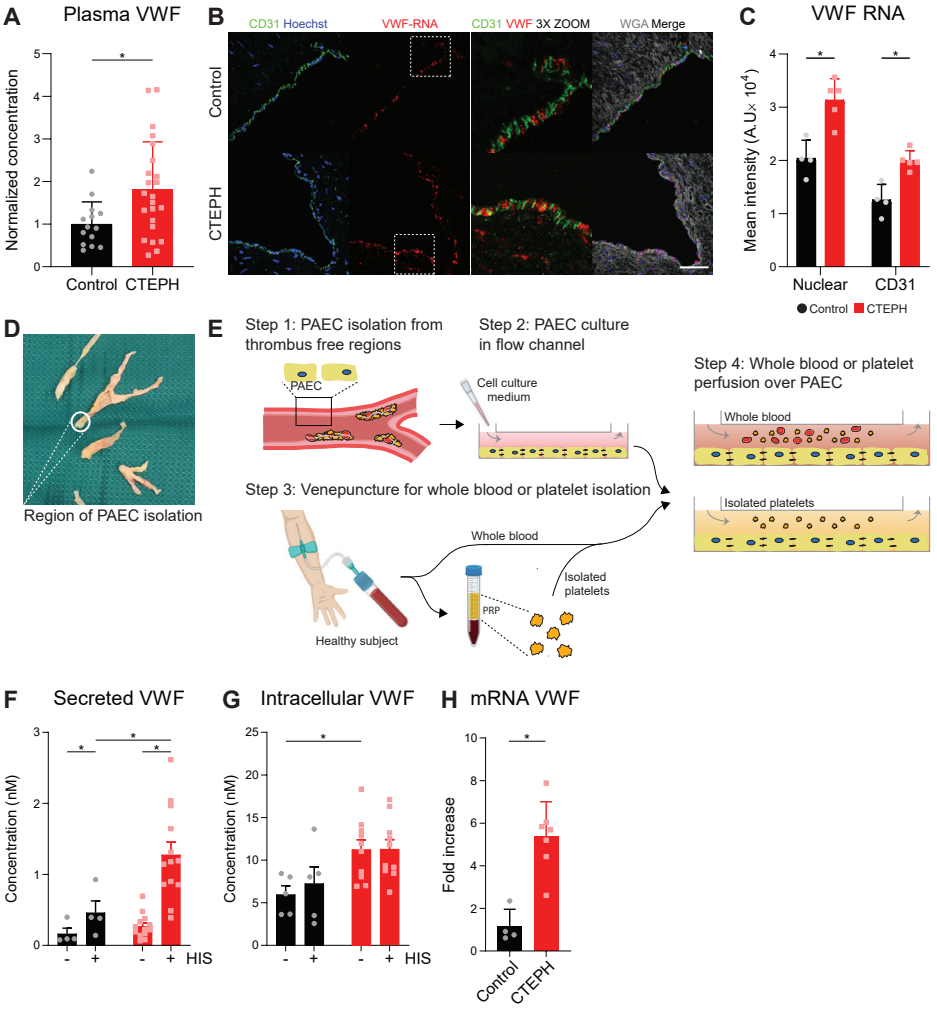

Figure 1. Von Willebrand factor (VWF) levels are upregulated in chronic thromboembolic pulmonary hypertension (CTEPH) plasma and pulmonary endothelium. (A) Plasma VWF levels from patients with CTEPH and healthy control subjects ($n_{control}$ = 14, n_{CTEPH} = 21). (B) Fluorescent images of fluorescent detection of VWF RNA (red) in formalin-fixed paraffin-embedded pulmonary artery tissue. Localized expression was determined with nuclei (blue), CD31 (green), or wheat germ agglutinin (WGA) (gray). Scale bar, 50 µm. (C) Comparison of mean fluorescent intensity of VWF RNA expression in nuclei and CD31-positive tissue between CTEPH and control. Each dot represents the average per donor; donor average includes five regions of interest for each left and right pulmonary artery ($n_{control}$ = 4, n_{CTEPH} = 5). (D) Example of pulmonary endarterectomy material for the isolation of CTEPH–pulmonary artery endothelial cells (PAEC). (E) Schematic overview of experimental procedure for studying in vitro pulmonary artery thrombosis. (F) Endothelial VWF release from PAEC with or without histamine activation ($n_{control}$ = 6, n_{CTEPH} = 13). (G) Protein expression of VWF from PAEC lysates measured by ELISA ($n_{control}$ = 5, n_{CTEPH} = 10). (H) Relative VWF gene expression in CTEPH-PAEC compared with control ($n_{control}$ = 4, n_{CTEPH} = 7). (*A*, *C*, *F*, and *G*) Data are presented as mean ± SD. Significance is indicated with *P < 0.05 after (A) unpaired Welch's t test, (*C* and *H*) Mann-Whitney U test, (*F*) two-way ANOVA with Grenhouse-Geisser correction for Tukey's multiple comparisons test when P-interaction <0.05. A.U. = arbitrary units; HIS = histamine; PRP = platelet-rich plasma.

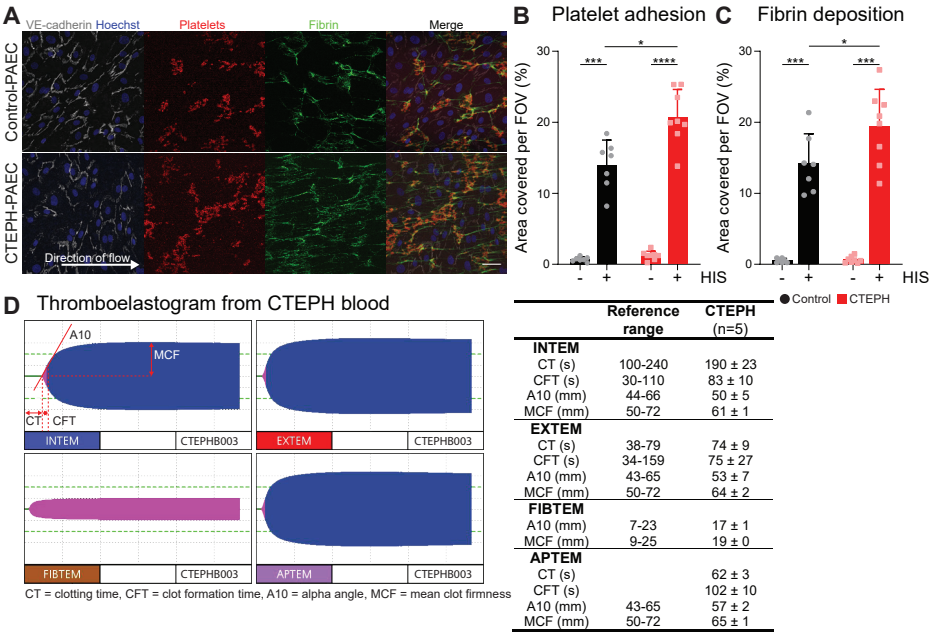

	Reference range	CTEPH (n=5)
INTEM		
CT (s)	100-240	190 ± 23
CFT (s)	30-110	83 ± 10
A10 (mm)	44-66	50 ± 5
MCF (mm)	50-72	61 ± 1
EXTEM		
CT (s)	38-79	74 ± 9
CFT (s)	34-159	75 ± 27
A10 (mm)	43-65	53 ± 7
MCF (mm)	50-72	64 ± 2
FIBTEM		
A10 (mm)	7-23	17 ± 1
MCF (mm)	9-25	19 ± 0
APTEM		
CT (s)		62 ± 3
CFT (s)		102 ± 10
A10 (mm)	43-65	57 ± 2
MCF (mm)	50-72	65 ± 1

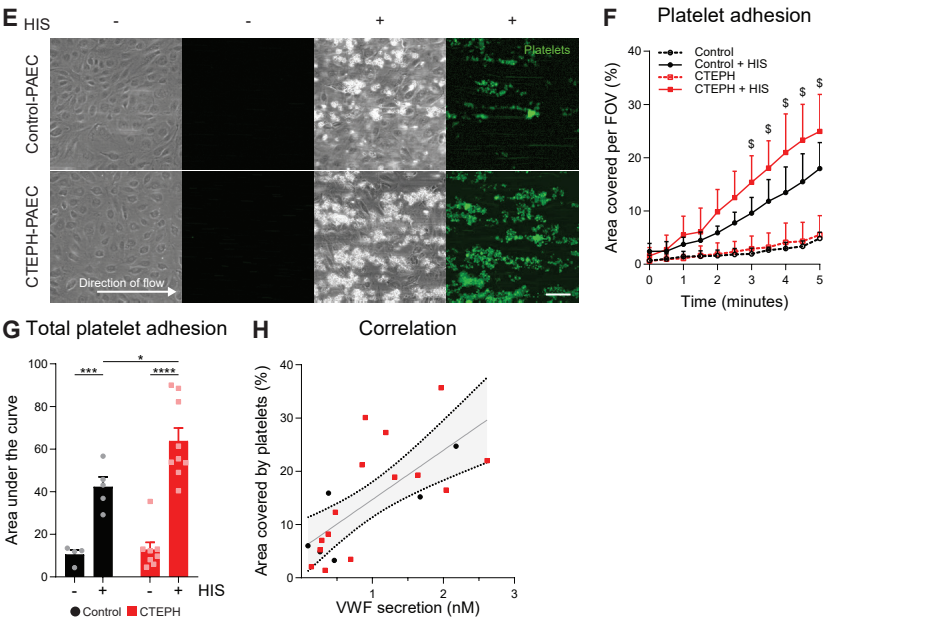

Figure 2. Pulmonary artery endothelial cells (PAEC) from patients with chronic thromboembolic pulmonary hypertension (CTEPH) show enhanced primary hemostasis. (A) Immunofluorescence images of thrombus formation on histamine-activated PAEC. Whole blood was perfused over PAEC for 5 minutes. Endothelial monolayers were characterized by VE-cadherin (gray), and thrombi were formed by Cd42b-labeled platelets (red) and Alexa488-fibrinogen (green); nuclei were stained with Hoechst (blue). Scale bar, 50 µm. (B) Quantification of the area covered by fluorescence platelets and (C) fibrin. Each dot represents the average of three regions of interest per donor ($n_{control}$ = 7, n_{CTEPH} = 8). (D) Thromboelastogram of citrated blood from a patient with CTEPH. CT, CFT, A10, and MCF were measured during intrinsic and extrinsic coagulation (INTEM and EXTEM), fibrin formation

(FIBTEM), and fibrinolysis (APTEM) (n_{CTEPH} = 5). Blood was taken from patients with CTEPH who were off anticoagulant therapy for at least 24 hours. **(E)** Bright-field and fluorescence images of adhered platelets (green) on PAEC monolayers with or without HIS activation. Platelets were perfused over PAEC for 5 minutes. Scale bar, 100 µm. **(F)** Time-dependent accumulation of adhered platelets on PAEC ($n_{control}$ = 4, n_{CTEPH} = 8). Significance compared with control PAEC is indicated with $P < 0.05. **(G)** Comparison of total adhered platelets by calculating the area under the curve. Each dot represents the average of three regions of interest per donor. **(H)** Correlation analysis between endothelial-released VWF and total platelet adhesion on PAEC. Statistics were performed with Pearson's rank correlation coefficient (n = 21; r = 0.736; P < 0.001). (*B*, *C*, *F*, and *G*) Data are presented as mean ± SD. Significance is indicated with *P < 0.05, ***P < 0.001, and ****P < 0.0001 after two-way ANOVA with Grenhouse-Geisser correction for (*B*, *C*, and *F*) Tukey's or (*G*) Sidak's multiple comparison test. A10 = clot firmness after 10 minutes; CFT = clot formation time; CT = clotting time; FOV = field of view; HIS = histamine; MCF = maximal clot firmness; VE = vascular endothelial; VWF = von Willebrand factor.

Excessive platelet adhesion on CTEPH-PAEC is mediated by VWF

Platelets bind to the A1 domain of VWF via the GPIβ receptor[25-27] and can interact with other ligands besides VWF, such as collagens, P-selectin, and integrins[28,29]. To verify a VWF-mediated mechanism, platelet binding was inhibited by using CLB-RAg35, a monoclonal antibody against the A1 domain of VWF[26]. The finding of increased VWF in CTEPH-PAEC was supported by a dose-dependent response to CLB-RAg35. One micromolar of CLB-RAg35 was sufficient to inhibit platelet adhesion to histamine-activated PAEC (**Figure 3A**). Increasing the concentration of CLB-RAg35 to, respectively, 10 or 100 µM did not have an additional effect in control-PAEC, while CTEPH-PAEC showed a further dose-dependent reduction in platelet adhesion (Figure 3B). These data show that platelet adhesion is regulated by VWF secretion and support a functional role of VWF in the increase platelet adhesion in CTEPH.

To further validate the functional relevance of endothelial VWF in PAEC, VWF expression was inhibited. PAEC transfected with silencing RNA or transduced with shRNA against VWF showed reduced VWF protein levels, leading to a loss of Weibel-Palade bodies and decreased VWF protein (Figures E2A–E2E). Knockdown of VWF significantly reduced platelet adhesion to CTEPH monolayers, with adhesion values almost reaching control levels (**Figures 3C** and **3D**; Figures E2F and E2G).

Increased NFκB2 expression in CTEPH-PAEC is associated with elevated VWF gene-expression

To elucidate possible signaling networks involved in the increased VWF transcription in CTEPH, we performed mass spectrometry-based quantitative proteomics to compare the proteomes of CTEPH and control PAEC. In total, 5,212 proteins were identified. An unbiased cluster analysis of the protein expression data showed separate clustering of CTEPH-PAEC and control, indicating different expression profiles (**Figure 4A**). Ninety-nine proteins were differentially expressed in CTEPH versus control (**Figure 4B**). From these, ICAM-1 and NFκB2 were the most significantly increased and with a high fold change. These two proteins are known to be involved in inflammation and form central nodes in the network of regulated proteins in our data (**Figure 4C**)[11]. In line with these findings, gene ontology enrichment analysis on the 99 upregulated proteins showed an increase in blood coagulation and cytokine signaling pathways (Figure E3A). Although enrichment of inflammatory pathways in CTEPH is acknowledged, its role in the etiology of the disease is unclear[2,30,31].

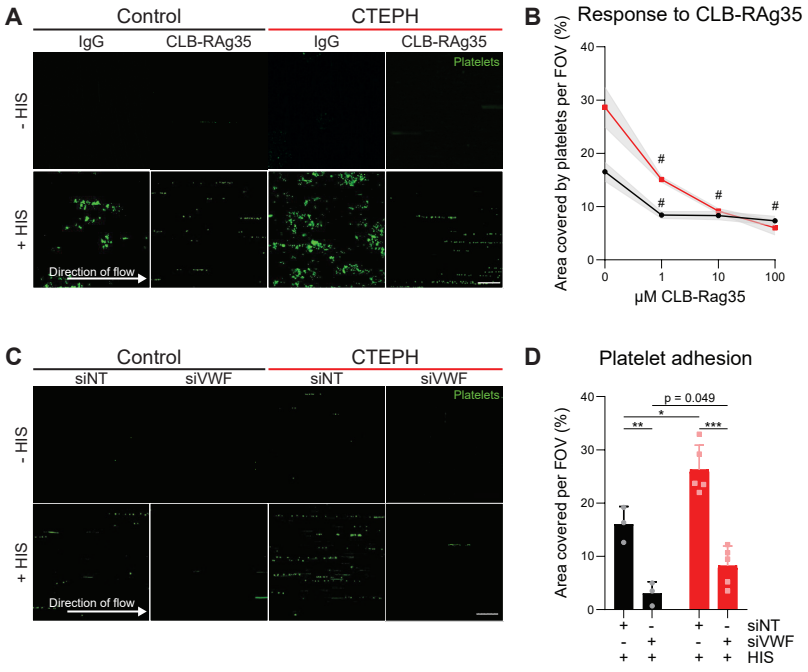

Figure 3. Excessive platelet adhesion on chronic thromboembolic pulmonary hypertension (CTEPH)–pulmonary artery endothelial cells (PAEC) is mediated by von Willebrand factor (VWF). (A) Fluorescence imaging of adhered platelets (green) on histamine-activated PAEC monolayers. Platelets were preincubated for 30 minutes with 10 μM CLB-RAg35 or IgG and perfused over PAEC for 5 minutes. Scale bar, 100 μm. (B) Dose-dependent response of adhered platelets on histamine-activated PAEC when platelets were preincubated with a dosage of 1, 10, or 100 μM CLB-RAg35. Each dot represents the average of three regions of interest per donor ($n_{control}$ = 3, n_{CTEPH} = 5). Data are presented as mean ± SD; statistics were performed with two-way ANOVA with Grenhouse-Geisser correction for Sidak's multiple comparison test; significance compared with nontreated platelets is indicated with #P < 0.05. (C) Fluorescence images of adhered platelets (green) on histamine-activated PAEC monolayers. PAECs were treated with siRNA against VWF or NT, and platelets were perfused for 5 minutes. Scale bar, 100 μm. (D) Comparison of total fluorescence of adhered platelets on PAEC. Each dot represents the average of three regions of interest per donor ($n_{control}$ = 3, n_{CTEPH} = 5). Data are presented as mean ± SD; statistics were performed with two-way ANOVA, Grenhouse-Geisser correction for Tukey's multiple comparisons test was performed when P-interaction <0.05, significance is indicated with *P < 0.05, **P < 0.01, and ***P < 0.001. FOV = field of view; HIS = histamine; NT = nontargeting.

The NF-κB transcription factor is a central mediator of inflammation and is involved in molecular pathways of inflammation and thrombosis, where NFκB2 is a central node in the network of regulated proteins in our data (**Figure 4C**)[11]. The NF-κB family forms a group of transcription factors that consists of five genes, NF-κB1 (p105/p50), RelA (p65), NFκB2 (p100/p52), RelB, and c-Rel[32]. These interact to form transcriptionally active homo- and heterodimeric complexes that bind the NF-κB consensus sequence, originally described as 5'–GGRRNNYYCC–3'[33], in target genes[34,35]. To validate our finding, we verified increased NFκB2 protein expression on Western blot (**Figure 4D**). Measuring gene expression of various NF-κB members, we found that NF-κB2, but not RelB or NF-κB1, was increased

at mRNA level in CTEPH-PAEC compared with control (Figures E3B–E3D). These data suggest the association of inflammation with CTEPH, dominated by NF-κB2.

To investigate the underlying mechanism of inflammation in thrombosis, we evaluated VWF expression and in vitro thrombosis after knockdown of various NF-κB members. Silencing of NFκB2 or RelB reversed VWF expression in CTEPH-PAEC while silencing of NF-κB1 did not affect VWF expression (**Figure 4E**). The increased expression of VWF in CTEPH endothelium is therefore specifically regulated by NF-κB2, while NF-κB1 is not involved in the transcriptional regulation of VWF.

Next, we studied the functional consequences of NFκB2 depletion for platelet adhesion. Inhibition of either NFκB2 or RelB resulted in a significant reduction in platelet adhesion in both CTEPH and control-PAEC (**Figure 4F**; Figure E3E), indicating that VWF-mediated platelet adhesion in CTEPH-PAEC is among others driven by NF-κB2.

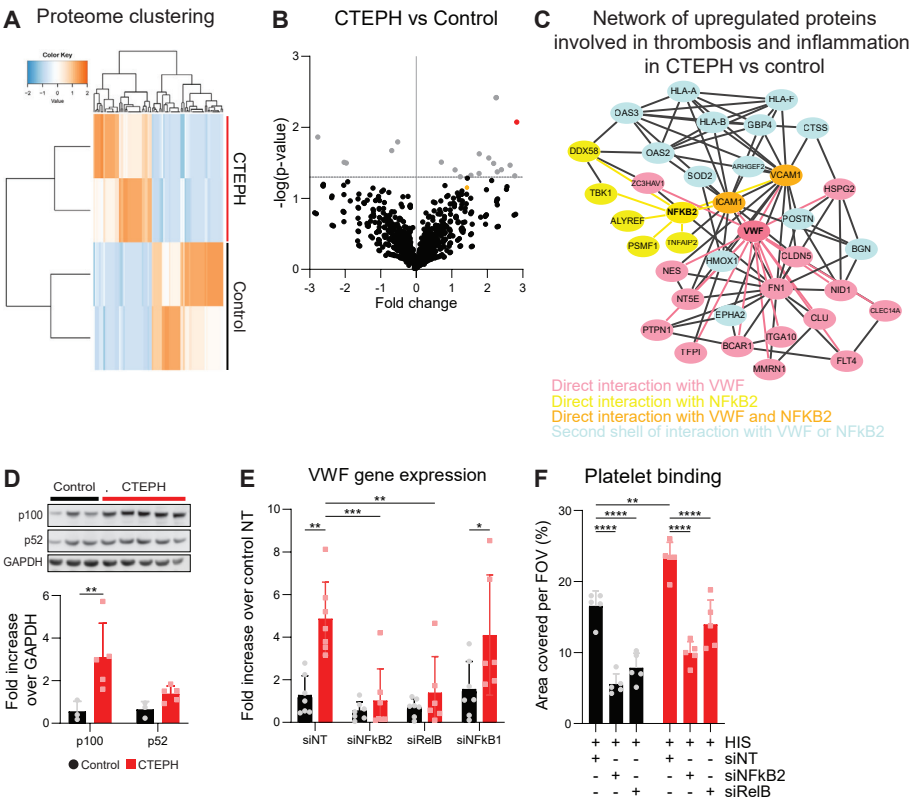

Figure 4. Increased nuclear factor (NF)-κB2 expression in chronic thromboembolic pulmonary hypertension (CTEPH)–pulmonary artery endothelial cells (PAEC) is associated with elevated von Willebrand factor (VWF) gene expression. **(A)** Unsupervised clustering and group comparison of all proteins that are differently expressed in CTEPH-PAEC compared with control ($n_{control}$ = 2, n_{CTEPH} = 2). **(B)** Volcano plot of up- and downregulated proteins of CTEPH-PAEC compared with control. Significant markers are displayed in gray, NFκB2 in red, and ICAM-1 in orange. **(C)** Protein interaction cluster of significantly upregulated proteins involved in thrombosis and

inflammation in CTEPH-PAEC compared with control. **(D)** Western blot with quantification of NFκB2 protein expression from whole PAEC lysates. **(E)** Relative VWF gene expression in CTEPH-PAEC with knockdown of NF-κB2, RelB, and NF-κB1 compared with control ($n_{control}$ = 6, n_{CTEPH} = 7). **(F)** Comparison of total fluorescence of adhered platelets on histamine-activated PAEC with siRNA against NF-κB2, RelB, or NT. Each dot represents the average of three regions of interest per donor ($n_{control}$ = 3, n_{CTEPH} = 5). (*D* and *E*) Data are presented as mean ± SD. Significance is indicated with *P < 0.05, **P < 0.01, ***P < 0.001, and ****P < 0.0001 after two-way ANOVA with Grenhouse-Geisser correction for (*A*) Sidak's or (*E* and *F*) Tukey's multiple comparison test. FOV = field of view; HIS = histamine; NT = nontargeting.

Epigenetic alterations in the VWF promoter support NFκB2 binding that enhances transcription

We showed that increased endothelial VWF is predominantly regulated at mRNA levels, mediated by NF-κB2. NF-κB is known to interact with the VWF promoter, thereby affecting VWF mRNA levels[35]. Because we demonstrated that the higher VWF transcription in CTEPH is preserved after isolation and culturing of PAEC for several passages, we explored the possibility that NFκB2 epigenetically regulates VWF gene transcription[36].

To test this hypothesis, we performed in silico analysis using the University of California Santa Cruz (UCSC) Genome Browser to interrogate a region 1013 bp upstream and 271 bp downstream the TCA transcription start site (TSS) of VWF[37]. In endothelial cells, we found strong histone trimethylation (H3K27me3, transcription repressive) and histone acetylation (H3K27Ac, transcription permissive)[38] downstream of the transcription start site around exon 1; strong histone acetylation was observed around the TSS, while >1 kbp upstream the TSS, hardly any histone modification was found. Furthermore, putative binding sites for NF-κB were found at -803 bp and +71 bp from the TSS (**Figure 5A**)[37]. These in silico analyses suggest that most epigenetic modification and NFκB2 binding occurs around and downstream of the VWF TSS.

To validate these in silico findings, chromatin immunoprecipitation was performed for H3K27me3, H3K27Ac, and NFκB2 in CTEPH versus control PAEC. Primers were designed for the region downstream of the VWF-TSS covering exon 1 (region 1), the region around the TSS (region 2), and a region >900 bp upstream of the TSS serving as control region (region 3) (**Figure 5A**). H3K27me3 was significantly reduced in CTEPH-PAEC compared with control both in regions 1 and 2 (**Figure 5B**), while significantly higher H3K27Ac was found in CTEPH in region 2 of the VWF promoter (**Figure 5C**). No histone modifications were observed in region 3, which aligns with the epigenetic profile of the VWF promoter as found in the UCSC browser (**Figure 5A**).

As these epigenetic modifications modulate the binding of transcription factors, we evaluated NFκB2 binding to the VWF promoter region. In silico analysis revealed NFκB2 binding sites close to the chosen primer regions, and chromatin immunoprecipitation revealed a 2- to 10-fold increased binding of NFκB2 to regions 1 and 2 along the VWF promoter in CTEPH-PAEC as compared with the control (**Figure 5D**). Altogether, these data show histone modification of the VWF promoter in CTEPH endothelium, allowing enhanced binding of NFκB2 to the promoter leading to constitutively higher transcription of VWF.

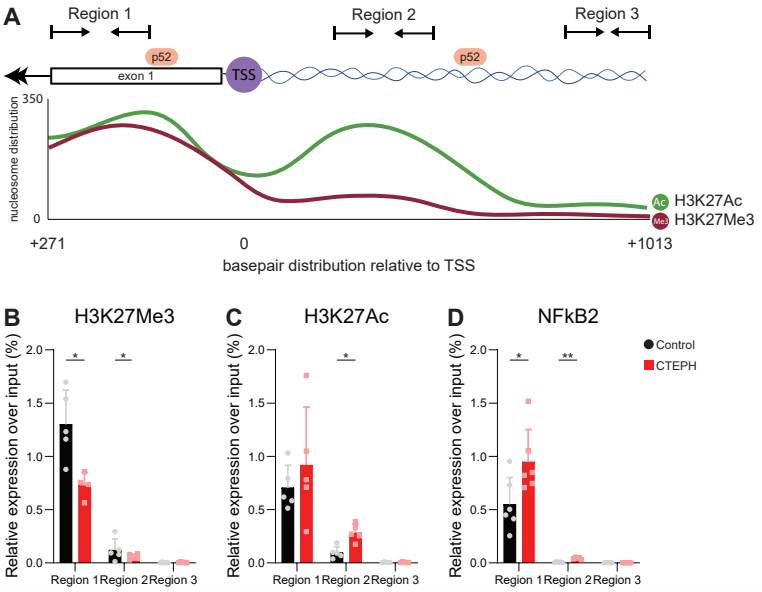

Figure 5. Epigenetic alterations in the von Willebrand factor (VWF) promoter support nuclear factor (NF)-κB2 binding that enhances transcription. **(A)** Illustration of the UCSC Genome Map of regions around the transcription start site (TSS) of VWF with NFκB2 binding sites. Primers were designed across the VWF promoter region, after the TSS (Region 1), close by TSS (Region 2), and early before TSS (Region 3). **(B)** Quantification of chromatin immunoprecipitation for H3K27Me3, **(C)** H3K27Ac, and **(D)** NFκB2 on nuclear extracts of CTEPH-PAEC compared with control ($n_{control} = 5$, $n_{CTEPH} = 5$). (*B* and *D*) Data are presented as mean ± SD. Significance is indicated with *P < 0.05 and **P < 0.01 after two-way ANOVA with Grenhouse-Geisser correction for Sidak's comparison test. CTEPH = chronic thromboembolic pulmonary hypertension; PAEC = pulmonary artery endothelial cells; UCSC = University of California Santa Cruz.

Discussion

Here, we show that the pulmonary endothelium in CTEPH recruits more platelets as a consequence of higher VWF transcription and secretion. The increase in VWF mRNA expression is driven by histone modification of the VWF promoter region and increased NFκB2 binding (**Figure 6**). These data provide the first experimental evidence that links increased VWF expression to an inflammatory stimulus. Our study explains increased VWF plasma levels in CTEPH and demonstrates the involvement of VWF in creating a local prothrombotic environment in the pulmonary arterial endothelium in CTEPH.

First, our findings reveal a novel mechanism for the control of VWF in chronic inflammatory conditions. To our knowledge, neither epigenetic regulation of the VWF promoter in the context of disease nor increased binding of inflammatory transcription factors to the VWF promoter have been reported previously. While established mechanisms of VWF regulation like the release from Weibel-Palade bodies and ADAMTS-13 cleavage mediate acute adaptations in VWF function[12], our current findings indicate that epigenetic regulation mediates changes in VWF levels in CTEPH.

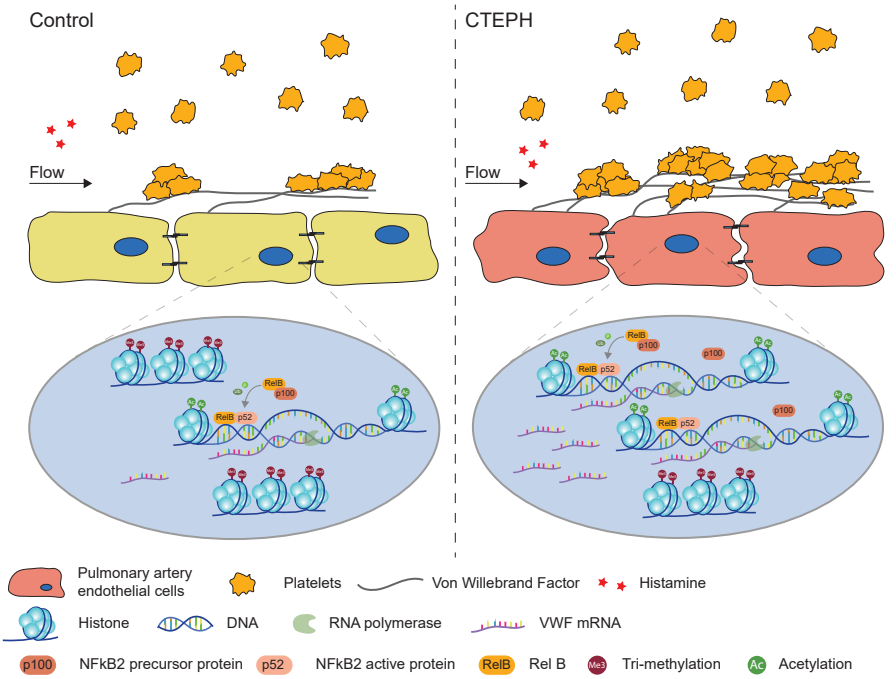

Figure 6. Illustration of the proposed mechanism of in situ thrombosis. Pulmonary artery endothelial cells from patients with chronic thromboembolic pulmonary hypertension (CTEPH) show enhanced platelet adhesion as a consequence of increased von Willebrand factor (VWF) expression. VWF transcription is enhanced by epigenetic modifications in its promoter. Reduced histone trimethylation (H3K27me3) and enhanced histone acetylation (H3K27Ac) allow more binding of nuclear factor (NF)-κB2 transcription factor, which increases transcription. P = phosphorylation; Ub = ubiquitination.

Inflammatory responses and elevated VWF plasma concentrations are acknowledged in patients with CTEPH[10,13,14], which is in line with our findings of an inflammation-mediated VWF-dependent mechanism of thrombosis in CTEPH-PAEC. Various studies have shown a prominent role of inflammation in the enhancement of fibrotic thrombus remodeling after a PE[13,39,40], but local inflammation is also associated with a prothrombotic activation of the vascular wall (e.g., neutrophils or macrophages)[41,42], as recently observed in coronavirus disease (COVID-19)[43]. Macrophages from severely ill patients induce an inflammatory response that contributes to pulmonary endothelial thrombosis, which is promoted by persistent supraphysiological levels of VWF[43,44].

It is well recognized that environmental and genetic factors play an important role in the onset and progression of various chronic diseases. Epigenetic modification is an important link between environmental factors and gene expression[45]. We observed epigenetic modifications by reduced trimethylation and enhanced acetylation of histone H3 reflected increased binding of NFκB2 transcription factor on the VWF promoter, although VWF transcription is primarily activated by GATA, Ets, H1, and NFAT5 transcription factors[46]. NFκB2 is not constitutively expressed and is activated in

inflammatory conditions only[47]. Although previous studies have established the presence of inflammation or enhanced coagulation in CTEPH, our study provides a mechanistic link between inflammation and local thrombosis, which rests upon the interaction of NFκB2 with the VWF promoter in the CTEPH endothelium.

The primary current treatment option for CTEPH is PEA, followed by lifelong anticoagulation[1,48]. Although this medication is supposed to prevent recurrent thromboembolic events after successful surgery, some patients still suffer from recurrent thromboembolic lesions[49]. This may be explained by the fact that anticoagulant drugs act on the coagulation cascade[50] when platelets have already been activated to form a stable aggregate. Our data reveal an endothelial VWF-mediated mechanism, where VWF levels are dependent on NFκB2 levels. NFκB2 inhibition may therefore serve as a therapeutic target to reduce inflammatory VWF-mediated thrombosis while the process of hemostasis is maintained.

This study introduces a novel method to study the early stages of thrombosis in humans, specifically CTEPH. For some time, the pathophysiology of CTEPH has remained elusive due to a lack of appropriate disease models[51]. Large animal models have provided valuable insight into the hemodynamic consequences of CTEPH but also have failed to reproduce the characteristic vascular lesions as observed in CTEPH, as prothrombotic conditions are difficult to mimic in these in vivo models[52]. The most commonly used thrombosis models involve mice with intravenous administration of clotting agents, such as collagen or thrombin, to induce acute PEs[53]. Although these models can be used to study clot resolution, both the artificial means of thrombus induction in these mouse models as well as the important differences between mice and humans in thrombus formation preclude the use of these models for the investigation of in situ thrombus formation. Furthermore, the main focus of the current study is to evaluate the link between the thrombogenic endothelium in CTEPH and epigenetic regulation of the VWF promoter. It is well established that VWF is the main ligand for platelets and is critical for thrombus development, as VWF-deficient mice do not form a stable thrombus[28,54,55]. However, specific epigenetic alteration of the specific VWF promoter cannot be captured in transgenic models, whereas pharmacological ways to induce epigenetic alteration (e.g., HDAC inhibitors) induce epigenetic changes in a wide array of genes. To overcome this, we have used a humanized in vitro platform of thrombosis that recapitulates the vascular intima layer of pulmonary arteries. For this, we use human-derived primary endothelial cells that accurately represent the characteristics of ECs in the lungs of patients[56].

To our knowledge, we are the first to report endothelium-platelet interaction under flow using endothelial cells derived from patients with CTEPH, and the current study demonstrates the model as a powerful tool to characterize and modulate endothelial function in relation to thrombosis. Considering the importance of VWF in thrombosis, we were able to interfere with VWF in human primary endothelial cells and could reverse the diseased endothelial phenotype to a control condition.

The relevance of this model and the mechanisms elucidated by the model were validated in tissue sections by RNA in situ hybridization experiments, demonstrating a similar increase in VWF levels in vitro and in vivo. Our humanized model allows for various forms of interference to evaluate therapeutic strategies for CTEPH. Finally, as this model well captured human endothelium–platelet interaction, it may be used to study endothelium–platelet interaction in other pathological conditions, and therefore has its relevance beyond CTEPH.

Besides thrombosis, endothelial cells play a key role in thrombus resolution via angiogenesis and recanalization. This study focused on VWF regulation in PAEC and VWF effects on platelet adhesion. Our model is limited by its inability to observe the progression of thrombus formation and resolution that causes persistent clot formation. Although impaired fibrinolysis and angiogenesis are generally more accepted hypotheses of the pathophysiology of CTEPH, initial clot formation typically starts with endothelial activation that can be easily studied in our model (57). The strength of this study is the use of primary isolated cells, even though this approach has its limitations. Although CTEPH-PAECs were derived from thrombus-free PEA material, the cells may have been affected by thrombotic events. However, it is impossible to obtain completely uninvolved pulmonary vessels from patients with CTEPH. Furthermore, control-PAECs were isolated from lobectomy material, mostly from patients with a lung malignancy. We made sure to only include material distal from the tumor, and excluded patients with prior thromboembolic events and/or severe cardiovascular comorbidities.

Finally, this study suggests that CTEPH is not merely the consequence of embolism but that also local thrombosis contributes to CTEPH. Although our results do not prove that in situ thrombosis is the primary source of clot formation in CTEPH, they do suggest that it contributes to the disease. Whether our finding is a primary event in the pulmonary endothelium that results in in situ thrombosis or whether it is a consequence of nonresolving emboli needs to be determined. Additional follow-up questions that need to be addressed in future studies are which upstream events invoke the observed epigenetic changes in CTEPH and whether the phenomenon of chronic VWF derangement is also present in other cardiovascular diseases.

In conclusion, this study reveals enhanced platelet aggregation on CTEPH-derived endothelial cells, resulting from epigenetic modifications to the VWF promoter and increased binding of the transcription factor NFκB2 to the VWF promoter. VWF-mediated in situ thrombosis may therefore play an important role in the development and/or progression of CTEPH. Interference at the NFκB2 or VWF level reduced thrombocyte aggregation, yielding novel targets for therapies in CTEPH (**Figure 6**).

References

1. Wilkens H, Konstantinides S, Lang IM, Bunck AC, Gerges M, Gerhardt F, et al. Chronic thromboembolic pulmonary hypertension (CTEPH): updated recommendations from the Cologne Consensus Conference 2018. Int J Cardiol 2018;272S:69–78.
2. Yan L, Li X, Liu Z, Zhao Z, Luo Q, Zhao Q, et al. Research progress on the pathogenesis of CTEPH. Heart Fail Rev 2019;24:1031–1040.
3. Pepke-Zaba J, Delcroix M, Lang I, Mayer E, Jansa P, Ambroz D, et al. Chronic thromboembolic pulmonary hypertension (CTEPH): results from an international prospective registry. Circulation 2011;124:1973–1981.
4. Lang IM, Madani M. Update on chronic thromboembolic pulmonary hypertension. Circulation 2014;130:508–518.
5. Braams NJ, Boon G, de Man FS, van Es J, den Exter PL, Kroft LJM, et al. Evolution of CT findings after anticoagulant treatment for acute pulmonary embolism in patients with and without an ultimate diagnosis of chronic thromboembolic pulmonary hypertension. Eur Respir J 2021;58:2100699.
6. Peyvandi F, Garagiola I, Baronciani L. Role of von Willebrand factor in the haemostasis. Blood Transfus 2011;9:s3–s8.
7. Lenting PJ, Christophe OD, Denis CV. von Willebrand factor biosynthesis, secretion, and clearance: connecting the far ends. Blood 2015;125:2019–2028.
8. Tomaiuolo M, Brass LF, Stalker TJ. Regulation of platelet activation and coagulation and its role in vascular injury and arterial thrombosis. Interv Cardiol Clin 2017;6:1–12.
9. Edvardsen MS, Hindberg K, Hansen ES, Morelli VM, Ueland T, Aukrust P, et al. Plasma levels of von Willebrand factor and future risk of incident venous thromboembolism. Blood Adv 2021;5:224–232.
10. Newnham M, South K, Bleda M, Auger WR, Barberà JA, Bogaard H, et al. The ADAMTS13-VWF axis is dysregulated in chronic thromboembolic pulmonary hypertension. Eur Respir J 2019;53:1801805.
11. Mussbacher M, Salzmann M, Brostjan C, Hoesel B, Schoergenhofer C, Datler H, et al. Cell type-specific roles of NF-κB linking inflammation and thrombosis. Front Immunol 2019;10:85
12. Chen J, Chung DW. Inflammation, von Willebrand factor, and ADAMTS13. Blood 2018;132:141–147.
13. Zabini D, Heinemann A, Foris V, Nagaraj C, Nierlich P, Bálint Z, et al. Comprehensive analysis of inflammatory markers in chronic thromboembolic pulmonary hypertension patients. Eur Respir J 2014;44:951–962.
14. Skoro-Sajer N, Gerges C, Gerges M, Panzenböck A, Jakowitsch J, Kurz A, et al. Usefulness of thrombosis and inflammation biomarkers in chronic thromboembolic pulmonary hypertension-sampling plasma and surgical specimens. J Heart Lung Transplant 2018;37:1067–1074.
15. Manz XD, Pan X, Symersky P, Majolée J, Hordijk P, Voorberg J, et al. Elevated von Willebrand factor expression in the activated pulmonary endothelium of chronic thromboembolic pulmonary hypertension patients enhances platelet adhesion [abstract]. Eur Respir J 2020;56:1551.
16. Manz XD, Pan X, Symersky P, Majolee J, Tura O, Hordijk P, et al. The activated pulmonary endothelium of chronic thromboembolic pulmonary hypertension patients exhibits elevated platelet adhesion [abstract]. Am J Respir Crit Care Med 2020;201:A2044.
17. Manz XD, Albers HJ, Symersky P, Aman J, van der Meer AD, Bogaard HJ, et al. In vitro microfluidic disease model to study whole blood-endothelial interactions and blood clot dynamics in real-time. J Vis Exp 2020;159. DOI: 10.3791/61068
18. Smeets MWJ, Mourik MJ, Niessen HWM, Hordijk PL. Stasis promotes erythrocyte adhesion to von Willebrand factor. Arterioscler Thromb Vasc Biol 2017;37:1618–1627.
19. Barco S, Klok FA, Konstantinides SV, Dartevelle P, Fadel E, Jenkins D, et al. Sex-specific differences in chronic thromboembolic pulmonary hypertension: results from the European CTEPH registry. J Thromb Haemost 2020;18:151–161.
20. Wong CL, Szydlo R, Gibbs S, Laffan M. Hereditary and acquired thrombotic risk factors for chronic thromboembolic pulmonary hypertension. Blood Coagul Fibrinolysis 2010;21:201–206.
21. Bonderman D, Turecek PL, Jakowitsch J, Weltermann A, Adlbrecht C, Schneider B, et al. High prevalence of elevated clotting factor VIII in chronic thromboembolic pulmonary hypertension. Thromb Haemost 2003;90:372–376.
22. Smith JM, Meinkoth JH, Hochstatter T, Meyers KM. Differential distribution of von Willebrand factor in canine vascular endothelium. Am J Vet Res 1996;57:750–755.
23. Mahmud E, Madani MM, Kim NH, Poch D, Ang L, Behnamfar O, et al. Chronic thromboembolic pulmonary hypertension: evolving therapeutic approaches for operable and inoperable disease. J Am Coll Cardiol 2018;71:2468–2486.

24. Crochemore T, Piza FMT, Rodrigues RDR, Guerra JCC, Ferraz LJR, Corrêa TD. A new era of thromboelastometry. Einstein (Sao Paulo) 2017;15:380–385.
25. Reininger AJ, Heijnen HF, Schumann H, Specht HM, Schramm W, Ruggeri ZM. Mechanism of platelet adhesion to von Willebrand factor and microparticle formation under high shear stress. Blood 2006;107:3537–3545.
26. Sixma JJ, Sakariassen KS, Stel HV, Houdijk WP, In der Maur DW, Hamer RJ, et al. Functional domains on von Willebrand factor: recognition of discrete tryptic fragments by monoclonal antibodies that inhibit interaction of von Willebrand factor with platelets and with collagen. J Clin Invest 1984;74:736–744.
27. Bridges DJ, Bunn J, van Mourik JA, Grau G, Preston RJ, Molyneux M, et al. Rapid activation of endothelial cells enables plasmodium falciparum adhesion to platelet-decorated von Willebrand factor strings. Blood 2010;115:1472–1474.
28. Denis CV, Wagner DD. Platelet adhesion receptors and their ligands in mouse models of thrombosis. Arterioscler Thromb Vasc Biol 2007;27:728–739.
29. Stegner D, Nieswandt B. Platelet receptor signaling in thrombus formation. J Mol Med (Berl) 2011;89:109–121.
30. Matthews DT, Hemnes AR. Current concepts in the pathogenesis of chronic thromboembolic pulmonary hypertension. Pulm Circ 2016;6:145–154.
31. Xi Q, Liu Z, Song Y, Gan H, Huang Z, Luo Q, et al. Proteomic analyses of endarterectomized tissues from patients with chronic thromboembolic pulmonary hypertension. Cardiology 2020;145:48–52.
32. Oeckinghaus A, Ghosh S. The NF-kappaB family of transcription factors and its regulation. Cold Spring Harb Perspect Biol 2009;1:a000034.
33. Wong D, Teixeira A, Oikonomopoulos S, Humburg P, Lone IN, Saliba D, et al. Extensive characterization of NF-κB binding uncovers non-canonical motifs and advances the interpretation of genetic functional traits. Genome Biol 2011;12:R70.
34. Wynants M, Vengethasamy L, Ronisz A, Meyns B, Delcroix M, Quarck R. NF-κB pathway is involved in CRP-induced effects on pulmonary arterial endothelial cells in chronic thromboembolic pulmonary hypertension. Am J Physiol Lung Cell Mol Physiol 2013;305:L934–L942.
35. Keightley AM, Lam YM, Brady JN, Cameron CL, Lillicrap D. Variation at the von Willebrand factor (VWF) gene locus is associated with plasma VWF:Ag levels: identification of three novel single nucleotide polymorphisms in the VWF gene promoter. Blood 1999;93:4277–4283.
36. Bannister AJ, Kouzarides T. Regulation of chromatin by histone modifications. Cell Res 2011;21:381–395.
37. Collins CJ, Underdahl JP, Levene RB, Ravera CP, Morin MJ, Dombalagian MJ, et al. Molecular cloning of the human gene for von Willebrand factor and identification of the transcription initiation site. Proc Natl Acad Sci USA 1987;84:4393–4397.
38. Miller JL, Grant PA. The role of DNA methylation and histone modifications in transcriptional regulation in humans. Subcell Biochem 2013;61:289–317.
39. Sharma S, Hofbauer TM, Ondracek AS, Chausheva S, Alimohammadi A, Artner T, et al. Neutrophil extracellular traps promote fibrous vascular occlusions in chronic thrombosis. Blood 2021;137:1104–1116.
40. Simonneau G, Torbicki A, Dorfmüller P, Kim N. The pathophysiology of chronic thromboembolic pulmonary hypertension. Eur Respir Rev 2017;26:160112.
41. Corbett V, Hassouna H, Girgis R. In situ thrombosis of the pulmonary arteries: an emerging new perspective on pulmonary embolism. Med Student Res J 2015;4:54–58.
42. Gaertner F, Massberg S. Blood coagulation in immunothrombosis: at the frontline of intravascular immunity. Semin Immunol 2016;28:561–569.
43. Hoepel W, Chen H-J, Geyer CE, Allahverdiyeva S, Manz XD, de Taeye SW, et al. High titers and low fucosylation of early human anti-SARS-CoV-2 IgG promote inflammation by alveolar macrophages. Sci Transl Med 2021;13:eabf8654.
44. Ward SE, Curley GF, Lavin M, Fogarty H, Karampini E, McEvoy NL, et al.; Irish COVID-19 Vasculopathy Study (ICVS) Investigators. von Willebrand factor propeptide in severe coronavirus disease 2019 (COVID-19): evidence of acute and sustained endothelial cell activation. Br J Haematol 2021;192:714–719.
45. Wang G, Walker SO, Hong X, Bartell TR, Wang X. Epigenetics and early life origins of chronic noncommunicable diseases. J Adolesc Health 2013; 52(Suppl 2)S14–S21.
46. Xiang Y, Hwa J. Regulation of VWF expression, and secretion in health and disease. Curr Opin Hematol 2016;23:288–293.
47. Sun SC. The non-canonical NF-κB pathway in immunity and inflammation. Nat Rev Immunol 2017;17:545–558.
48. Gavilanes-Oleas FA, Alves JL Jr, Fernandes CJC, Prada LFL, Salibe Filho W, Terra Filho M, et al. Use of direct oral anticoagulants for chronic thromboembolic pulmonary hypertension. Clinics (São Paulo) 2018;73:e216.

49. Cannon JE, Su L, Kiely DG, Page K, Toshner M, Swietlik E, et al. Dynamic risk stratification of patient long-term outcome after pulmonary endarterectomy: results from the United Kingdom National Cohort. Circulation 2016;133:1761–1771.
50. Mekaj YH, Mekaj AY, Duci SB, Miftari EI. New oral anticoagulants: their advantages and disadvantages compared with vitamin K antagonists in the prevention and treatment of patients with thromboembolic events. Ther Clin Risk Manag 2015;11:967–977.
51. Mercier O, Fadel E. Chronic thromboembolic pulmonary hypertension: animal models. Eur Respir J 2013;41:1200–1206.
52. Stam K, Clauss S, Taverne YJHJ, Merkus D. Chronic thromboembolic pulmonary hypertension: what have we learned from large animal models. Front Cardiovasc Med 2021;8:574360.
53. Jagadeeswaran P, Cooley BC, Gross PL, Mackman N. Animal models of thrombosis from zebrafish to nonhuman primates: use in the elucidation of new pathologic pathways and the development of antithrombotic drugs. Circ Res 2016;118:1363–1379.
54. Brill A, Fuchs TA, Chauhan AK, Yang JJ, De Meyer SF, Köllnberger M, et al. von Willebrand factor-mediated platelet adhesion is critical for deep vein thrombosis in mouse models. Blood 2011;117:1400–1407.
55. Chen J, Tan K, Zhou H, Lo HF, Tronik-Le Roux D, Liddington RC, et al. Modifying murine von Willebrand factor A1 domain for in vivo assessment of human platelet therapies. Nat Biotechnol 2008;26:114–119.
56. Comhair SA, Xu W, Mavrakis L, Aldred MA, Asosingh K, Erzurum SC. Human primary lung endothelial cells in culture. Am J Respir Cell Mol Biol 2012;46:723–730.
57. Yau JW, Teoh H, Verma S. Endothelial cell control of thrombosis. BMC Cardiovasc Disord 2015;15:130.

Supplementary materials

Immuno-Fluorescent In Situ Hybridization (iFISH)

Formalin fixed and paraffin embedded surgical specimen of pulmonary artery tissue samples were acquired from the Biobank Pathology (Amsterdam UMC, location VU University Medical Center, The Netherlands), and RNA fluorescent in situ hybridization was performed using RNAscope® Multiplex Fluorescent Reagent Kit v2 (Advanced Cell Diagnostics, #323135). Briefly, 4 µm sections were cut and baked at a 60°C oven for 1 hour. Samples were pre-treated by deparaffinization, dehydration, and 20 minutes target retrieval using RNAscope®Co-Detection Target Retrieval (Advanced Cell Diagnostics, #323165). RNA probe against VWF (Advanced Cell Diagnostics, #560461) was incubated for 2 hours at 40°C, and amplification was performed according to manufacturer's protocol. Opal570 (Akoya, #FP1488001KT) was used to detect fluorescent signal. After hybridization, cells were washed three times in PBS and immunofluorescence was performed. Samples were blocked with 1% Donkey serum (Sigma-Aldrich, #D9663), and stained for CD31 (1:100, Santa Cruz C-20, #sc-1505), WGA (1:200, Invitrogen, #W32466) and nuclei. Tissue slides were mounted with Mowiol (Sigma-Aldrich, #81381) supplemented with DABCO (Sigma-Aldrich, #290734). Confocal images were acquired with Nikon A1R and signal was quantified in at least five different ROI per donor. Images were blinded and automatically analyzed by using a macro to measure fluorescent intensity in Image J. This macro creates first a mask of CD31 positive areas, and secondly a nuclear mask. VWF mean fluorescent intensity was measured within this nuclear and CD31 mask to distinguish nuclear and cytoplasm VWF. The quantified values indicate average intensity per area.

Rotational thromboelastometry

Blood samples from CTEPH patients were analyzed for blood coagulation disorders with rotational thromboelastometry (ROTEM©, Pentapharm GmbH, Munich, Germany). Clotting time (CT), clot formation time (CFT), clot firmness after 10 minutes (A10) and maximal cloth firmness (MCF) were measured according to the manufacturer's procedures. Intrinsic and extrinsic blood coagulation were measured with INTEM and EXTEM, platelet function and fibrinolysis were tested with FIBTEM and EXTEM (1).

Primary cell isolation

Pulmonary artery endothelial cells (PAEC) were isolated from resected pulmonary artery tissue according to the previously published protocol[2]. In brief, control tissue was obtained from lobectomies of suspected or proven lung malignancies (non-PH control) and CTEPH tissue was obtained from pulmonary endarterectomy (PEA) material, both surgeries performed at the Amsterdam UMC, location VU University Medical Center, The Netherlands. PAEC were isolated by carefully scraping the endothelial layer onto fibronectin-coated (5 µg/mL) CellBIND culture dishes (Corning, #3295). PAEC were cultured in endothelial cell medium (ECM, ScienCell, #1001) supplemented with 1% Penicillin/Streptomycin, 1% endothelial cell growth supplement (ECGS), 5% fetal bovine serum (FBS), and 1% non-essential amino acids (NEAA, Biowest, #X055-100). further

referred to as cECM. Isolated cells were maintained in a physiological environment at 37°C with 5% CO2. Cells were expanded on 0.1% gelatin coated culture flasks until passage 4-6 was reached for experiments.

siRNA transfection

PAEC were grown until 80% confluence and medium was refreshed 24 hours before transfection. ON-TARGETplus human siRNA against VWF (#LQ-009754-00-0002), NFκB2 (#LQ-003918-00-0005), RelB (#LQ-004767-00-0005), NFκB1 (#LQ-003520-00-0005) and non-targeting control (NT, #D-001810-10-05) were purchased from Dharmacon (Supplementary Table 2). PAEC were transfected with a final concentration of 25 nM siRNA using DharmaFECT1 (Dharmacon, #T2001-03). Transfection was performed overnight with 20% new born calf serum (NBCS) in ECM. Medium was refreshed with cECM the next day. Cells were used for experiments at least 72 hours after transfection.

Lentiviral shRNA knockdown

Pre-tested short hairpin RNA (shRNA) constructs from Sigma MISSION® TRC-Hs 2.0 shRNA library were used in VWF knockdown experiments[3]. The results shown were obtained with TRCN0000373864, targeting VWF RefSeq NM_000552.3 and TRCN0000SHC002 as non-targeting negative control (Supplementary Table 2). shRNA constructs were packed into lentiviral particles with second-generation packaging plasmids (pHDM-G, pHDM-HgpM2, pRC-CMV-Rev1b, and pHDM-TAT1B) in HEK293T cells after transfection using TransIT®LT1 (Mirus, #MIR2300) according to manufacturer's instructions. Virus-containing supernatant was collected at 48 and 72 hours post transfection and filtered through a 0.45 µm polyvinylidene fluoride filter (Whatman, #10462100). At 80% confluency, PAEC were infected with the virus containing supernatant at a 1:6 virus:cECM ratio. After 24 hours, medium was changed to cECM and infected cells were selected for 72 hours with puromycin (Gibco, #A11138-03), before used for experiments.

Platelet isolation

Platelets were isolated as previously described[4]. In short, platelet rich plasma (PRP) was obtained by centrifugation at 150 ×g for 15 minutes. Subsequently, 10% acid citrate dextrose (85 mM sodium citrate, 65 mM citric acid and 100 mM D-glucose, pH 4.5) was added to PRP prior to centrifugation at 2000 ×g for 5 minutes. The platelet pellet was washed with wash buffer (36 mM citric acid, 103 mM NaCl, 5mM KCl, 5 mM EDTA, 56 mM D-glucose, 0.35% bovine serum albumin (BSA), pH 6.5), and fluorescently tagged with calcein AM (1:1000, Invitrogen, #C3099) for 10 minutes at 37°C. Platelets were suspended in HEPES+ buffer (132 mM NaCl, 20 mM HEPES, 6 mM KCl, 1 mM MgSO4 × 7 H2O, 1.2 mM K2HPO4 × 3 H2O, 2.5mM CaCl2, 5.5mM D-glucose, 1% BSA, pH 7.4) and allowed to equilibrate at 37°C to restore their function. If indicated, platelets were treated for 30 minutes with monoclonal antibody raised to the A1 domain of VWF (CLB-RAg-35, gifted from Sanquin, The Netherlands) prior to perfusion experiments.

Platelet adhesion under flow

PAEC were seeded in 0.1% gelatin-coated µ-Slide VI 0.4 ibiTreat flow slides (ibidi, #80606) and cultured for at least 7 days to form a stable monolayer. PAEC were starved for 1 hour in ECM supplemented with 1% FBS, and stimulated with 1 µM histamine (Sigma-Aldrich, #H7125) for 30 minutes prior to start of perfusion of platelets. Fluorescently labeled platelets were perfused over PAEC with a syringe pump (Word Precision Instruments, #AL4000) with a unidirectional shear rate of 2.5 dyne/cm2. Phase-contrast and fluorescent images of three chosen region of interest (ROI) were taken every 30 seconds with an Etaluma LS720 microscope using a 20X phase-contrast objective. Platelet adhesion was quantified in ImageJ by determining the area covered by platelets per Field of View (FOV). Images were blinded and automatically analyzed by using a macro to measure area covered by platelets in Image J.

Enzyme Linked Immunosorbent Assay (ELISA)

Supernatant of histamine stimulated PAEC was collected and VWF levels were measured as previously described[5]. In brief, a 96-well ELISA plate was coated with polyclonal anti-VWF (1:1000, Dako, #A0082) overnight at 4°C and subsequently blocked with 2% BSA for 2 hours at RT. Samples were loaded for 2 hours at RT and HRP-conjugated rabbit polyclonal anti-VWF (1:2500, Dako, #A0082) was used for detection of bound VWF. HRP activity was detected with substrate solution (1.1 M NaAc, TMB/DMSO, 30% H2O2) and the reaction was stopped with H2SO4. Normal plasma with a stock concentration of 50 nM VWF was used as a standard for determination of VWF levels, measured at 450 nm and 540 nm.

Real-Time (Quantative) Polymerase Chain Reaction (RT-qPCR)

PAEC were lysed in TRIzol (Invitrogen, #15596018) and RNA was isolated with Direct-zol RNA kit (Zymo Research, #R2051). Total RNA was reverse transcribed with iScript cDNA synthesis kit (BioRad, #1708890). RT-qPCR was performed in a C1000 Thermo Cycler (BioRad) using iQ SYBR Green (BioRad, #1708886) and specific primers for VWF, NFκB2, RelB, NFκB1, P0 and RPL27 were designed with NCBI Primer-BLAST (Supplementary Table 3). Threshold cycle values (Ct) were analyzed and expression was quantified using the 2−ddCt method.

Immunofluorescence imaging

PAEC were fixed with warm 4% paraformaldehyde (PFA) for 10 minutes at room temperature (RT). Cells were permeabilized with 0.2% Triton X-100 in PBS for 10 minutes and blocked with 1% BSA for 1 hour at RT. Cells were stained with VE-cadherin (1:200, Cell Signaling, D87F2, #2500), CD31 (1:200, Invitrogen, #37-0700) or VWF (1:200, SantaCruz, #14014) overnight at 4°C and fluorescently labelled secondary antibodies were added for 1 hour at RT. Actin fibers, nuclei and platelets were stained for 30 minutes at RT with Phalloidin (1:200, Cytoskeleton, #PHDN1-A), Hoechst (1:1000, Invitrogen, #H1399) and CD42b (Miltenyi Biotec, #130-100-186) respectively. In between incubation steps, cells were washed three times with PBS with 0.05%Tween. Coverslips were mounted with Mowiol (Sigma-

Aldrich, #81381) supplemented with DABCO (Sigma-Aldrich, #290734). Confocal images were acquired with Nikon A1R. Z-stacks of 3 µm were taken with 60X oil-immersion objective. Images were blinded and automatically analyzed by using a macro to measure fluorescent intensity in Image J.

Proteomics

Approximately 10 cm2 of PAEC were used for proteomics. Proteins were lysed in 1X NuPage LDS sample buffer (Invitrogen, #NP0007) and 50 µM DTT. Lysates were sonicated for 30 seconds and equal volumes were loaded on a 12.5% acrylamide/bis-acrylamide gel. Equal loading and protein quality were checked on separate gels before electrophoresis was applied for 20 minutes at 100V. Gels were fixed for 15 minutes in 50% ethanol containing 3% phosphoric acid and stained with Coomassie Brilliant Blue G-250 in 34% methanol and 3% phosphoric acid. Each sample was processed for in-gel digestion and measured by liquid chromatography-mass spectrometry (LC-MS) as described before[6]. MS/MS spectra were searched against a Uniprot human reference proteome FASTA file (swissprot_2018_01_human_canonical_and_isoform.fasta (42258 entries)) using MaxQuant version 1.6.0.16[7]. The mass spectrometry proteomics data are provided on request. Beta-binominal statistics were used to assess differential protein expression between groups, after normalization on the sum of the counts for each sample[8, 9]. Proteins with a significant change with $p<0.05$ were selected for pathway analysis. Protein networks were generated using STRING (Search Tool for the Retrieval of Interacting Genes/Proteins) and visualized with Cytoscape software version 3.2.1.

Chromatin immunoprecipitation (ChIP)

DNA for chromatin immunoprecipitation (ChIP) was obtained from a confluent PAEC monolayer of a Ø10 cm culture dish. Chromatins were cross linked with 1% formaldehyde for 5 minutes at RT, followed by lysis for 10 minutes in cell lysis buffer (50 mM Tris-HCl, 2 mM EDTA, 0.1% Igepal, 10% glycerol and protease inhibitor). Lysates were centrifuged and nuclear extracts were obtained by nuclear lysis buffer (50 mM Tris-HCl, 5 mM EDTA, 0.1% SDS). Nuclear lysates were fragmented by sonication to an average fragment size of 200-1000 base pairs (4 cycles of pulses for 30s on and 30s off). Chromatin immunoprecipitation was performed using Magna ChIP© G Kit (Sigma-Aldrich, #17-611). Samples were pre-cleared by 2 hours incubation with protein G magnetic beads at 4°C. Supernatants were collected and overnight incubated at 4°C with Mouse IgG (Millipore, #12-371B), H3K27me3 (Abcam #6002), H3K27Ac (Diagenode, #C15410174) and NFκB2 (R&D Systems, # MAB28881) antibodies, while bead complexes were washed and blocked in dilution buffer with 1% BSA. Blocked beads and antibodies were incubated for 2 hours at 4°C on a turning wheel. Bead-bound antigen/antibody complexes were collected using DynaMagTM-2 Magnet (Invitrogen, #12321D) and washed with high salt buffer, low salt buffer, LiCl buffer and TE buffer followed by two times elution for 15 minutes at RT. Samples were processed with 1 U proteinase K for 1h at 55°C, followed by reverse crosslinking with an additional 4 hours at 65°C and 10 minutes at 95°C. DNA was isolated with QIAamp DNA Mini Kit (Qiagen, #51304) according to the manufacturers protocol.

Western Blot

PAEC protein lysates were obtained in lysis buffer (1 M Tris-HCl, 3M NaCl, 3M KCl, 500 mM EDTA-NaOH, 5% Igepal, 0.5% Triton X-100, pH 8.0) containing phosphatase and protease inhibitor cocktail (Roche, #4906845001 and #11697498001). Lysates were prepared with 1X NuPage LDS sample buffer (Invitrogen, #NP0007) and 50 µM DTT. Samples were loaded on 7% SDS-Page gels or NuPageTM 4-12% Bis-Tris gel (Invitrogen, #NP0336) and electrophoresed at 130V. Separated proteins were transferred to 0.45 µM Amersham Hybond ECL nitrocellulose membranes (Invitrogen, #88018) and blocked with 5% BSA in Tris-buffered saline (pH 7.6) with 0.1% Tween (TBS-T) for 1 hour at RT. Membranes were incubated overnight at 4°C in 5% BSA with rabbit NFκB2 (Cell Signaling, #4882), rabbit polyclonal anti-VWF (1:1000, Dako, #A0082) and mouse Vinculin (1:1000, Sigma-Aldrich, #V9131). HRP-conjugated secondary antibodies (1:4000, Dako, #P0448) and HRP-conjugated GAPDH (Invitrogen, #G9295) were incubated in 5% BSA for 1 hour at RT. Bands were visualized with Amersham ECL Prime Blotting Detection Reagent (GE Healthcare Life Sciences, #RPN2108) and detected with the AmershamTM Imager 600.

Supplementary Table 1. Clinical group characteristics of healthy controls and CTEPH patients used for plasma VWF analysis

	CTEPH (n=21)	Control (n=14)
Sex (M/F)	11/10	7/7
Age (years)	64.3 ± 12.0	49.3 ± 15.6
mPAP (mmHg)	43.2 ± 12.8	N/A
PVR (dyn/s/cm^{-5})	632.7 ± 450.5	N/A
CO (L/min)	5.3 ± 1.6	N/A
SvO_2 (%)	64.9 ± 9.8	N/A

CTEPH = chronic thromboembolic pulmonary hypertension; mPAP = mean pulmonary artery pressure; PVR = pulmonary vascular resistance; CO = cardiac output; SvO_2 = mixed venous oxygen saturation; N/A = not available.

Supplementary Table 2. **Individual characteristics of CTEPH patients used for PAEC isolation**

Donor	Age	Sex	sPAP (mmHg)	dPAP (mmHg)	mPAP (mmHg)	PCWP (mmHg)	saturation VCI (%)	CO (L/min)	PVR (dyn/s/cm^{-5})	BMI	Comorbidities	Experiment
CTEPH01	79	M	78	27	45	14	57	5.4	460.1	28	hypertension, dyslipidemia, spinal disc hernia, prostate cancer, pancreatic adenocarcinoma	b, c, e, f, h, i
CTEPH02	52	M	113	38	61	12	N/A	3.3	1192.0	32	hypertension, dpinal disc hernia, BPH	b, c, d, e, f
CTEPH03	47	F	40	18	27	9	81	5.0	286.0	26	dyslipidemia, spinal disc hernia, hypothyroidism, Cutane LE	a, b, c, e, f, h, i
CTEPH04	70	F	98	37	59	19	73	4.9	653.1	38	hypertension, OSAS	a, b, e
CTEPH05	68	M	84	32	50	8	44	4.0	840.0	28	dyslipidemia	b, c, e, f, i
CTEPH06	56	M	80	31	49	13	N/A	6.7	382.1	27	hypertension, colitis ulcerosa, asthma, nephrolithiasis	b, d, e, f, h
CTEPH07	69	M	81	25	42	10	70	5.5	465.5	26	peripheral vascular disease	b, d, g
CTEPH09	49	F	86	32	52	12	N/A	7.5	427.0	29	asthma, antiphospholipid antibodies	a, b, c, d, e, f, i, j
CTEPH10	65	F	80	36	52	9	N/A	4.4	782.0	31	hypertension	b, e, h
CTEPH11	55	M	64	31	44	13	N/A	5.1	486.0	23	none	a, b, c, e, f, i
CTEPH12	69	F	84	34	51	20	N/A	5.1	486.0	43	hypertension, breast cancer, OSAS	b, c, f
CTEPH13	59	M	86	30	50	14	N/A	4.4	655.0	24	none	a, b, c, e, f, g, i, j
CTEPH14	68	M	104	35	62	16	N/A	5.8	635.0	32	none	b, c, e, h

Donor	Age	Sex	sPAP (mmHg)	dPAP (mmHg)	mPAP (mmHg)	PCWP (mmHg)	saturation VCI (%)	CO (L/min)	PVR (dyn/s/cm^{-5})	BMI	Comorbidities	Experiment
CTEPH31	69	M	60	24	38	15	52	5.6	328.6	30	hypertension, B-cell lymphoma, peripheral vascular disease	k
CTEPH32	59	M	91	34	55	13	N/A	5.5	610.9	30	hypertension, BPH, essential thrombocytosis	k
CTEPH33	77	M	67	34	46	15	66	5.4	462.7	33	hypertension, BPH, knee replacement	k
CTEPH34	34	M	39	16	24	13	75	5.5	160.0	29	viral myocarditis	k
CTEPH35	77	M	67	88	25	49	52	5.7	561.4	26	sigmoid colon carcinoma	k

CTEPH = chronic thromboembolic pulmonary hypertension; sPAP = systolic pulmonary artery pressure; dPAP = diastolic pulmonary artery pressure; mPAP = mean pulmonary artery pressure; PCWP = pulmonary capillary wedge pressure SvO_2 = mixed venous oxygen saturation; CO = cardiac output; PVR = pulmonary vascular resistance; N/A = not available | BPH = Benign prostatic hyperplasia; LE = Lupus erythematodes; OSAS = obstructive sleep apneasyndrome | a = Fluorescent In Situ Hybridization; b = Enzyme Linked Immunosorbent Assay; c = Quantative Polymerase Chain Reaction; d = Whole blood perfusion; e = isolated platelet perfusion; f = knockdown with silencing RNA; g = proteomics; h = Western blot; i = Chromatin immunoprecipitation; j = knockdown with short hairpin RNA; k = rotational thromboelastometry

Supplementary Table 3. **Knockdown sequences**

Gene of interest		Sequence
Smartpool siRNA	VWF	CCAGCGAGGUCUUGAAAUA, GAGGAGAGUUGAGCUGUU, AAACGCUCCUUCUCGAUUA, CAACGGGAUGUCCCGGAACU
	RelB	CUGCGGAUUUGCCGAAUUA, GCACAGAUGAAUUGGAGAU, CCAUUGAGCGGAAGAUUCA, GCCCGUCUAUGACAAGAAA
	NT	UGGUUUACAUGUCGACUAA, UGGUUUACAUGUUGUGUGA, UGGUUUACAUGUUUUCUGA, UGGUUUACAUGUUUUCCUA
Single target siRNA	NFκB2	CGAACAGCCUUGCAUCUAG
	NFκB1	GAAAUUAGGUCUGGGGAUA
shRNA	VWF	GAAACGCTCCTTCTCGATTAT
	NT	CAACAAGATGAAGAGCACCAA

VWF = Von Willebrand Factor, NT = non-targeting, NFκB = Nuclear Factor κB

Supplementary Table 4. **Primer sequences**

Gene of interest		Sequence
VWF	Forward	ATGTCTGCTTCAGGACCACG
	Reverse	AGCCACCCCTCAGTGAAATG
NFκB2	Forward	ATGGAGAGTTGCTACAACCCA
	Reverse	CTGTTCCACGATCACCAGGTA
RelB	Forward	TGTGGTGAGGATCTGCTTCCAG
	Reverse	TCGGCAAATCCGCAGCTCTGAT
NFκB1	Forward	ATGTGGAGATCATTGAGCAGC
	Reverse	CCTGGTCCTGTGTAGCCATT
Housekeeping genes		**Sequence**
P0	Forward	TCGACAATGGCAGCATCTAC
	Reverse	ATCCGTCTCCACAGACAAGG
RPL27	Forward	ATCGCCAAGAGATCAAAGATAA
	Reverse	TCTGAAGACATCCTTATTGACG
VWF promoter regions		**Sequence**
Region 1	Forward	AGCCAGCTCTCCTTCCAAAG
	Reverse	CCTGATTGAGCCTTTGCAGC
Region 2	Forward	GCCAGGGGGAATCACAGTAG
	Reverse	CCTGGGGTGCATAGGAAGTG
Region 3	Forward	CCCACATACCTCGCACTCTG
	Reverse	ATTCTGCCTCTGGTGCCATT

VWF = Von Willebrand Factor, NFκB = Nuclear Factor κB, RPL27 = Ribosomal Protein L27

Supplementary Figures

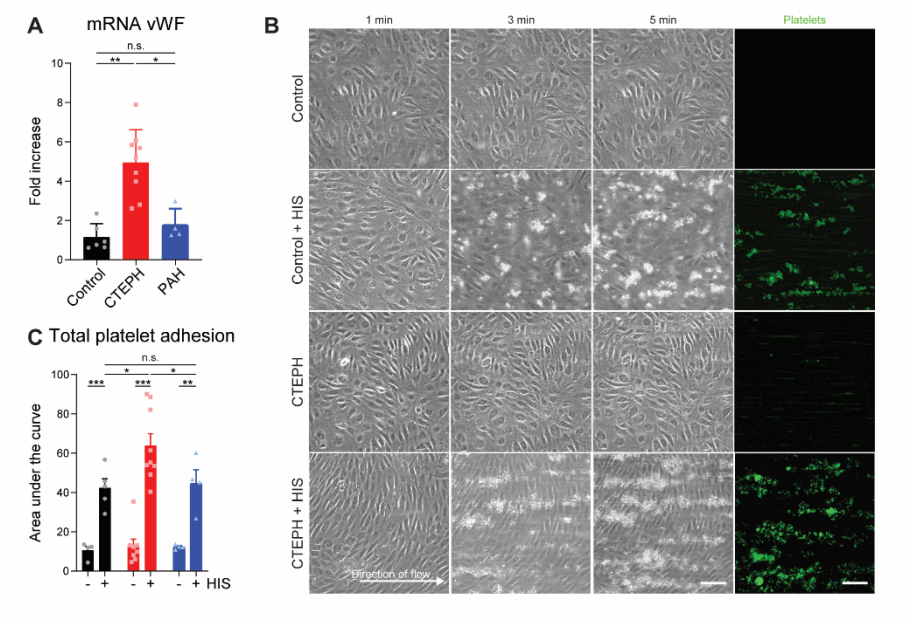

Supplementary Figure 1. **(A)** Relative VWF gene-expression in CTEPH-PAEC compared to control ($n_{control}$=6, n_{CTEPH}=9, n_{PAH}=4). **(B)** Bright field and fluorescent imaging of adhered platelets (green) on a PAEC monolayers with or without 30 minutes of histamine activation. Platelets were perfused over PAEC for 1, 3 and 5 minutes. Scale bar = 100 µm. **(C)** Comparison of total adhered platelets by calculating area under the curve. Each dot represents the average of three ROI per donor ($n_{control}$=5, n_{CTEPH}=9, n_{PAH}=4). ***(a-c)*** Data is presented as mean±SD. Significance is indicated with *p<0.05, **p<0.01, ***p<0.001, after *(a)* Kruskal-Wallis test, *(b)* two-way ANOVA with Grenhouse-Geisser correction for Tukey's multiple comparison test.

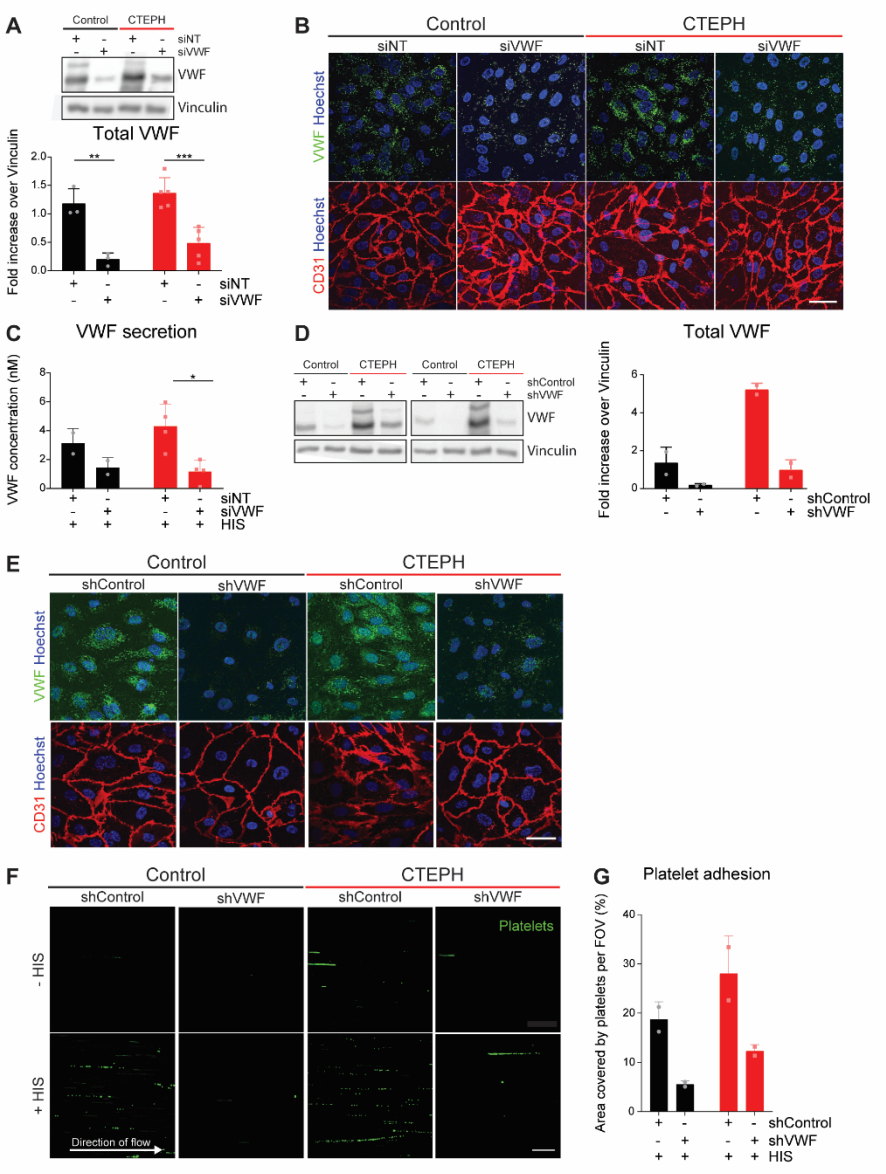

Supplementary Figure 2. **(A)** Western blot of VWF protein expression from whole PAEC lysates after treatment with siRNA against VWF or non-targeting (NT) ($n_{control}$=3, n_{CTEPH}=5). Data is presented as mean±SD, statistics were performed with two-way ANOVA with Grenhouse-Geisser correction for Tukey's multiple comparisons test, significance was indicated with **p<0.01, ***p<0.001. **(B)** Immunofluorescence staining of Weibel Palade bodies (WPB) from PFA fixed PAEC after treatment with siRNA against VWF or non-targeting (NT). **(C)** Endothelial VWF release into supernatant from siRNA treated PAEC after 30 minutes stimulation with histamine ($n_{control}$=2, n_{CTEPH}=4). Data is presented as mean±SD, statistics were performed with two-way ANOVA with Grenhouse-Geisser correction for Tukey's multiple comparisons test, significance was indicated with *p<0.05. **(D)** Western blot of VWF protein expression from whole PAEC lysates with or without short hairpin RNA knockdown of VWF ($n_{control}$=2, n_{CTEPH}=2). Data is presented as mean±SD. **(E)** Immunofluorescence staining of Weibel Palade Bodies (WPB) from PFA fixed PAEC with or without short hairpin RNA knockdown of VWF. **(F)** Fluorescence imaging of calcein AM labeled

platelets (green) on PAEC after 5 minutes of perfusion. VWF expression in endothelial cells was inhibited with siRNA against VWF or non-targeting (NT). Scale bar = 100 µm. **(G)** Comparison of total fluorescence of adhered platelets on PAEC treated with or without knockdown of VWF. Each dot represents the average of three ROI per donor ($n_{control}$=2, n_{CTEPH}=2). Data is presented as mean±SD.

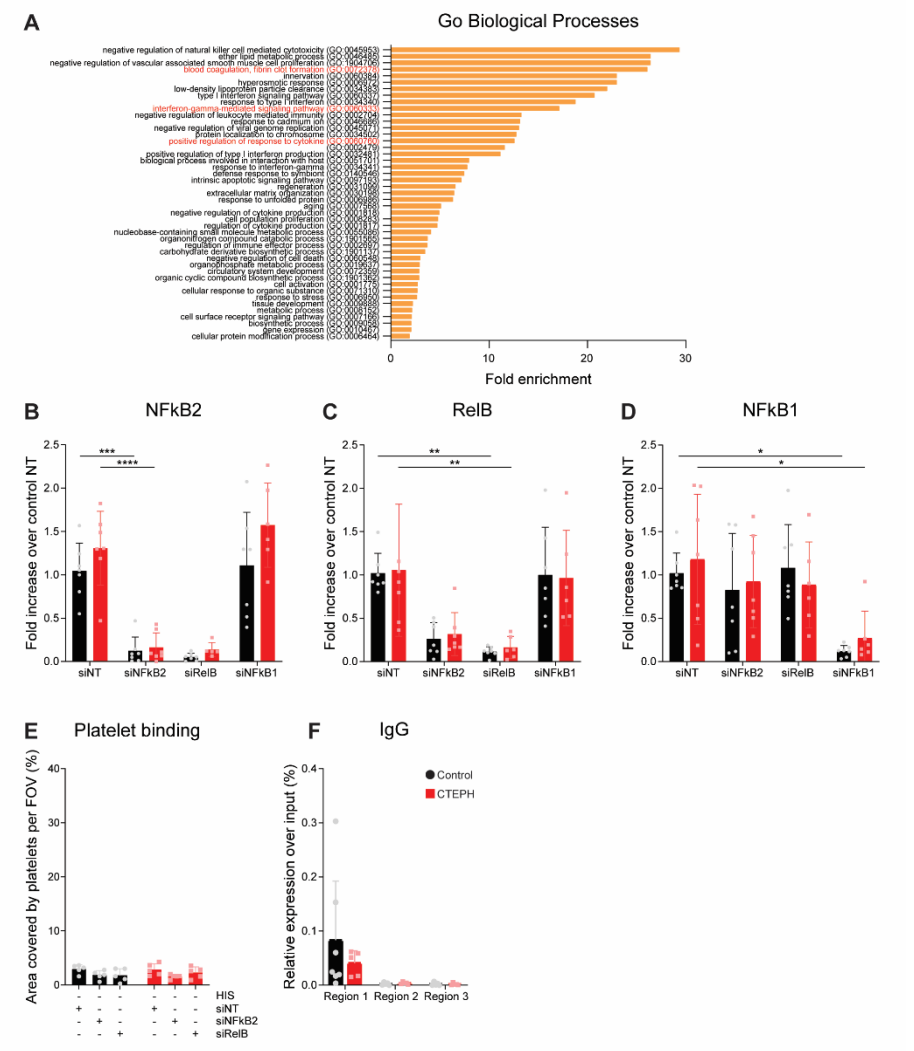

Supplementary Figure 3. **(A)** GO enrichment analysis of upregulated proteins in CTEPH compared to control involved in biological processes. **(B)** Relative NFκB2, **(C)** RelB and **(D)** NFκB1 mRNA expression in CTEPH-PAEC with knockdown of respectively NFκB2, RelB and NFκB1 compared to control ($n_{control}$=6, n_{CTEPH}=7). Data is presented as mean±SD, statistics were performed with two-way ANOVA with Grenhouse-Geisser correction for Tukey's multiple comparisons test, significance was indicated with *p<0.05, **p<0.01, ***p<0.001, ****p<0.0001. **(E)** Comparison of total fluorescence of adhered platelets on unstimulated PAEC with siRNA against NFκB2 and RelB. Each dot represents the average of three ROI per donor ($n_{control}$=3, n_{CTEPH}=5). Data is presented as mean±SD, statistics were performed with two-way ANOVA with Grenhouse-Geisser correction for Tukey's multiple comparisons test. Data was not significant. **(F)** Quantification of ChIP-qPCR of the VWF promotor region on IgG on nuclear extracts of CTEPH-PAEC compared to control. Data is presented as mean±SD, statistics were performed with two-way ANOVA with Grenhouse-Geisser correction for Sidak's multiple comparisons test. Data was not significant.

Supplementary references

1. Crochemore T, Piza FMT, Rodrigues RDR, Guerra JCC, Ferraz LJR, Correa TD. A new era of thromboelastometry. Einstein (Sao Paulo) 2017; 15: 380-385.
2. 2. Manz XD, Albers HJ, Symersky P, Aman J, van der Meer AD, Bogaard HJ, Szulcek R. In Vitro Microfluidic Disease Model to Study Whole Blood-Endothelial Interactions and Blood Clot Dynamics in Real-Time. J Vis Exp 2020.
3. Root DE, Hacohen N, Hahn WC, Lander ES, Sabatini DM. Genome-scale loss-of-function screening with a lentiviral RNAi library. Nat Methods 2006; 3: 715-719.
4. Smeets MWJ, Mourik MJ, Niessen HWM, Hordijk PL. Stasis Promotes Erythrocyte Adhesion to von Willebrand Factor. Arterioscler Thromb Vasc Biol 2017; 37: 1618-1627.
5. Schillemans M, Karampini E, van den Eshof BL, Gangaev A, Hofman M, van Breevoort D, Meems H, Janssen H, Mulder AA, Jost CR, Escher JC, Adam R, Carter T, Koster AJ, van den Biggelaar M, Voorberg J, Bierings R. Weibel-Palade Body Localized Syntaxin-3 Modulates Von Willebrand Factor Secretion From Endothelial Cells. Arterioscler Thromb Vasc Biol 2018; 38: 1549-1561.
6. Piersma SR, Fiedler U, Span S, Lingnau A, Pham TV, Hoffmann S, Kubbutat MH, Jimenez CR. Workflow comparison for label-free, quantitative secretome proteomics for cancer biomarker discovery: method evaluation, differential analysis, and verification in serum. J Proteome Res 2010; 9: 1913-1922.
7. Cox J, Mann M. MaxQuant enables high peptide identification rates, individualized p.p.b.-range mass accuracies and proteome-wide protein quantification. Nat Biotechnol 2008; 26: 1367-1372.
8. Pham TV, Jimenez CR. An accurate paired sample test for count data. Bioinformatics 2012; 28: i596-i602.
9. Pham TV, Piersma SR, Warmoes M, Jimenez CR. On the beta-binomial model for analysis of spectral count data in label-free tandem mass spectrometry-based proteomics. Bioinformatics 2010; 26: 363-369.

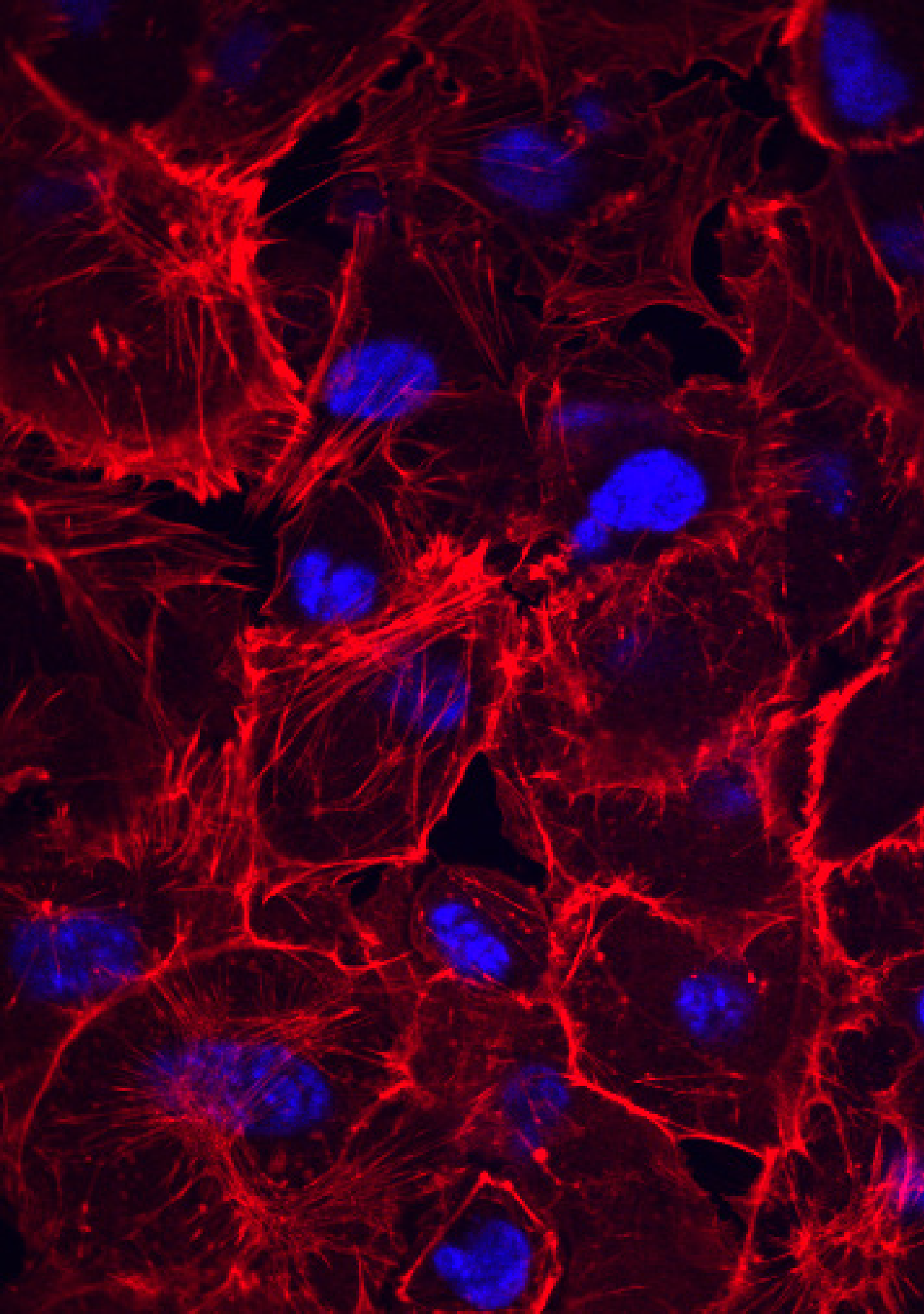

CHAPTER 5

Multi-omic profiling of the pulmonary arterial endothelium reveals disturbed cell adhesion and extracellular matrix reorganization in chronic thromboembolic pulmonary hypertension

Xue D. Manz[1], Xiaoke Pan[1], Robert Szulcek[1,2], Koen Prange[3], Guillermo Griffith[3], Aldo Jongejan[4], Mo Arkani[1], Petr Symersky[5,6], Chris Dickhoff[5], Connie Jimenez[6], Menno de Winther[3], Harm Jan Bogaard[1], Jurjan Aman[1]

[1]PHEniX Laboratory, Department of Pulmonary Medicine, Amsterdam UMC, VU University Medical Center, Amsterdam Cardiovascular Sciences, Amsterdam, The Netherlands
[2]Institute of Physiology, Charité Universitätsmedizin Berlin, corporate member of Freie Universität Berlin and Humboldt-Universität zu Berlin and German Heart Center Berlin, Germany
[3]Department of Medical Biochemistry, Experimental Vascular Biology, Amsterdam UMC, University of Amsterdam, Amsterdam Cardiovascular Sciences, Amsterdam Infection and Immunity, Amsterdam, The Netherlands
[4]Department of Clinical Epidemiology, Biostatistics and Bioinformatics, Amsterdam UMC, University of Amsterdam, Amsterdam, The Netherlands
[5]Department of Cardio-thoracic surgery, Amsterdam UMC, VU University Medical Center, Amsterdam, The Netherlands
[6]Department of Cardiothoracic Surgery, OLVG Hospital, Amsterdam, the Netherlands
[7]Department of Medical Oncology, Amsterdam UMC, VU University Medical Center, Cancer Center Amsterdam (CCA), Amsterdam, The Netherlands

Manuscript in preparation

Abstract

Chronic thromboembolic pulmonary hypertension (CTEPH) is characterized by occlusion of pulmonary arteries by organized blood clots and occlusive vascular remodeling. Recent studies have stressed the contribution of the endothelium to a local prothrombotic environment in CTEPH. However, the full scale of mechanisms by which the endothelium may contribute to the development and progression of CTEPH remains unknown. In this study, we performed a transcriptome and proteome analysis of CTEPH pulmonary artery endothelial cells, and evaluated whether expression was epigenetically regulated. The aim of this study was to identify novel regulators that contribute to the pro-thrombotic phenotype of pulmonary artery endothelial cells from CTEPH patients. Therefore, we performed multi-layer omic profiling of the endothelium and revealed that CTEPH-PAEC show altered cell adhesion, extracellular matrix organization and platelet signaling.

Embargo

Embargo

5

Embargo

5

Embargo

5

Embargo

Embargo

5

Embargo

Embargo

5

Embargo

5

Embargo

5

Embargo

Embargo

5

Embargo

5

Embargo

5

Embargo

Embargo

5

Embargo

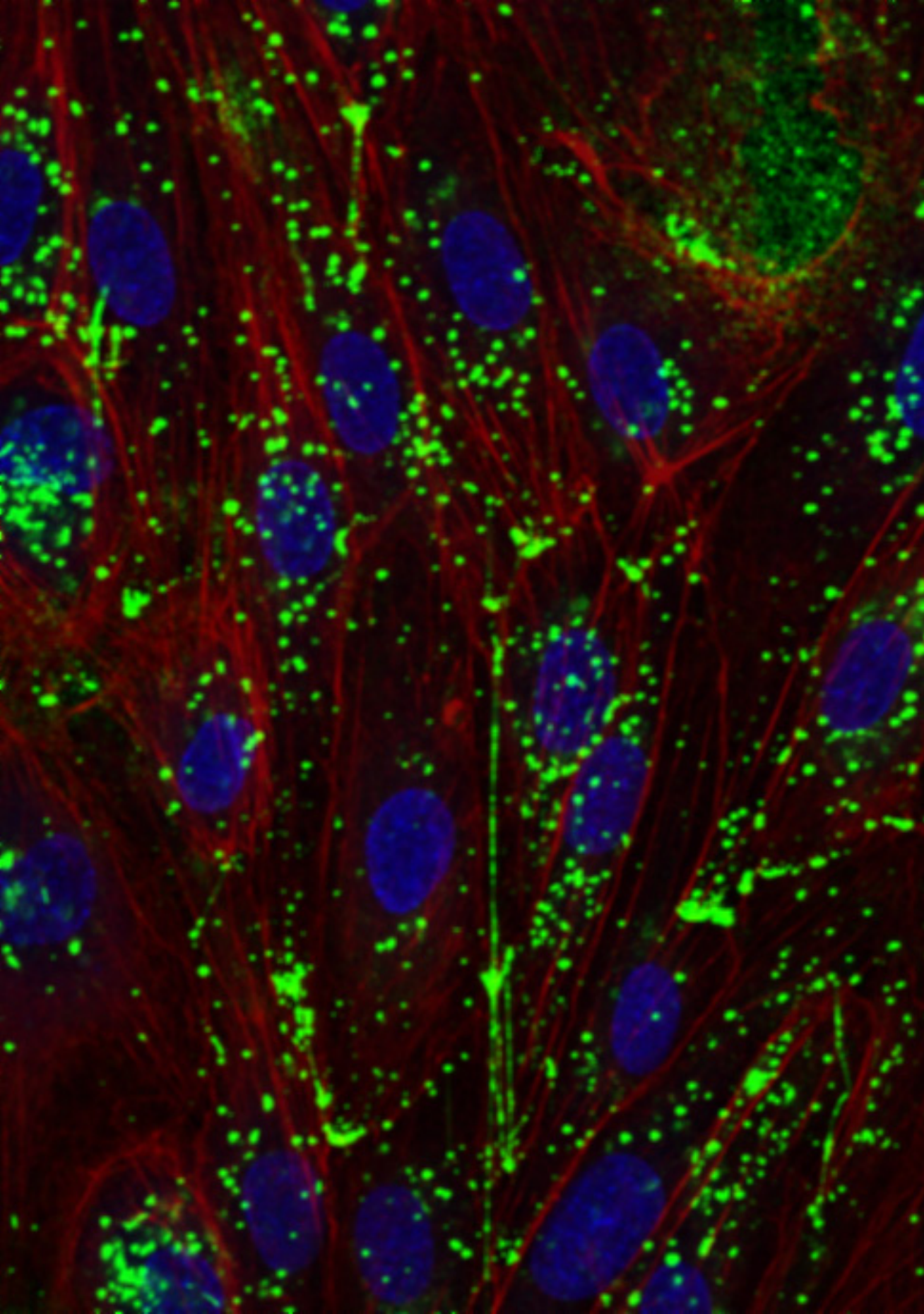

CHAPTER 6

Riociguat inhibits ultra large VWF string formation on pulmonary artery endothelial cells from chronic thromboembolic pulmonary hypertension patients

Takayuki Jujo Sanada[1,2*], **Xue D. Manz[1*]**, Petr Symersky[3,4], Xiaoke Pan[1], Keimei Yoshida[1,5], Jurjan Aman[1], Harm Jan Bogaard[1]

[1]Department of Pulmonary Medicine, Amsterdam UMC, VU University Medical Center, Amsterdam Cardiovascular Sciences (ACS), Amsterdam, The Netherlands
[2]Department of Respirology, Graduate School of Medicine, Chiba University, Chiba, Japan
[3]Department of Cardio-thoracic Surgery, Amsterdam UMC, VU University Medical Center, Amsterdam, The Netherlands
[4]Department of Cardiothoracic Surgery, OLVG Hospital, Amsterdam, The Netherlands
[5]Kyushu University, Faculty of Medicine, Graduate School of Medical Sciences, Fukoka, Japan

*Equal contribution

6 October 2022, Pulmonary Circulation

Abstract

Chronic thromboembolic pulmonary hypertension (CTEPH) is characterized by elevated pulmonary arterial pressure and organized thrombi within pulmonary arteries. Riociguat is a soluble guanylate cyclase stimulator, and is approved for patients with inoperable CTEPH or residual pulmonary hypertension after pulmonary endarterectomy (PEA). Previous work suggested that riociguat treatment is associated with an increased risk of bleeding, although the mechanism is unclear. The aim of this study is to assess how riociguat affects primary hemostasis by studying its effect on the interaction between platelets and endothelial cells derived from CTEPH patients. Pulmonary artery endothelial cells (PAECs) were isolated from thrombus-free regions of PEA material. Purified PAECs were cultured in flow chambers and were stimulated with 0.1 and 1 μM riociguat for 24 hours before flow experiments. After stimulation with histamine, PAECs were exposed to platelets under shear stress. Platelet adhesion and expression of von Willebrand Factor (VWF) were evaluated to assess the role of riociguat in hemostasis. Under dynamic conditions, 0.1 and 1.0 μM of riociguat suppressed platelet adhesion on the surface of PAECs. Although riociguat did not affect intracellular expression and secretion of VWF, PAECs stimulated with riociguat produced fewer VWF strings than unstimulated PAECs. Flowcytometry suggested that decreased VWF string formation upon riociguat treatment may be associated with suppressed cell surface expression of P-selectin, a protein that stabilizes VWF anchoring on the endothelial surface. In conclusion, Riociguat inhibits VWF string elongation and platelet adhesion on the surface of CTEPH-PAECs, possibly by reduced P-selectin cell surface expression.

Introduction

Chronic thromboembolic pulmonary hypertension (CTEPH) is diagnosed when despite effective anticoagulation treatment, persistent thromboembolic obstruction of pulmonary arteries leads to an elevated mean pulmonary arterial pressure[1]. Patients left untreated may die from right heart failure[1,2]. Treatment options for CTEPH are pulmonary endarterectomy (PEA), balloon pulmonary angioplasty (BPA) and medical therapies[1,3], which together significantly improve the prognosis of CTEPH[4]. PEA is the first choice of treatment and involves removal of organized thrombi from the pulmonary arteries[1,3,5]. Nevertheless, 16 to 50% of patients who underwent PEA suffer from residual or recurrent pulmonary hypertension (PH)[6]. In addition, according to an international registry, 30-40% of CTEPH patients are inoperable due to surgical inaccessibility, compromised hemodynamics, and/or comorbidities[7]. Medical treatments with specific pulmonary vasodilators serve as alternatives to patients with inoperable CTEPH or residual PH after PEA and BPA. Riociguat was the first medical therapy specifically approved for CTEPH patients[1,3]. This selective pulmonary vasodilator acts on the nitric oxide pathway, and reduces pulmonary vasoconstriction by stimulating soluble guanylate cyclase (sGC)[8]. Clinically, it has been shown that riociguat improved exercise capacity, hemodynamics and cardiac function in CTEPH patients in the short and longer term[9-11].

Life-long anticoagulation is required in all CTEPH patients to prevent de novo pulmonary embolism[3]. However, the combined use of selective pulmonary vasodilators and anticoagulants seems to be associated with an increased risk of bleeding[12]. In our previous study, riociguat treatment increased the bleeding risk in CTEPH patients treated with vitamin K antagonists[13]. However, the mechanism by which vasodilators elicit bleeding remains enigmatic.

Vascular thrombosis is initiated when platelets bind to von Willebrand Factor (VWF) secreted from endothelial cells (ECs)[14]. Under physiological flow, endothelial cells have a negative charge and release prostaglandin I2 and nitric oxide to prevent platelet adhesion[15,16]. Activation of ECs by e.g. a stress response or inflammation leads to the release of VWF from Weibel-Palade bodies (WPB)[17], and the formation of ultra large VWF (ULVWF) strings, which serves as a platform for platelets to adhere to initiate coagulation[18]. VWF strings are anchored and stabilized on the endothelial surface by P-Selectin and αvβ3 integrin[19,20]. We have recently demonstrated that VWF-mediated platelet adhesion is increased in PAEC derived CTEPH patients[21]. However, the effect of riociguat on these cells has never been investigated. It has been known that riociguat can suppress activation and aggregation of platelets via suppression of glycoprotein IIb/IIIa[22], but the effect on endothelial cells is unclear We hypothesized that riociguat would affect ULVVWF string formation and platelet adhesion, thereby possibly contributing to bleeding.

The aim of this study was to evaluate the effect of riociguat on VWF and endothelium-platelet interactions under dynamic conditions. We found that platelet adhesion on the CTEPH endothelium

was inhibited by riociguat, which was associated with decreased VWF string formation and reduced endothelial surface expression of P-selectin.

Methods

Reagents

Riociguat was purchased from Sigma Aldrich (St. Louis, MO, USA), dissolved in dimethyl sulfoxide (DMSO) in a concentration of 1 mol/L and stored at -80°C. Histamine was purchased from Sigma Aldrich, dissolved in supplemental free endothelial cell medium in a concentration of 1 M and stored ad -20°C. Antibodies against the following proteins were used: VWF (1:1000, A0082, Dako)), β-actin (1:1000, SC-47778, Santa Cruz Biotechnology). Primary antibodies were detected with secondary antibodies for polyclonal goat anti-rabbit (1:2500, P0448, Dako) or anti-mouse antibodies (1:2500, P0449, Dako) conjugated with horseradish peroxidase (HRP).

Isolation and culture of pulmonary arterial endothelial cells

PAECs were isolated and purified according to the previously published protocol[21,23]. Briefly, chronic thrombi were surgically resected from pulmonary endarterectomy material obtained from CTEPH patients. The endothelial inner layer was scratched with a scalpel, transplanted onto a 60 mm culture dish (Corning, USA) coated with 5 µg/mL fibronectin, and incubated with complete endothelial cell medium (cECM, ScienCell Research Laboratories, USA) at 37°C and 5% CO2 in a humidified incubator. For purification, the outgrown endothelial cells were separated with CD144 positive magnetic beads (Miltenyi Biotec, Germany). Purified cells were expanded on 0.1% gelatin until passage 4-6 was reached for the following experiments.

Flow experiment

PAECs were cultured on µ-Slide VI 0.4 ibidi flow chambers (ibidi GmbH, Germany) coated with 0.1% gelatin until confluence. Prior to the flow experiments, PAECs were stimulated with 0.1 and 1 µM riociguat for 24 hours. After stimulation, PAECs were additionally stimulated with 1 µM histamine for 5 minutes to induce VWF secretion.

Platelets were freshly collected and prepared on the day of experiments. Citrated blood was centrifuged at 150g and platelet-rich plasma (PRP) was collected in a new tube. 10% acid citrate dextrose (ACD, 85 mM sodiumcitrate, 65 mM citric acid, 100 mM glucose) was added for anticoagulation and PRP was centrifuged at 2000g. The supernatant was removed and platelets were fluorescently stained with Calcein AM (1:1000, Thermo Fisher Scientific, USA) for 15 minutes. Platelets were washed with platelet wash buffer (36 mM citric acid, 103 mM NaCl, 5 mM KCl, 5 mM EDTA, 56 mM D-glucose, 0.35% bovine serum albumin (BSA), pH 6.5) three times before resuspended in HEPES containing 1% BSA. Platelets were diluted in a concentration of 200-400×106 cells/mL and allowed to equilibrate at 37°C to restore their function. Platelets were not stimulated with riociguat in this study.

Flow experiments were performed as previously described[21,23]. Isolated platelets were perfused with a shear stress of 2.5 dyne/cm2 for 5 minutes over stimulated PAEC and phase-contrast and fluorescent images were taken with an Etaluma LS720 microscope (Etaluma, USA) using a 20X phase-contrast objective. Platelet adhesion was quantified in ImageJ by determining the area covered by platelets per Field of View (FOV). Quantification represents the average of 5 FOV, per channel per donor.

Real-Time quantative polymerase chain reaction (qPCR)

Total RNA of PAEC stimulated with 0.1 or 1.0 µM riociguat was isolated with RNeasy Mini Kit (Qiagen, Germany) according to the manufacturer's protocol. Isolated RNA was transcribed to cDNA with iScript (Biorad Laboratories, USA) and qPCR was performed with SYBR Green (Biorad Laboratories, USA) in a C1000 Thermo Cycler (Biorad Laboratories, USA). Genes were normalized using the 2-ddCt method to quantify expression with the following primers: VWF (Fw, ATGTCTGCTTCAGGACCACG; Rv, AGCCACCCCTCAGTGAAATG) and RPL27 (Fw, ATCGCCAAGAGATCAAAGATAA; Rv, TCTGAAGACATCCTTATTGACG)

Protein isolation and Western blot analysis

Total protein lysates were collected from PAECs stimulated with 0.1 or 1.0 µM riociguat for 24 hours, using lysis buffer (20 mM Tris/HCl, pH 8.0, 150 mM NaCl, 100 mM KCl, 2 mM EDTA-NaOH, 5% Igepal and 0.5% Triton-X) supplemented with phosphatase and protease inhibitor cocktail (Roche, Switzerland). Western blot analysis was performed according to our previously published report[24]. In brief, lysates were prepared with 1× NuPage LDS sample buffer (Thermofisher Scientific, USA) and 50 µM DTT (Thermofisher Scientific, USA). Protein samples were separated on 4–12% NuPageTM Bis-Tris protein gel (Thermofisher Scientific, USA) and transferred to 0.45 µM nitrocellulose membranes (Thermofisher Scientific, USA). Protein membranes were blocked with 5% BSA in Tris-buffered saline containing Tween-20 (TBS-T, pH 7.6) and overnight incubated at 4 ^{o}C with primary antibodies. Secondary antibodies were incubated for 1h at room temperature. Protein bands were detected using ECL Prime Blotting Detection Reagent (GE Healthcare Life Sciences, The Netherlands) and imaged by AmershamTM Imager 600 (GE Healthcare Life Sciences, The Netherlands). Bands were quantified with ImageJ and normalized to loading control.

Enzyme-linked immuno sorbent assay (ELISA)

Supernatant was collected from PAECs stimulated with 0.1 or 1.0 µM riociguat for 24 hours and secreted VWF levels were measured as previously described 25. In brief, PBS containing anti-VWF antibody (1:1000, A0082, Dako) was coated into each well of a 96-well plate and incubated overnight at 4°C. The wells were washed with PBS and blocked using PBS containing 2% BSA at room temperature for 2 hours. After blocking, supernatants were applied into each well and incubated at room temperature for 2 hours. After washing, HRP-conjugated rabbit polyclonal anti-VWF was added at room temperature for 2 hours. VWF levels were detected using substrate solution and the reaction

was stopped by stop solution 20 minutes later. Absorbance of 450 nm and 540 nm were read using a plate reader. The VWF concentration was determined by a standard curve.

Immunofluorescence imaging of secreted VWF

PAECs were cultured on µ-Slide VI 0.4 ibidi flow chambers coated with 0.1% gelatin until confluence. PAECs were stimulated with 0.1 or 1.0 µM riociguat for 24 hours and additionally stimulated with histamine to induce VWF secretion. VWF elongation was induced by applying shear stress of 2.5 dyne/cm2 for 5 minutes, after which PAECs were fixed with 4% paraformaldehyde (PFA) for 10 minutes at RT. Cells were blocked with 1% BSA for 30 minutes at RT, and stained with FITC conjugated VWF (1:1000), Phalloidin (1:400, Cytoskeleton) and Hoechst (1:1000, Thermofisher Scientific) for 30 minutes at RT. Confocal images were acquired with Nikon A1R and Z-stacks of 2 µm were taken with 60X oil-immersion objective.

Flow cytometry

PAECs were pretreated with riociguat and stimulated with histamine to evaluate P-selectin surface expression. Cells were detached, blocked for 10 minutes with 10% BSA, and stained for P-selectin (1:50, CD62P, 1E3, sc-19672) for 1h at 4°C. Fluorescently labeled secondary antibody was incubated for 30 minutes at 4°C and signal were measured using Attune™ NxT Flow Cytometer. Unstained and secondary antibody stained were used as negative controls. Mean fluorescent intensity (MFI) of P-selectin was analyzed with FCS Express version 7.

Statistical analysis

Continuous variables were described as mean ± standard deviation (SD) unless otherwise stated. All analysis were performed using GraphPad prism ver.9.0 (GraphPad Software Inc, San Diego, CA, USA). Comparison between two groups with normal distribution were performed using an unpaired Student's t-test. If not normally distributed, a Mann-Whitney U test was used. For comparison with more than two groups, two-way ANOVA with Grenhouse-Geisser correction was used, followed by Tukey's post hoc for multiple comparison. P-values < 0.05 was considered significant.

Results

Riociguat inhibits platelet adhesion on CTEPH pulmonary artery endothelium

PAECs were isolated from the surgical specimens of 12 CTEPH patients (**Table 1**). The baseline hemodynamic characteristics from CTEPH patients are displayed in Supplementary Table 1.

Table 1. Baseline characteristics of CTEPH patients used for PAEC isolation

CTEPH patients	All (n=12)
Sex (M/F)	7/5
Age (years)	60.9 ± 14.0
mPAP (mmHg)	51.3 ± 7.5
PVR (dyne/s/cm^{-5})	634.7 ± 280.7
CO (L/min)	5.1 ± 1.4
SvO_2 (%)	63.7 ± 12.9

CTEPH = chronic thromboembolic pulmonary hypertension; mPAP = mean pulmonary artery pressure; PVR = pulmonary vascular resistance; CO = cardiac output; SvO2 = mixed venous oxygen saturation

To assess the *in vitro* effect of riociguat on platelet adhesion to CTEPH endothelium, freshly isolated platelets were perfused over PAEC monolayers which were incubated with riociguat for 24 hours, followed by histamine stimulation for 30 minutes (**Figure 1A**). The area covered by platelets after histamine stimulation dropped by 60% on PAECs pretreated with riociguat (15.94 ± 1.19% vs. 6.15 ± 3.38%) (**Figure 1B**), with a comparable decrease observed for 0.1uM and 1.0uM. These data indicate that riociguat suppresses platelet adhesion.

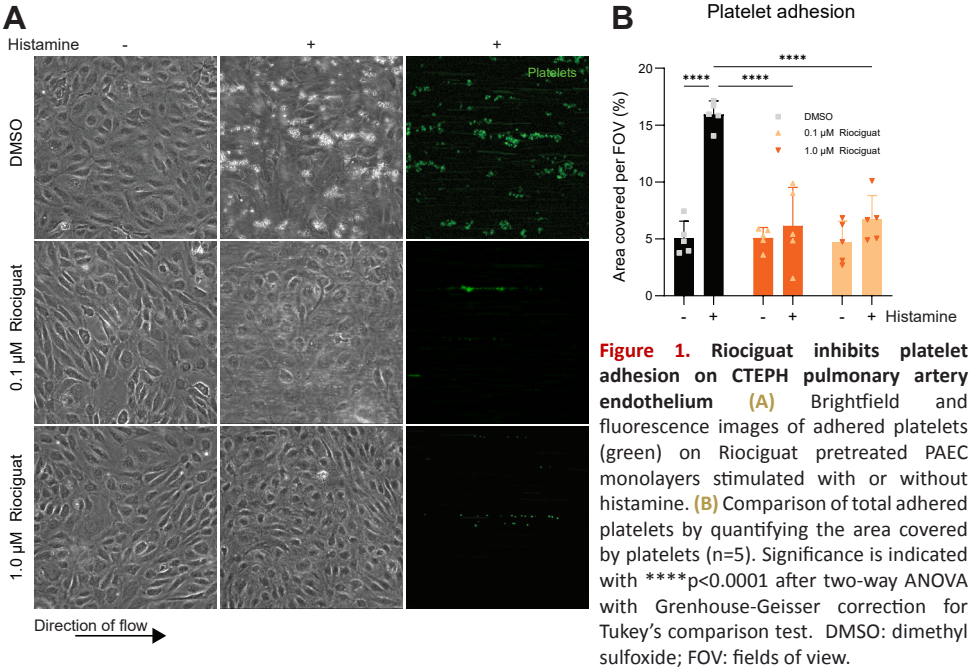

Figure 1. Riociguat inhibits platelet adhesion on CTEPH pulmonary artery endothelium **(A)** Brightfield and fluorescence images of adhered platelets (green) on Riociguat pretreated PAEC monolayers stimulated with or without histamine. **(B)** Comparison of total adhered platelets by quantifying the area covered by platelets (n=5). Significance is indicated with ****p<0.0001 after two-way ANOVA with Grenhouse-Geisser correction for Tukey's comparison test. DMSO: dimethyl sulfoxide; FOV: fields of view.

Riociguat did not affect VWF intracellular expression and secretion in CTEPH-PAEC

We have recently shown that platelet adhesion on CTEPH endothelium is driven by excessive VWF expression[21]. In order to examine the effect of riociguat on VWF expression in CTEPH-PAEC, analysis on RNA and protein expression was performed. Stimulation with riociguat did not alter VWF mRNA expression (**Figure 2A**) or the levels of intracellular VWF protein in CTEPH PAECs (**Figure 2B-C**). Since platelets bind to secreted VWF, we next evaluated the effect of riociguat on VWF release upon histamine stimulation. However, no changes in VWF release were observed after riociguat pretreatment (**Figure 2D**). Together, these data show that riociguat did not suppress intracellular VWF expression or release from CTEPH-PAEC in static conditions.

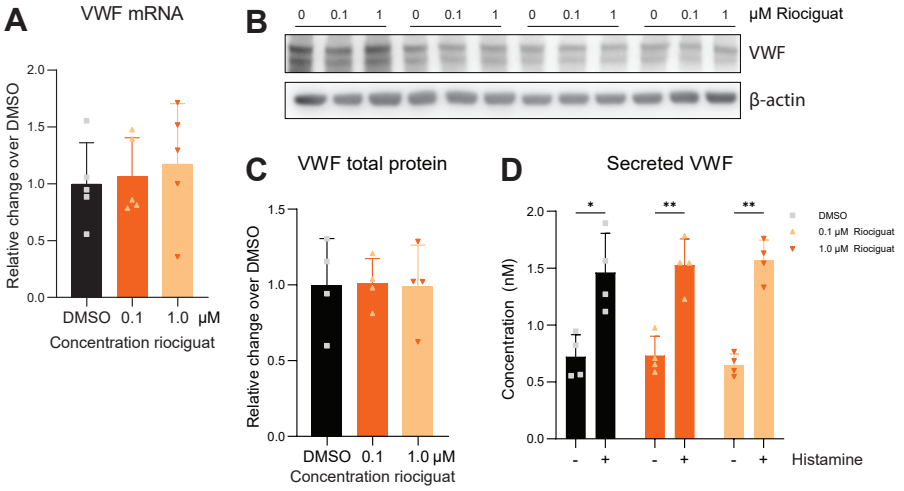

Figure 2. Riociguat did not affect VWF expression and secretion in CTEPH-PAEC. CTEPH-PAECs were pretreated with riociguat and total cell lysates were used to determine **(A)** VWF mRNA expression (n=5) and **(B-C)** total protein expression (n=4). Data was not significant. **(D)** Endothelial VWF release from PAEC with or without histamine activation (n=4). Significance is indicated with *p<0.05 and **p<0.01 after two-way ANOVA with Grenhouse-Geisser correction for Tukey's comparison test. VWF: von Willebrand factor; DMSO: dimethyl sulfoxide.

VWF string formation under shear was inhibited by Riociguat

Under laminar flow, confluent endothelial monolayers release VWF that form strings parallel to the direction of flow. These extend to several hundreds of micrometers and are stabilized on the surface of the endothelium[20]. Alterations in VWF strings may disturb hemostasis. To evaluate whether riociguat interfered with this mechanism, VWF string formation under shear was studied after immunofluorescence visualization (**Figure 3A**). Upon shear, riociguat treatment significantly reduced the number of VWF strings (**Figure 3B**) and individual VWF strings tended to be shorter after riociguat treatment of PAEC, although the difference was not statistically significant (**Figure 3C**). Total string length of VWF was significantly lower (**Figure 3D**). This effect may lead to decreased stabilization of platelet binding under flow.

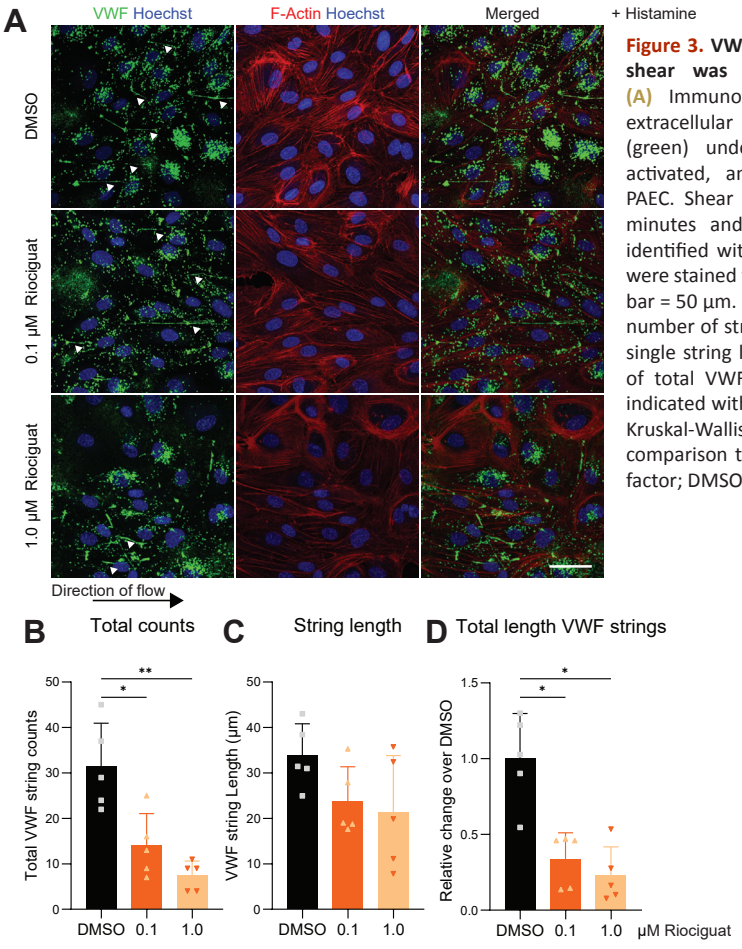

Figure 3. VWF string formation under shear was inhibited by Riociguat (A) Immunofluorescence images of extracellular VWF string formation (green) under shear on histamine activated, and riociguat pre-treated PAEC. Shear stress was applied for 5 minutes and endothelial cells were identified with Phalloidin (red), nuclei were stained with Hoechst (blue). Scale bar = 50 µm. (B) Quantification of total number of strings (C) Quantification of single string length (D) Quantification of total VWF length. Significance is indicated with *p<0.05, **p<0.01 after Kruskal-Wallis test with Dunn's multiple comparison test VWF: von Willebrand factor; DMSO: dimethyl sulfoxide.

Riociguat inhibits P-selectin surface expression

To explain our observation of fewer and shorter VWF strings, we considered that some factors associated with VWF stabilization under shear stress were affected by riociguat. It has been reported that P-selectin and αvβ3 integrin are involved in the stabilization of VWF on the cell surface[19,20]. Thus, the effect of riociguat on the expression of these adhesion molecules in CTEPH-ECs were assessed. Total P-selectin and αvβ3 protein expression were not affected by riociguat (**Figure 4A-B**, Supplementary Figure 1A-B). However, because VWF anchoring depends on cell surface expression of these adhesion molecules, we performed flow cytometry analysis (**Figure 4C**). Stained and unstained cells were mixed to determine the range of positive signal (**Figure 4D**), which was used to quantify cell surface expression.

Pretreatment with riociguat did not affect the percentage of P-selectin positive cells of cells positive. P-selectin surface expression was low under basal conditions, but increased after stimulation with

histamine for 30 minutes (**Figure 4E**). The histamine-induced surface expression of P-selectin was abrogated by riociguat, independent of concentration (**Figure 4F**). However, paired analysis of the mean fluorescent intensity was negatively influenced by riociguat after stimulation with histamine (**Figure 4G**). Riociguat treatment did not affect αvβ3 integrin expression (Supplementary Figure 1). Although the effect of riociguat on P-selectin was modest, these data suggest that P-selectin is involved in riociguat mediated suppression of platelet adhesion on activated PAEC.

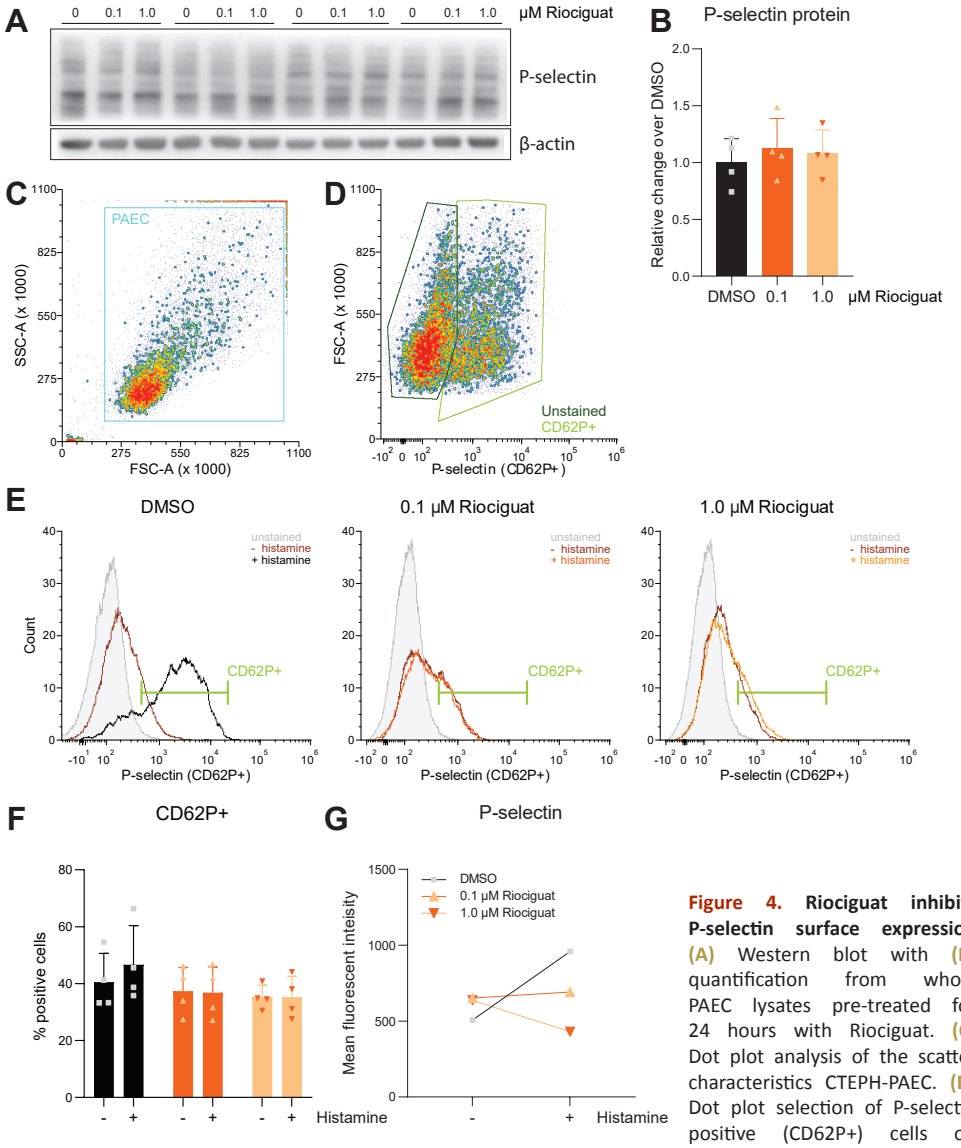

Figure 4. Riociguat inhibits P-selectin surface expression **(A)** Western blot with **(B)** quantification from whole PAEC lysates pre-treated for 24 hours with Riociguat. **(C)** Dot plot analysis of the scatter characteristics CTEPH-PAEC. **(D)** Dot plot selection of P-selectin positive (CD62P+) cells on gated PAEC. **(E)** P-selectin (CD62P) expression demonstrated by fluorescence histogram on PAEC population **(F)** Percentage of PAEC positive for CD62P+ **(G)** Paired analysis of mean fluorescent intensity of P-selectin on PAEC. Data was not significant. DMSO: dimethyl sulfoxide.

Discussion

As riociguat has been reported to increase the risk of bleeding as a side effect, the present study aimed to understand how riociguat affects primary hemostasis. Investigating the effect of riociguat on platelet adhesion to CTEPH PAECs, we found that riociguat reduced VWF strings formation on PAEC contributing to reduced platelet adhesion on the endothelial surface under laminar flow. Conversely, VWF protein and mRNA expression was not altered by riociguat treatment. Finally, we observed that riociguat decreased P-selectin expression on the cell surface, which was associated with decreased ULVWF stabilization and platelet adhesion.

The effects of riociguat on CTEPH-PAECs were evaluated at the concentration of 0.1 to 1.0 μM, which was similar to the physiological plasma concentration of 150-500 nM when CTEPH patients receive up to 2.5 mg riociguat per dose[26]. It has been reported that more than a 10-fold higher concentration is necessary to increase cGMP concentration and reduce ADP-induced platelet aggregation[22]. As such, clinical observations of increased bleeding in riociguat treated patients are unlikely explained by reduced ADP-induced platelet aggregation. This suggests an additional role for disturbed platelet-endothelial interaction as a cause of bleeding. The primary response to vascular trauma or injury is a repair mechanism that includes the release of VWF. Under shear conditions, VWF is unfolded and serves as a ligand for platelets to adhere to, thereby participating in wound healing. We have shown that treatment of endothelial cells with riociguat results in reduced VWF string formation and platelet adhesion. VWF expression and secretion into the circulation can be regulated via various transcriptional and (post)translational mechanisms[27]. Although recent data from our group has shown that VWF expression in PAECs from CTEPH patients is regulated on the transcriptional level under inflammatory conditions[21], and that previous studies showed that mRNA levels of VWF were decreased in endothelial progenitor cells from patients receiving riociguat[28], we were not able to observe an anti-inflammatory effect that reduced VWF mRNA expression in PAEC after in vitro riociguat stimulation. From these results, we considered that the suppressed VWF strings formation was unrelated to VWF expression.

P-selectin is an adhesion molecule localized in WPBs in ECs and α-granules in platelets[29], and plays an important role in interactions between endothelial cells, platelets (aggregation) and leukocytes (cell rolling and adhesion)[30]. In WPBs, the luminal domain of P-selectin binds to the D'-D3 domains of VWF, and they are co-stored in WPBs 31. In response to stimulation including histamine, VWF and P-selectin are secreted by exocytosis of WPBs on the surface of ECs[14,29], and VWF is unfolded and tethered to the endothelial surface by P-selectin, which is associated with the stabilization of secreted VWF strings against the shear stress[19,20]. Our data showed that specifically P-selectin surface expression on PAECs was suppressed by riociguat treatment, which is supported by a previous study showing that a sGC stimulator (BAY 22-2272) similar to riociguat downregulates histamine induced P-selectin expression in human umbilical vein endothelial cells[32]. The detailed mechanism is unclear from the results of the previous and current study. It has been reported that the endothelial secretory response is not binary

and can be influenced by multiple factors, P-selectin and VWF are therefore not always co-released[33], which may explain our finding that P-selectin surface expression was reduced in response to riociguat, while VWF remained similar.

This study has some limitation. First, appropriate CTEPH animal models reflecting the pathogenesis of CTEPH are currently not available[34], which prohibits the study of the effect of riociguat on in vivo bleeding events. Further investigation for in vivo application is needed to find robust evidence of the effect of riociguat on bleeding in CTEPH. Second, PAECs derived from different patients were used for different experiments, because the number of isolated cells from surgical specimens was limited. Some heterogeneity between samples may have affected the results.

In conclusion, riociguat inhibits VWF elongation and platelet adhesion on the surface of PAECs by reduced P-selectin expression. Although the underlying mechanism by which riociguat suppresses the surface expression of P-selectin remains to be determined, we have shown that riociguat affects primary hemostasis on PAEC from CTEPH patients, which may explain the increased bleeding risk associated with this treatment in CTEPH patients.

References

1. Kim NH, Delcroix M, Jais X, et al. Chronic thromboembolic pulmonary hypertension. Eur Respir J 2019; 53: 1801915.
2. Riedel M, Stanek V, Widimsky J, et al. Longterm follow-up of patients with pulmonary thromboembolism. Late prognosis and evolution of hemodynamic and respiratory data. Chest 1982; 81: 151-158.
3. Galiè N, Humbert M, Vachiery JL, et al. 2015 ESC/ERS guidelines for the diagnosis and treatment of pulmonary hypertension: the joint task force for the diagnosis and treatment of pulmonary hypertension of the European Society of Cardiology (ESC) and the European Respiratory Society (ERS) : endorsed by: Association for European Paediatric and Congenital Cardiology (AEPC), International Society for Heart and Lung Transplantation (ISHLT). Eur Respir J 2015; 46: 903-975.
4. Miwa H, Tanabe N, Jujo T, et al. Long-term outcome of chronic thromboembolic pulmonary hypertension at a single Japanese pulmonary endarterectomy center. Circ J 2018; 82: 1428-1436.
5. Delcroix M, Lang IM, Pepke-Zaba J, et al. Long-term outcome of patients with chronic thromboembolic pulmonary hypertension: results from an international prospective registry. Circulation 2016; 133: 859-871.
6. Braams NJ, Ruigrok D, Schokker MGM, et al. Pulmonary vascular imaging characteristics after pulmonary endarterectomy for chronic thromboembolic pulmonary hypertension. J Heart Lung Transplant 2020; 39: 248-256.
7. Pepke-Zaba J, Delcroix M, Lang I, et al. Chronic thromboembolic pulmonary hypertension (CTEPH): results from an international prospective registry. Circulation 2011; 124: 1973-1981.
8. Humbert M, Lau EM, Montani D, et al. Advances in therapeutic interventions for patients with pulmonary arterial hypertension. Circulation 2014; 130: 2189-2208.
9. Ghofrani HA, D'Armini AM, Grimminger F, et al. Riociguat for the treatment of chronic thromboembolic pulmonary hypertension. N Engl J Med 2013; 369: 319-329.
10. Simonneau G, D'Armini AM, Ghofrani HA, et al. Riociguat for the treatment of chronic thromboembolic pulmonary hypertension: a long-term extension study (CHEST-2). Eur Respir J 2015; 45: 1293-1302.
11. Simonneau G, D'Armini AM, Ghofrani HA, et al. Predictors of long-term outcomes in patients treated with riociguat for chronic thromboembolic pulmonary hypertension: data from the CHEST-2 open-label, randomised, long-term extension trial. Lancet Respir Med 2016; 4: 372-380.
12. Opitz CF, Kirch W, Mueller EA, et al. Bleeding events in pulmonary arterial hypertension. Eur J Clin Invest 2009; 39 Suppl 2: 68-73.
13. Jujo-Sanada T, Tanabe N, Sakao S, et al. The anticoagulant effects of warfarin and the bleeding risk associated with its use in patients with chronic thromboembolic pulmonary hypertension at a specialist center in Japan: a retrospective cohort study. Pulm Circ 2017; 7: 684-691.
14. Lenting PJ, Christophe OD and Denis CV. von Willebrand factor biosynthesis, secretion, and clearance: connecting the far ends. Blood 2015; 125: 2019-2028.
15. Badimon L, Vilahur G, Rocca B, et al. The key contribution of platelet and vascular arachidonic acid metabolism to the pathophysiology of atherothrombosis. Cardiovasc Res 2021; 117: 2001-2015.
16. van den Berg BM, Nieuwdorp M, Stroes ES, et al. Glycocalyx and endothelial (dys) function: from mice to men. Pharmacol Rep 2006; 58 Suppl: 75-80.
17. McCormack JJ, Lopes da Silva M, Ferraro F, et al. Weibel-Palade bodies at a glance. J Cell Sci 2017; 130: 3611-3617.
18. De Meyer SF, De Maeyer B, Deckmyn H, et al. Von Willebrand factor: drug and drug target. Cardiovasc Hematol Disord Drug Targets 2009; 9: 9-20.
19. Padilla A, Moake JL, Bernardo A, et al. P-selectin anchors newly released ultralarge von Willebrand factor multimers to the endothelial cell surface. Blood 2004; 103: 2150-2156.
20. Huang J, Roth R, Heuser JE, et al. Integrin alpha(v)beta(3) on human endothelial cells binds von Willebrand factor strings under fluid shear stress. Blood 2009; 113: 1589-1597.
21. Manz XD, Szulcek R, Pan X, et al. Epigenetic Modification of the VWF Promotor Drives Platelet Aggregation on the Pulmonary Endothelium in Chronic Thromboembolic Pulmonary Hypertension. Am J Respir Crit Care Med 2022: in press.
22. Reiss C, Mindukshev I, Bischoff V, et al. The sGC stimulator riociguat inhibits platelet function in washed platelets but not in whole blood. Br J Pharmacol 2015; 172: 5199-5210.
23. Manz XD, Albers HJ, Symersky P, et al. In vitro microfluidic disease model to study whole blood-endothelial interactions and blood clot dynamics in real-time. J Vis Exp 2020.
24. Sanada TJ, Sun XQ, Happé C, et al. Altered TGFβ/SMAD signaling in human and rat models of pulmonary hypertension: an old target needs attention. Cells 2021; 10: 84.

25. Schillemans M, Karampini E, van den Eshof BL, et al. Weibel-Palade Body Localized Syntaxin-3 Modulates Von Willebrand Factor Secretion From Endothelial Cells. Arterioscler Thromb Vasc Biol 2018; 38: 1549-1561.
26. Frey R, Becker C, Saleh S, et al. Clinical Pharmacokinetic and Pharmacodynamic Profile of Riociguat. Clin Pharmacokinet 2018; 57: 647-661.
27. Xiang Y and Hwa J. Regulation of VWF expression, and secretion in health and disease. Curr Opin Hematol 2016; 23: 288-293.
28. Yamamoto K, Nishimura R, Kato F, et al. Protective role of endothelial progenitor cells stimulated by riociguat in chronic thromboembolic pulmonary hypertension. Int J Cardiol 2020; 299: 263-270.
29. Purdy M, Obi A, Myers D, et al. P- and E- selectin in venous thrombosis and non-venous pathologies. J Thromb Haemost 2022; 20: 1056-1066.
30. Purdy M, Obi A, Myers D, et al. P- and E- selectin in venous thrombosis and non-venous pathologies. J Thromb Haemost 2022.
31. Michaux G, Pullen TJ, Haberichter SL, et al. P-selectin binds to the D'-D3 domains of von Willebrand factor in Weibel-Palade bodies. Blood 2006; 107: 3922-3924.
32. Ahluwalia A, Foster P, Scotland RS, et al. Antiinflammatory activity of soluble guanylate cyclase: cGMP-dependent down-regulation of P-selectin expression and leukocyte recruitment. Proc Natl Acad Sci U S A 2004; 101: 1386-1391.
33. Cleator JH, Zhu WQ, Vaughan DE, et al. Differential regulation of endothelial exocytosis of P-selectin and von Willebrand factor by protease-activated receptors and cAMP. Blood 2006; 107: 2736-2744.
34. Alba GA, Atri D, Darbha S, et al. Chronic thromboembolic pulmonary hypertension: the bench. Curr Cardiol Rep 2021; 23: 141.

Supplementary Table 1. **Individual Baseline characteristics of CTEPH patients used for PAEC isolation**

Donor	Age	Sex	sPAP (mmHg)	dPAP (mmHg)	mPAP (mmHg)	PCWP (mmHg)	saturation VCI (%)	CO (L/min)	PVR (dyne/s/cm^{-5})	Medication	Experiment
CTEPH01	79	M	78	27	45	14	57	5,4	460,1		a, b, c, e, f
CTEPH02	52	M	113	38	61	12		3,3	1192		a, f
CTEPH04	70	F	98	37	59	19	73	4,9	653,1		b, c, f
CTEPH05	68	M	84	32	50	8	44	4	840	Riociguat	a, b, c, d, e
CTEPH06	56	M	80	31	49	13		6,7	382,1		a, b, f
CTEPH09	49	F	86	32	52	12		7,5	427		d, f
CTEPH11	55	M	64	31	44	13		5,1	486		d,f
CTEPH13	59	M	86	30	50	14		4,4	655		e, f
CTEPH17	29	F	77	45	56	11		3		Riociguat	e, f
CTEPH19	66	F	70	21	39	6	81	7,13	370,3		b, c, e, f
CTEPH21	71	F	106	42	64	10	61	4,1	1053,7	Riociguat	d, f
CTEPH33	77	M	67	34	46	15	66	5,4	462,7		f

CTEPH = chronic thromboembolic pulmonary hypertension; sPAP = systolic pulmonary artery pressure; dPAP = diastolic pulmonary artery pressure; mPAP = mean pulmonary artery pressure; PCWP = pulmonary capillary wedge pressure SvO2 = mixed venous oxygen saturation; CO = cardiac output; PVR = pulmonary vascular resistance; N/A = not available | a = isolated platelet perfusion; b = Quantative Polymerase Chain Reaction; c = Western blot; d = Enzyme Linked Immunosorbent Assay; e = immunofluorescence staining | f = FACS

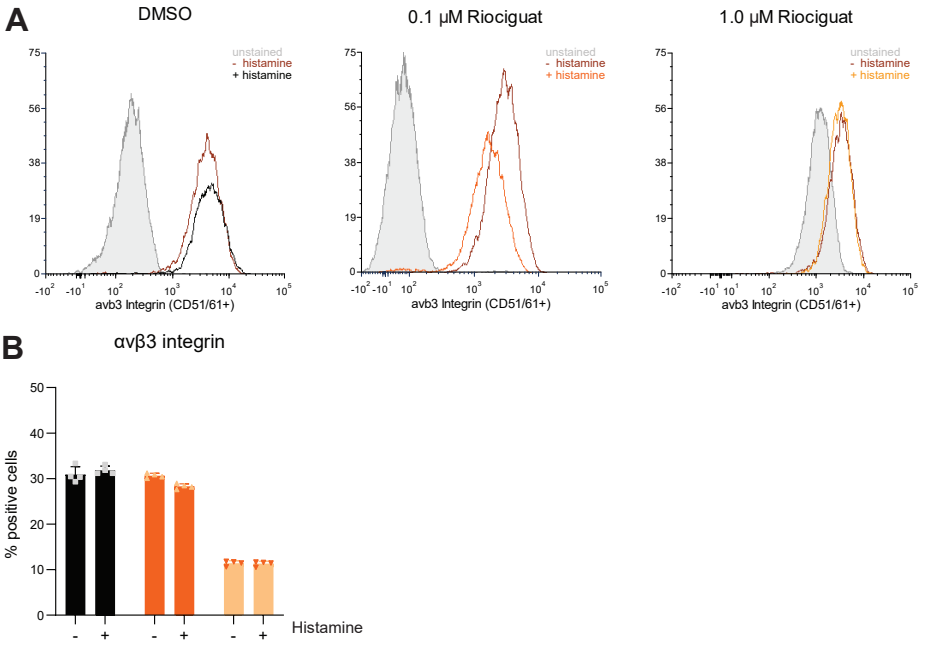

Supplementary Figure 1. αvβ3 (CD51/61+) Integrin surface expression (A) FACS analysis demonstrated by fluorescence histogram on PAEC gated population (B) Percentage of PAEC positive for CD51/61+. Data is expressed as mean ± SD and was not significant.

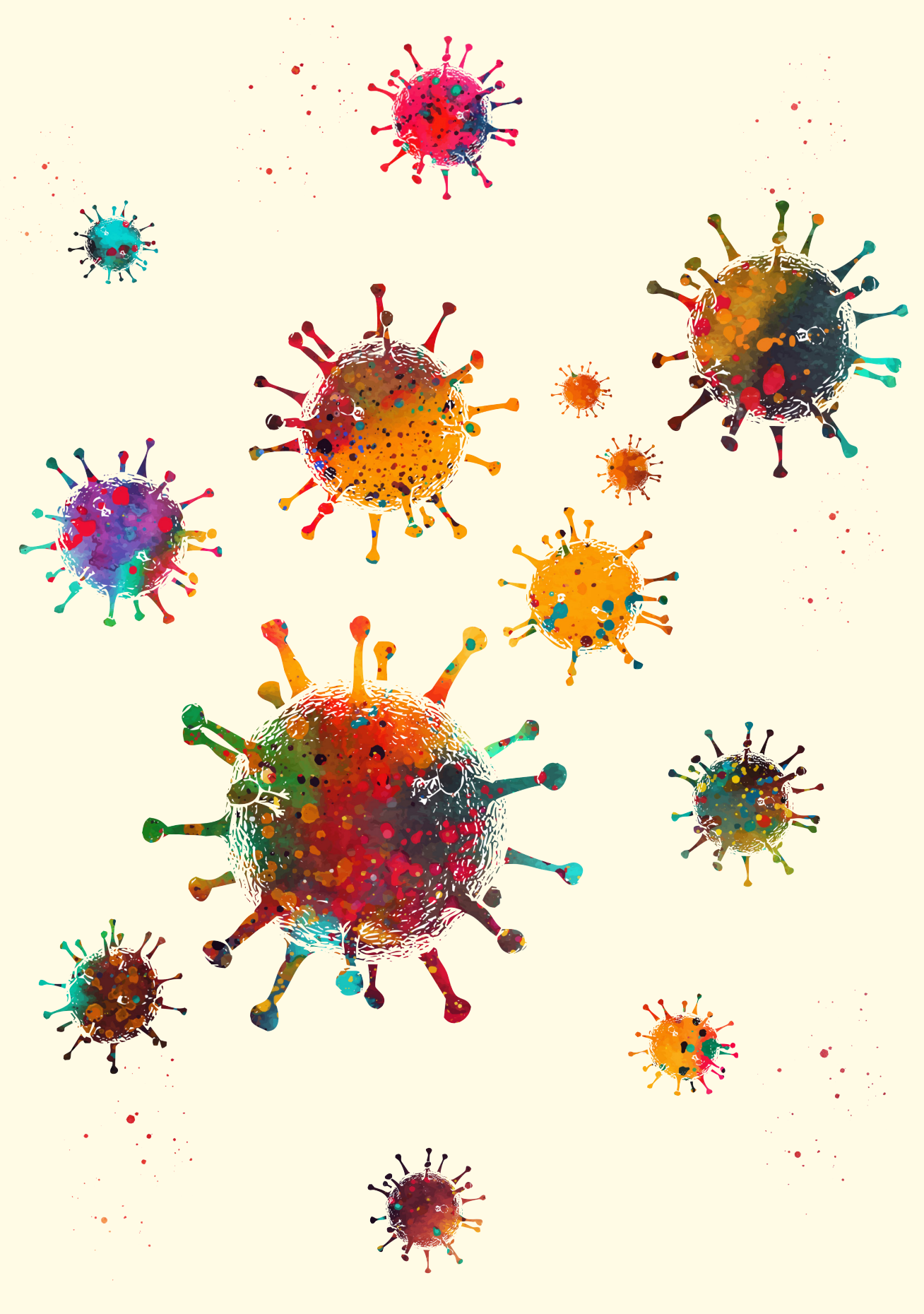

PART III

Corona virus disease 2019

CHAPTER 7

High titers and low fucosylation of early human anti–SARS-CoV-2 IgG promote inflammation by alveolar macrophages

Willianne Hoepel[1,2]*, Hung-Jen Chen[3]*, Chiara E. Geyer*[1,2], Sona Allahverdiyeva[1,2,4], **Xue D. Manz**[5], Steven W. de Taeye[4,6,7], Jurjan Aman[5], Lynn Mes[1,2,4], Maurice Steenhuis[6], Guillermo R. Griffith[3], Peter I. Bonta[8], Philip J.M. Brouwer[4], Tom G. Caniels[4], Karlijn van der Straten[4,9], Korneliusz Golebski[10], René E. Jonkers[8], Mads D. Larsen[7], Federica Linty[7], Jan Nouta[11], Cindy P.A.A. van Roomen[3], Frank E.H.P. van Baarle[12], Cornelis M. van Drunen[13], Gertjan Wolbink[6,14], Alexander P.J. Vlaar[12], Goedelieve J. de Bree[9], Rogier W. Sanders[4,15], Lisa Willemsen[3], Annette E. Neele[3], Diederik van de Beek[16], Theo Rispens[6], Manfred Wuhrer[11], Harm Jan Bogaard[5], Marit J. van Gils[4], Gestur Vidarsson[7], Menno de Winther[3#], Jeroen den Dunnen[1,2#]

[1]Department of Rheumatology and Clinical Immunology, Amsterdam UMC, Amsterdam Rheumatology and Immunology Center
[2]Department of Experimental Immunology, Amsterdam UMC, University of Amsterdam, Amsterdam Infection and Immunity Institute
[3]Department of Medical Biochemistry, Experimental Vascular Biology, Amsterdam UMC, University of Amsterdam, Amsterdam Cardiovascular Sciences, Amsterdam Infection and Immunity
[4]Department of Medical Microbiology, Amsterdam UMC, University of Amsterdam, Amsterdam Infection and Immunity Institute
[5]Department of Pulmonary Medicine, Amsterdam UMC, VU University Medical Center, Amsterdam Cardiovascular Sciences
[6]Department of Immunopathology, Sanquin Research and Landsteiner Laboratory, Amsterdam UMC, University of Amsterdam
[7]Department of Experimental Immunohematology, Sanquin Research and Landsteiner Laboratory, Amsterdam UMC, University of Amsterdam
[8]Department of Pulmonology, Amsterdam UMC, University of Amsterdam
[9]Department of Internal Medicine, Amsterdam UMC, University of Amsterdam, Amsterdam Infection and Immunity Institute
[10]Department of Respiratory Medicine, Amsterdam UMC, University of Amsterdam
[11]Center for Proteomics and Metabolomics, Leiden University Medical Center
[12]Department of Intensive Care Medicine, Amsterdam UMC, University of Amsterdam
[13]Department of Otorhinolaryngology, Amsterdam UMC, University of Amsterdam
[14]Department of Rheumatology, Amsterdam Rheumatology and Immunology Center, Reade Amsterdam
[15]Weill Medical College of Cornell University, New York, USA.
[16]Departments of Neurology and Neuroscience, University of Amsterdam

2 June 2021, Science Translational Medicine

Abstract

Patients diagnosed with coronavirus disease 2019 (COVID-19) become critically ill primarily around the time of activation of the adaptive immune response. Here, we provide evidence that antibodies play a role in the worsening of disease at the time of seroconversion. We show that early-phase severe acute respiratory distress syndrome coronavirus 2 (SARS-CoV-2) spike protein–specific immunoglobulin G (IgG) in serum of critically ill COVID-19 patients induces excessive inflammatory responses by human alveolar macrophages. We identified that this excessive inflammatory response is dependent on two antibody features that are specific for patients with severe COVID-19. First, inflammation is driven by high titers of anti-spike IgG, a hallmark of severe disease. Second, we found that anti-spike IgG from patients with severe COVID-19 is intrinsically more proinflammatory because of different glycosylation, particularly low fucosylation, of the antibody Fc tail. Low fucosylation of anti-spike IgG was normalized in a few weeks after initial infection with SARS-CoV-2, indicating that the increased antibody-dependent inflammation mainly occurs at the time of seroconversion. We identified Fcγ receptor (FcγR) IIa and FcγRIII as the two primary IgG receptors that are responsible for the induction of key COVID-19–associated cytokines such as interleukin-6 and tumor necrosis factor. In addition, we show that anti-spike IgG–activated human macrophages can subsequently break pulmonary endothelial barrier integrity and induce microvascular thrombosis in vitro. Last, we demonstrate that the inflammatory response induced by anti-spike IgG can be specifically counteracted by fostamatinib, an FDA- and EMA-approved therapeutic small-molecule inhibitor of Syk kinase.

Introduction

Coronavirus disease 2019 (COVID-19), which is caused by severe acute respiratory syndrome coronavirus 2 (SARS-CoV-2), is characterized by mild flu-like symptoms in most patients[1,2]. However, about 20% of the cases have more severe disease outcomes, with bilateral pneumonia that may rapidly deteriorate into acute respiratory distress syndrome and even death by respiratory failure. With high numbers of infected people worldwide and limited treatments available, safe and effective therapies for the most severe cases of COVID-19 are urgently needed.

Many of the COVID-19 patients with severe disease show a marked worsening of the disease around 1 to 2 weeks after onset of symptoms[2,3]. This is suggested not to be a direct effect of viral infection but instead to be caused by the overactivation of the immune system in response to infection because worsening of disease coincides with the activation of adaptive immunity[2]. This excessive immune response is frequently described as a "cytokine storm," characterized by high concentrations of proinflammatory cytokines[3,4]. A detailed assessment of the cytokine profile in severe cases of COVID-19 indicates that some cytokines and chemokines are strongly elevated, such as interleukin (IL)-6, IL-8, and tumor necrosis factor (TNF)[5-7]. In contrast, type I and III interferon (IFN) responses, which are critical for early antiviral immunity, appear to be suppressed[8,9]. Together, high proinflammatory cytokines, known to induce collateral damage to tissues, and muted antiviral responses suggest that an unfavorable immune response may be driving disease patients with severe cases of COVID-19.

Antibodies pose a potential candidate of the adaptive immune system that could explain the observed worsening of disease during SARS-CoV-2 infection. Previous studies on dengue virus identified that immunoglobulin G (IgG) antibodies can increase the infection of cells by a process known as antibody-dependent enhancement (ADE)[10]. However, thus far, there is little evidence for antibody-enhanced infection in COVID-19[11]. In addition to ADE (which increases viral infection of cells), human IgG antibodies can also worsen pathology by increasing the release of proinflammatory cytokines. Initial studies identified this phenomenon in autoimmune disorders such as rheumatoid arthritis, where IgG autoantibodies promote synovial inflammation[12,13]. More recently, antibody-dependent inflammation (ADI) has also been observed upon infection with SARS-CoV-1, and this was induced by anti-spike IgG[14]. In both rheumatoid arthritis and SARS-CoV-1 infection, IgG antibodies convert wound-healing "M2" macrophages to a proinflammatory phenotype[12,14,15]. Combined, these data hint toward a pathogenic role for IgG in severe cases of COVID-19. In this study, we explored the hypothesis that anti–SARS-CoV-2 antibodies drive excessive inflammation in severe cases of COVID-19 and define therapeutic approaches to suppress these responses.

Results

High titers of anti-spike IgG promote inflammation by alveolar macrophages

We assessed the effect of anti-spike antibodies from serum of patients who were critically ill with COVID-19 on human M2-polarized macrophages. Our previous transcriptional analysis revealed that

macrophage colony-stimulating factor (M-CSF) and IL-10 induce M2 monocyte differentiation that generates macrophages that most closely resemble primary human lung macrophages[16]. Because activation of immune cells by IgG antibodies requires immune complex formation by binding of IgG to its cognate antigen[17,18], we generated spike-IgG immune complexes by incubating SARS-CoV-2 spike–coated wells with diluted serum from patients with severe COVID-19 treated in the intensive care unit (ICU) at the Amsterdam University Medical Centers (UMC) who tested positive for anti–SARS-CoV-2 IgG (Supplementary Figure 1A). Stimulation with spike protein alone did not induce cytokine production, whereas spike-IgG immune complexes elicited small amounts of IL-1β, IL-6, and TNF but very high IL-8 production by human macrophages (**Figure 1A**). However, because in the later phase of infection (1 to 2 weeks after initial exposure) lung macrophages are simultaneously exposed to virus-associated stimuli and anti-spike IgG immune complexes, we also assessed the effect of the combination of these two stimuli. Combined stimulation of anti-spike IgG immune complexes and the Toll-like receptor 3 agonist, polyinosinic:polycytidylic acid [poly(I:C)], increased the production of COVID-19–associated proinflammatory cytokines IL-1β, IL-6, and TNF compared to IgG or poly(I:C) alone (**Figure 1A**). Similar effects were observed with other viral and bacterial co-stimuli (Supplementary Figure 1B). Induction of the anti-inflammatory cytokine IL-10 was also increased (**Figure 1A**), similar to what is observed in patients with COVID-19[19]. We confirmed these findings in primary human alveolar macrophages that were obtained by bronchoalveolar lavage (BAL), which showed similar responses (**Figure 1B**). Phenotypical analysis of these human alveolar macrophages showed significantly decreased expression of M2 markers upon costimulation with anti-spike IgG immune complexes, indicating the polarization toward a more inflammatory phenotype [$P < 0.0001$ (CD163) and $P = 0.001$ (CD209); Supplementary Figure 1C].

To assess whether the inflammatory response is dependent on anti-spike antibodies, we compared the effect of sera from 33 intensive care lung disease patients that either (i) did not have COVID-19, (ii) had COVID-19 but were still negative for anti-spike IgG, or (iii) had COVID-19 and were positive for anti-spike IgG (Supplementary table 1). Whereas serum of non–COVID-19 patients and anti-spike IgG–negative COVID-19 patients showed no up-regulation of proinflammatory cytokines compared to individual poly(I:C) stimulation, IL-1β, IL-6, IL-8, and TNF production was amplified by serum of COVID-19 patients with anti-spike IgG ($P < 0.0001$; **Figure 1C**). To further confirm that the observed inflammation is induced by anti-spike IgG and not by other inflammatory components in serum, we purified IgG from serum of critically ill COVID-19 patients that were seropositive and healthy controls that were seronegative for anti–SARS-CoV-2. Whereas proinflammatory cytokine production was strongly amplified by purified IgG from severely ill COVID-19 patients, no amplification was observed by purified IgG from controls (Supplementary Figure 1D).

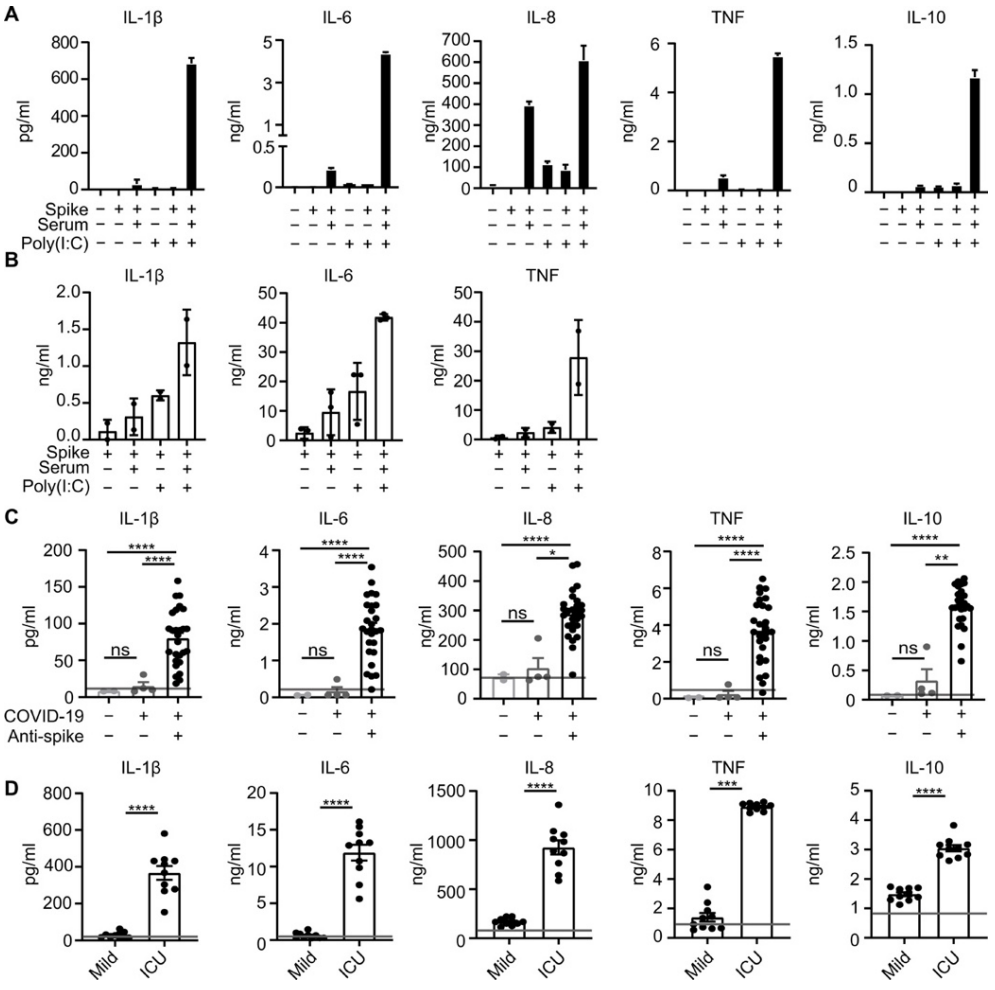

Figure 1. High titers of anti-spike IgG induce inflammation by macrophages. **(A)** Cytokine production by human macrophages after 24 hours of stimulation with combinations of spike protein, COVID-19 serum (50× diluted), and poly(I:C). Triplicate values from a representative experiment with serum from five different patients with COVID-19 and two different macrophage donors (means ± SD). **(B)** Cytokine production by primary alveolar macrophages obtained from BAL, stimulated as in (A). Every dot represents cytokine production after 24 hours by a different macrophage donor performed in triplicate (means ± SEM). **(C)** Macrophages stimulated with spike protein and poly(I:C) were costimulated with serum from patients in the ICU for lung disease that either did not have COVID-19 (n = 2), had COVID-19 but were negative for anti-spike IgG (n = 4), or had COVID-19 and were positive for anti-spike IgG (n = 27). Horizontal gray line depicts cytokine induction upon stimulation with poly(I:C) + spike protein. Significance was calculated with Brown-Forsythe and Welch's ANOVA test and corrected by Dunnett T3 test for multiple test correction (means ± SEM). **(D)** Macrophages stimulated with spike protein and poly(I:C) were costimulated with serum isolated from patients with mild COVID-19 (n = 10) and were compared to serum from patients in the ICU for COVID-19 (n = 10). Significant differences were calculated with an unpaired t test. Each dot represents cytokine production after 24 hours by macrophages stimulated with a different serum donor (mean ± SEM). Horizontal gray line depicts cytokine induction upon stimulation with poly(I:C) plus spike protein. *P < 0.05; **P < 0.01; ***P < 0.001; ****P < 0.0001; ns, not significant.

To determine whether the inflammatory responses are specific for severely ill COVID-19 patients or are also induced by patients who have mild symptoms, we directly compared cytokine amplification by serum obtained from patients with mild COVID-19 or patients in the ICU (Supplementary Table 2). Amplification of proinflammatory cytokine production was specific for severely ill patients ($P < 0.0001$; **Figure 1D**), which was in line with the substantially lower anti-spike titers in mild patients (Supplementary Figure 1E), whereas the fucosylation was comparable (Supplementary Figure 1F).

RNA sequencing analysis of macrophages stimulated with sera from anti-spike IgG–positive COVID-19 patients showed induction of a proinflammatory gene program, as highlighted by induction of TNF, ILs, chemokines, and macrophage differentiation factors (**Figure 2A**). IFN-β and IFN-γ were induced also by anti-spike–positive serum, whereas the classical downstream IFN response gene, CXCL10, was reduced ($P < 0.0001$; Supplementary Figure 1, G to I), which is in line with recent findings by others[20].

In patients with COVID-19, high anti-spike IgG titers are strongly associated with disease severity[21,22]. To determine whether anti-spike titers correlate with higher cytokine responses by human macrophages, we performed a principal component analysis of the combined cytokine production data for all samples that, upon overlaying with anti-spike IgG titers, suggested that the inflammatory response of macrophages was associated with IgG titers (**Figure 2B**). Subsequent analysis similarly demonstrated that anti–receptor binding domain (RBD) IgG titers and cytokine production correlate for the cytokines IL-1β ($P < 0.0001$), IL-6 ($P < 0.0001$), IL-8 ($P < 0.0001$), IL-10 ($P < 0.0001$), and TNF ($P < 0.0001$; **Figure 2C** and Supplementary Figure 1J). Similar correlations were observed for IL-6 and total anti-spike IgG ($P < 0.0001$; Supplementary Figure 1K). IFN-β ($P = 0.0004$) and IFN-γ ($P < 0.0001$) also showed a positive correlation, whereas CXCL10 showed a negative correlation ($P < 0.0001$; Supplementary Figure 1J), which may be related to reduced expression of IFN receptors (Supplementary Figure 1L). Stimulation with immune complexes made from three serum samples with different titers using serial-step dilutions showed a dose-dependent induction of proinflammatory cytokines (**Figure 2D**), thereby confirming that high anti-spike titers drive proinflammatory cytokine production by human macrophages.

To assess whether inflammatory responses are induced directly upon virus opsonization or whether this requires spike expression by infected cells, we stimulated macrophages with anti-spike IgG-opsonized pseudo-typed virus. Virus opsonization had no detectable effect on cytokine production (Supplementary Figure 1M), which is in line with previous findings that small IgG immune complexes are unable to trigger cytokine production[23]. In contrast, IgG-opsonized spike-expressing 293F cells, which mimic SARS-CoV-2–infected cells and induce the formation of larger immune complexes, did amplify IL-6 production by macrophages (Supplementary Figure 1N). These results indicate that anti-spike–induced inflammation requires large IgG immune complexes, as occurs upon host cell infection. Combined, these data demonstrate that high titers of anti-spike IgG from serum of severely ill COVID-19 patients induce a strong proinflammatory response by otherwise

immunosuppressive human M2 macrophages, which is characterized by the production of classical cytokine storm mediators such as IL-1β, IL-6, IL-8, and TNF.

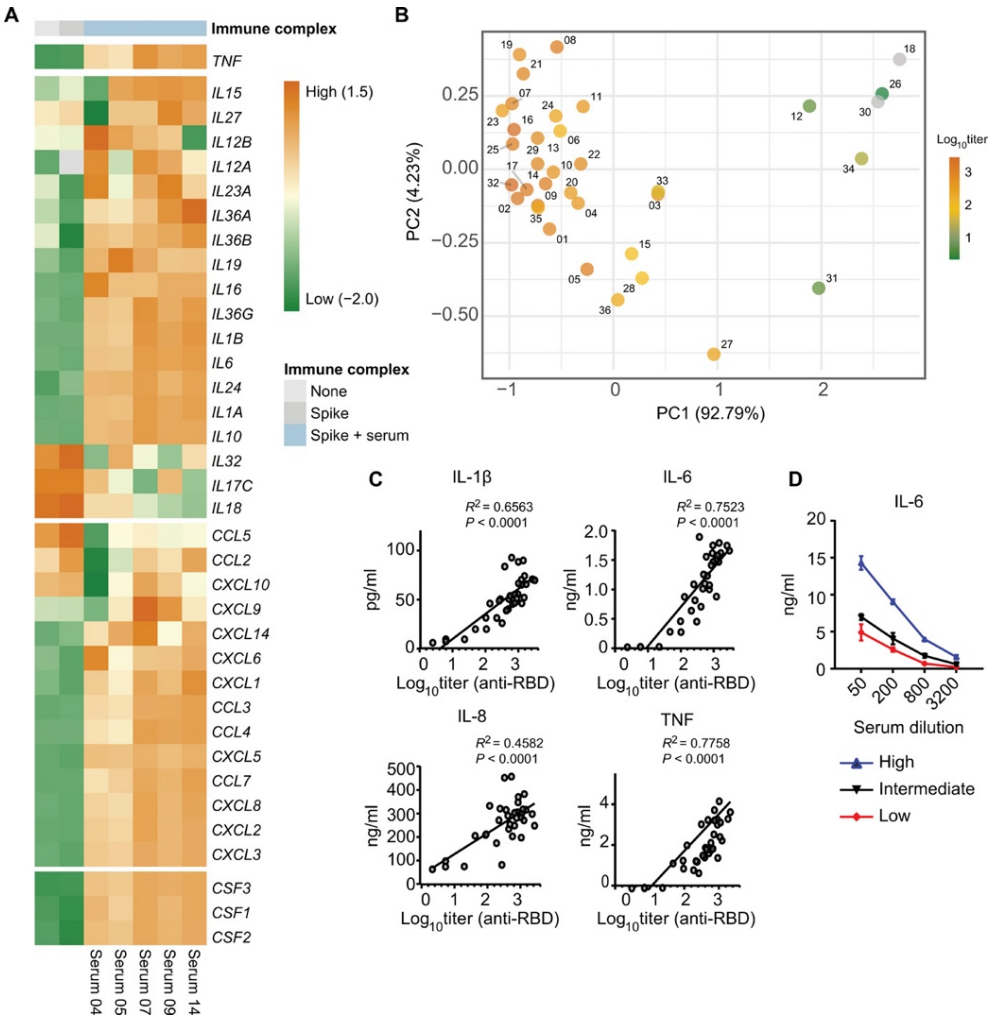

Figure 2. High titers of anti-spike IgG induce inflammation by macrophages. **(A)** Heatmap showing scaled log2 expression (z score) of genes assessed by RNA sequencing after a 6-hour stimulation of human macrophages with poly(I:C) with or without spike protein and serum from five patients with COVID-19 that tested positive for anti-spike IgG. **(B)** Principal component analysis of the combined cytokine profile (IL-1β, IL-6, IL-8, IL-10, TNF, IFN-β, IFN-γ, and CXCL10) for all serum samples overlaid with log10 anti-RBD IgG titers. Titers of each serum sample are represented by the color scale. Samples with anti-RBD IgG titer below detection limit are colored gray. Numbers represent the patients' sample number. **(C)** Correlation graphs of anti-RBD IgG titer from COVID-19 serum against cytokine production of macrophages after stimulation. The square of Pearson correlation coefficient (R2) and P value are stated in each graph. **(D)** Macrophages stimulated with spike protein and poly(I:C) were costimulated with different dilutions of serum from patients with varying anti-spike titers. Titers were from patient 2 (high titer), 5 (intermediate titer), or 6 (low titer). IL-6 production was determined after 24 hours.

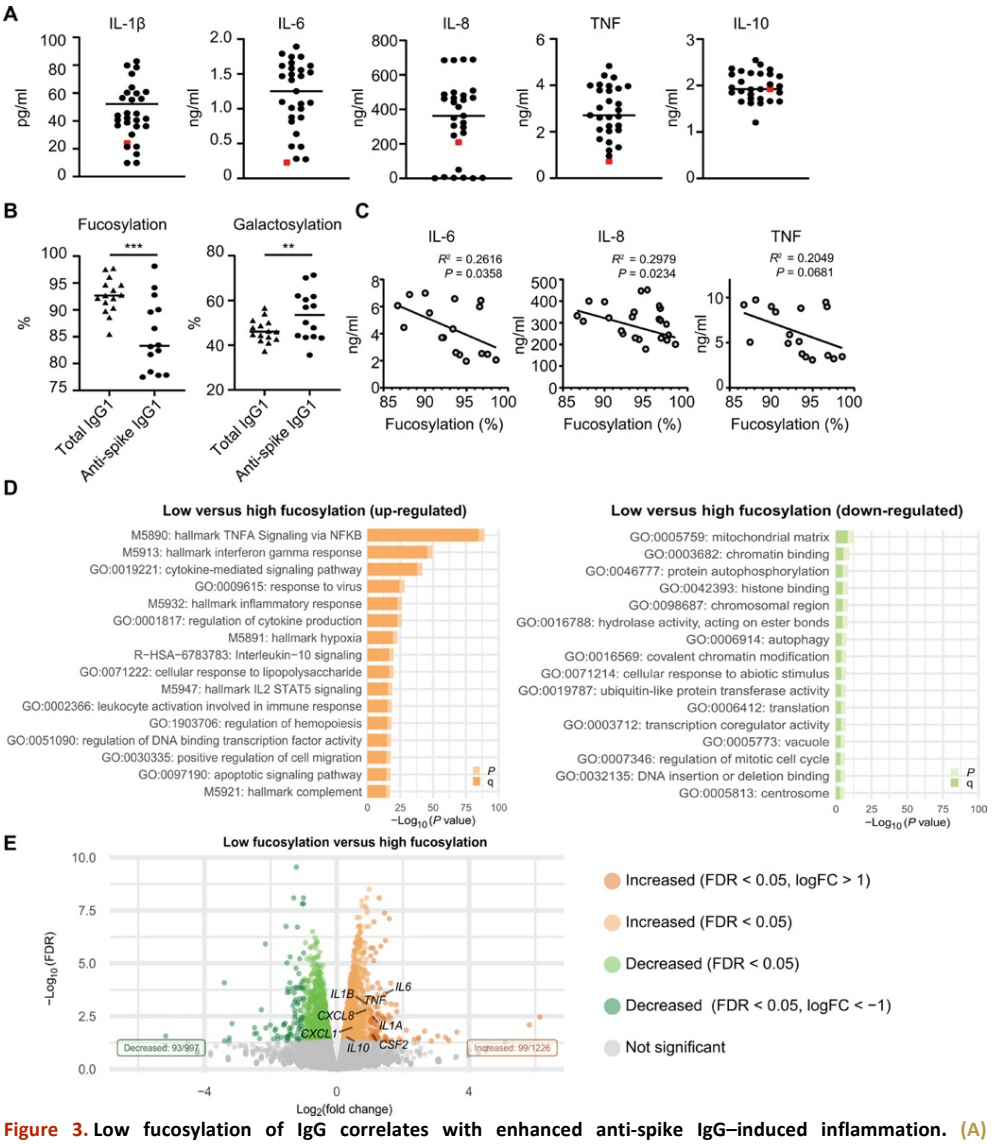

Figure 3. Low fucosylation of IgG correlates with enhanced anti-spike IgG–induced inflammation. **(A)** Macrophages stimulated with spike protein and poly(I:C) were costimulated with either 50× diluted serum from different anti-spike+ patients with COVID-19 (black dots) or with recombinant anti-spike antibody COVA1-18 (red dot). Representative example of four independent macrophages donors is shown. Cytokine production was measured after 24 hours. **(B)** Fucosylation and galactosylation of total and anti-spike–specific IgG1 antibodies. Statistics were calculated with a paired t test. **P < 0.01; ***P < 0.001. **(C)** Correlation graphs of fucosylation percentages of anti-spike IgG1 from COVID-19 serum against cytokine production of macrophages after stimulation. The square of Pearson correlation coefficient (R2) and P value are stated in each graph. **(D)** Pathway analysis of differentially expressed genes (DEGs). DEGs were defined by a false discovery rate (FDR) of <0.05 and an absolute log2 fold change higher or lower than 0. Pathway enrichment analyses were performed using the Metascape on 29 July 2020. P = P value; q = FDR-corrected P value. **(E)** Volcano plot depicting up- and down-regulated genes when comparing macrophages stimulated for 6 hours with spike, poly(I:C), and serum with low-fucosylated IgG to the same stimulation with high-fucosylated IgG.

Aberrant glycosylation of anti-spike IgG contributes to inflammation

In addition to the anti-spike antibodies from serum, we tested the effect of the recombinant anti-spike IgG COVA1-18, which we generated previously from B cells isolated from a patient with COVID-19[24]. We stimulated macrophages with anti-spike immune complexes made with a high concentration of recombinant anti-spike antibody COVA1-18 (mimicking a serum concentration of 100 µg/ml in our assay). This concentration is higher than the average anti–SARS-CoV-2 IgG concentration in patients with severe COVID-19, which, according to previous studies, on average peaks at 16.5 µg/ml[25]. The high concentration of COVA1-18 immune complexes elicited substantially less IL-1β, IL-6, and TNF than anti-spike immune complexes made from COVID-19 serum (**Figure 3A**). We did not observe this difference for the induction of anti-inflammatory cytokine IL-10 (**Figure 3A**). These data suggest that the anti-spike IgG in severe cases of patients with COVID-19 is intrinsically more proinflammatory than a recombinant IgG against the same target.

One of the critical characteristics that determine IgG pathogenicity is the glycosylation of the IgG Fc tail at position 297[26,27]. Recently, we and others[28, 29] have shown that anti-spike IgG of patients with severe COVID-19 have aberrant fucosylation and galactosylation, both compared to the total IgG within these individual patients, as well as compared to anti-spike IgG from mild or asymptomatic patients. We determined the glycosylation pattern of a subset of COVID-19 serum samples in the present study, which showed significantly decreased fucosylation (P = 0.0003) and increased galactosylation of anti-spike IgG compared to total IgG within the tested patients (P = 0.0096; **Figure 3B**), similar to the study of Larsen et al[28]. Fucosylation of anti-spike IgG correlated negatively with macrophage production of proinflammatory cytokines IL-6 (P = 0.0358) and IL-8 (P = 0.0234; **Figure 3C**). No correlation was observed for TNF, IL-1β, or IL-10 (**Figure 3C** and Supplementary Figure 2A). CXCL10 showed a positive correlation (P = 0.0443; Supplementary Figure 2A). RNA sequencing data from patients with relatively low fucosylation (sera 07, 09, and 14) and from patients with relatively normal fucosylation (sera 04 and 05) showed a very pronounced induction of inflammatory mediators and proinflammatory pathways specifically in low-fucosylation patients (**Figure 3D-E**).

To determine whether anti-spike glycosylation directly modulates cytokine induction, we stimulated macrophages with regular monoclonal COVA1-18 or modified COVA1-18 that had low fucosylation or high galactosylation (Supplementary Table 3). COVA1-18 with low fucosylation showed an increased capacity for amplification of proinflammatory cytokines (P < 0.0001; **Figure 4A**). High galactosylation alone or in combination with low IgG fucosylation did not lead to elevated cytokine production (**Figure 4A**). COVA1-18 with low fucose and high galactose showed a similar amplification of IL6, IL8, and TNF mRNA expression over time (**Figure 4B**), whereas CXCL10 mRNA expression was again inhibited (Supplementary Figure 2B). To gain more insight into the molecular mechanisms that underlie the enhanced inflammatory response induced by anti-spike IgG with aberrant glycosylation, we focused on the transcriptional responses induced by the anti-spike IgGs. Motif analyses of genes differentially induced by anti–SARS-CoV-2 monoclonal IgG COVA1-18 showed clear enrichment for classical

inflammatory transcription factors like EGR, p65 (RELA), and Maf (**Figure 4C**). Upon comparison of genes affected by the differential glycosylation in patient samples, we identified IFN-stimulated response elements as a key enriched motif (**Figure 4D**), suggesting amplification of macrophage activation via IFN pathways. This was further indicated by increased IFN-β and IFN-γ secretion (Supplementary Figure 2C) by afucosylated IgG compared to IgG with normal fucosylation and by increased expression of a series of classical IFN response genes (**Figure 4E**)[30]. These data suggest that afucosylated anti–SARS-CoV-2 IgG promotes inflammation by engagement of IFN pathways, which are classical cofactors to promote macrophage activation[31].

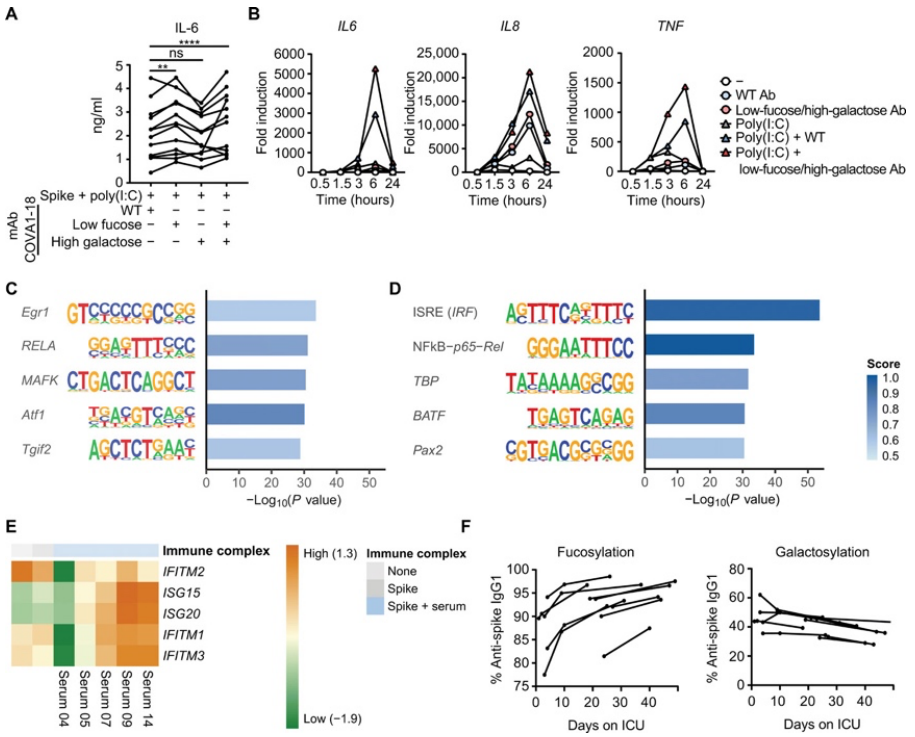

Figure 4. Low fucosylation of IgG promotes inflammatory cytokine production. **(A)** Macrophages stimulated with spike protein were costimulated with combinations of poly(I:C), COVA1-18 [wild-type (WT), recombinant anti-spike IgG1], or COVA1-18 that had been modified to express low fucose or high galactose. IL-6 production was measured after 24 hours. Each line represents one macrophage donor, performed in triplicate. Statistics were calculated with two-way ANOVA. **P < 0.01; ****P < 0.0001. mAb, monoclonal antibody. **(B)** Time-dependent fold changes (to 0-hour unstimulated M2 macrophages) in gene expression are depicted in line chart for IL6, IL8, and TNF. Macrophages stimulated with poly(I:C) were costimulated with immune complexes of wild-type antibody (Ab) or an antibody that had been modified to express low fucose or high galactose. Representative example of six independent macrophages donors is shown. Cytokine production was measured after 0.5, 1.5, 3, 6, and 24 hours. **(C)** Enriched motifs for significantly up-regulated genes when comparing macrophages stimulated for 6 hours with spike and poly(I:C), with or without anti-spike IgG. **(D)** Enriched motifs for significantly up-regulated genes when comparing macrophages stimulated for 6 hours with spike, poly(I:C), and serum with low-fucosylated IgG to the same stimulation with high-fucosylated IgG. **(E)** Heatmap showing scaled log2 expression (z score) of IFN-stimulated genes assessed by RNA sequencing after a 6-hour stimulation of human macrophages with poly(I:C) with or without spike protein and serum from five seropositive patients with COVID-19. **(F)** IgG1 fucosylation and galactosylation of anti-spike specific antibodies were determined in serum samples over time for patients in the ICU with COVID-19. Each line represents one donor.

Last, we determined whether the aberrant glycosylation pattern of anti-spike IgG is stable over time, by analyzing fucosylation and galactosylation over time of the patients in our study. Both fucosylation and galactosylation normalized within days to weeks after ICU admission (**Figure 4F**). Similar results were observed for the other types of IgG glycosylation (Supplementary Figure 2D). These data indicate that, in patients critically ill with COVID-19, the first anti-spike IgG antibodies that are produced after infection are intrinsically more inflammatory by bearing different glycosylation patterns.

Anti-spike IgG induces activation of endothelium and platelets *in vitro*

The excessive lung inflammation in severely ill COVID-19 patients often leads to pulmonary edema, after disruption of the microvascular endothelium[32], and coagulopathy, which in many patients is characterized by pulmonary thrombosis[33]. To test whether the excessive macrophage activation by anti-spike IgG may contribute to pulmonary edema and thrombosis, we applied in vitro models for endothelial barrier integrity (34) and in situ thrombosis[35] using primary human pulmonary artery endothelial cells (HPAECs), where thrombocytes are added under flow conditions. For this, we stimulated macrophages and used the supernatant to assess endothelium and platelet activation. Although conditioned medium of poly(I:C)-stimulated macrophages induced only a transient drop in endothelial barrier integrity, costimulation of macrophages with spike protein and serum isolated from patients with severe COVID-19 induced long-lasting endothelial barrier disruption (**Figure 5A**). In addition, during platelet perfusion, we observed significantly increased platelet adhesion to endothelium exposed to conditioned medium of macrophages that had been costimulated with spike protein and serum ($P < 0.0001$; **Figure 5B**). This effect was paralleled by an increase in von Willebrand factor release from the endothelial cells (**Figure 5C**), indicative of an active procoagulant state of the endothelium. These data suggest that anti-spike IgG–induced inflammation by macrophages may contribute to permeabilization of pulmonary endothelium, microvascular thrombosis, and subsequent severe pulmonary problems.

Fostamatinib counteracts inflammation induced by anti-spike IgG

Anti-spike IgG from severely ill COVID-19 patients promoted inflammatory cytokines, endothelial barrier disruption, and microvascular thrombosis in vitro, which are key phenomena underlying pathology in patients with severe COVID-19. Hence, counteracting this antibody-induced aberrant immune response could be of potential therapeutic interest. To determine how to counteract this ADI, we first set out to investigate which receptors on human macrophages are activated by the anti–SARS-CoV-2 IgG immune complexes. IgG immune complexes can be recognized by Fcγ receptors (FcγRs), which include FcγRI, FcγRIIa, and FcγRIII[18], which are all expressed on our human M2 macrophages (**Figure 6A**). To determine whether FcγRs are involved in activation by anti-spike immune complexes, we blocked the different FcγRs with specific antibodies during stimulation and analyzed cytokine production after exposure to anti-spike immune complexes. All FcγRs contributed to anti-spike–induced cytokine induction, but the most pronounced inhibition was observed upon blockade of FcγRIIa (**Figure 6B**). No inhibition was observed upon blocking of FcαRI, suggesting that IgA does not play a substantial role in the observed cytokine induction (**Figure 6B**).

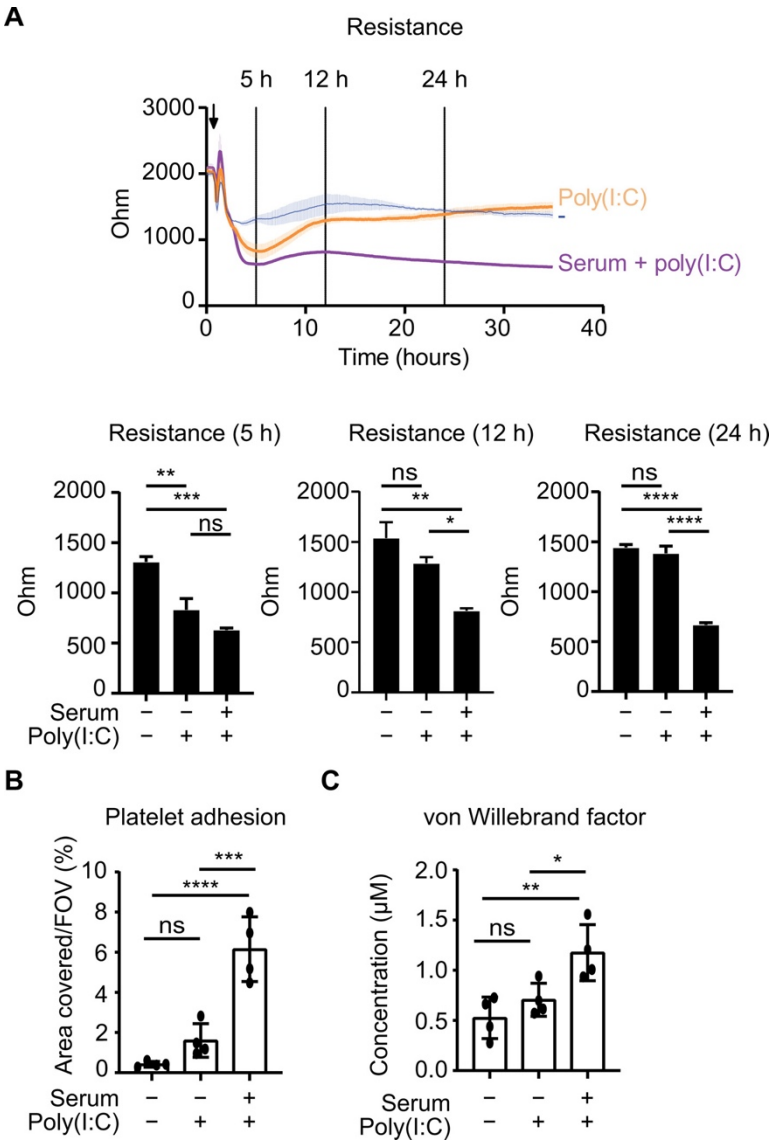

Figure 5. Anti-spike IgG breaks endothelial barrier integrity and activates platelets *in vitro*. **(A)** Human pulmonary arterial endothelial cells were exposed to supernatants of macrophages that were unstimulated or had been stimulated with poly(I:C) and spike protein, with or without serum from patients with COVID-19. Endothelial barrier integrity was quantified by measuring the resistance over time using electrical cell-substrate impedance sensing. Statistics were calculated using an ordinary one-way ANOVA and corrected with Tukey's comparisons test. **(B)** Endothelium stimulated as in (A) for 24 hours was perfused with platelets for 5 min, after which the area covered by platelets was quantified. FOV, field of view. **(C)** Flow supernatant was collected after perfusion under (B), and von Willebrand factor concentrations were measured with ELISA. Statistics were calculated using an ordinary one-way ANOVA and corrected using Sidak's multiple comparison test. *P < 0.05; **P < 0.01; ***P < 0.001; ****P < 0.0001.

Because changes in glycosylation of the Fc tail can differentially affect the interaction of IgG with the different FcγRs, we also blocked the three different FcγRs upon costimulation with monoclonal IgG that either had conventional Fc glycosylation or low fucose and high galactose. Cytokine induction by both IgG with conventional glycosylation and low fucose and high galactose was mostly dependent on FcγRIIa (**Figure 6C**). However, FcγRIII appeared to be the primary receptor responsible for the enhanced cytokine production by aberrant IgG glycosylation, because blocking FcγRIII specifically counteracted IL-6 and TNF production induced by IgGs with low fucose and high galactose (**Figure 6C**). We did not observe this for IL-1β (Supplementary Figure 3A), which may be related to the activation of caspase-1 that is known to be mainly dependent on FcγRIIa[36].

FcγRs are known to induce signaling that critically depends on the kinase Syk[12,36]. To determine whether we could counteract anti-spike–induced immune activation, we blocked Syk using R406, the active component of the small-molecule inhibitor fostamatinib, a U.S. Food and Drug Administration (FDA)– and European Medicines Agency (EMA)–approved drug for the treatment of immune thrombocytopenia (ITP)[37]. R406 significantly reduced proinflammatory cytokine production induced by anti-spike IgG from patients with severe COVID-19 ($P < 0.0001$; **Figure 6D-E**). Inhibition by R406 appeared to be specific, because it selectively blocked anti-spike–induced amplification of cytokines but did not substantially affect cytokine production induced by poly(I:C) alone (**Figure 6D**). Similar effects were observed with primary human macrophages obtained from BAL fluid (Supplementary Figure 3B).

To assess the consequences of inhibition by fostamatinib in greater detail, we analyzed the effects of R406 on macrophages stimulated with spike, serum from patients with COVID-19, and poly(I:C) by RNA sequencing. In total, 4386 genes were suppressed by R406 treatment, whereas 3976 genes were induced [false discovery rate (FDR) < 0.05; **Figure 6F**]. Many of the classical proinflammatory mediators were present in the list of genes down-regulated by R406 treatment, including TNF, IL1B, IL6, and CCL2. Pathway analyses showed no clear pathways in the up-regulated genes, although suppressed genes were linked to inflammatory pathways (Supplementary Figure 3C). Last, gene set enrichment analysis (GSEA) showed that genes associated with several proinflammatory pathways, including IL-1 signaling and TNF production and response, were significantly down-regulated by R406 ($P = 0.013$; **Figure 6G**). Response to type I IFN, FcγR signaling, glycolysis, and platelet activation gene sets were suppressed (Supplementary Figure 3D). These data demonstrate that the excessive inflammatory response by anti-spike IgG from severely ill COVID-19 patients can be counteracted by the Syk inhibitor fostamatinib.

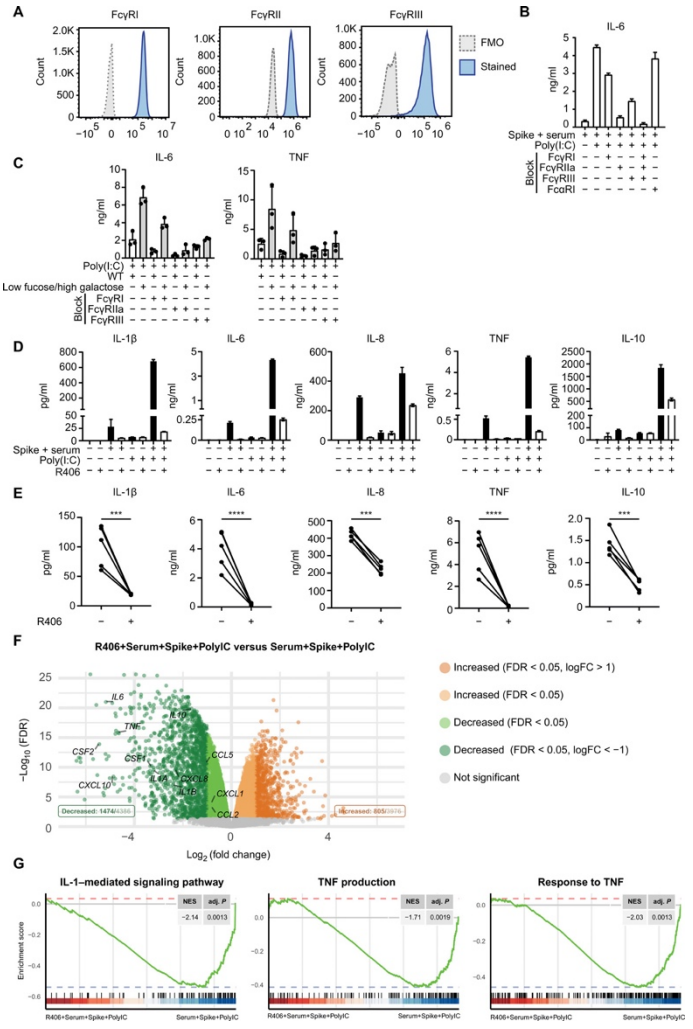

Figure 6. Anti-spike IgG–induced inflammation is FcγR dependent and can be counteracted by fostamatinib. **(A)** Membrane expression of FcγRI, FcγRII, and FcγRIII by human macrophages was determined by flow cytometry. FMO, fluorescence minus one control. **(B)** FcγRI, FcγRII, FcγRIII, and FcαRI were blocked by specific antibodies, after which macrophages were stimulated with spike, COVID-19 serum, poly(I:C), or a combination. IL-6 production was measured after 24 hours. Triplicate values from a representative experiment with serum from three different patients with COVID-19 and two different macrophage donors (means ± SD). **(C)** FcγRI, FcγRII, and FcγRIII were blocked by specific antibodies, after which macrophages stimulated with poly(I:C) and immune complexes of wild-type antibody or an antibody that had been modified to express low fucose and high galactose. Each dot represents cytokine production after 24 hours by a different macrophage donor (means ± SEM). **(D and E)** Macrophages were preincubated with Syk inhibitor R406, after which cells were stimulated as in (B). Cytokine production was measured after 24 hours. A representative donor is shown (D), and data are presented as means ± SD. The response for multiple donors with or without preincubation with R406 is shown (E). Every pair of dots represents cytokine production after 24 hours by a different serum donor. Statistics were calculated with a ratio paired t test. ***P < 0.001; ****P < 0.0001. **(F)** Volcano plot depicting up- and down-regulated genes when comparing macrophages stimulated for 6 hours with spike, poly(I:C), and serum to the same stimulation in the presence of R406. **(G)** Gene set enrichment analysis (GSEA) of curated gene sets suppressed by R406: IL-1–mediated signaling pathway (GO: 0070498), TNF production (GO: 0032640), response to TNF (GO: 0034612). NES, normalized enrichment score; adj. P, Benjamini-Hochberg (BH)–adjusted P value.

Discussion

It is still not well understood why many patients with COVID-19 become critically ill around the time of activation of adaptive immune responses. Here, we identified the induction of pathogenic IgG antibody responses against the spike protein as a potential cause, which not only amplifies proinflammatory responses by human macrophages but also induces subsequent endothelial barrier

disruption and thrombosis (Supplementary Figure 4). The induction of inflammation by anti–SARS-CoV-2 IgG is both dependent on anti-spike IgG titers and on low fucosylation of these antibodies, which increases their inflammatory potential, most likely by overactivation through FcγRIII. During the course of infection, both these inflammatory parameters change. Anti-spike IgG titers rapidly increase after seroconversion followed by a gradual decline[38]. In contrast, only the first wave of anti-spike IgG displays aberrant Fc glycosylation (characterized by low fucose and high galactose), which rapidly normalizes in the following days to weeks. On the basis of these two parameters, the induction of excessive inflammation by anti-spike IgG is particularly likely to occur in the days right after seroconversion, when titers are high and glycosylation is most aberrant. This correlates with the observed pathology in severely ill COVID-19 patients, which show a peak in inflammation, edema, and thrombosis around the time of seroconversion[2,3]. In addition, this also correlates with the common absence of excessive inflammation in people that become reinfected with SARS-CoV-2[39,40], because the anti-spike IgG in these reinfected individuals will have lower titers and most likely will have normalized Fc glycosylation.

In general, antibodies are beneficial for host defense by providing various mechanisms to counteract infections, including pathogen neutralization, phagocytosis, complement activation, antibody-dependent cellular cytotoxicity (ADCC), and cytokine production[41]. These different effector functions of antibodies are induced to a greater or lesser extent depending on antibody-intrinsic characteristics, such as isotype, subclass, allotype, and glycosylation[26]. In patients who are severely ill with COVID-19, the glycosylation of anti-spike IgG is changed, which can lead to pathology by overactivation of IgG effector functions, as we show here by particularly amplifying the production of COVID-19–associated cytokines such as IL-6 and TNF[5,42]. Decreased IgG fucosylation, as observed in severe cases of COVID-19, has previously been observed in patients infected with HIV or dengue virus[43, 44] and may actually be a general phenomenon in a response to enveloped viruses[28]. For dengue virus, decreased IgG fucosylation has been described to contribute to the worsening of the course of disease after reinfection[10]. However, it is important to realize that the underlying mechanism by which low-fucose IgG contributes to disease exacerbation is very different between dengue virus and SARS-CoV-2. In dengue virus infections, decreased IgG fucosylation worsens the pathology by binding to the virus and increasing the infection of host cells through enhanced uptake by FcγRs, a process known as ADE[10]. For SARS-CoV-2, there is very little evidence for ADE. Instead, increased pathology by afucosylated IgG in patients with COVID-19 likely results from excessive immune activation. To make this difference clear, we propose to not use the term ADE but instead to use ADI to denote antibody-induced pathology as observed in patients with COVID-19.

The combination of decreased fucosylation and increased galactosylation of IgG is known to increase the affinity for FcγRIII[26]. Whereas FcγRIII was the primary receptor responsible for the inflammatory responses that were specifically induced by IgG with low fucose and high galactose, FcγRIIa contributed most to anti-spike–induced inflammation overall. These findings indicate that

collaboration between multiple FcγRs is required for ADI by anti-spike IgG. The observed FcγR-dependent overactivation of human alveolar macrophages, which generally have a wound-healing M2 phenotype, is in line with the general concept that the effect of ADI is most pronounced in immune cells that have a tolerogenic or anti-inflammatory phenotype, such as synovial M2 macrophages[12] or intestinal CD103+ dendritic cells[45]. Although we focused on alveolar macrophages in this study, FcγRII and FcγRIII are also expressed by various other myeloid immune cells that are found in the inflamed lungs of patients with severe COVID-19, such as monocytes and neutrophils[3,46]. Overactivation of neutrophils by COVID-19 patient plasma can also be inhibited by fostamatinib[47]. In addition, the high degree of aberrantly glycosylated anti-spike IgG could also contribute to pathology by activating nonimmune cells. For example, airway epithelial cells express FcγRIII, are one of the main target cells of infection by SARS-CoV-2, closely interact with activated macrophages[48], and are a major source of IL-6[49]. In addition, anti-spike IgG may activate platelets through FcγRIIa[50,51], which would provide a direct way of platelet activation in addition to the indirect activation by macrophages and pulmonary endothelium that we observed in this study, thereby further promoting microvascular thrombosis.

It is still unclear how severe SARS-CoV-2 infections lead to the generation of IgG antibodies with aberrant glycosylation. Regarding the total amount of IgG in circulation, changes in glycosylation are associated with age and sex, which results in slightly decreased IgG fucosylation with age[52,53]. However, in severely ill patients with COVID-19, it is specifically the anti-spike IgG that shows lower fucosylation. Although production of afucosylated IgG seems to be a general mechanism in response to enveloped viruses[28], it is unclear why afucosylation is more pronounced in patients with COVID-19 who develop severe disease as compared to mild disease. The quick normalization of glycosylation of anti-spike IgG after seroconversion hints toward the aberrant activation of B cells that are responsible for the first wave of anti–SARS-CoV-2 antibodies, mostly likely the short-lived plasmablasts. Critically ill COVID-19 patients are characterized by extrafollicular B cell activation, which coincides with early production and high concentrations of SARS-CoV-2–specific neutralizing antibodies[54]. The molecular processes that underlie the production of IgG with aberrant glycosylation in these cells are still unclear but could be related to increased endoplasmic reticulum stress or different expression of proteins such as Jagunal homolog 1[55]. For future studies, it would be very interesting to study how risk factors of severe COVID-19 (such as age, obesity, and comorbidities) affect these glycosylation processes in B cells. In addition to IgG, the extrafollicular B cells also produce IgM and IgA[54]. Whether these isotypes are also aberrantly glycosylated in patients with severe COVID-19 is still unknown. However, in particular, antibodies of the IgA isotype can promote inflammation depending on the glycosylation profile[56]. On top of this, IgG subclasses (IgG1 to IgG4) could also play a role in both the amplitude and the kinetics of anti-spike–induced inflammatory responses[57]. For example, IgG3 is typically the first IgG subclass to be produced in response to viruses and generally shows a glycosylation pattern similar to IgG1[26,58]. Last, cell-intrinsic differences in macrophages may also contribute to increased or decreased susceptibility of particular individuals to IgG glycosylation differences. This could be related to genetic polymorphisms, such as FCGR2A and FCGR3A single-nucleotide polymorphisms or

downstream signaling molecules, but could also be related to epigenetic differences in macrophages or their precursors.

A limitation of our current study is that we have not been able to perfectly match mild and severe COVID-19 patients in terms of age and several other parameters because of practical limitations. This study required serum from mild patients quickly after seroconversion, which is generally difficult to obtain because mildly ill patients with COVID-19 are not hospitalized (or even diagnosed) and therefore difficult to follow over time. Although, here, we were able to match for the most important parameter (day of onset), it will be relevant to additionally match for age, sex, body mass index, and comorbidities in future studies. In addition, it is not yet clear whether ADI is specific for severe SARS-CoV-2 infection or whether it may also occur upon infection with other viruses. Although induction of afucosylated IgG may be a common trait of enveloped viruses[28], excessive inflammation right after seroconversion appears to be a rare event for most viral infections in humans, with the exception of SARS-CoV-1[14]. However, theoretically, ADI may still occur during other viral infections but in a less pronounced manner that does not lead to pathology. Last, it is important to realize that, although we specifically focused on ADI in this study, antibodies have additional effector functions that will be activated simultaneously in patients with COVID-19. Whereas overactivation of ADI leads to pathology, increased activation of ADCC or phagocytosis of infected cells by afucosylated IgG could simultaneously have beneficial effects such as increasing viral clearance. Therefore, in future work, it will be interesting to determine how afucosylation affects other antiviral IgG effector functions in patients with COVID-19.

We here showed that the observed inflammatory response induced by anti-spike IgG from severe patients could be specifically counteracted by the Syk inhibitor R406, the active component of fostamatinib. Fostamatinib is an FDA- and EMA-approved drug that is currently used for the treatment of ITP[37], which may facilitate repurposing for the treatment of patients with severe COVID-19. A study indicates that fostamatinib may also counteract acute lung injury by inhibiting Mucin-1 expression on epithelial cells, suggesting that fostamatinib may target multiple pathways simultaneously[59]. In addition to fostamatinib, other drugs that also interfere with FcγR activation could be efficacious to counteract anti-spike IgG–induced inflammation in patients with COVID-19. Previous studies already showed the beneficial effects of treatment with intravenous immunoglobulin, which can interfere with FcγR activation[60]. Alternatively, it could be interesting to target critical molecules in FcγR downstream signaling. For example, the Syk-dependent FcγR signaling pathway critically depends on the transcription factor IFN regulatory factor 5 (IRF5)[17,36], which can be targeted using cell-penetrating peptides[61]. Furthermore, FcγR stimulation is known to induce metabolic reprogramming of human macrophages[36], which is also observed in patients with COVID-19[62], and therefore may provide additional targets for therapy. These findings may not only be valuable to find new ways to treat the most severely ill COVID-19 patients but may also have implications for the therapeutic use of convalescent serum, for which it may be wise to omit the afucosylated IgGs that are present in

severely ill patients. Similarly, for recombinant neutralizing antibodies, the composition of the Fc tail needs to be carefully considered, because extreme activation of Fc effector functions by afucosylation needs to be prevented, while at the same time, Fc effector functions should remain partially intact to provide optimal therapeutic protection[63]. Because ADI appears to lead to excessive inflammation upon infection with both SARS-CoV-1[14] and SARS-CoV-2 viruses, these findings may also be relevant in case of an emergence of a future outbreak with related coronaviruses. In conclusion, our data indicate a pathogenic role for anti–SARS-CoV-2 antibodies in patients who are severely ill with COVID-19 caused by high titers and low fucosylation of anti-spike IgG. Moreover, we define therapeutically relevant approaches to suppress the induced cytokine release. These data thus warrant future investigations into the therapeutic potential of targeting this inflammatory mechanism in patients with COVID-19.

Materials and Methods

Study design

The study was designed to investigate the effect of SARS-CoV-2 immune complexes on macrophage activation and clinically relevant in vitro parameters. We applied a human monocyte-derived macrophage model of IL-10–polarized macrophages, resembling human alveolar macrophages[16]. We verified these data in primary human macrophages obtained via BAL. In the studies, we analyzed sera from patients hospitalized at Amsterdam UMC ICUs (n = 27) and compared these to sera from ICU patients negative for SARS-CoV-2 (n = 2), sera from patients positive for SARS-CoV-2 but negative for IgG against spike protein (n = 4), and to the response induced by recombinant anti-spike IgG, COVA1-18[24]. The patients with COVID-19 were included on the basis of serology (positive for anti-spike), except for the control COVID-19 patients in **Figure 1D**, who not only needed to have a positive quantitative polymerase chain reaction (qPCR) result but also had to be seronegative. No other selection criteria were used, and there were no outliers. For the comparison with mild patients, we worked with sera from patients who tested positive for SARS-CoV-2 but were not hospitalized (n = 10). Mild patients' sera were selected by matching gender and serum collection date as comparable as possible with the ICU sera. Smaller subsets of sera were used for selected experiments as described in the respective methods. Cytokine production assays were repeated at least in two donors. Investigators were not blinded for the patient status of the serum used. Samples were randomly assigned to positions in culture plates.

Cells

Buffy coats from healthy anonymous donors were acquired from the Sanquin blood supply in Amsterdam, The Netherlands. All the individuals provided written informed consent before donation to Sanquin. Monocytes were isolated from the buffy coats through density centrifugation using Lymphoprep (Axis-Shield) followed by human CD14 magnetic bead purification with the MACS cell separation columns (Miltenyi Biotec) as previously described (16). The resulting monocytes were seeded on tissue culture plates and subsequently differentiated to macrophages for 6 days in the

presence of human M-CSF (50 ng/ml; Miltenyi Biotec) with Iscove's modified Dulbecco's medium (Lonza) containing 5% fetal bovine serum (FBS; Biowest) and gentamicin (86 µg/ml; Gibco). The medium was renewed on the third day. After a 6-day differentiation period, the medium was replaced by culture medium without M-CSF and supplemented with IL-10 (50 ng/ml; R&D Systems) for 24 hours to generate alveolar macrophage-like monocyte-derived macrophages. These macrophages were then detached with TrypLE Select (Gibco) for further treatment and stimulation.

PAECs were obtained from resected pulmonary artery tissue, obtained from lobectomy surgery performed at Amsterdam UMC, and isolated according to the previously published protocol (35). Briefly, the endothelial cell layer was carefully scraped onto fibronectin-coated (5 µg/ml) culture dishes (Corning, #3295) and maintained in culture in endothelial cell medium (ECM; ScienCell, #1001) supplemented with 1% penicillin/streptomycin, 1% endothelial cell growth supplement (ECGS), 5% FBS, and 1% nonessential amino acids (NEAA; Biowest, #X055-100). Cells were grown until passages 4 to 6 for experiments.

Primary macrophages were prepared from BAL fluid that was obtained as spare material from the ongoing DIVA study (Netherlands Trial Register: NL6318; AMC Medical Ethical Committee approval number: 2014_294). The DIVA study includes healthy male volunteers aged 18 to 35. In this study, the individuals are given lipopolysaccharide (LPS) intravenously and, 2 hours later, a dose of either fresh or aged platelet concentrate or 0.9% NaCl intravenously. Six hours after the platelet or NaCl treatment, a BAL was performed by a trained pulmonologist according to national guidelines. Fractions 2 to 8 were pooled and split in two, one-half is centrifuged (4°C, 1750g, 10 min), the cell pellet of which was used in this research. Because of the COVID-19 pandemic, individuals are also screened for SARS-CoV-2 via throat swab PCR 2 days before the BAL. All individuals in the DIVA study have signed an informed consent form. The frequency of macrophages (80 to 85%) in the BAL was determined by counting the cells that did not adhere to the plate after 30 min at 37°C. For our experiments, complete cell pellets were stimulated.

Coating

To mimic spike protein–specific immune complexes, soluble prefusion-stabilized spike proteins of SARS-CoV-2 (2 µg/ml) were coated overnight on a 96-well high-affinity plate (Nunc). Plates were blocked with 10% fetal calf serum (FCS) in phosphate-buffered saline (PBS) for 1 hour at 37°C. Then, diluted serum or 2 µg/ml of anti–SARS-CoV-2 monoclonal antibodies or purified IgG was added and incubated for 1 hour at 37°C. The spike and anti–SARS-CoV-2 monoclonal antibody COVA1-18 were generated as described previously[24]. When using anti-D glyco-variants, soluble antibodies (2 µg/ml) were coated overnight on a 96-well high-affinity plate (Nunc), and plates were blocked afterward with 10% FCS in PBS for 1 hour at 37°C. Patient sera were provided by the Amsterdam UMC COVID-19 Biobank based on a deferred consent procedure for the usage of materials and clinical information for research purposes, approved by the medical ethics committees of Amsterdam UMC. Patients with

COVID-19 were included on the basis of serology (positive for anti-spike), except for the control COVID-19 patients in **Figure 1D**, who not only needed to have a positive qPCR result but also had to be seronegative. Patients with severe COVID-19 were defined as hospitalized at the ICU, whereas mild patients were defined as symptomatic but not hospitalized.

The anti-D glyco-variant antibodies were made as previously described[64].The specific glyco-engineered antibodies were made from the potent SARS-CoV-2 neutralizing antibody COVA1-18 produced in 293F cells as previously described[24]. Glyco-engineering tools were used to alter N-linked glycosylation of the N297 glycan in the Fc domain and thereby generated several COVA1-18 glycoforms[65]. To decrease fucosylation of the N-linked glycan, 0.2 mM of the decoy substrate for fucosylation, 2-deoxy-2-fluoro-L-fucose (2FF) (Carbosynth, MD06089), was added 1 hour before transfection. To produce a COVA1-18 variant with elevated galactosylation, 293F cells were cotransfected (1% of total DNA) with a plasmid expressing β-1,4-galactosyltransferase 1 (B4GALT1). In addition, 5 mM D-galactose was added 1 hour before transfection. Antibodies were purified with protein G affinity chromatography as previously described[24] and stored in PBS at 4°C. To determine the glycosylation of COVA1-18, aliquots of the monoclonal antibody samples (5 µg) were subjected to acid denaturation (100 mM formic acid, 5 min), followed by vacuum centrifugation. Subsequently, samples were trypsinized, and Fc glycopeptides were measured as described previously[28]. Relative abundances of Fc glycopeptides were determined, and amounts of bisection, fucosylation, galactosylation, and sialylation were determined as described before[28].

Total IgG from individual donors was purified from about 10 µl of serum diluted in PBS using the AssayMAP Bravo platform (Agilent Technologies) with protein G–coupled cartridges as described elsewhere[28]. Samples were eluted into neutralization buffer (214 mM tris and 22 mM sodium phosphate buffer) to obtain neutral pH. Concentrations of purified IgG were determined by absorbance at 280 nm (NanoDrop, Thermo Fisher Scientific).

Titer determination

Total IgG to RBD was measured as described previously (66), using RBD proteins as described by Vogelzang et al[67]. In short, MaxiSorp plates were coated with RBD (1.0 µg/ml) in PBS overnight. After washing, samples were diluted 10,800-fold in PBS supplemented with 0.02% polysorbate 20 and 0.3% gelatin (PTG) and incubated for 1 hour at room temperature. After washing, horseradish peroxidase (HRP)–conjugated monoclonal mouse anti-human IgG (0.5 µg/ml; MH16, Sanquin) was added for 1 hour at room temperature, diluted in PTG. Afterward, enzymatic conversion of the tetramethylbenzidine substrate was used to evaluate antibody binding by measuring the difference in absorbance at 450 and 540 nm. Antibody binding was quantified using a serially diluted calibrator consisting of pooled convalescent plasma that was included on each plate. This calibrator was arbitrarily assigned a value of 100 arbitrary units (AU)/ml. Results are expressed as arbitrary units per milliliter and represent a semiquantitative measure of the concentrations of IgG antibodies.

Stimulation

Macrophages (50,000 per well) were stimulated in precoated plates as described above in combination with poly(I:C) (20 µg/ml; Sigma-Aldrich), LPS (100 ng/ml; from Escherichia coli o111:B4, Sigma-Aldrich), CL097 (5 µg/ml; InvivoGen), R848 (100 ng/ml; Sigma-Aldrich), or Pam3CSK (10 µg/ml; InvivoGen). To block Syk, cells were preincubated with 0.5 µM R406 (Selleckchem) or dimethyl sulfoxide (Sigma-Aldrich) as a control, for 30 min at 37°C. To block the different FcRs, cells were preincubated with 20 µg/ml of the antibodies anti-FcγRI (CD64; 10.1; BD Biosciences), anti-FcγRIIa (CD32a; IV.3; STEMCELL Technologies), anti-FcγRIII (CD16; 3G8; BD Biosciences), and anti-FcαRI (CD89; MIP8a; Abcam) for 30 min at 4°C. Then, media was added to a final antibody concentration of 5 µg/ml.

Virus and HEK293F opsonization

To mimic opsonized SARS-CoV-2 or infected cells, SARS-CoV-2 pseudovirus or SARS-CoV-2 spike–expressing human embryonic kidney (HEK) 293F cells were generated. Transient transfection of HEK293F cells with SARS-2 spike was performed as previously described[24]. To obtain spike surface expression, 62.5 ml of HEK293F cells (at a density of 1 × 106/ml) was transfected with 20 µg of SARS-CoV-2 full-length spike plasmid DNA and 60 µg of PEI MAX. After 60 to 72 hours, cells were harvested and preincubated with COVA1-18. Then, HEK293F cells were washed three times and added to the macrophages at a 1:1 ratio in combination with or without poly(I:C). After 24 hours, supernatant was harvested, and cytokine production was assessed with enzyme-linked immunosorbent assay (ELISA). To produce a SARS-CoV-2 S–pseudo-typed HIV-1 virus, a SARS-CoV-2 spike expression plasmid was cotransfected in HEK293T cells (American Type Culture Collection, CRL-11268) with an HIV backbone expressing firefly luciferase (pNL4-3.Luc.R-E-) as previously described[24]. After 3 days, culture supernatants were harvested and stored at −80°C. To quantify pseudovirus production and determine the viral input for the macrophage activation assay, a capsid p24 antigen ELISA was performed[68]. Monocyte-derived macrophages were incubated in 96-well flat-bottom plates at 37°C with SARS-CoV-2 pseudo-typed particles (an equivalent of 0.2 ng of CA p24 antigen) in the presence or absence of poly(I:C) (20 µg/ml; Sigma-Aldrich) and COVA1-18 antibody (0.4 ng/ml). After 24 hours, supernatant was harvested, and cytokine production was assessed by ELISA.

Endothelial barrier function

PAEC passage 4 to 6 cells were seeded 1:1 in 0.1% gelatin-coated 8-well (8W10E) or 96-well (96W10idf PET) ibidi culture slides for electrical cell-substrate impedance sensing, as previously described[34]. Cells were maintained in culture in ECM (ScienCell, #1001) supplemented with 1% penicillin/streptomycin, 1% ECGS, 5% FBS, and 1% NEAA (Biowest, #X055-100), with medium change every other day. From seeding onward, electrical impedance was measured at 4000 Hz every 5 min. Cells were grown to confluence, and after 72 hours, ECM medium was removed and replaced by the supernatant of alveolar macrophage–like monocyte-derived macrophages stimulated for 6 hours as described above with poly(I:C) or in combination with patient serum. Within every experiment, triplicate

measurements were performed for each condition. For every experiment, PAECs and macrophages obtained from different donors were used.

Platelet adhesion on PAEC under flow

PAECs were seeded in 0.1% gelatin-coated µ-Slide VI 0.4 ibiTreat flow slides (ibidi, #80606) and cultured for 7 days. PAECs were preincubated for 24 hours with the supernatant of alveolar macrophage–like monocyte-derived macrophages stimulated for 6 hours as described above with poly(I:C) or in combination with patient serum before flow experiments were performed. On the day of perfusion, citrated blood was collected from healthy volunteers, and platelets were isolated as previously described[69]. Platelets were perfused for 5 min, and phase-contrast and fluorescent images were taken with an Etaluma LS720 microscope using a 20× phase-contrast objective. Platelet adhesion was quantified in ImageJ by determining the area covered by platelets per field of view.

Enzyme-linked immunosorbent assay

To determine cytokine production, supernatants were harvested after 24 hours of stimulation, and cytokines were detected using the following antibody pairs: IL-1β and IL-6 (U-CyTech Biosciences), TNF (eBioscience), and IL-8 (Invitrogen). Concentration of (anti-spike) antibodies present in patient serum was determined as described before[28].

Flow supernatant was collected after perfusion, and von Willebrand factor concentrations were measured with ELISA. A 96-well high-affinity ELISA plate was coated with polyclonal anti–von Willebrand factor (1:1000; Dako, #A0082) and blocked with 2% bovine serum albumin. Samples were loaded, and bound von Willebrand factor was detected with HRP-conjugated rabbit polyclonal anti–von Willebrand factor (1:2500; Dako, #A0082). Normal plasma with a stock concentration of 50 nM von Willebrand factor (gifted from Sanquin) was used as a standard for determination of concentration, measured at 450 and 540 nm.

Quantitative polymerase chain reaction

Total RNA was isolated with the RNeasy Mini Kit (Qiagen) and RNase-Free DNase Set (Qiagen) as per the manufacturer's protocol. RNA was then converted to complementary DNA (cDNA) with iScript (Life Technologies). qPCR was performed with SYBR Green Fast on a ViiA7 PCR machine (Applied Biosystems). All genes were normalized to the mean of the relative expression values of two housekeeping genes, HPRT1 and RACK1. Primers used are as follows: IL6 (hsIL6-FW, GAGTAGTGAGGAACAAGCCAG; hsIL6-RV, TTGTCATGTCCTGCAGCC); IL8 (CXCL8) (hsIL8-FW, ATACTCCAAACCTTTCCACC; hsIL8-RV, TCCAGACAGAGCTCTCTTCC); TNF (hsTNFa-FW, GGCGTGGAGCTGAGAGAT; hsTNFa-RV, TGGTAGGAGACGGCGATG); CXCL10 (hsCXCL10-FW, GAAAGCAGTTAGCAAGGAAAGGT; hsCXCL10-RV, GACATATACTCCATGTAGGGAAGTGA); HPRT1 (hsHPRT1_FW, GACCAGTCAACAGGGGACAT; hsHPRT1_RV, AACACTTCGTGGGGTCCTTTTC); RACK1 (hsRACK1_FW, GAGTGTGGCCTTCTCCTCTG; hsRACK1_RV, GCTTGCAGTTAGCCAGGTTC); CD163

(hsCD163_FW, AGTCCCAAACACTGTCCTCG; hsCD163_RV, GGCGAAGTTGACCACTCTCTAT); CD209 (hsCD209_FW, AATGGCTGGAACGACGACAAA; hsCD209_RV, CAGGAGGCTGCGGACTTTTT).

Meso Scale Discovery multiplex assay

V-PLEX Custom Human Cytokine 10-plex kits for Proinflammatory Panel 1 and Chemokine Panel 1 (K151A0H-2, for IL-1β, IL-6, IL-8, IL-10, TNF, CCL2, and CXCL10) and U-PLEX human Interferon Combo SECTOR (K15094K-2, for IFN-α2a, IFN-β, IFN-γ, and IFN-λ1) were purchased from Meso Scale Discovery (MSD). The lyophilized cocktail mix calibrators for Proinflammatory Panel 1 and Chemokine Panel 1 and four calibrators for U-PLEX Biomarker Group 1 (calibrators 1, 3, 6, and 9) were reconstituted in provided assay diluents, respectively. U-PLEX plates were coated with supplied linkers and biotinylated capture antibodies according to the manufacturer's instructions. Proinflammatory cytokines and chemokines in supernatant collected at 24 hours after stimulation were detected with precoated V-PLEX, and IFNs in the 6-hour supernatant were measured by coated U-PLEX plates. The assays were performed according to the manufacturer's protocol with overnight incubation of the diluted samples and standards at 4°C. The electrochemiluminescence signal was detected by a MESO QuickPlex SQ 120 plate reader (MSD) and analyzed with Discovery Workbench Software (v4.0, MSD). The concentration of each sample was calculated on the basis of the four-parameter logistic fitting model generated with the standards (concentration was determined according to the certificate of analysis provided by MSD). Log10 values of the measured concentrations of IL-1β, IL-6, IL-8, IL-10, TNF, IFN-β, IFN-γ, and CXCL10 were used for the principal component analysis. Log10 IgG titers [half-maximal effective concentration (EC50)] were used for the color overlay.

RNA sequencing

Cells were stimulated as described above and lysed after 6 hours. Total RNA was isolated with the RNeasy Mini Kit (Qiagen) and RNase-Free DNase Set (Qiagen) as per the manufacturer's protocol. cDNA libraries were prepared using the standard protocol of KAPA mRNA HyperPrep Kits (Roche) with input of 300 ng of RNA per sample. Size-selected cDNA libraries were pooled and sequenced on a HiSeq 4000 sequencer (Illumina) to a depth of 16 to 20 M per sample according to the 50–base pair single-end protocol at the Amsterdam UMC, location Vrije Universiteit Medical Center. Raw FASTQ files were aligned to the human genome GRCh38 by STAR (v2.5.2b) with default settings[70]. Indexed binary alignment map files were generated and filtered on MAPQ>15 with SAMTools (v1.3.1)[71]. Raw tag counts and reads per kilobase million (RPKM) per gene were calculated using HOMER2's analyzeRepeats.pl script with default settings and the -noadj or -rpkm options for raw counts and RPKM reporting[72] for further analyses.

Flow cytometry

After detachment, macrophages were stained with antibodies against FcγRs: FcγRI (CD64, catalog no. 305014, BioLegend), FcγRII (CD32, catalog no. 555448, BD Biosciences), and FcγRIII (CD16, catalog no. 562293, BD Biosciences). Fluorescence was measured with the CytoFLEX flow cytometer and analyzed

with FlowJo software version 7.6.5 (FlowJo LLC). Fluorescence Minus One (FMO) controls were used for each staining as negative controls.

Functional analyses of transcriptomic data

All analyses were performed in the R statistical environment (v3.6.3). Differential expression was assessed using the Bioconductor package edgeR (v3.28.1)[73]. Lowly expressed genes were filtered with the filterByExpr function, and gene expression was called differential with an FDR < 0.05. Pathway enrichment analyses were performed on the differentially regulated genes with an absolute log2(fold change) higher than 1 using the Metascape (http://metascape.org/gp/index.html)[74] on 26 June 2020. For heatmaps, normalized expression values (counts per million) of each gene were calculated and plotted using pheatmap (v1.0.12) with values scaled by gene. GSEA was performed with Bioconductor package fgsea (v1.12.0)[75] with genes ranked by effect size (Cohen's d) with respect to the "R406+serum+spike+poly(I:C) vs serum+spike+poly(I:C)" against the curated gene sets obtained from gene ontology (GO) by Bioconductor package biomaRt (v2.42.1) (76). A total of 5000 permutations were performed to estimate the empirical P values for the gene sets. Normalized enrichment scores and the Benjamini-Hochberg (BH)–adjusted P values are provided in the Figures. De novo transcription factor motif analysis was performed by using HOMER (v4.11)[77] using the following parameters: -start -200 -end 100 -len 8, 10, 12.

Statistical analysis

Statistical significance of the data was performed in GraphPad Prism version 8 (GraphPad Software). For t tests or nonparametric analysis comparing two sets of measurements, data were first examined with D'Agostino-Pearson normality test with $\alpha = 0.05$. For the data following normal distribution, paired or unpaired t tests were conducted on the basis of the experiment design. For unpaired data not following a normal distribution, Mann-Whitney test was applied. For multiple comparison tests, one-way or two-way analysis of variance (ANOVA) was applied on the basis of the addressed scientific question. Brown-Forsythe and Welch's ANOVA test was applied when not assuming that the compared groups were sampled from populations with equal variances (examined by Brown-Forsythe test), otherwise an ordinary one-way ANOVA was performed. For differential analysis and GSEA of transcriptomic data, P values were adjusted by BH procedure to control the FDR. The analysis methods applied for each figure are stated in the legends.

References

1. R. T. Gandhi, J. B. Lynch, C. del Rio, Mild or moderate COVID-19. N. Engl. J. Med. 383, 1757–1766 (2020).
2. M. Z. Tay, C. M. Poh, L. Rénia, P. A. MacAry, L. F. P. Ng, The trinity of COVID-19: Immunity, inflammation and intervention. Nat. Rev. Immunol. 20, 363–374 (2020).
3. M. Merad, J. C. Martin, Pathological inflammation in patients with COVID-19: A key role for monocytes and macrophages. Nat. Rev. Immunol. 20, 355–362 (2020).
4. N. Mangalmurti, C. A. Hunter, Cytokine storms: Understanding COVID-19. Immunity 53, 19–25 (2020).
5. D. Blanco-Melo, B. E. Nilsson-Payant, W. C. Liu, S. Uhl, D. Hoagland, R. Møller, T. X. Jordan, K. Oishi, M. Panis, D. Sachs, T. T. Wang, R. E. Schwartz, J. K. Lim, R. A. Albrecht, B. R. tenOever, Imbalanced host response to SARS-CoV-2 drives development of COVID-19. Cell 181, 1036–1045.e9 (2020).
6. E. J. Giamarellos-Bourboulis, M. G. Netea, N. Rovina, K. Akinosoglou, A. Antoniadou, N. Antonakos, G. Damoraki, T. Gkavogianni, M. E. Adami, P. Katsaounou, M. Ntaganou, M. Kyriakopoulou, G. Dimopoulos, I. Koutsodimitropoulos, D. Velissaris, P. Koufargyris, A. Karageorgos, K. Katrini, V. Lekakis, M. Lupse, A. Kotsaki, G. Renieris, D. Theodoulou, V. Panou, E. Koukaki, N. Koulouris, C. Gogos, A. Koutsoukou, Complex immune dysregulation in COVID-19 patients with severe respiratory failure. Cell Host Microbe 27, 992–1000.e3 (2020).
7. T. Herold, V. Jurinovic, C. Arnreich, B. J. Lipworth, J. C. Hellmuth, M. von Bergwelt-Baildon, M. Klein, T. Weinberger, Elevated levels of IL-6 and CRP predict the need for mechanical ventilation in COVID-19. J. Allergy Clin. Immunol. 146, 128–136.e4 (2020).
8. J. Hadjadj, N. Yatim, L. Barnabei, A. Corneau, J. Boussier, N. Smith, H. Péré, B. Charbit, V. Bondet, C. Chenevier-Gobeaux, P. Breillat, N. Carlier, R. Gauzit, C. Morbieu, F. Pène, N. Marin, N. Roche, T. A. Szwebel, S. H. Merkling, J. M. Treluyer, D. Veyer, L. Mouthon, C. Blanc, P. L. Tharaux, F. Rozenberg, A. Fischer, D. Duffy, F. Rieux-Laucat, S. Kernéis, B. Terrier, Impaired type I interferon activity and inflammatory responses in severe COVID-19 patients. Science 369, 718–724 (2020).
9. M. Sa Ribero, N. Jouvenet, M. Dreux, S. Nisole, Interplay between SARS-CoV-2 and the type I interferon response. PLOS Pathog. 16, e1008737 (2020).
10. S. B. Halstead, Dengue antibody-dependent enhancement: Knowns and unknowns. Microbiol Spectr. 2, 6 (2014).
11. T. Zohar, G. Alter, Dissecting antibody-mediated protection against SARS-CoV-2. Nat. Rev. Immunol. 20, 392–394 (2020).
12. L. T. Vogelpoel, I. S. Hansen, T. Rispens, F. J. Muller, T. M. van Capel, M. C. Turina, J. B. Vos, D. L. Baeten, M. L. Kapsenberg, E. C. de Jong, J. den Dunnen, Fc gamma receptor-TLR cross-talk elicits pro-inflammatory cytokine production by human M2 macrophages. Nat. Commun. 5, 5444 (2014).
13. J. Sokolove, X. Zhao, P. E. Chandra, W. H. Robinson, Immune complexes containing citrullinated fibrinogen costimulate macrophages via Toll-like receptor 4 and Fcγ receptor. Arthritis Rheum. 63, 53–62 (2011).
14. L. Liu, Q. Wei, Q. Lin, J. Fang, H. Wang, H. Kwok, H. Tang, K. Nishiura, J. Peng, Z. Tan, T. Wu, K. W. Cheung, K. H. Chan, X. Alvarez, C. Qin, A. Lackner, S. Perlman, K. Y. Yuen, Z. Chen, Anti-spike IgG causes severe acute lung injury by skewing macrophage responses during acute SARS-CoV infection. JCI Insight 4, e123158 (2019).
15. M. Liao, Y. Liu, J. Yuan, Y. Wen, G. Xu, J. Zhao, L. Cheng, J. Li, X. Wang, F. Wang, L. Liu, I. Amit, S. Zhang, Z. Zhang, Single-cell landscape of bronchoalveolar immune cells in patients with COVID-19. Nat. Med. 26, 842–844 (2020).
16. H.-J. Chen, A. Y. F. Li Yim, G. R. Griffith, W. J. de Jonge, M. M. A. M. Mannens, E. Ferrero, P. Henneman, M. P. J. de Winther, Meta-analysis of in vitro-differentiated macrophages identifies transcriptomic signatures that classify disease macrophages in vivo. Front. Immunol. 10, 2887 (2019).
17. W. Hoepel, K. Golebski, C. M. van Drunen, J. den Dunnen, Active control of mucosal tolerance and inflammation by human IgA and IgG antibodies. J. Allergy Clin. Immunol. 146, 273–275 (2020).
18. L. T. Vogelpoel, D. L. Baeten, E. C. de Jong, J. den Dunnen, Control of cytokine production by human Fc gamma receptors: Implications for pathogen defense and autoimmunity. Front. Immunol. 6, 79 (2015).
19. C. Huang, Y. Wang, X. Li, L. Ren, J. Zhao, Y. Hu, L. Zhang, G. Fan, J. Xu, X. Gu, Z. Cheng, T. Yu, J. Xia, Y. Wei, W. Wu, X. Xie, W. Yin, H. Li, M. Liu, Y. Xiao, H. Gao, L. Guo, J. Xie, G. Wang, R. Jiang, Z. Gao, Q. Jin, J. Wang, B. Cao, Clinical features of patients infected with 2019 novel coronavirus in Wuhan, China. Lancet 395, 497–506 (2020).
20. J. Combes, T. Courau, N. F. Kuhn, K. H. Hu, A. Ray, W. S. Chen, N. W. Chew, S. J. Cleary, D. Kushnoor, G. C. Reeder, A. Shen, J. Tsui, K. J. Hiam-Galvez, P. Munoz-Sandoval, W. S. Zhu, D. S. Lee, Y. Sun, R. You, M. Magnen, L. Rodriguez, K. W. Im, N. K. Serwas, A. Leligdowicz, C. R. Zamecnik, R. P. Loudermilk, M. R. Wilson, C. J. Ye, G. K. Fragiadakis, M. R. Looney, V. Chan, A. Ward, S. Carrillo, U. C. Consortium, M. Matthay, D. J. Erle, P. G.

Woodruff, C. Langelier, K. Kangelaris, C. M. Hendrickson, C. Calfee, A. A. Rao, M. F. Krummel, Global absence and targeting of protective immune states in severe COVID-19. Nature 591, 124–130 (2021).
21. Q.-X. Long, B.-Z. Liu, H.-J. Deng, G.-C. Wu, K. Deng, Y.-K. Chen, P. Liao, J.-F. Qiu, Y. Lin, X.-F. Cai, D.-Q. Wang, Y. Hu, J.-H. Ren, N. Tang, Y.-Y. Xu, L.-H. Yu, Z. Mo, F. Gong, X.-L. Zhang, W.-G. Tian, L. Hu, X.-X. Zhang, J.-L. Xiang, H.-X. Du, H.-W. Liu, C.-H. Lang, X.-H. Luo, S.-B. Wu, X.-P. Cui, Z. Zhou, M.-M. Zhu, J. Wang, C.-J. Xue, X.-F. Li, L. Wang, Z.-J. Li, K. Wang, C.-C. Niu, Q.-J. Yang, X.-J. Tang, Y. Zhang, X.-M. Liu, J.-J. Li, D.-C. Zhang, F. Zhang, P. Liu, J. Yuan, Q. Li, J.-L. Hu, J. Chen, A.-L. Huang, Antibody responses to SARS-CoV-2 in patients with COVID-19. Nat. Med. 26, 845–848 (2020).
22. K. K.-W. To, O.-T. Tsang, W.-S. Leung, A.-R. Tam, T.-C. Wu, D.-C. Lung, C.-C. Yip, J.-P. Cai, J.-M. Chan, T.-S. Chik, D.-P. Lau, C.-Y. Choi, L.-L. Chen, W.-M. Chan, K.-H. Chan, J.-D. Ip, A.-C. Ng, R.-W. Poon, C.-T. Luo, V.-C. Cheng, J.-F. Chan, I.-F. Hung, Z. Chen, H. Chen, K.-Y. Yuen, Temporal profiles of viral load in posterior oropharyngeal saliva samples and serum antibody responses during infection by SARS-CoV-2: An observational cohort study. Lancet Infect. Dis. 20, 565–574 (2020).
23. L. T. Vogelpoel, I. S. Hansen, M. W. Visser, S. Q. Nagelkerke, T. W. Kuijpers, M. L. Kapsenberg, E. C. de Jong, J. den Dunnen, FcγRIIa cross-talk with TLRs, IL-1R, and IFNγR selectively modulates cytokine production in human myeloid cells. Immunobiology 220, 193–199 (2015).
24. P. J. M. Brouwer, T. G. Caniels, K. van der Straten, J. L. Snitselaar, Y. Aldon, S. Bangaru, J. L. Torres, N. M. A. Okba, M. Claireaux, G. Kerster, A. E. H. Bentlage, M. M. van Haaren, D. Guerra, J. A. Burger, E. E. Schermer, K. D. Verheul, N. van der Velde, A. van der Kooi, J. van Schooten, M. J. van Breemen, T. P. L. Bijl, K. Sliepen, A. Aartse, R. Derking, I. Bontjer, N. A. Kootstra, W. J. Wiersinga, G. Vidarsson, B. L. Haagmans, A. B. Ward, G. J. de Bree, R. W. Sanders, M. J. van Gils, Potent neutralizing antibodies from COVID-19 patients define multiple targets of vulnerability. Science 369, 643–650 (2020).
25. H. Ma, W. Zeng, H. He, D. Zhao, D. Jiang, P. Zhou, L. Cheng, Y. Li, X. Ma, T. Jin, Serum IgA, IgM, and IgG responses in COVID-19. Cell. Mol. Immunol. 17, 773–775 (2020).
26. G. Vidarsson, G. Dekkers, T. Rispens, IgG subclasses and allotypes: From structure to effector functions. Front. Immunol. 5, 520 (2014).
27. M. F. Jennewein, G. Alter, The immunoregulatory roles of antibody glycosylation. Trends Immunol. 38, 358–372 (2017).
28. M. D. Larsen, E. L. de Graaf, M. E. Sonneveld, H. R. Plomp, J. Nouta, W. Hoepel, H.-J. Chen, F. Linty, R. Visser, M. Brinkhaus, T. Šuštić, S. W. de Taeye, A. E. H. Bentlage, S. Toivonen, C. A. M. Koeleman, S. Sainio, N. A. Kootstra, P. J. M. Brouwer, C. E. Geyer, N. I. L. Derksen, G. Wolbink, M. de Winther, R. W. Sanders, M. J. van Gils, S. de Bruin, A. P. J. Vlaar, T. Rispens, J. den Dunnen, H. L. Zaaijer, M. Wuhrer, C. E. van der Schoot, G. Vidarsson, Afucosylated IgG characterizes enveloped viral responses and correlates with COVID-19 severity. Science 371, eabc8378 (2021).
29. S. Chakraborty, J. Gonzalez, K. Edwards, V. Mallajosyula, A. S. Buzzanco, R. Sherwood, C. Buffone, N. Kathale, S. Providenza, M. M. Xie, J. R. Andrews, C. A. Blish, U. Singh, H. Dugan, P. C. Wilson, T. D. Pham, S. D. Boyd, K. C. Nadeau, B. A. Pinsky, S. Zhang, M. J. Memoli, J. K. Taubenberger, T. Morales, J. M. Schapiro, G. S. Tan, P. Jagannathan, T. T. Wang, Proinflammatory IgG Fc structures in patients with severe COVID-19. Nat. Immunol. 22, 67–73 (2021).
30. J. S. Lee, S. Park, H. W. Jeong, J. Y. Ahn, S. J. Choi, H. Lee, B. Choi, S. K. Nam, M. Sa, J. S. Kwon, S. J. Jeong, H. K. Lee, S. H. Park, S. H. Park, J. Y. Choi, S. H. Kim, I. Jung, E. C. Shin, Immunophenotyping of COVID-19 and influenza highlights the role of type I interferons in development of severe COVID-19. Sci. Immunol. 5, eabd1554 (2020).
31. S. H. Park, K. Kang, E. Giannopoulou, Y. Qiao, K. Kang, G. Kim, K. H. Park-Min, L. B. Ivashkiv, Type I interferons and the cytokine TNF cooperatively reprogram the macrophage epigenome to promote inflammatory activation. Nat. Immunol. 18, 1104–1116 (2017).
32. L. Li, Q. Huang, D. C. Wang, D. H. Ingbar, X. Wang, Acute lung injury in patients with COVID-19 infection. Clin. Transl. Med. 10, 20–27 (2020).
33. R. C. Becker, COVID-19 update: COVID-19-associated coagulopathy. J. Thromb. Thrombolysis 50, 54–67 (2020).
34. L. Botros, M. C. A. Pronk, J. Juschten, J. Liddle, S. K. H. Morsing, J. D. van Buul, R. H. Bates, P. R. Tuinman, J. S. M. van Bezu, S. Huveneers, H. J. Bogaard, V. W. M. van Hinsbergh, P. L. Hordijk, J. Aman, Bosutinib prevents vascular leakage by reducing focal adhesion turnover and reinforcing junctional integrity. J. Cell Sci. 133, jcs240077 (2020).
35. X. D. Manz, H. J. Albers, P. Symersky, J. Aman, A. D. van der Meer, H. J. Bogaard, R. Szulcek, In vitro microfluidic disease model to study whole blood-endothelial interactions and blood clot dynamics in real-time. J. Vis. Exp. 2020, (2020).

36. W. Hoepel, M. Newling, L. T. C. Vogelpoel, L. Sritharan, I. S. Hansen, M. L. Kapsenberg, D. L. P. Baeten, B. Everts, J. den Dunnen, FcγR-TLR cross-talk enhances TNF production by human monocyte-derived DCs via IRF5-dependent gene transcription and glycolytic reprogramming. Front. Immunol. 10, 739 (2019).
37. N. T. Connell, N. Berliner, Fostamatinib for the treatment of chronic immune thrombocytopenia. Blood 133, 2027–2030 (2019).
38. Wajnberg, F. Amanat, A. Firpo, D. R. Altman, M. J. Bailey, M. Mansour, M. McMahon, P. Meade, D. R. Mendu, K. Muellers, D. Stadlbauer, K. Stone, S. Strohmeier, V. Simon, J. Aberg, D. L. Reich, F. Krammer, C. Cordon-Cardo, Robust neutralizing antibodies to SARS-CoV-2 infection persist for months. Science 370, 1227–1230 (2020).
39. K. K.-W. To, I.-F. Hung, J.-D. Ip, A.-W. Chu, W.-M. Chan, A.-R. Tam, C.-H. Fong, S. Yuan, H.-W. Tsoi, A.-C. Ng, L.-L. Lee, P. Wan, E. Tso; W.-K. To, D. Tsang, K.-H. Chan, J.-D. Huang, K.-H. Kok, V.-C. Cheng, K.-Y. Yuen, COVID-19 re-infection by a phylogenetically distinct SARS-coronavirus-2 strain confirmed by whole genome sequencing. Clin. Infect. Dis. 2020, ciaa1275 (2020).
40. W. Deng, L. Bao, J. Liu, C. Xiao, J. Liu, J. Xue, Q. Lv, F. Qi, H. Gao, P. Yu, Y. Xu, Y. Qu, F. Li, Z. Xiang, H. Yu, S. Gong, M. Liu, G. Wang, S. Wang, Z. Song, Y. Liu, W. Zhao, Y. Han, L. Zhao, X. Liu, Q. Wei, C. Qin, Primary exposure to SARS-CoV-2 protects against reinfection in rhesus macaques. Science 369, 818–823 (2020).
41. M. Guilliams, P. Bruhns, Y. Saeys, H. Hammad, B. N. Lambrecht, The function of Fcγ receptors in dendritic cells and macrophages. Nat. Rev. Immunol. 14, 94–108 (2014).
42. D. M. D. Valle, S. Kim-Schulze, H.-H. Huang, N. Beckmann, S. Nirenberg, B. Wang, Y. Lavin, T. Swartz, D. Madduri, A. Stock, T. U. Marron, H. Xie, M. Patel, O. van Oekelen, A. Rahman, P. Kovatch, J. A. Aberg, E. Schadt, S. Jagannath, M. Mazumdar, A. Charney, A. Firpo-Betancourt, D. R. Mendu, J. Jhang, D. Reich, K. Sigel, C. Cordon-Cardo, M. Feldmann, S. Parekh, M. Merad, S. Gnjatic, An inflammatory cytokine signature helps predict COVID-19 severity and death. medRxiv 2020.2005.2028.20115758 (2020).
43. M. E. Ackerman, M. Crispin, X. Yu, K. Baruah, A. W. Boesch, D. J. Harvey, A.-S. Dugast, E. L. Heizen, A. Ercan, I. Choi, H. Streeck, P. A. Nigrovic, C. Bailey-Kellogg, C. Scanlan, G. Alter, Natural variation in Fc glycosylation of HIV-specific antibodies impacts antiviral activity. J. Clin. Invest. 123, 2183–2192 (2013).
44. T. T. Wang, J. Sewatanon, M. J. Memoli, J. Wrammert, S. Bournazos, S. K. Bhaumik, B. A. Pinsky, K. Chokephaibulkit, N. Onlamoon, K. Pattanapanyasat, J. K. Taubenberger, R. Ahmed, J. V. Ravetch, IgG antibodies to dengue enhanced for FcγRIIIA binding determine disease severity. Science 355, 395–398 (2017).
45. S. Hansen, L. Krabbendam, J. H. Bernink, F. Loayza-Puch, W. Hoepel, J. A. van Burgsteden, E. C. Kuijper, C. J. Buskens, W. A. Bemelman, S. A. J. Zaat, R. Agami, G. Vidarsson, G. R. van den Brink, E. C. de Jong, M. E. Wildenberg, D. L. P. Baeten, B. Everts, J. den Dunnen, FcαRI co-stimulation converts human intestinal CD103+ dendritic cells into pro-inflammatory cells through glycolytic reprogramming. Nat. Commun. 9, 863 (2018).
46. B. J. Barnes, J. M. Adrover, A. Baxter-Stoltzfus, A. Borczuk, J. Cools-Lartigue, J. M. Crawford, J. Daßler-Plenker, P. Guerci, C. Huynh, J. S. Knight, M. Loda, M. R. Looney, F. McAllister, R. Rayes, S. Renaud, S. Rousseau, S. Salvatore, R. E. Schwartz, J. D. Spicer, C. C. Yost, A. Weber, Y. Zuo, M. Egeblad, Targeting potential drivers of COVID-19: Neutrophil extracellular traps. J. Exp. Med. 217, e20200652 (2020).
47. J. R. Strich, M. J. Ramos-Benitez, D. Randazzo, S. R. Stein, A. Babyak, R. T. Davey, A. F. Suffredini, R. W. Childs, D. S. Chertow, Fostamatinib inhibits neutrophils extracellular traps induced by COVID-19 patient plasma: A potential therapeutic. J. Infect. Dis. 223, 981–984 (2021).
48. R. L. Chua, S. Lukassen, S. Trump, B. P. Hennig, D. Wendisch, F. Pott, O. Debnath, L. Thürmann, F. Kurth, M. T. Völker, J. Kazmierski, B. Timmermann, S. Twardziok, S. Schneider, F. Machleidt, H. Müller-Redetzky, M. Maier, A. Krannich, S. Schmidt, F. Balzer, J. Liebig, J. Loske, N. Suttorp, J. Eils, N. Ishaque, U. G. Liebert, C. von Kalle, A. Hocke, M. Witzenrath, C. Goffinet, C. Drosten, S. Laudi, I. Lehmann, C. Conrad, L. E. Sander, R. Eils, COVID-19 severity correlates with airway epithelium-immune cell interactions identified by single-cell analysis. Nat. Biotechnol. 38, 970–979 (2020).
49. K. Golebski, W. Hoepel, D. van Egmond, E. J. de Groot, G. D. Amatngalim, J. M. Beekman, W. J. Fokkens, C. M. van Drunen, J. den Dunnen, FcγRIII stimulation breaks the tolerance of human nasal epithelial cells to bacteria through cross-talk with TLR4. Mucosal Immunol. 12, 425–433 (2019).
50. Y. Zuo, S. K. Estes, R. A. Ali, A. A. Gandhi, S. Yalavarthi, H. Shi, G. Sule, K. Gockman, J. A. Madison, M. Zuo, V. Yadav, J. Wang, W. Woodard, S. P. Lezak, N. L. Lugogo, S. A. Smith, J. H. Morrissey, Y. Kanthi, J. S. Knight, Prothrombotic autoantibodies in serum from patients hospitalized with COVID-19. Sci. Transl. Med. 12, eabd3876 (2020).
51. P. Bye, W. Hoepel, J. L. Mitchell, S. Jégouic, S. Loureiro, T. Sage, S. de Taeye, M. van Gils, N. Kriek, N. Cooper, I. Jones, J. den Dunnen, J. M. Gibbins, Aberrant glycosylation of anti-SARS-CoV-2 IgG is a pro-thrombotic stimulus for platelets. bioRxiv 2021.2003.2026.437014 (2021).

52. N. de Haan, K. R. Reiding, G. Driessen, M. van der Burg, M. Wuhrer, Changes in healthy human IgG Fc-glycosylation after birth and during early childhood. J. Proteome Res. 15, 1853–1861 (2016).
53. X. Yu, Y. Wang, J. Kristic, J. Dong, X. Chu, S. Ge, H. Wang, H. Fang, Q. Gao, D. Liu, Z. Zhao, H. Peng, M. Pucic Bakovic, L. Wu, M. Song, I. Rudan, H. Campbell, G. Lauc, W. Wang, Profiling IgG N-glycans as potential biomarker of chronological and biological ages: A community-based study in a Han Chinese population. Medicine (Baltimore) 95, e4112 (2016).
54. M. C. Woodruff, R. P. Ramonell, D. C. Nguyen, K. S. Cashman, A. S. Saini, N. S. Haddad, A. M. Ley, S. Kyu, J. C. Howell, T. Ozturk, S. Lee, N. Suryadevara, J. B. Case, R. Bugrovsky, W. Chen, J. Estrada, A. Morrison-Porter, A. Derrico, F. A. Anam, M. Sharma, H. M. Wu, S. N. Le, S. A. Jenks, C. M. Tipton, B. Staitieh, J. L. Daiss, E. Ghosn, M. S. Diamond, R. H. Carnahan, J. E. Crowe Jr., W. T. Hu, F. E. Lee, I. Sanz, Extrafollicular B cell responses correlate with neutralizing antibodies and morbidity in COVID-19. Nat. Immunol. 21, 1506–1516 (2020).
55. Hagelkruys, G. Wirnsberger, J. Stadlmann, M. Wohner, M. Horrer, B. Vilagos, G. Jonsson, M. Kogler, L. Tortola, M. Novatchkova, P. Bonelt, D. Hoffmann, R. Koglgruber, U. Steffen, G. Schett, M. Busslinger, A. Bergthaler, C. Klein, J. M. Penninger, A crucial role for Jagunal homolog 1 in humoral immunity and antibody glycosylation in mice and humans. J. Exp. Med. 218, e20200559 (2021).
56. U. Steffen, C. A. Koeleman, M. V. Sokolova, H. Bang, A. Kleyer, J. Rech, H. Unterweger, M. Schicht, F. Garreis, J. Hahn, F. T. Andes, F. Hartmann, M. Hahn, A. Mahajan, F. Paulsen, M. Hoffmann, G. Lochnit, L. E. Munoz, M. Wuhrer, D. Falck, M. Herrmann, G. Schett, IgA subclasses have different effector functions associated with distinct glycosylation profiles. Nat. Commun. 11, 120 (2020).
57. W. Hoepel, S. Allahverdiyeva, H. Harbiye, S. W. de Taeye, A. J. van der Ham, L. de Boer, S. A. J. Zaat, M. van Weeghel, D. L. P. Baeten, R. H. Houtkooper, B. Everts, G. Vidarsson, J. den Dunnen, IgG subclasses shape cytokine responses by human myeloid immune cells through differential metabolic reprogramming. J. Immunol. 205, 3400–3407 (2020).
58. M. E. Sonneveld, C. A. M. Koeleman, H. R. Plomp, M. Wuhrer, C. E. van der Schoot, G. Vidarsson, Fc-glycosylation in human IgG1 and IgG3 Is similar for both total and anti-red-blood cell anti-K Antibodies. Front. Immunol. 9, 129 (2018).
59. M. Kost-Alimova, E.-H. Sidhom, A. Satyam, B. T. Chamberlain, M. Dvela-Levitt, M. Melanson, S. L. Alper, J. Santos, J. Gutierrez, A. Subramanian, P. J. Byrne, E. Grinkevich, E. Reyes-Bricio, C. Kim, A. R. Clark, A. J. B. Watts, R. Thompson, J. Marshall, J. L. Pablo, J. Coraor, J. Roignot, K. A. Vernon, K. Keller, A. Campbell, M. Emani, M. Racette, S. Bazua-Valenti, V. Padovano, A. Weins, S. P. McAdoo, F. W. K. Tam, L. Ronco, F. Wagner, G. C. Tsokos, J. L. Shaw, A. Greka, A high-content screen for mucin-1-reducing compounds identifies fostamatinib as a candidate for rapid repurposing for acute lung injury. Cell Rep. Med. 1, 100137 (2020).
60. N. Gharebaghi, R. Nejadrahim, S. J. Mousavi, S. R. Sadat-Ebrahimi, R. Hajizadeh, The use of intravenous immunoglobulin gamma for the treatment of severe coronavirus disease 2019: A randomized placebo-controlled double-blind clinical trial. BMC Infect. Dis. 20, 786 (2020).
61. J. Banga, D. Srinivasan, C.-C. Sun, C. D. Thompson, F. Milletti, K.-S. Huang, S. Hamilton, S. Song, A. F. Hoffman, Y. G. Qin, B. Matta, M. LaPan, Q. Guo, G. Lu, D. Li, H. Qian, D. R. Bolin, L. Liang, C. Wartchow, J. Qiu, M. Downing, S. Narula, N. Fotouhi, J. A. DeMartino, S.-L. Tan, G. Chen, B. J. Barnes, Inhibition of IRF5 cellular activity with cell-penetrating peptides that target homodimerization. Sci. Adv. 6, eaay1057 (2020).
62. B. Shen, X. Yi, Y. Sun, X. Bi, J. Du, C. Zhang, S. Quan, F. Zhang, R. Sun, L. Qian, W. Ge, W. Liu, S. Liang, H. Chen, Y. Zhang, J. Li, J. Xu, Z. He, B. Chen, J. Wang, H. Yan, Y. Zheng, D. Wang, J. Zhu, Z. Kong, Z. Kang, X. Liang, X. Ding, G. Ruan, N. Xiang, X. Cai, H. Gao, L. Li, S. Li, Q. Xiao, T. Lu, Y. Zhu, H. Liu, H. Chen, T. Guo, Proteomic and metabolomic characterization of COVID-19 patient sera. Cell 182, 59–72.e15 (2020).
63. E. S. Winkler, P. Gilchuk, J. Yu, A. L. Bailey, R. E. Chen, Z. Chong, S. J. Zost, H. Jang, Y. Huang, J. D. Allen, J. B. Case, R. E. Sutton, R. H. Carnahan, T. L. Darling, A. C. M. Boon, M. Mack, R. D. Head, T. M. Ross, J. E. Crowe Jr., M. S. Diamond, Human neutralizing antibodies against SARS-CoV-2 require intact Fc effector functions for optimal therapeutic protection. Cell 184, 1804–1820.e16 (2021).
64. G. Dekkers, L. Treffers, R. Plomp, A. E. H. Bentlage, M. de Boer, C. A. M. Koeleman, S. N. Lissenberg-Thunnissen, R. Visser, M. Brouwer, J. Y. Mok, H. Matlung, T. K. van den Berg, W. J. E. van Esch, T. W. Kuijpers, D. Wouters, T. Rispens, M. Wuhrer, G. Vidarsson, Decoding the human immunoglobulin G-glycan repertoire reveals a spectrum of fc-receptor- and complement-mediated-effector activities. Front. Immunol. 8, 877 (2017).
65. G. Dekkers, R. Plomp, C. A. Koeleman, R. Visser, H. H. von Horsten, V. Sandig, T. Rispens, M. Wuhrer, G. Vidarsson, Multi-level glyco-engineering techniques to generate IgG with defined Fc-glycans. Sci. Rep. 6, 36964 (2016).
66. M. Steenhuis, G. van Mierlo, N. I. L. Derksen, P. Ooijevaar-de Heer, S. Kruithof, F. L. Loeff, L. C. Berkhout, F. Linty, C. Reusken, J. Reimerink, B. Hogema, H. Zaaijer, L. van de Watering, F. Swaneveld, M. J. van Gils, B. J.

Bosch, M. van Ham, A. ten Brinke, G. Vidarsson, E. C. van der Schoot, T. Rispens, Dynamics of antibodies to SARS-CoV-2 in convalescent plasma donors. medRxiv 2021.2001.2006.20249035 (2021).
67. E. H. Vogelzang, F. C. Loeff, N. I. L. Derksen, S. Kruithof, P. O.-d. Heer, G. van Mierlo, F. Linty, J. Y. Mok, W. van Esch, S. de Bruin, A. P. J. Vlaar, B. Seppen, M. Leeuw, A. J. G. van Oudheusden, A. G. M. Buiting, K. K. Jim, H. Vrielink, F. Swaneveld, G. Vidarsson, C. E. van der Schoot, P. C. Wever, W. Li, F. van Kuppeveld, J. L. Murk, B. J. Bosch, G. J. Wolbink, T. Rispens, Development of a SARS-CoV-2 total antibody assay and the dynamics of antibody response over time in hospitalized and nonhospitalized patients with COVID-19. J. Immunol. 205, 3491–3499 (2020).
68. R. E. Jeeninga, B. Jan, H. van den Berg, B. Berkhout, Construction of doxycyline-dependent mini-HIV-1 variants for the development of a virotherapy against leukemias. Retrovirology 3, 64 (2006).
69. M. W. J. Smeets, M. J. Mourik, H. W. M. Niessen, P. L. Hordijk, Stasis promotes erythrocyte adhesion to von willebrand factor. Arterioscler. Thromb. Vasc. Biol. 37, 1618–1627 (2017).
70. Dobin, C. A. Davis, F. Schlesinger, J. Drenkow, C. Zaleski, S. Jha, P. Batut, M. Chaisson, T. R. Gingeras, STAR: Ultrafast universal RNA-seq aligner. Bioinformatics 29, 15–21 (2013).
71. H. Li, B. Handsaker, A. Wysoker, T. Fennell, J. Ruan, N. Homer, G. Marth, G. Abecasis, R. Durbin, The sequence alignment/map format and SAMtools. Bioinformatics 25, 2078–2079 (2009).
72. M. I. Love, W. Huber, S. Anders, Moderated estimation of fold change and dispersion for RNA-seq data with DESeq2. Genome Biol. 15, 550 (2014).
73. D. J. McCarthy, Y. Chen, G. K. Smyth, Differential expression analysis of multifactor RNA-Seq experiments with respect to biological variation. Nucleic Acids Res. 40, 4288–4297 (2012).
74. Y. Zhou, B. Zhou, L. Pache, M. Chang, A. H. Khodabakhshi, O. Tanaseichuk, C. Benner, S. K. Chanda, Metascape provides a biologist-oriented resource for the analysis of systems-level datasets. Nat. Commun. 10, 1523 (2019).
75. G. Korotkevich, V. Sukhov, A. Sergushichev, Fast gene set enrichment analysis. bioRxiv, 060012 (2019).
76. S. Durinck, P. T. Spellman, E. Birney, W. Huber, Mapping identifiers for the integration of genomic datasets with the R/Bioconductor package biomaRt. Nat. Protoc. 4, 1184–1191 (2009).
77. S. H. Duttke, M. W. Chang, S. Heinz, C. Benner, Identification and dynamic quantification of regulatory elements using total RNA. Genome Res. 29, 1836–1846 (2019).

Supplementary Materials

Supplementary material can be found on:

stm.sciencemag.org/cgi/content/full/13/596/eabf8654/DC1

Supplementary Figure 1 – 4

Supplementary Table 1 – 3

Supplementary Data file 1

CHAPTER 8

General discussion and conclusion

In this thesis, we investigated the role of the endothelium in pulmonary thrombosis (**Figure 1**). In part one, we provide an overview of the role of VWF in thrombosis and how its expression is regulated on a transcriptional and translational level in inflammatory conditions such as atherosclerosis, chronic thromboembolic pulmonary hypertension (CTEPH) and corona virus disease 2019 (COVID-19). To investigate the role of inflammation in endothelium-platelet interaction we developed a preclinical model to study *in situ* pulmonary thrombosis.

In the second part of this thesis, we investigated how the pulmonary artery endothelium contributes to thrombus formation and platelet adhesion in CTEPH. It is acknowledged that VWF levels are upregulated in CTEPH, and we present evidence of an inflammation-driven mechanism of *in situ* thrombosis in which VWF plays a central role. We followed up on this by performing transcriptomics and proteomics of CTEPH-PAEC and evaluated whether differential expression was due to epigenetic modifications. Subsequently, those expression profiles were linked to pathways involved in platelet signaling and increased thrombosis.

The current treatment options for CTEPH are limited to pulmonary endarterectomy surgery, balloon pulmonary angioplasty or medical treatment with vasodilators. In addition, patients receive lifelong anticoagulation to prevent recurrent thrombi. However, the combined use of vasodilators with anticoagulative drugs can be associated with an increased risk of bleeding. In the final part of this thesis, we identified a mechanism by which riociguat affects endothelial function which may lead to increased risk of bleeding.

Finally, we investigated why severe COVID-19 patients experience vascular leakage by pulmonary edema and thrombosis, and identified mechanisms that play a key role in the progression of the disease.

Preclinical models of thrombosis

Starting in the early 1970s, flow chambers were used to study thrombus formation on extracellular matrix components of the vascular wall[1,2]. However, the first devices required a large amount of blood, and caused pre-activation of platelets that only provided end-stage outcomes of thrombus formation[3]. Throughout the years, many efforts have been put into overcoming these issues which resulted in several *in vitro* techniques to study thrombus formation. Nowadays, microfluidics are widely used to recapitulate and unravel complex dynamic cellular and extracellular interactions[4].

In **chapter 3** we investigated how we can study such interaction processes between endothelial cells and platelets under conditions of blood flow. First, we described a method for custom-made microfluidic channels to study the effect of vascular geometry on thrombus formation. Endothelial cells are constantly subjected to flow and mechanical stresses: processes that continuously influence biophysical, biochemical and genetic regulatory responses of endothelial cells[5].. Biophysical properties are determined by vessel architecture and flow-conditions. Vascular bifurcations, for example, induce non-laminar flow that alters endothelial function towards an inflammatory phenotype[6].

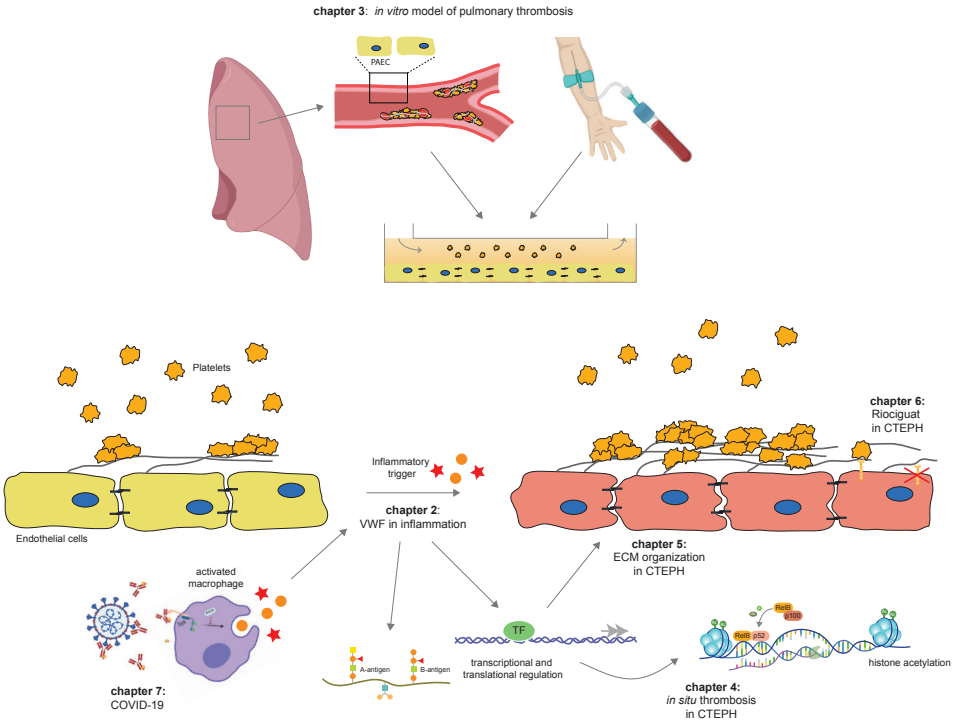

Figure 1. Graphical illustration of the work presented in this thesis

The most commonly used microfluidic models to study thrombosis are parallel chambers with unidirectional flow. A monolayer of cells is created at the bottom of the channel after which blood flow and shear stresses induce endothelial signaling. This method has been widely used to study endothelial cell signaling in responses in dynamic physical conditions and blood cell adhesion to endothelial cells. Various strategies can be employed to control the coagulation process, e.g. endothelial modifications, treatment with specific medication, addition of a selected thrombogenic marker or adaptation of the blood flow rate[7]. However, these simple systems do not recapitulate vascular geometries and hemodynamic forces as observed in vascular diseases. A soft lithography technique has been used to study a variety of microfluidic systems capable of mimicking vascular geometries such as bifurcations and stenosis[4]. Yet, these models still have rectangular cross-sections that have non-physiological edge-effects. Therefore, many studies have tried to improve the vascular mimicry by designing round channel geometries for example with 3D bio-printing or electrospinning[8,9].

The major drawback of these advanced techniques is the use of bio-inert materials that challenges the efficiency of cell seeding, usually requiring a high number of cells for sufficient cell adhesion and growth[10]. Current techniques to isolate primary pulmonary endothelial cells do not yield such high cell numbers. The most commonly method for cell isolation involves tissue digestion and yields endothelial cell populations that are contaminated with other cell types, requiring purification with a resultant further loss of cells[11,12]. We have optimized a technique that immediately yields endothelial cell growth from pulmonary artery tissue, limiting the contamination of unwanted cell types. However, a limitation of this method is that it is only feasible using material from patients who underwent surgery. Recently, a new protocol was developed to isolate PAEC from Swan-Ganz pulmonary arterial catheters, which are used during routine diagnostic or follow up right heart catheterization to diagnose pulmonary hypertension. The use of this technique allows non-invasive patient specific pulmonary artery endothelial isolation, excluding circulating endothelial cells[13,14].

Current animal models poorly reflect the pathophysiology of thromboembolic processes. The most common animal species utilized for thrombosis research are rodents, such as mice, rats, hamsters and rabbits. Pulmonary embolism can be induced via four main methods: 1) induction of acute embolism via intravenous administration of clotting agents, such as collagen or thrombin, 2) induction of thromboembolism via injection of an *in vitro* prepared blood clot, 3) administration of non-thrombotic particles such as microspheres and 4) surgical procedures to ligate pulmonary arteries in order to create occlusion[15]. The choice for a specific model or animal species is based on the objectives of the proposed study. At present, such models are primarily applied to study the consequences of thrombosis or for drug testing[16]. Understanding the exact pathobiology of thrombosis in the different blood vessels of these animal models is hampered by the complex interaction between platelets and endothelial cells. The use of microfluidics is promising technology because it permits the inclusion of

primary human cells and blood obtained from patients. With the model presented in this thesis, we provided novel insights into the response of human disease-specific endothelial cells in thrombosis.

Inflammation and thrombosis

Although inflammation-induced thrombosis is a well-known entity, its pathogenesis remains complicated. There are complex interactions between inflammation and hemostasis, involving proinflammatory cytokines, chemokines, adhesion molecules, tissue factor expression, platelet and endothelial activation[17]. The role of endothelial VWF at the interface of platelet activation and coagulation has been well established. Epidemiological studies have shown a strong relationship between elevated plasma VWF levels and the risk of thrombosis. In **chapter 2**, we discussed the role of VWF in inflammation-mediated thrombosis. Elevated VWF levels are not specific for an inflammatory acute phase response, but may be regarded as an indicator of vascular dysfunction. As such, VWF connects the hemostatic and inflammatory pathways.

In this thesis we have shown a strong role of inflammation in pulmonary thrombosis. Both physiological hemostasis and immuno-thrombosis represent normal responses to trauma or invading microorganisms; any deregulation of these processes can lead to aberrant intravascular coagulation and pathological obstruction of blood flow, which is generally defined as thrombosis[18]. In **chapter 4**, we showed that CTEPH endothelial cells are characterized by increased VWF expression, resulting in enhanced platelet accumulation under flow. The increased VWF expression is induced by NFκB2. NFκB is a central mediator of inflammation and thus fundamentally involved in the molecular links between inflammatory and thrombotic processes[18]. The major biological function of NFκB is to change cellular programs in all different kinds of stress situations. In **chapter 5**, we showed that CTEPH endothelial cells show altered extracellular matrix organization and cell-cell adhesion pathways, which affects endothelial barrier integrity. The function of endothelial integrity is to respond to rapid changes as a result from environmental events. In addition, it functions to bind other cellular components, to regulate membrane properties and endothelial barrier. Disruption of endothelial integrity influences the thrombotic response by exposure of subendothelial proteins that mediates initial platelet adhesion from the circulation[19], initiating the process of thrombosis.

In **chapter 7** we found that the pro-inflammatory response of human alveolar macrophages from severely ill COVID-19 patients is amplified by altered glycosylation of the anti-spike IgG. In general, antibodies are activated for host defense by providing various mechanisms to counteract infections, including pathogen neutralization, phagocytosis, complement activation and cytokine production[20]. However, these antibody alterations lead to overactivation of IgG effector function, thereby inducing an excessive inflammatory response[21]. This antibody induced inflammation (ADI) has been suggested to be a common immune response against all enveloped viruses[22].

A crucial event in immunothrombosis is the activation of platelets and immune cells, resulting in clot formation and vessel occlusion. Inflammation causes local thrombus formation and thrombosis can amplify the inflammatory response. It has been shown that sustained inflammation is involved in thrombus nonresolution and fibrotic remodeling of the vasculature[23] and that inflammation propagates progression of thrombosis[24]. Whether inflammation is a driver of chronic thrombosis or a consequence thereof, remains elusive.

Epigenetic regulation of endothelial cells in pulmonary thrombosis

The sequence of events leading to the generation of functional VWF protein that participates in thrombosis includes numerous factors. Genetic and epigenetic factors have been associated with the regulation of VWF levels. External stimuli such as hypoxia, trauma or inflammation can activate transcription factors that can either stimulate or repress VWF transcription, depending on the binding site on the promoter region, as described in **chapter 2**. Epigenetic modifications are an important link between environmental factors and gene expression[25]. External factors such as diet, environment or lifestyle can impose aberrant gene expression by controlling DNA methylation and histone modification[26]. Increased acetylation and tri-methylation of histone H3 are associated with accessible, actively transcribed euchromatins, whereas low acetylation or methylation are linked with transcriptionally inactive heterochromatin. Gene expression requires physical interaction between a transcription factor and DNA, depending on the conformation of chromatin. It has been shown that epigenetic factors are mediators of inflammation and chronic inflammatory disease. For example, DNA hypermethylation in peripheral blood mononuclear cells is associated with high CRP levels and cardiovascular mortality[27]. In addition, inflammatory cytokines such as IL-6 or IL-8 have reduced promoter methylation, which have been found to be increased in atheromatous plaques of coronary artery disease patients[28,29].

In **chapter 4** we found that the VWF promoter was epigenetically regulated in the endothelium of CTEPH patients, which supports the hypothesis that *in situ* thrombosis propagates disease development. VWF expression is modulated in response to external stimuli such as shear stress, vascular bed-specific heterogeneity and inflammatory responses. With our study, we identified a novel mechanism for the control of VWF in chronic inflammatory condition. Neither epigenetic regulation of the VWF promoter in the context of disease, nor increased binding of inflammatory transcription factors to the VWF promoter have been reported previously. We observed reduced tri-methylation and enhanced acetylation of histone H3 in the VWF promotor reflected by increased NFkB2 binding. But it has also been shown that the traditional transcription factor for VWF, GATA, is highly susceptible to inflammation. For example, in inflammatory condition there is more EC angiogenesis[28,30]. In addition, other epigenetic regulators, including the HDAC4 histone lysine methyltransferase EHMT2, play a role in vascular inflammation and thrombosis[31,32]. This suggests epigenetic regulation of immunothrombosis in diseases such as CTEPH.

In **chapter 5**, we showed that cytoskeletal cell-cell and extracellular matrix organization is altered in CTEPH-PAEC due to the transcription permissive epigenome of these extracellular matrix genes in endothelial cells. We demonstrated that CTEPH-PAEC show increased endothelial permeability upon stimulation with TNFα. This rapid response in barrier integrity may be induced by the altered histone acetylation in these cell-cell and extracellular matrix genes, but this mechanism requires further investigation. A possible explanation may be that inflammatory activation by for example the NFκB pathway can activate histone acetyl/methyl transferases or deacetylases[33,34].

Treatment options

CTEPH patients who are not eligible for surgery to remove the blood clots, are receiving the soluble guanylate cyclase stimulator riociguat[35]. However, combining riociguat treatment with anticoagulation may increase the risk of bleeding [36]. In **chapter 6**, we aimed to understand how riociguat affects primary hemostasis. Investigating the effect of riociguat on platelet adhesion to CTEPH PAECs, we found that riociguat reduced VWF string formation by decreased P-selectin expression on the cell surface. P-selectin expression on the surface of endothelial cells initiates leukocyte rolling along the vessel wall, and has been shown to be increased in inflammatory conditions. In response to stimuli, VWF is unfolded and anchored by P-selectin to the endothelial surface, which stabilizes VWF string formation and enhances platelet adhesion[37]. Inhibition of P-selectin has been shown to reduce venous thromboembolisms and vascular fibrosis without an increase in bleeding[38]. In addition, studies have demonstrated that leukocyte adhesion and transmigration contribute to the initiation of thrombosis by disrupting the endothelial barrier and exposing the underlying basement membrane, providing a surface for the activation of coagulation[38]. Blocking P-selectin expression has been shown to effectively inhibit inflammatory cell adhesion to the vascular wall and consequently, a reduction of thrombosis[39].

Inflammation can start local thrombosis, and thrombosis can amplify inflammation. Specific anti-VWF targets have been tested and proven to be effective to reduce the thrombotic response, as discussed in **chapter 2**. However, dampening the inflammatory response would serve as a potential antithrombotic agent that may suppress inflammation and help breaking the vicious cycle. Inflammation is often induced by a response from immune cells. Interacting with these cells, would therefore inhibit the inflammatory response, while the hemostatic response remains unaffected. As we showed in **chapter 7** with fostamatinib. Fostamatinib inhibits Syk signaling by reducing the formation of neutrophil extracellular traps[40]. We showed that by using the active compound of Fostamatinib, R406, inflammation elicited by inflammatory antibodies from severely ill COVID-19 patients could be abolished. In addition, R406 reversed the potentiation of VWF induced thrombus formation[41], which finding was confirmed in a clinical trial for COVID-19 therapy[42,43]. The pro-thrombotic environment in critically ill COVID-19 patients is exacerbated by a cytokine storm that may be driven by activated macrophages. This induces VWF secretion from endothelial cells to recruit

platelets to initiate a thrombus. As this effect is caused by inflammation, blocking ADI or macrophage activation has the potential to reduce thrombosis in COVID-19 infection.

Future perspectives

Collectively, this thesis showed that inflammatory mechanisms are an early and catalyzing event in *in situ* thrombosis in the pulmonary arteries, which challenges the embolic hypothesis of CTEPH. We showed that in COVID-19, cytokines play an important role as initiators of microvascular thrombosis. Cytokines and neutrophils play an important role in chronic inflammation. It would be of interest to investigate the effect of these immune cells on endothelial modifications in CTEPH. Besides platelets, neutrophils play an important role in inflammation and thrombosis. Neutrophils are the most abundant immune cell, constituting approximately for 70% of leukocytes in human blood and are regarded as first responders of the innate immune system. It has been shown that neutrophils and the formation of neutrophil extracellular traps (NETs) are increased in CTEPH, thereby contributing to chronic thrombosis[23]. NETs have been predominantly described in early stages of thrombus formation[44], which is further supported by the identification of in situ microvascular thrombi in the progression of SARS-CoV-2 pulmonary infection[45]. It would therefore be of interest, whether neutrophils induce the inflammatory response of VWF.

In addition, to date, proper animal models to study in vivo pathophysiology are still lacking. Existing thrombosis models involve intravenous administration of clotting agents, such as collagen or thrombin to induce acute pulmonary embolisms, but are not suitable to study mechanisms of primary hemostasis. In addition, CTEPH animal models consist of large animal models that allow studying the hemodynamic consequences of CTEPH, but fail to reproduce the characteristic vascular lesions. As such, there remains a translational gap in the study of mechanisms involved in in vivo thrombosis.

Lastly, the exact role of platelets in immunothrombosis remains open for discussion. Although we showed absence of coagulation abnormalities in CTEPH blood, it has been reported that platelets from CTEPH patients are hyperresponsive to environmental stimulation[46,47]. The direct interaction of CTEPH platelets with endothelium has not been studied and could be for interest to evaluate current anticoagulation therapy with anti-platelet therapy.

General conclusion

We propose that inflammation plays a critical role in *in situ* thrombosis by interfering with VWF-mediated platelet adhesion. Our findings may provide interesting therapeutic treatment options for inflammatory induced VWF mediated thrombosis, interfering between inflammation, coagulation and homeostasis.

References

1. Cadroy Y, Sakariassen K, Grandjean H, Thalamas C, Boneu B, Sie P. The effect of platelet PlA polymorphism on experimental thrombus formation in man depends on blood flow and thrombogenic substrate. Thromb Haemost. 2001;85:1097-1103.
2. Sakariassen KS, Aarts PA, de Groot PG, Houdijk WP, Sixma JJ. A perfusion chamber developed to investigate platelet interaction in flowing blood with human vessel wall cells, their extracellular matrix, and purified components. J Lab Clin Med. 1983;102:522-535.
3. De Groot PS, JJ. Perfusion chambers. Platelets.; 2002.
4. Mannino RG, Qiu Y, Lam WA. Endothelial cell culture in microfluidic devices for investigating microvascular processes. Biomicrofluidics. 2018;12:042203. doi: 10.1063/1.5024901
5. Davies PF. Flow-mediated endothelial mechanotransduction. Physiol Rev. 1995;75:519-560. doi: 10.1152/physrev.1995.75.3.519
6. Gebb S, Stevens T. On lung endothelial cell heterogeneity. Microvasc Res. 2004;68:1-12. doi: 10.1016/j.mvr.2004.02.002
7. Nagy M, Heemskerk JWM, Swieringa F. Use of microfluidics to assess the platelet-based control of coagulation. Platelets. 2017;28:441-448. doi: 10.1080/09537104.2017.1293809
8. Awad NK, Niu H, Ali U, Morsi YS, Lin T. Electrospun Fibrous Scaffolds for Small-Diameter Blood Vessels: A Review. Membranes (Basel). 2018;8. doi: 10.3390/membranes8010015
9. Zhang YS, Davoudi F, Walch P, Manbachi A, Luo X, Dell'Erba V, Miri AK, Albadawi H, Arneri A, Li X, et al. Bioprinted thrombosis-on-a-chip. Lab Chip. 2016;16:4097-4105. doi: 10.1039/c6lc00380j
10. Akther F, Yakob SB, Nguyen NT, Ta HT. Surface Modification Techniques for Endothelial Cell Seeding in PDMS Microfluidic Devices. Biosensors (Basel). 2020;10. doi: 10.3390/bios10110182
11. van Beijnum JR, Rousch M, Castermans K, van der Linden E, Griffioen AW. Isolation of endothelial cells from fresh tissues. Nat Protoc. 2008;3:1085-1091. doi: 10.1038/nprot.2008.71
12. Kaneko FT, Arroliga AC, Dweik RA, Comhair SA, Laskowski D, Oppedisano R, Thomassen MJ, Erzurum SC. Biochemical reaction products of nitric oxide as quantitative markers of primary pulmonary hypertension. Am J Respir Crit Care Med. 1998;158:917-923. doi: 10.1164/ajrccm.158.3.9802066
13. Tielemans B, Stoian L, Wagenaar A, Leys M, Belge C, Delcroix M, Quarck R. Incremental Experience in In Vitro Primary Culture of Human Pulmonary Arterial Endothelial Cells Harvested from Swan-Ganz Pulmonary Arterial Catheters. Cells. 2021;10. doi: 10.3390/cells10113229
14. Passineau MJ, Gallo PH, Williams G, Perez R, Benza RL. Harvest of Endothelial Cells from the Balloon Tips of Swan-Ganz Catheters after Right Heart Catheterization. J Vis Exp. 2019. doi: 10.3791/58353
15. Karpov AA, Vaulina DD, Smirnov SS, Moiseeva OM, Galagudza MM. Rodent models of pulmonary embolism and chronic thromboembolic pulmonary hypertension. Heliyon. 2022;8:e09014. doi: 10.1016/j.heliyon.2022.e09014
16. Jagadeeswaran P, Cooley BC, Gross PL, Mackman N. Animal Models of Thrombosis From Zebrafish to Nonhuman Primates: Use in the Elucidation of New Pathologic Pathways and the Development of Antithrombotic Drugs. Circ Res. 2016;118:1363-1379. doi: 10.1161/CIRCRESAHA.115.306823
17. Aksu K, Donmez A, Keser G. Inflammation-induced thrombosis: mechanisms, disease associations and management. Curr Pharm Des. 2012;18:1478-1493. doi: 10.2174/138161212799504731
18. Mussbacher M, Salzmann M, Brostjan C, Hoesel B, Schoergenhofer C, Datler H, Hohensinner P, Basilio J, Petzelbauer P, Assinger A, et al. Cell Type-Specific Roles of NF-kappaB Linking Inflammation and Thrombosis. Front Immunol. 2019;10:85. doi: 10.3389/fimmu.2019.00085
19. Yau JW, Teoh H, Verma S. Endothelial cell control of thrombosis. BMC Cardiovasc Disord. 2015;15:130. doi: 10.1186/s12872-015-0124-z
20. Guilliams M, Bruhns P, Saeys Y, Hammad H, Lambrecht BN. The function of Fcgamma receptors in dendritic cells and macrophages. Nat Rev Immunol. 2014;14:94-108. doi: 10.1038/nri3582
21. Vidarsson G, Dekkers G, Rispens T. IgG subclasses and allotypes: from structure to effector functions. Front Immunol. 2014;5:520. doi: 10.3389/fimmu.2014.00520
22. Larsen MD, de Graaf EL, Sonneveld ME, Plomp HR, Nouta J, Hoepel W, Chen HJ, Linty F, Visser R, Brinkhaus M, et al. Afucosylated IgG characterizes enveloped viral responses and correlates with COVID-19 severity. Science. 2021;371. doi: 10.1126/science.abc8378
23. Sharma S, Hofbauer TM, Ondracek AS, Chausheva S, Alimohammadi A, Artner T, Panzenboeck A, Rinderer J, Shafran I, Mangold A, et al. Neutrophil extracellular traps promote fibrous vascular occlusions in chronic thrombosis. Blood. 2021;137:1104-1116. doi: 10.1182/blood.2020005861

24. Esmon CT. The impact of the inflammatory response on coagulation. Thromb Res. 2004;114:321-327. doi: 10.1016/j.thromres.2004.06.028
25. Wang G, Walker SO, Hong X, Bartell TR, Wang X. Epigenetics and early life origins of chronic noncommunicable diseases. J Adolesc Health. 2013;52:S14-21. doi: 10.1016/j.jadohealth.2012.04.019
26. Fraga MF, Ballestar E, Paz MF, Ropero S, Setien F, Ballestar ML, Heine-Suner D, Cigudosa JC, Urioste M, Benitez J, et al. Epigenetic differences arise during the lifetime of monozygotic twins. Proc Natl Acad Sci U S A. 2005;102:10604-10609. doi: 10.1073/pnas.0500398102
27. Stenvinkel P, Karimi M, Johansson S, Axelsson J, Suliman M, Lindholm B, Heimburger O, Barany P, Alvestrand A, Nordfors L, et al. Impact of inflammation on epigenetic DNA methylation - a novel risk factor for cardiovascular disease? J Intern Med. 2007;261:488-499. doi: 10.1111/j.1365-2796.2007.01777.x
28. Patsouras MD, Vlachoyiannopoulos PG. Evidence of epigenetic alterations in thrombosis and coagulation: A systematic review. J Autoimmun. 2019;104:102347. doi: 10.1016/j.jaut.2019.102347
29. Apostolakis S, Vogiatzi K, Amanatidou V, Spandidos DA. Interleukin 8 and cardiovascular disease. Cardiovasc Res. 2009;84:353-360. doi: 10.1093/cvr/cvp241
30. Benincasa G, Costa D, Infante T, Lucchese R, Donatelli F, Napoli C. Interplay between genetics and epigenetics in modulating the risk of venous thromboembolism: A new challenge for personalized therapy. Thromb Res. 2019;177:145-153. doi: 10.1016/j.thromres.2019.03.008
31. Wei X, Yi X, Zhu XH, Jiang DS. Histone methylation and vascular biology. Clin Epigenetics. 2020;12:30. doi: 10.1186/s13148-020-00826-4
32. Rai V, Agrawal DK. Transcriptional and Epigenetic Factors Associated with Early Thrombosis of Femoral Artery Involved in Arteriovenous Fistula. Proteomes. 2022;10. doi: 10.3390/proteomes10020014
33. Barroso M, Kao D, Blom HJ, Tavares de Almeida I, Castro R, Loscalzo J, Handy DE. S-adenosylhomocysteine induces inflammation through NFkB: A possible role for EZH2 in endothelial cell activation. Biochim Biophys Acta. 2016;1862:82-92. doi: 10.1016/j.bbadis.2015.10.019
34. Barnes PJ, Adcock IM, Ito K. Histone acetylation and deacetylation: importance in inflammatory lung diseases. Eur Respir J. 2005;25:552-563. doi: 10.1183/09031936.05.00117504
35. Delcroix M, Torbicki A, Gopalan D, Sitbon O, Klok FA, Lang I, Jenkins D, Kim NH, Humbert M, Jais X, et al. ERS statement on chronic thromboembolic pulmonary hypertension. Eur Respir J. 2021;57. doi: 10.1183/13993003.02828-2020
36. Jujo-Sanada T, Tanabe N, Sakao S, Sugiura T, Sekine A, Nishimura R, Suda R, Naito A, Miwa H, Yamamoto K, et al. The anticoagulant effects of warfarin and the bleeding risk associated with its use in patients with chronic thromboembolic pulmonary hypertension at a specialist center in Japan: a retrospective cohort study. Pulm Circ. 2017;7:684-691. doi: 10.1177/2045893217717258
37. Padilla A, Moake JL, Bernardo A, Ball C, Wang Y, Arya M, Nolasco L, Turner N, Berndt MC, Anvari B, et al. P-selectin anchors newly released ultralarge von Willebrand factor multimers to the endothelial cell surface. Blood. 2004;103:2150-2156. doi: 10.1182/blood-2003-08-2956
38. Purdy M, Obi A, Myers D, Wakefield T. P- and E- selectin in venous thrombosis and non-venous pathologies. J Thromb Haemost. 2022;20:1056-1066. doi: 10.1111/jth.15689
39. Briggs JB, Oda Y, Gilbert JH, Schaefer ME, Macher BA. Peptides inhibit selectin-mediated cell adhesion in vitro, and neutrophil influx into inflammatory sites in vivo. Glycobiology. 1995;5:583-588. doi: 10.1093/glycob/5.6.583
40. Connell NT, Berliner N. Fostamatinib for the treatment of chronic immune thrombocytopenia. Blood. 2019;133:2027-2030. doi: 10.1182/blood-2018-11-852491
41. Bye AP, Hoepel W, Mitchell JL, Jegouic S, Loureiro S, Sage T, Vidarsson G, Nouta J, Wuhrer M, de Taeye S, et al. Aberrant glycosylation of anti-SARS-CoV-2 spike IgG is a prothrombotic stimulus for platelets. Blood. 2021;138:1481-1489. doi: 10.1182/blood.2021011871
42. Strich JR, Ramos-Benitez MJ, Randazzo D, Stein SR, Babyak A, Davey RT, Suffredini AF, Childs RW, Chertow DS. Fostamatinib Inhibits Neutrophils Extracellular Traps Induced by COVID-19 Patient Plasma: A Potential Therapeutic. J Infect Dis. 2021;223:981-984. doi: 10.1093/infdis/jiaa789
43. Strich JR, Tian X, Samour M, King CS, Shlobin O, Reger R, Cohen J, Ahmad K, Brown AW, Khangoora V, et al. Fostamatinib for the Treatment of Hospitalized Adults With Coronavirus Disease 2019: A Randomized Trial. Clin Infect Dis. 2022;75:e491-e498. doi: 10.1093/cid/ciab732
44. Bonaventura A, Liberale L, Carbone F, Vecchie A, Diaz-Canestro C, Camici GG, Montecucco F, Dallegri F. The Pathophysiological Role of Neutrophil Extracellular Traps in Inflammatory Diseases. Thromb Haemost. 2018;118:6-27. doi: 10.1160/TH17-09-0630
45. Middleton EA, He XY, Denorme F, Campbell RA, Ng D, Salvatore SP, Mostyka M, Baxter-Stoltzfus A, Borczuk AC, Loda M, et al. Neutrophil extracellular traps contribute to immunothrombosis in COVID-19 acute respiratory distress syndrome. Blood. 2020;136:1169-1179. doi: 10.1182/blood.2020007008

46. Yaoita N, Shirakawa R, Fukumoto Y, Sugimura K, Miyata S, Miura Y, Nochioka K, Miura M, Tatebe S, Aoki T, et al. Platelets are highly activated in patients of chronic thromboembolic pulmonary hypertension. Arterioscler Thromb Vasc Biol. 2014;34:2486-2494. doi: 10.1161/ATVBAHA.114.304404
47. Remkova A, Simkova I, Valkovicova T. Platelet abnormalities in chronic thromboembolic pulmonary hypertension. Int J Clin Exp Med. 2015;8:9700-9707.

APPENDIX

English summary
Nederlandse samenvatting
Bibliography
List of Publications
Dankwoord

English summary

With every heartbeat, the body ensures sufficient blood supply to and from all tissues and organs. The heart pumps oxygen and nutrients to, and eliminates carbon dioxide and waste products from the organs via a closed circulatory network of blood vessels. The inner layer of these blood vessels is formed by endothelial cells, and form the interface between the bloodstream and tissues. To prevent fluid leakage or bleeding, endothelial cells are highly active to sense and respond to extracellular signals. Alterations and/or damage of the endothelium plays a central role in several cardiovascular diseases such as atherosclerosis, thrombosis and pulmonary hypertension.

Various factors such as inflammation or disturbed blood flow can damage the vessel wall and activate endothelial cells to form a blood clot. Endothelial cells secrete a sticky protein string, called Von Willebrand Factor (VWF) that captures blood platelets from the circulation. This initiates the recruitment of other proteins that continue the process for the formation of a stable blood clot. When the blood vessel is repaired, the body has a mechanism that breaks down the blood clot. However, if there is excessive blood clot formation that limits or blocks continuous blood flow, it is called thrombosis.

The aim of this thesis was to investigate the role of endothelial cells in thrombosis in the lung vessels. In **chapter 1**, we provide general background information about the pulmonary vessels, and the role of inflammation in thrombosis. In **chapter 2**, we reviewed the regulation of VWF production and how this is altered in inflammation. In **chapter 3**, we have implemented a model to study endothelial function in pulmonary thrombosis. We demonstrated a protocol for the isolation of pulmonary artery endothelial cells that can be used to study endothelial-platelet interaction.

If blood clots in the lungs do not break down by its own body mechanisms, patients receive medication, also known as anticoagulation therapy. If there is no improvement after at least three months of medication, it will result in chronic narrowing of the pulmonary vessels which makes it harder for the heart to pump blood through the lungs. This impaired blood flow results in reduced gas exchange and an increased work load for the heart, which in the end results in heart failure. If this is caused by these chronic thrombi in the lung vessels, this disease condition is called chronic thromboembolic pulmonary hypertension (CTEPH).

In **chapter 4** we tried to find out why these CTEPH patients have chronic thrombus formation. We provided evidence of a mechanism of *in situ* thrombosis, where the local formation of a blood clot contributes to the progression of the disease. We found a strong link between inflammation and VWF expression, consequently leading to increased platelet adhesion on the pulmonary endothelium of CTEPH patients. This is caused by genetic alterations in that increases the production of VWF in inflammatory condition.

In **chapter 5**, we found that the pulmonary endothelium of CTEPH cells show disrupted signaling in their cell-cell contacts and cell-matrix contacts, which are also caused by similar genetic alterations as we have found in chapter 4. This makes the vessel more susceptible to leakage and exposure to coagulation proteins, which induces thrombosis.

Some CTEPH patients are eligible for a surgery that removes blood clots from the lung vessels. However, operability is based on the criteria that the lesions are surgically accessible and the absence of relevant comorbidities. As an alternative, blood flow can be restored with a balloon catheter that opens the vessels. This is often performed in combination with medical therapy that widens the blood vessels, known as vasodilators. However, the combined use of vasodilators with anticoagulation medication, can be associated with an increased risk of bleeding. In **chapter 6**, we attempted to find a mechanism how a specific vasodilator, riociguat, affect endothelial function and found that endothelial cells stimulated with riociguat inhibited ultra large VWF formation. This reduced initial platelet binding which may lead to increased risk of bleeding.

Finally, we have investigated why intensive care COVID-19 patients experience severely symptoms compared to ward or non-hospitalized patients. Severely ill COVID-19 patients experience vascular leakage by pulmonary edema and thrombosis that play a key role the progression of the disease. In **chapter 7**, we have shown that antibodies from critically ill COVID-19 patients are different than less ill patients. These antibodies induce an excessive inflammatory response, that subsequently induces endothelial barrier disruption and pulmonary thrombosis.

The main conclusion of this thesis provides strong evidence of inflammation and thrombosis leading to excessive production of VWF, involved in the primary initiation of thrombosis. In **chapter 8** we have discussed our findings with current literature and provided new options for future research to improve understanding of pulmonary thrombosis.

Nederlandse leken samenvatting

De vorming van een **bloedstolsel** omvat een complexe interactie tussen de vaatwand en het bloed. In dit proefschrift hebben we onderzocht hoe deze interactie verstoord is tijdens longziekten, met in het bijzonder: **chronische trombo-embolische pulmonale hypertensie (CTEPH)**, letterlijk vertaald als verhoogde bloeddruk in de longen door langdurige bloedstolsels in de longbloedvaten.

We hebben dit onderzoek mogelijk gemaakt door een methode te ontwikkelen waarmee we deze interactie tussen de vaatwand en het bloed in het lab kunnen bestuderen. De belangrijkste ontdekking was dat CTEPH patiënten meer bloedplaatjes uit de bloedcirculatie vangen doordat hun vaatwand meer eiwit maakt waar deze bloedplaatjes aan binden. Dit komt door genetische veranderingen die door omgevingsfactoren worden veroorzaakt. Met name tijdens een ontstekingsreactie kunnen hierdoor extra veel bloedplaatjes binden, waardoor er een overmatige vorming van bloedstolsels ontstaat die de doorstroom van het bloed verstoren en voor ziekte kan zorgen. De hoofdbevindingen van dit proefschrift zijn samengevat in **Figuur 1**, welke hierna verder zullen worden toegelicht.

De vorming van een bloedstolsel

Hoofdstuk 1 beschrijft algemene achtergrondinformatie over de inhoud van dit proefschrift. Een bloedstolsel vormt zich in het vaatstelsel van de bloedsomloop. De bloedsomloop bestaat uit het hart- en vaatstelsel. Het hart werkt als een pomp en zorgt ervoor dat de bloedsomloop tijdens elke hartklopping in beweging blijft. Het vaatstelsel vormt een netwerk van buisvormige structuren die het bloed langs alle weefsels en organen van het lichaam brengt. De binnenkant van dit bloedvatenstelsel is bekleed met een enkele laag cellen, welke **endotheelcellen** worden genoemd. Endotheelcellen liggen als stoeptegels tegen elkaar aan en reguleren de uitwisseling van gassen zoals zuurstof en koolstofdioxide, en de doorlaatbaarheid van voedingsstoffen zoals suikers, eiwitten en vetten, naar de weefsels en organen. In een gezond bloedvat maken endotheelcellen stofjes aan die voorkomen dat bloedcellen aan de vaatwand kunnen binden, en het bloed dus goed blijft stromen. Bij beschadiging van een bloedvat, door bijvoorbeeld een ontsteking, wordt een reparatiemechanisme gestart dat het vloeibare stromende bloed kan omzetten in een vaste substantie, een **bloedstolsel**. Als het bloed dusdanig goed stolt en daarmee de doorstroom van het bloed blokkeert, spreekt men van **trombose** en wordt het bloedstolsel een trombus genoemd. De vorming van een trombus begint met endotheelcellen die een stollingseiwit afgeven in het bloed. Dit stollingseiwit heet **Von Willebrand Factor** (VWF) en vormt lange plakkerige draden in de vaatwand waar bloedplaatjes uit de bloedcirculatie aan kunnen blijven hangen. Op deze manier wordt het begin van een bloedplaatjesprop gemaakt, die zich door de interactie met andere stollingsfactoren verder ontwikkelt tot een stabiel bloedpropje.

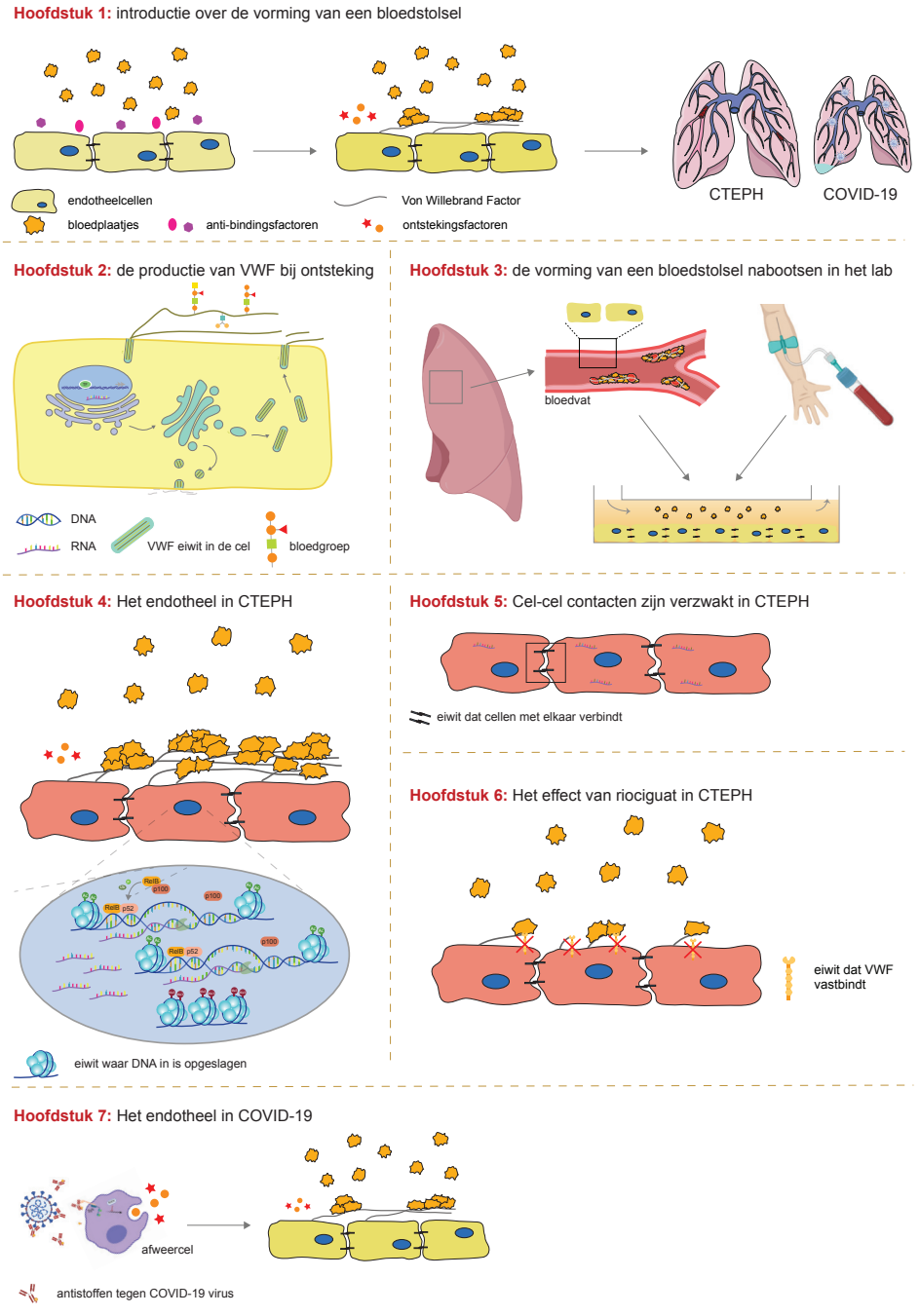

Figuur 1. Een illustratie van de belangrijkste bevindingen van dit proefschrift

In **hoofdstuk 2** hebben we geprobeerd te begrijpen hoe de eerste interactie tussen endotheelcellen en bloedplaatjes plaats vindt, en hoe deze acuut wordt beïnvloed tijdens infectie met het coronavirus, of bij langdurige ziektes zoals slagaderverkalking en terugkerende longembolieën. We beschrijven hoe VWF wordt geproduceerd in endotheelcellen en hoe een ontstekingsreactie in de bloedvaten de aanmaak van dit stofje kan verstoren. Voordat endotheelcellen het VWF uitscheiden, wordt eerst het DNA omgezet in RNA, dat de genetische code die het functionele VWF eiwit kan maken. Een genetische verandering in het DNA of een ontstekingsreactie kan er voor zorgen dat stofjes worden geactiveerd die meer RNA zullen maken. Het gevolg is dat er meer van het functionele VWF eiwit wordt gemaakt. Voordat het wordt uitgescheiden in de bloedsomloop, wordt het eerst opgeslagen in de endotheelcellen. Hier worden nog extra moleculen afknipt of bijgehangen aan het eiwit, waardoor mensen meer of minder gevoelig zijn voor een ontsteking en het ontwikkelen van een bloedstolsel. Bij mensen met bloedgroep O ontbreken er bijvoorbeeld moleculen die het VWF eiwit minder functioneel maken.

In **hoofdstuk 3** hebben we een methode opgezet waarmee de interactie tussen endotheelcellen en bloed kan worden bestudeerd in het lab. Allereerst hebben we een manier ontwikkeld waarbij endotheelcellen uit de bloedvaten van de long, in het lab kunnen worden gekweekt. Deze bloedvaten zijn van patiënten bij wie bloedstolsels operatief uit de long worden verwijderd. Hierbij komt naast de trombus, ook een stuk van de vaatwand mee waaruit we gemakkelijk cellen konden isoleren voor gebruik in het lab. Deze cellen worden vervolgens in zogenaamde mini kanaaltjes gekweekt om zo een bloedvat na te bootsen. Vervolgens worden bloedplaatjes geïsoleerd uit het bloed, waarna deze over de endotheelcellen worden gestroomd. Door het gebruik van patiënten materiaal, hebben we een methode ontwikkeld om patiënt en ziekte specifieke bloedvaten na te maken in het lab. Hiermee hebben we bijvoorbeeld in het lab kunnen aantonen dat endotheelcellen van patiënten die veel bloedstolsels in hun longen hebben, inderdaad ook veel meer bloedplaatjes vangen uit het bloed dan endotheelcellen van niet-zieke patiënten.

Trombose in de longen

Als een bloedstolsel in de longen terechtkomt, heet het een longembolie. Het kan echter ook voorkomen dat een trombus plaatselijk in de longen wordt gevormd. Vaak krijgen patiënten dan antistollingsmedicatie, in de volksmond bekend als bloedverdunners. Deze antistollingsmedicatie helpt het lichaam om de vorming van een bloedstolsel te voorkomen. Het komt soms echter ook voor dat dit niet effectief genoeg werkt waardoor bloedvaten verstopt en of vernauwd achter blijven. Omdat dezelfde hoeveelheid bloed dan door minder of smallere bloedvaten moet gaan, stijgt de bloeddruk in de longen. Als deze bloeddruk dusdanig hoog is waardoor het hart harder moet pompen, heet dit **chronische trombo-embolische pulmonale hypertensie** (CTEPH), een verhoogde bloeddruk in de longen door langdurige bloedstolsels.

In **hoofdstuk 4** hebben we aangetoond dat de plaatselijke vorming van een bloedstolsel in de longen bijdraagt aan de ontwikkeling van CTEPH. We vonden dat dit komt doordat endotheelcellen van CTEPH patiënten meer bloedplaatjes vangen doordat zij meer VWF aanmaken. De verhoogde VWF aanmaak wordt veroorzaakt doordat het DNA van dit eiwit in CTEPH patiënten beter toegankelijk is voor eiwitten die het DNA omzetten tot het functionele stollingseiwit. Tijdens een ontstekingsreactie, wat veelal voorkomt in CTEPH patiënten, wordt dit proces extra gestimuleerd waardoor het VWF eiwit productie als een sneeuwbaleffect bloedplaatjes uit de bloedcirculatie vangt.

Naast VWF spelen ook andere eiwitten een belangrijke rol in de vorming van een bloedstolsel. In **hoofdstuk 5** hebben we van een ingewikkelde labtechniek gebruik gemaakt die in één keer vele genetisch materiaal en eiwitstructuren uit cellen kan identificeren. De resultaten uit dit onderzoek laten zien dat genen en eiwitten in de cel die een rol spelen tijdens de zogenaamde barrière functie van een bloedvat, veranderd zijn in endotheelcellen van CTEPH patiënten. Deze barrière functie zorgt ervoor dat het bloed wordt gescheiden van weefsels en er geen bloed kan weglekken. Als dit niet goed functioneert, worden er moleculen aan het bloed blootgesteld die de vorming van een bloedstolsel kunnen initiëren. Echter is er meer onderzoek nodig om te achterhalen of deze ook van belang zijn in de interactie tussen endotheel en bloedplaatjes.

Overmatige bloedstolsels van CTEPH patiënten worden momenteel operatief verwijderd via de longslagader. Het kan echter voorkomen dat zulke operaties een te groot risico zijn voor de patiënt, of dat de bloedvaten dusdanig diep zitten waardoor een operatie niet mogelijk is. Als alternatief kan een bloedvat weer worden geopend door een ballon die middels een katheter in het bloedvat wordt geplaatst. Dit verwijdert echter niet de bloedprop, waardoor patiënten vaak nog vaatverwijdende medicatie moeten slikken. Echter, als CTEPH patiënten zulk medicijn slikken in combinatie met antistollingsmedicatie, ontstaan er soms overmatige bloedingen. In **hoofdstuk 6** hebben we geprobeerd te ontdekken hoe een veelgebruikt vaatverwijdend medicijn, riociguat, endotheelcellen en VWF productie aantasten. We hebben gevonden dat riociguat de vorming van de lange plakkerige VWF draden remt. Endotheelcellen blijven wel voldoende VWF aanmaken, maar het eiwit plakt niet meer goed tegen de vaatwand doordat riociguat de expressie van dit bindingseiwit remt. Doordat het VWF eiwit niet meer goede plakdraden vormt, kunnen minder bloedplaatjes binden. Dit kan als gevolg hebben dat er een verhoogd risico op bloeding ontstaat.

Tenslotte hebben we naast CTEPH patiënten ook coronapatiënten onderzocht. In **hoofdstuk 7** hebben we aangetoond dat ernstig zieke coronapatiënten die op de spoedeisende hulp liggen niet ziek worden van het virus zelf, maar voornamelijk door hun afweerreactie tegen het virus. Deze patiënten maken andere antistoffen aan dan coronapatiënten die minder ernstig ziek zijn. Deze veranderde antistoffen activeren juist afweercellen die een ernstige ontstekingsreactie induceren. Deze ontstekingsreactie zorgt voor meer lekkage en vaatschade in de longen. Dit zien we terug in endotheelcellen die worden geïnfecteerd met het bloed van deze zieke patiënten. De endotheelcellen

liggen niet meer netjes tegen elkaar aan waardoor er vocht in de longen kan lekken en het stollingsmechanisme wordt geactiveerd. Er wordt meer VWF aangemaakt en uitgescheiden wat weer een verhoogd risico op longtrombose geeft, dat uiteindelijk leidt tot een ernstiger ziekteproces.

De hoofdconclusie uit dit proefschrift is dat ontstekingsreacties in het bloed nauw zijn verbonden met de productie van het stollingseiwit Von Willebrand Factor, dat het ontstaan van bloedpropjes initieert. We hebben deze bevindingen toegepast in een ziekte waarbij patiënten last hebben van een langdurige lichte ontsteking in de longen zoals in CTEPH, maar ook in een acutere fase van ontsteking zoals tijdens een infectie met het coronavirus. In **hoofdstuk 8** hebben we de meest belangrijke bevindingen van dit proefschrift besproken. Daarnaast hebben we gespeculeerd over mogelijke vervolgstappen van dit proefschrift die voor een verbeterde diagnose en behandeling voor de patiënt kunnen zorgen.

Bibliography

Xue Manz was born on 29 October 1993. After obtaining her bachelor's degree in biomedical sciences at Maastricht University in 2015, she continued her master degree in cardiovascular disease at Utrecht University. During her studies, she chose to obtain abroad experience and went to Sydney, Australia for 6 months. Immediately after graduation in 2017, she started her PhD at VU medical center in Amsterdam, at the department of Pulmonology. Under supervision of prof.dr. Harm Jan Bogaard, dr. Jurjan Aman and dr. Robert Szulcek she investigated the role of endothelial cells in pulmonary thrombosis. By doing her PhD in a preclinical and clinical department, she obtained a broad experience in cellular and molecular laboratory techniques, as well as clinical application. After almost 10 years of research education, she broadened her horizon outside academia and started working at the Dutch Heart Foundation. In March 2023, she will start her training laboratorium medicine in clinical chemistry at Meander medical center in Amersfoort, where she can combine her biomedical background and enthousiasm for research with patient care and laboratory management.

List of publications

Published manuscripts

Hartl L, Maarschalkerweerd PAF, Butler JM, **Manz XD**, de Man FS, Thijssen V, Blijsma MF, Duitman JW, Spek CA. *C/EBPδ Suppresses Motility-Associated Gene Signatures and Reduces PDAC Cell Migration.* Cells. October 2022.

Sanada-Jujo T*, **Manz XD***, Pan X, Symersky P, Yoshida K, Aman J, Bogaard HJ. *Riociguat inhibits ultra large VWF string formation on pulmonary artery endothelial cells from chronic thromboembolic pulmonary hypertension patients*. Pulmonary Circulation. October 2022. *equal contribution

Manz XD, Bogaard HJ, Aman J. *Regulation of Von Willebrand Factor in inflammatory thrombosis.* Arteriosclerosis, Thrombosis and Vascular Biology (ATVB). September 2022.

Man K, Joukhdar H, **Manz XD**, Brunet MY, Jiang LH, Rnjak-Kovacina J, Yang XB. Bone tissue engineering using 3D silk scaffolds and human dental pulp stromal cells epigenetic reprogrammed with the selective histone deacetylase inhibitor MI192. Cell Tissue Research. April 2022.

Manz XD, Szulcek R, Pan X, Symersky P, Dickhoff C, Majolée J, Kremer V, Michielon E, Jordanova ES, Radonic T, Bijnsdorp IV, Piersma SR, Pham TV, Jimenez CR, Vonk Noordergraaf A, de Man FS, Boon RA, Voorberg J, Hordijk PL, Aman J*, Bogaard HJ*. *Epigenetic modification of the Von Willebrand Factor promotor drives platelet aggregation in chronic thromboembolic pulmonary hypertension.* American Journal of Respiratory and Critical Care Medicine. April 2022. *equal contribution

Llucià-Valldeperas A, Smal R, Bekedam F, Ce M, Pan X, **Manz XD**, Wijnker PJM, Vonk Noordegraaf A, Bogaard HJ, Goumans MJ, de Man FS. *Development of a 3-dimensional model to study right heart dysfunction in pulmonary arterial hypertension: first observations*. Cells. December 2021.

Hoepel W*, Chen HJ*, Geyer CE, Allahverdiyeva S, **Manz XD**, de Taeye SW, Aman J, Mes L, Steenhuis M, Griffith GR, Bonta PI, Brouwer PJM, Caniels TG, van der Straten K, Golebski K, Jonkers RE, Larsen MD, Linty F, Nouta J, van Roomen CPAA, van Baarle FEHP, van Drunen CM, Wolbink G, Vlaar APJ, de Bree GJ, Sanders RW, Willemsen L, Neele AE, van de Beek D, Rispens T, Wuhrer M, Bogaard HJ, van Gils MJ, Vidarsson G, de Winther M#, den Dunnen J#. *High titers and low fucosylation of early human anti-SARS-CoV-2 IgG promote inflammation by alveolar macrophages.* Science Translational Medicine. June 2021 *,#equal contribution

Szulcek R, Sanchez-Duffhues G, Rol N, Pan X, Tsonaka R, Dickhoff C, Yung LM, **Manz XD**, Kurakula K, Kiełbasa SM, Mei H, Timens W, Yu PB, Bogaard HJ, Goumans MJ. *Exacerbated inflammatory signaling underlies aberrant response to BMP9 in pulmonary arterial hypertension lung endothelial cells.* Angiogenesis. November 2020

Manz XD, Albers HJ, Symersky P, Aman J, van der Meer AD, Bogaard HJ, Szulcek R. *In Vitro Microfluidic Disease Model to Study Whole Blood-Endothelial Interactions and Blood Clot Dynamics in Real-Time*. Journal of Visualized Experiments: JoVE. May 2020

Tang F, **Manz XD**, Bongers A, Odell RA, Joukhdar H, Whitelock JM, Lord MS, Rnjak-Kovacina J. *Microchannels Are an Architectural Cue That Promotes Integration and Vascularization of Silk Biomaterials in Vivo*. ACS Biomaterials Science & Engineering. March 2020

Submitted manuscripts

Geyer C*, Chen HJ*, Bye AP, **Manz XD**, Guerra D, Caniels TG, Bijl TPL, Griffith GR, Hoepel W, de Taeye SW, Veth J, Vlaar APJ, Amsterdam UMC COVID-19 Biobank, Vidarsson G, Bogaard HJ, Aman J, Gibbins JM, van Gils MJ, de Winther MPJ#, den Dunnen J#. *Identification of new drugs to counteract anti-spike IgG-induced hyperinflammation in severe COVID-19.* Under review at Cell Reports. *, #equal contribution.

Manuscripts in preparation

Manz XD, Pan X, Szulcek R, Prange K, Griffith G, Jongejan A, Arkani M, Symersky P, Dickhoff C, Jimenez C, de Winther M, Bogaard HJ, Aman J. *Multi-omic profiling of the pulmonary arterial endothelium reveals disturbed cell adhesion and extracellular matrix reorganization in chronic thromboembolic pulmonary hypertension*

Published abstracts

Manz XD, Szulcek R, Pan X, Symersky P, Dickhoff C, Majolée J, Kremer V, Michielon E, Jordanova ES, Radonic T, Bijnsdorp IV, Piersma SR, Pham TV, Jimenez CR, de Man FS, Boon RA, Voorberg J, Hordijk PL, Aman J*, Bogaard HJ*. *Epigenetic Modification of the Von Willebrand Factor Promotor Drives in situ Thrombosis in Chronic Thromboembolic Pulmonary Hypertension.* AHA Scientific Sessions – Circulation. November 2021.

Manz XD, Pan X, Symersky P, Majolée J, Hordijk P, Voorberg J, Aman J, Bogaard HJ, Szulcek R. *Elevated Von Willebrand Factor expression in the activated pulmonary endothelium of chronic thromboembolic pulmonary hypertension patients enhances platelet adhesion*. ERS International Congress – European Respiratory Journal. September 2020.

Manz XD, Pan X, Symersky P, Majolée J, Tura-Ceide O, Hordijk, PL, Voorberg J, Bogaard, HJ, Szulcek R. *The Activated Pulmonary Endothelium of Chronic Thromboembolic Pulmonary Hypertension Patients Exhibits Elevated Platelet Adhesion*. ATS International Conference – American Journal of Respiratory and Critical Care Medicine. May 2020.

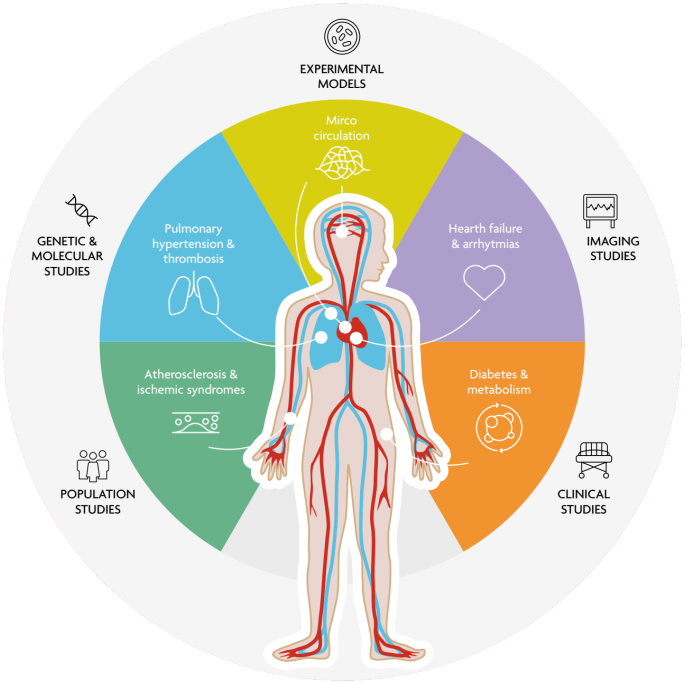

Amsterdam Cardiovascular Sciences

Amsterdam UMC
Universitair Medische Centra